Title
New Paradigms for eIF4E in Translating the Genome of Normal and Cancer Cells

Author
Truitt, Morgan Lee

Publication Date
2014

Peer reviewed|Thesis/dissertation

New Paradigms for eIF4E in Translating the Genome of Normal and Cancer Cells

by

Morgan Lee Truitt

DISSERTATION

Submitted in partial satisfaction of the requirements for the degree of

DOCTOR OF PHILOSOPHY

in

Biomedical Sciences

in the

[redacted]

Acknowledgements

First and foremost, I would like to thank my graduate advisor Dr. Davide Ruggero for his excellent support and guidance over the years. I joined Davide's lab during my third year of graduate school after my original graduate advisor, Dough Hanahan, announced he would be taking a director position in Switzerland. Davide saw immense potential in me the first time we met and his enthusiasm and support has never wavered over the years. He has given me innumerable opportunities to grow and succeed as a scientist and any claims to future success in science I may have will be in no small part due to the time I spent under his guidance. Davide may not be aware of this but he has also been, along with Dr. Maria Barna, a great example that a relationship between two successful scientists cannot only survive the pressures of the scientific world but also help to drive each individual to even greater success. In that regard, I must add that it has been an immense pleasure getting to work with Dr. Maria Barna, a tremendous scientist who has been invaluable in helping to shape and direct my graduate project over the years.

Although your graduate advisor is your primary scientific mentor, if you're in the right environment, just as much of your mentoring comes from the people you are surrounded by in the lab, and I have been fortunate enough to be surrounded by a fantastic group of people in the Ruggero lab. They are all scientists of the highest caliber and have been my scientific sounding board throughout my graduate career. In particular I would like to acknowledge, Tom Cunningham and Craig Stumpf, who have always taken time out from their own scientific endeavors to give me feedback and guidance. In addition, I am grateful for the opportunities I have had to collaborate with Andrew Hsieh, Michael Pourdehnad, and Crystal Conn, each of whom has been incredibly rewarding to work with. Finally, I would like to thank the entire Ruggero lab, but in particular Adrian Contreras and Mary McMahon, for making the lab a fun place to be- there is no better cure than laughter for a failed experiment or generally crappy lab day.

Graduate school has been a long and trying process, but as my original graduate advisor, Doug Hanahan, once told me- struggle is an inevitable part of doing science and it is important to learn how to deal with and overcome adversities if one wishes to become a successful scientist. Although the time I got to work with Doug was limited, I have the deepest respect for him as both a scientist and a mentor. He has steered an ever increasing and impressive list of people towards their own successful careers. I was very fortunate to work closely with one of those scientists, Dr. Neta Erez, a terrific colleague and an even better friend. She is an amazingly strong woman, who juggled a successful science career while basically single-handedly raising two beautiful children. I hope that one day I can be even half as efficient as she is and more importantly that I can always count her as one of my cherished friends.

I must also thank the members of my thesis committee, Dr. William Weiss and Dr. Kevan Shokat, who have given me excellent feedback and scientific support over the years but must be somewhat relieved that I am finally graduating. I should also acknowledge the wonderful support crew that the BMS program has provided us, in particular Lisa Magargal and Monique Piazza who have been there for most of my graduate career to answer any question I may have and help fix any issue that arises.

Although most of my time in graduate school may have been spent in the lab, some of the most memorable and important moments of the past years have occurred nowhere near a pipette. Indeed, I have always believed that in order to do your best science, sometimes you need to walk away from the bench and clear your head, and I have had a great group of friends in town to help me do just that. Whether skiing or backpacking with Kelley and Roko Kruze, surfing with David DeNardo, kayaking with my old roommate Ekuike Falorca, drinking great wine and beer with Dan Diephouse, venting to my classmate Michelle (Tofty) Graham, hanging out with my old friends from Medarex, or playing card games with Ali’s classmates, I have had an amazing support network outside of the lab that has helped to keep me grounded and motivated.

I really must also thank my parents, Anne and Barry Truitt. In more ways than one, I wouldn't be here without them. They have been excellent role models and fantastic parents. By exposing me to the natural beauty of the landscape where I grew up on the Eastern Shore of Virginia, they helped instill a scientific curiosity in me from an early age. They've also helped to nurture that curiosity throughout the years, supporting me in college and putting up with my prolonged graduate career on the opposite side of the country. I truly believe I get some of my best scientific attributes from them: my work ethic and persistence from my mom and my analytical and inquisitive nature from my dad. I hope that when I start my own family, which they are eagerly anticipating, I can live up to the example they have provided in raising me.

Finally, I would like to thank my wife Alison Coady. Although I met her prior to this, the first time we really talked was at a New Year's party. For two hours straight, while ignoring everyone else around us, I had one of the best conversations of my life. We've been together for seven years now and thankfully she's still interested in talking to me. She is a great scientist in her own right and has just finished her PhD studies. It's been amazing watching her grow as a scientist, while simultaneously helping me to grow both as a scientist and as a human being. I'm excited for the next steps of our careers and lives together and I can honestly say that I couldn't ask for a more supportive, caring, and loving partner.

Contributions

The Abstract, Chapter 2, and Chapter 4 are in part taken from a manuscript published in the *Proceedings of the National Academy of Sciences of the United States of America*. M. Pourdehnad and M.L. Truitt contributed equally to this work. M. Pourdehnad and M.L. Truitt designed and performed research, analyzed data, and wrote the manuscript. I.N. Siddiqi performed research, contributed new reagents/analytic tools, and analyzed the data. G.S. Ducker contributed new reagents/analytic tools. KM Shokat contributed new reagents/analytic tools and analyzed the data. D. Ruggero designed research, analyzed data, and wrote the manuscript.

> Pourdehnad M[1], Truitt ML[1], Siddiqi IN, Ducker GS, Shokat KM, Ruggero D. 2013. Myc and mTOR converge on a common node in protein synthesis control that confers synthetic lethality in Myc-driven cancers. *Proc Natl Acad Sci U S A*.

Chapter 1 is adapted from a review I co-authored with A.C. Hsieh and D. Ruggero published in the *British Journal of Cancer*.

> Hsieh AC, Truitt ML, Ruggero D. 2011. Oncogenic AKTivation of translation as a therapeutic target. *Br J Cancer* **105**: 329–36.

The Abstract, Chapter 3, and Chapter 4 are in part taken from a manuscript currently submitted for publication entitled “eIF4E dose is critical for the oncogenic translation program but not mammalian development and protein synthesis”. M.L. Truitt designed and performed research, analyzed data, and wrote the manuscript. C.S. Conn designed and performed research and analyzed data. Z. Shi analyzed data. X. pang designed new reagents. T. Tokuyasu analyzed data. M. Barna designed and performed research, analyzed data, and wrote the manuscript. D. Ruggero designed research, analyzed data, and wrote the manuscript.

> Truitt, ML, Conn CS, Shi Z, Pang X, Tokuyasu T, Barna M, Ruggero D. eIF4E dose is critical for the oncogenic translation program but not mammalian development and protein synthesis. (In submission).

Abstract

Although it was first observed nearly a century ago that transformed cells are marked by enlarged nucleoli, where ribosomal RNA synthesis and ribosome assembly occur, it has only recently become clear that deregulated protein synthesis plays a causal role in the development and progression of cancer. Indeed, aberrant mRNA translation has emerged as a hallmark of oncogenic transformation, underlying many cellular functions critical for tumorigenesis. Oncogenic signaling has been shown to enhance and alter the protein synthesis capacity of cancer cells to directly contribute to their survival, proliferation, metastasis, and genome instability. Therefore, inhibiting enhanced protein synthesis may represent a highly relevant strategy for the treatment of human cancers. For example, *Myc* is one of the most commonly deregulated oncogenes in human cancer, yet therapies directly targeting Myc hyperactivation are not presently available in the clinic. Although the ability to modulate protein synthesis control is critical to the Myc oncogenic program, components of the translation machinery that can be exploited as therapeutic targets for Myc-driven cancers remain poorly defined. Recently, the translation initiation factor eIF4E, which is considered the quantitatively rate limiting factor for translation initiation, has become a central focus for therapeutic approaches seeking to inhibit oncogenic activation of translation. Despite this, the requirements for eIF4E in normal mammalian development and physiology are largely unknown. Moreover, we still do not understand the specific roles that eIF4E plays in translating the genome of both normal and cancer cells.

Here, we uncover a surprising and important functional link between Myc and mammalian target of rapamycin (mTOR)-dependent phosphorylation of eukaryotic translation initiation factor 4E binding protein-1 (4EBP1), a master regulator of eIF4E-dependent protein synthesis control. Using a pharmacogenetic approach, we find that mTOR-dependent phosphorylation of 4EBP1 is required for cancer cell survival in Myc-dependent tumor initiation and maintenance. We further show that a clinical mTOR active site inhibitor, which is capable of blocking mTOR-dependent

4EBP1 phosphorylation, has remarkable therapeutic efficacy in Myc-driven hematological cancers. Moreover, we demonstrate the clinical implications of these results by delineating a significant link between Myc, mTOR-dependent phosphorylation of 4EBP1, and therapeutic response in human lymphomas. Together, these findings identify an important mTOR substrate hyperactivated downstream of Myc oncogenic activity, which promotes tumor cell survival and confers synthetic lethality, thereby revealing a unique therapeutic approach to render Myc druggable in the clinic.

Additionally, we have generated a novel *Eif4e* haploinsufficient mouse, allowing the requirements for eIF4E dose to be defined at the organismal level for the first time. Surprisingly, we find that a 50% reduction in eIF4E is compatible with normal development and global protein synthesis. Strikingly, however, *Eif4e*$^{+/-}$ cells and mice are remarkably resistant to oncogenic transformation. Unbiased genome-wide translational profiling of mRNAs induced by oncogenic transformation reveals eIF4E dosage is critical for translating key mRNA networks, including redox balance, signaling, and proteasome control, which are demarcated by a novel 5'UTR signature. In particular, eIF4E dose is essential for translating a novel class of mRNAs regulating reactive oxygen species (ROS), a hallmark of oncogene-induced stress. Translational control of intracellular ROS fuels cancer cell survival and underlies *Eif4e*$^{+/-}$ resistance to cellular transformation. Therefore, mammalian cells have evolved surplus eIF4E levels that are usurped by cancer cells to drive a translational program supporting tumor growth and survival.

Table of Contents

List of Figures

Chapter Figures

Supplementary Figures

List of Tables

List of Appendices

Chapter 1: Introduction

Protein synthesis is one of the most costly and tightly regulated energetic investments in the cell. It is controlled through regulation of the multistep process of mRNA translation at every stage from ribosome biogenesis to translation initiation and elongation. Importantly, protein synthesis control impinges on multiple cellular processes frequently altered in cancer, such as proliferation, cell growth, survival, and angiogenesis. In line with this, recent studies have highlighted the ability of oncogenic signaling pathways to drive cellular transformation by altering gene expression at the translational level. Oncogenic signaling can lead to both global changes in protein synthesis as well as specific changes in the translation of select mRNAs. Newly developed genetic and pharmacological tools, along with emerging technologies, are significantly advancing our ability to identify and functionally group these translationally controlled mRNAs into gene networks based on their modes of regulation. How oncogenic signaling activates distinct stages of protein synthesis to regulate these translational networks is an ongoing area of research. Importantly, the translation initiation factor eIF4E has emerged as a common node hyperactivated downstream of multiple oncogenic signaling pathways and the majority of therapeutics currently targeting translational control are focused on blocking translation initiation through inhibition of eIF4E hyperactivity. Although the specific requirements for eIF4E for normal mammalian development and tissue function still need to be fully explored, these therapeutic strategies for inhibiting eIF4E may offer novel and effective approaches for targeting cancers driven by oncogenes typically considered undruggable.

mRNA translation in cancer: deregulated at every step

Protein synthesis is regulated through the phosphorylation of multiple downstream targets that function together to control all stages of mRNA translation from ribosome biogenesis to translation initiation and elongation. Importantly, ribosome biogenesis, translation initiation, and translation elongation are all frequently deregulated in cancer, and oncogenic signaling pathways, including

Ras, PI3K, Akt, and various growth factor receptors, drive tumor development and progression in part through their ability to coordinately activate these various steps of the translational process (Figure 1.1).

Oncogenic signaling activates translation initiation

One of the most rapid ways that oncogenic signaling enhances protein synthesis is through the activation of translation initiation. Translation initiation is the process by which ribosomes are recruited to the 5′ untranslated region (5′ UTR) of mature mRNAs in the first step of protein synthesis. In this process, 40S ribosomal subunits are recruited to the 7-methyl guanosine cap (5′ cap) of mRNAs by the eIF4F translation initiation complex through interactions with eukaryotic initiation factor 3 (eIF3) (Emanuilov et al., 1978). eIF4F is a trimeric complex that resides at the cap. It is composed of the 5′ cap mRNA-binding protein eIF4E, the RNA helicase eIF4A, and the scaffolding molecule eIF4G (Haghighat and Sonenberg, 1997; Rogers et al., 1999). The majority of mRNA translation begins through eIF4F association with the cap and is known as cap-dependent translation. Translation initiation is considered the key regulatory step of cap-dependent translation and eIF4E is thought to be the rate-limiting factor in controlling this step (Duncan et al., 1987). This thought is based largely on the fact that eIF4E activity is highly regulated at both the mRNA and protein level. eIF4E is upregulated at the mRNA level by a number of transcription factors including the oncogene MYC (Jones et al., 1996). At the protein level, eIF4E activity is controlled through an activating phosphorylation at serine 209, as well as through inhibitory interactions with the eIF4E-binding proteins (4EBPs) (Gingras et al., 1998; Topisirovic et al., 2004). This tight regulation of eIF4E activity provides a rapid mechanism for cells to modulate translation initiation in response to numerous stimuli, including growth factor and oncogenic signaling.

Many oncogenic signaling pathways, including Ras and AKT, control translation initiation in large part through activation of the kinase mammalian target of rapamycin complex 1

(mTORC1). mTORC1 is responsible for phosphorylating ribosomal protein (RP) S6 kinase 1/2 (S6K1/2) and the 4EBPs (Brown et al., 1995; Gingras et al., 1998; von Manteuffel et al., 1997). The 4EBPs are a family of small proteins (4EBP1–3) that compete with eIF4G for binding to the dorsal surface of eIF4E. In a hypophosphorylated state, 4EBPs prevent the formation of the eIF4F complex on the 5′ UTR of mRNAs by binding to eIF4E and preventing eIF4G recruitment (Figure 1.2). However, upon growth factor stimulation, 4EBPs are phosphorylated at multiple serine/threonine residues in a series initiated by mTORC1 (Gingras et al., 1999a; Gingras et al., 2001a). This leads to a conformational change that releases 4EBPs from eIF4E and allows eIF4G to bind eIF4E and ultimately recruit the 40S ribosomal subunit to the 5′ end of mRNAs. As a result, eIF4E regulates global protein synthesis by controlling the rate that ribosomes are able to dock onto the 5′ cap of mRNAs.

In addition to global increases in protein synthesis, eIF4E hyperactivation is able to enhance the translation of select mRNAs (Mamane et al., 2007). The 5′ UTR of these mRNAs are believed to be the regulatory factors that impart this selectivity. 5′ UTRs can vary in length and GC nucleotide content, resulting in a range of secondary mRNA structures. These structures are thought to function as physical barriers that limit the ability of the 40S ribosome to reach the translation start site (Manzella and Blackshear, 1990). As such, mRNAs with complex 5′ UTRs have low basal rates of translation and are exquisitely sensitive to eIF4E hyperactivation due to the ability of eIF4E to recruit the eIF4A helicase. eIF4A recruitment allows for enhanced unwinding of secondary structures in the 5′ UTR, resulting in improved translation initiation efficiency. Genes that are sensitive to eIF4E-mediated translation cover a range of cellular functions, including cell cycle control (cyclin D1), angiogenesis (VEGF), metabolism (ODC), and apoptosis (survivin and Mcl-1) among others (Graff et al., 2007; Mamane et al., 2007; Mills et al., 2008; Rousseau et al., 1996).

Despite the identification of mRNA targets that rely on the eIF4F complex for efficient translation (see above), several unbiased screens have also identified transcripts that lack

complex 5′ UTRs, but are sensitive to eIF4E hyperactivation (Hsieh et al., 2012; Larsson et al., 2006; Mamane et al., 2007). One such class of genes is the 5′ TOP genes. 5′ TOP genes (terminal oligopyrimidine or tract of oligopyrimidine genes) are characterized by oligopyrimidine repeats in the 5′ UTR and predominantly encode for RPs, translation initiation factors, and translation elongation factors (Avni et al., 1997; Avni et al., 1994; Levy et al., 1991). While it is still unknown precisely how hyperactivated eIF4E regulates the translation of 5′ TOP genes, the fact that these genes do not possess complex 5′ UTRs suggests that there are other mechanisms of translational regulation downstream of eIF4E that have not been described.

Oncogenic signaling promotes translation elongation

Although significant attention has been focused on the ability of oncogenic signaling pathways to regulate translation initiation, evidence suggests that other steps of translation, such as translation elongation, are also regulated downstream of oncogenic signaling. Translation elongation is the process by which amino acid-charged tRNAs dock onto the ribosome/mRNA complex and incorporate amino acids into the growing nascent polypeptide chain. Multiple elongation factors are necessary to carry out this process efficiently. The eukaryotic translation elongation factor 2 (eEF2) mediates the translocation step of elongation, where tRNAs move between the P and A site on the ribosome as the ribosome migrates by one codon along the mRNA. One way oncogenic signaling can promote this elongation step is through mTOR by S6K1/2-dependent inhibition of eEF2 kinase, a negative regulator of eEF2 (Wang et al., 2001). Thus, oncogenic lesions not only affect translation initiation but also the efficiency of actively translating ribosomes. In addition, there is evidence that oncogenic signaling may more broadly impact translation elongation through the preferential translation of 5′ TOP genes (see above), many of which encode for translation elongation factors (Avni et al., 1997; Mamane et al., 2007). While many mechanistic gaps still exist, it will be important to understand the degree to which oncogenic activation of translation elongation enhances protein synthesis. Furthermore, it needs to be better

established how the ability to modulate translation elongation can directly contribute to tumorigenesis, either through increases in global protein synthesis or through preferential translation of selects mRNAs.

Oncogenic control of ribosome biogenesis

Protein synthesis depends on the generation of properly assembled, mature ribosomes. The biogenesis of mature ribosomes involves the synthesis and processing of rRNA, the synthesis of RPs, and the proper assembly of all these components within the nucleolus. Many oncogenic signaling pathways have been shown to modulate aspects of these processes, but perhaps the most well characterized and best example comes from the Myc oncogene. In addition to directly controlling the transcription of various translation factors, such as eIF4E, Myc is a potent activator of ribosome biogenesis through direct transcriptional control of ribosomal proteins, rRNA, and numerous factors responsible for the synthesis, processing, and assembly of the ribosome (Ruggero, 2009). In fact, protein synthesis control represents an evolutionarily conserved function of Myc and comprises one of the largest functional gene classes regulated by Myc (Dang et al., 2006). Another way oncogenic signaling can promote ribosome biogenesis is through mTOR. For example, mTOR enhances the transcription of rDNA through activation of transcription initiation factor 1A (TIF-1A), a RNA polymerase I (Pol I) transcription factor. Through an indirect mechanism, mTOR simultaneously promotes an activating phosphorylation and blocks an inhibitory phosphorylation of TIF-1A to enhance rRNA synthesis (Mayer et al., 2004). mTOR can also promote rRNA synthesis through activation of another Pol I transcription factor, upstream binding factor (UBF). Although the precise mechanism behind mTOR-dependent UBF activation has not been identified, S6K1 is thought to be required for UBF activation (Hannan et al., 2003). In addition, it has been demonstrated in yeast that RP synthesis can be positively regulated by mTOR. In this setting, mTOR promotes the transcription of RP genes by indirectly activating transcription factors such as FHL1 (Martin et al., 2004).

Despite evidence that oncogenic signaling can regulate ribosomal biogenesis through modulation of RP synthesis, rRNA synthesis and processing, and ribosome assembly, the connection between ribosomal biogenesis and protein synthesis remains poorly defined. While studies have shown that normal ribosomal biogenesis is in fact required for protein synthesis, it is not clear if enhanced ribosomal biogenesis is sufficient to drive increased protein synthesis downstream of oncogenic signaling.

IRES-mediated translation

Another mechanism of initiating translation is internal ribosome entry site (IRES)-mediated translation. IRES elements are mRNA secondary structures predominantly located within the 5′ UTR (and to a lesser extent in the coding sequence and intronic regions of mRNA) that can associate with IRES *trans*-acting factors (ITAFs) to initiate translation in a 5′ cap and eIF4E-independent manner. Only a subset of mRNAs contains IRES sequences. Thus, IRES-mediated translation is thought to be a fine-tuning mechanism that controls the translation of key mRNAs under specific physiological conditions such as the G0/quiescent and G2/M phases of the cell cycle, where it modulates proliferation, as well as under specific stress conditions such as hypoxia, where it promotes cell survival and angiogenesis (Braunstein et al., 2007; Kullmann et al., 2002; Miskimins et al., 2001; Pyronnet et al., 2000). Importantly, IRES-mediated translation has been shown to have a role in cancer. One example for this is in the setting of hypoxia in invasive breast cancer, where it has been demonstrated in a mouse model that eIF4E-mediated translation is downregulated through increased expression of 4EBP1 under hypoxic conditions. Despite a resulting decrease in overall protein synthesis levels, specific IRES containing mRNAs such as VEGF, HIF-1α, and Bcl-2 are translated at higher rates, thereby increasing the protein levels of these protumorigenic targets (Braunstein et al., 2007). In this manner, IRES-mediated translation may enhance tumor cell survival under specific cellular conditions.

Coordinate translational control

Oncogenic signaling functions as a critical regulator of mRNA translation, coordinating everything from ribosome biogenesis to translation initiation and elongation, to drive increased cellular protein synthesis. Despite strong evidence that oncogenic signaling can regulate ribosome biogenesis, translation initiation, and translation elongation, we still do not understand the relative role that these events play in driving both global and specific changes in protein synthesis. Further studies are needed to determine the extent to which activation of these translational steps, either alone or in combination, is sufficient to drive protein synthesis. In addition, it will be important to understand the requirement for activation of each of these translational stages in tumors driven by different oncogenic lesions. Moreover, it remains an outstanding question to what extent translation cooperates with other key downstream targets of oncogenic signaling, such as transcription, to regulate critical cellular events that promote tumorigenesis and cancer progression.

eIF4E: a critical mediator of oncogenic translation

Despite a wealth of knowledge on genetic mutations in pathways upstream of key steps of translation control and a growing appreciation for the ability of oncogenic signaling pathways to coordinately regulate mRNA translation, the extent to which deregulated translational control functions as an oncogenic driver remains largely undefined. Recent studies have, however, highlighted a critical requirement for enhanced translation initiation downstream of oncogenic signaling. Strikingly, many oncogenic signaling pathways seems to enhance translation initiation largely through hyperactivation of the eIF4E translation initiation factor, which is a bona-fide oncogene.

The oncogenic potential of eIF4E has been well described both *in vitro* and *in vivo*. Overexpression of eIF4E is sufficient to induce transformation of fibroblasts and primary epithelial cells in culture, and eIF4E overexpression in mice leads to increased cancer susceptibility in a

range of tissues (Avdulov et al., 2004; Lazaris-Karatzas et al., 1990; Ruggero et al., 2004). While these findings, along with evidence of eIF4E overexpression in human cancers (Flowers et al., 2009; Graff et al., 2009; Wang et al., 2009), support the notion that eIF4E is oncogenic, a direct connection between eIF4E and translational deregulation downstream of oncogenic signaling has only recently been described. Some of the first evidence for such a connection came from a study showing that pharmacological inhibition of oncogenic RAS and AKT in glioblastoma cells caused a rapid and profound change in mRNA translation that far outweighed transcriptional changes and was associated with loss of mTORC1-dependent phosphorylation of 4EBPs (Rajasekhar et al., 2003). This study identified translational regulation of several mRNA targets important for cancer development, and suggested that altered translational control downstream of eIF4E hyperactivation may be required for cellular transformation.

Previously, our group demonstrated *in vivo* that hyperactivation of eIF4E is necessary for AKT-mediated tumorigenesis. Using a T-cell lymphoma model driven by overexpression of constitutively active AKT, we showed that enhanced protein synthesis through eIF4E hyperactivation was required for AKT-mediated tumorigenesis. We found that AKT overexpressing pretumor progenitor T cells possessed a distinct survival advantage, which was abrogated when eIF4E hyperactivity was restored to wild-type levels. Using a candidate gene approach, we found that this survival advantage was due in part to translational upregulation of the antiapoptotic Mcl-1. Importantly, we were also able to pharmacologically inhibit eIF4E hyperactivity downstream of oncogenic AKT, which resulted in significant inhibition of tumor growth (see below) (Hsieh et al., 2010). As such, we identified the 4EBP/eIF4E axis as a druggable target that regulates translation downstream of oncogenic AKT.

The requirement for eIF4E hyperactivity in tumors has been further substantiated by more recent studies. For example, it was found that the efficacy of an AKT inhibitor in human cancer cell lines correlated with its ability to inhibit phosphorylation of 4EBPs and block cap-dependent translation. This study showed that in cell lines where AKT inhibition failed to block

phosphorylation of 4EBPs, the MAPK signaling pathway was frequently activated. The authors further demonstrated that combined pharmacological inhibition of AKT and MAPK signaling was able to inhibit phosphorylation of 4EBPs and prevent the *in vivo* growth of cell lines resistant to AKT inhibition alone. Importantly, the authors were able to attribute this combinatorial drug effect directly to the inhibition of eIF4E hyperactivity, as the overexpression of a non-phosphorylatable form of 4EBP1 was sufficient to block the growth of these cells in xenografts (She et al., 2010). In a separate study, the resistance of BRAF mutant melanomas to BRAF and MEK inhibitors has been attributed to sustained eIF4F activity. Interestingly this work uncovered multiple mechanisms of therapeutic resistance that all converged on eIF4E hyperactivation, including ERK-independent phosphorylation of 4EBP (Boussemart et al., 2014). In line with this, the authors found that inhibition of the eIF4F complex, for example by blocking eIF4E-eIF4G interaction, potently synergized with BRAF inhibitors to promote tumor cell death.

In addition to 4EBP-dependent control, eIF4E activity is positively regulated through phosphorylation at serine 209 by the MAP kinase targets MNK1/2. Whole body expression of a knock-in mutant of eIF4E, which can no longer be phosphorylated at this residue, was found to decrease the incidence and grade of prostatic intraepithelial neoplasia in a mouse prostate cancer model driven by PTEN loss (Furic et al., 2010). While this study supports a role for eIF4E hyperactivation downstream of oncogenic AKT signaling, it raises several questions: Do all tissues rely on phosphorylation of serine 209 for hyperactivation of eIF4E downstream of oncogenic AKT signaling? More broadly, what is the tissue-specific dependence of eIF4E hyperactivation, which could be achieved by different mechanisms, downstream of other oncogenic signaling pathways? Indeed, there is convincing genetic evidence that oncogenic eIF4E alone is sufficient to drive tumorigenesis in specific tissues. Transgenic mice that ubiquitously overexpress eIF4E show that distinct tissues, including the lungs, liver, and the lymphoid compartment, are more prone to oncogenic transformation (Ruggero et al., 2004). As such, we can speculate that there may be tissue-specific requirements for eIF4E oncogenic

activity in the development of tumors from distinct histological origins. Although many important questions remain to be addressed, the above studies suggest that eIF4E hyperactivation serves as a critical node on which multiple oncogenic signaling pathways converge, thus representing an attractive therapeutic target.

Therapeutic approaches for targeting eIF4E

Antisense targeting of eIF4E – eIF4E ASO

eIF4E is a bona-fide oncogene frequently hyperactivated downstream of numerous oncogenic signaling pathways, and thus represents an attractive target for rational drug design. There are currently several approaches being pursued to therapeutically inhibit eIF4E, but perhaps the most direct of these approaches is the use of specific antisense oligonucleotides (ASOs) that bind to eIF4E mRNA and mediate its destruction by RNase H. Nanomolar concentrations of eIF4E ASOs have been shown to decrease eIF4E protein levels in several human cancer cell lines *in vitro*, reducing protein levels of known eIF4E targets and inducing apoptosis. In tumor xenograft models, eIF4E ASOs inhibited tumor growth without any detectable changes in body weight or liver function. Strikingly, control mice treated with eIF4E ASOs for 3 weeks showed no signs of toxicity, despite reductions in eIF4E protein levels by up to 80% in the liver, implying a critical difference in the requirement of eIF4E for normal physiological function (Graff et al., 2007). These studies suggest that tumors may be sensitive to eIF4E inhibition while normal tissues are not, but for what duration and to what extent eIF4E can be inhibited system-wide without detriment remains an open question.

eIF4E–eIF4G interaction inhibitor – 4EGI-1

Additional attempts to target eIF4E have focused on blocking its ability to interact with eIF4G. The interaction between eIF4E and eIF4G is dependent on an eIF4G $Y(X)_4L\Phi$ motif, where X is

variable and Φ is hydrophobic (Altmann et al., 1997). High-throughput screens for inhibitors that could prevent eIF4E binding to the $Y(X)_4LΦ$motif identified 4EGI-1 as a candidate compound. 4EGI-1 was able to inhibit eIF4F complex formation at micromolar concentrations. Surprisingly, 4EGI-1 did not block the ability of eIF4E to bind to 4EBP1, which, similar to eIF4G, contains a $Y(X)_4LΦ$ motif. 4EGI-1 was shown to be cytostatic and cytotoxic in multiple cell lines and preferentially blocked the growth of transformed cells over untransformed cells (Moerke et al., 2007). Recently, it has been reported that 4EGI-1 functions through an eIF4G/eIF4E-independent mechanism to promote apoptosis in human lung cancer cells (Fan et al., 2010). Additionally, 4EGI-1 has been shown to suppress translation in primary human cells at concentrations below those required for eIF4E inhibition (McMahon et al., 2011). Collectively, these studies suggest that 4EGI-1 may have antitumor efficacy through more general inhibition of oncogenic pathways and that the full spectrum of protein–protein interactions and pathways that 4EGI-1 blocks still needs to be determined. Despite these concerns, specifically targeting the eIF4E/eIF4G protein–protein interaction is an attractive therapeutic approach, and subsequent generations of such inhibitors may provide a novel and important way of targeting eIF4E in human cancers.

Targeting the eIF4E-5′ cap interaction – Ribavirin

eIF4E function can also be directly inhibited by blocking its ability to interact with the 5′ cap of mRNAs. Ribavirin, a guanosine ribonucleoside currently used as an anti-viral therapy, has recently been shown to compete with endogenous mRNAs for binding to eIF4E, leading to decreased eIF4F complex formation *in vitro*. In line with this, ribavirin blocked eIF4E-mediated oncogenic transformation *in vitro* and demonstrated *in vivo* efficacy in preclinical models of acute myelogenous leukaemia (AML) and squamous cell carcinoma (Kentsis et al., 2004). In a phase I dose-escalation trial with ribavirin, 7 out of 11 AML patients were reported to have at least partial responses or stable disease (Assouline et al., 2009). Although ribavirin may ultimately prove to have clinical efficacy in human cancers, the specific function of ribavirin as a cap-mimetic has

been called into question by two independent groups (Westman et al., 2005; Yan et al., 2005). Therefore, it is not clear if the inhibition of cap-dependent translation underlies ribavirin's therapeutic efficacy.

Inhibition of eIF4E phosphorylation – MNK kinase inhibitors

The MNK kinases are activated downstream of MAP kinase signaling and directly phosphorylate eIF4E at serine 209 (Scheper et al., 2001). Mutation of eIF4E at this residue blocks its transforming potential *in vitro* and can inhibit PTEN-driven tumorigenesis *in vivo (Furic et al., 2010)*. Furthermore, mice doubly deficient for MNK1 and MNK2 are resistant to lymphomagenesis driven by PTEN loss, validating the MNKs as potential therapeutic targets upstream of eIF4E (Ueda et al., 2010). Recently, a high-throughput screen identified the antifungal cercosporamide as a potent inhibitor of MNK1 and MNK2 with limited activity towards other kinases. Cercosporamide was able to block eIF4E phoshorylation *in vivo* and inhibit the growth of human xenografts as well as the metastasis of mouse melanoma cells (Konicek et al., 2011). Although these results are promising and suggest that targeted inhibition of eIF4E phosphorylation may be a valid therapeutic approach, it remains unclear to what extent the efficacy of MNK kinase inhibitors can be attributed to their ability to block other downstream phosphorylation targets critical for tumor growth and maintenance. Regardless, the observation that both MNK kinase activity and eIF4E phosphorylation are dispensable for normal growth and development, but are required for tumorigenesis, makes the MNK kinases attractive therapeutic targets.

mTOR ATP active-site inhibitors

Perhaps one of the most promising approaches to therapeutically block eIF4E hyperactivity is the targeted inhibition of the mTOR kinase. First-generation allosteric mTOR inhibitors such as rapamycin, RAD001, and CCI-779 inconsistently inhibit phosphorylation of 4EBP1 downstream of mTORC1, despite potently inhibiting S6K phosphorylation (Choo et al., 2008; Hsieh et al., 2010). This suggests that phosphorylation of S6K or its downstream target rpS6 may not serve

as an accurate readout for inhibition of all mTORC1 kinase activity. Indeed, the poor clinical performance of rapamycin and its associated analogues in human cancer is most likely due to their inability to block mTORC1-dependent phosphorylation of 4EBPs and thus fully inhibit eIF4E activation (see above). In order to overcome the incomplete inhibition seen with allosteric mTOR inhibitors, our group and several others have identified mTOR ATP active-site inhibitors, such as PP242 and Torin1 (Feldman et al., 2009; Thoreen et al., 2009). These compounds reversibly compete with ATP for binding to the mTOR catalytic domain and thus block not only mTORC1 activity, but also mTORC2 activity. mTORC2, an mTOR complex distinct from mTORC1, is responsible for an activating phosphorylation of AKT at Serine 473. Using PP242, our group was the first to demonstrate that these ATP active-site inhibitors effectively inhibit phosphorylation of the 4EBPs, the S6Ks, and AKT. This is in striking contrast to rapamycin, which predominantly blocks the phosphorylation of S6Ks and infrequently blocks the phosphorylation of 4EBPs. As a result, PP242 inhibits the proliferation of cultured cell lines to a much greater extent than rapamycin. Furthermore, our group has shown that PP242 dramatically inhibits tumor growth in an AKT-driven mouse model of lymphoma that is inherently resistant to rapamycin. Strikingly, tumors from the same model that overexpressed a mutated non-phosphorylatable 4EBP1 transgene were completely insensitive to PP242 inhibition, suggesting that PP242 efficacy may be entirely due to its ability to block mTORC1-dependent 4EBP phosphorylation (Hsieh et al., 2010). In line with this, PP242 and Torin1 both retain their antiproliferative effects in mouse embryonic fibroblasts, in which the mTORC2 complex has been destabilized (Feldman et al., 2009; Thoreen et al., 2009). Moreover, our group has recently shown that a clinically relevant ATP site inhibitor of mTOR, MLN0128 (formerly INK128), can significantly block the *in vivo* metastasis of prostate cancer cells by inhibiting eIF4E-dependent translation of a pro-invasive gene network (Hsieh et al., 2012). Although these studies suggest that the antitumor effect of mTOR ATP active-site inhibitors is predominantly mediated by blocking phosphorylation of 4EBPs

and eIF4E hyperactivity, they cannot generally rule out a role for the inhibition of other translational regulators downstream of mTORC1.

Figures

Figure 1.1. Oncogenic signaling coordinately regulates translation. mRNA translation is activated downstream of various cellular and oncogenic signaling pathways, such as growth factor receptor signaling, to promote every stage of protein synthesis from ribosome biogenesis to translation initiation and elongation. Protein synthesis requires a full repertoire of mature ribosomes, and oncogenic signaling has been shown to promote ribosome biogenesis through both enhanced rRNA synthesis and enhanced ribosomal protein production. In addition, oncogenic signaling promotes protein synthesis through the activation of translation initiation factors that drive cap-dependent translation. This is one of the most rapid mechanisms by which oncogenic signaling can regulate protein synthesis, and it occurs in part through mTORC1-dependent hyperactivation of eIF4E. Furthermore, oncogenic signaling has been shown to affect the efficiency of translation through the control of translation elongation factors. Translation can also be regulated through additional mechanisms, such as IRES-mediated translation, to promote the expression of specific protumorigenic mRNAs. Through regulation of the multiple stages of translation, oncogenic signaling can drive both global changes in protein synthesis as well as selective changes in the translation of specific mRNAs.

Figure 1.2. Oncogenic hyperactivation of eIF4E. Oncogenic signaling can promote translation initiation through mTORC1-dependent hyperactivation of eIF4E. In the absence of signaling, hypophosphorylated 4EBP binds to and inhibits eIF4E, blocking its ability to interact with eIF4G. Oncogenic signaling through AKT activates mTORC1, initiating a series of phosphorylations that release 4EBP from eIF4E. This allows for eIF4G binding to eIF4E and the subsequent recruitment

of the 40S ribosomal subunit. In addition, it has been shown that Ras/MAP kinase signaling can promote eIF4E hyperactivation through downstream phosphorylation of eIF4E at Serine 209, and Myc can directly regulate eIF4E at the transcriptional level.

Figure 1.1

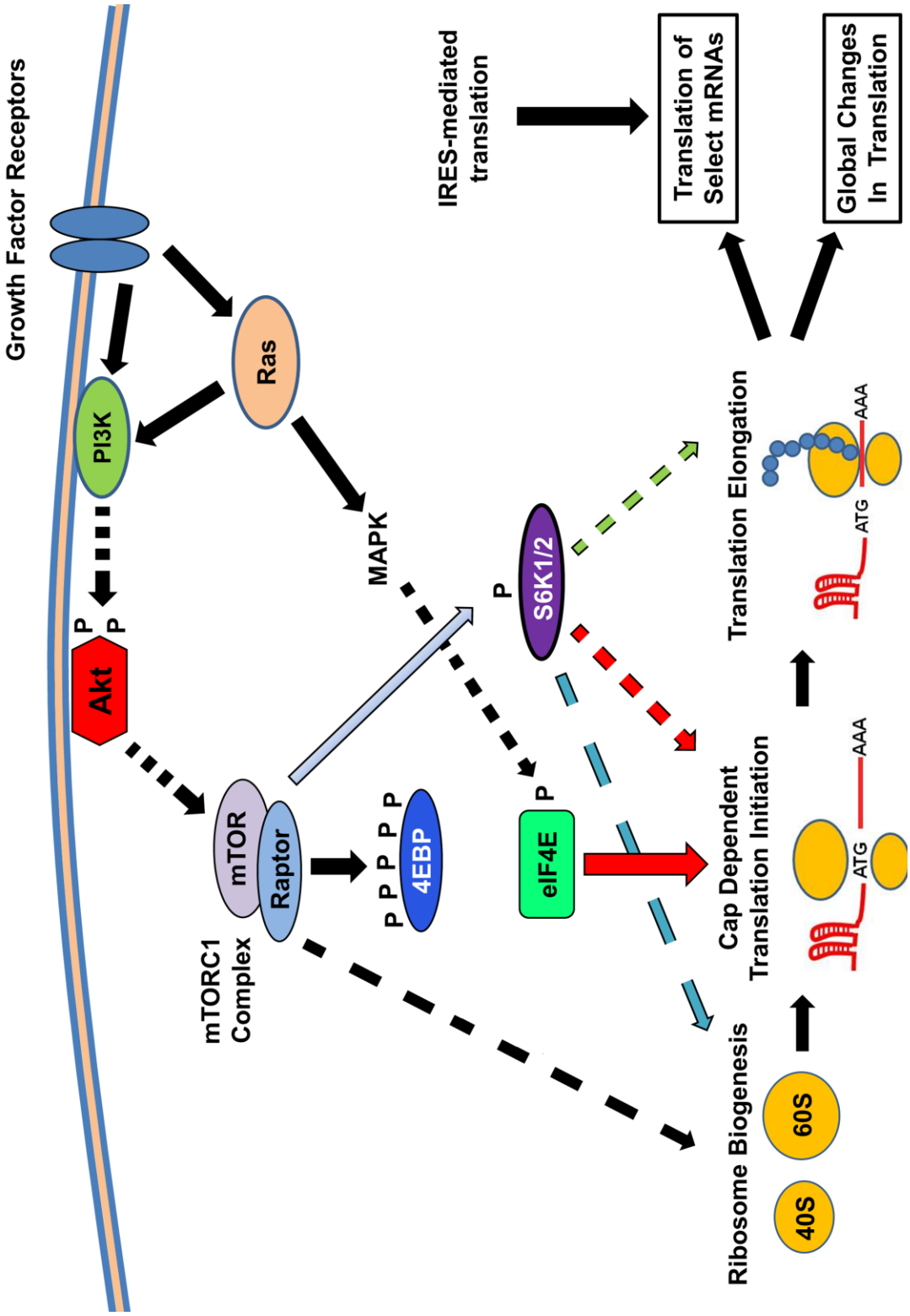
Growth Factor Receptors
PI3K
Ras
Akt
P
P
MAPK
mTOR
Raptor
mTORC1
Complex
P P P P
4EBP
P
S6K1/2
P
eIF4E
IRES-mediated
translation
Translation of
Select mRNAs
Global Changes
In Translation
Translation Elongation
AAA
ATG
Cap Dependent
Translation Initiation
AAA
ATG
Ribosome Biogenesis
60S
40S

Figure 1.2

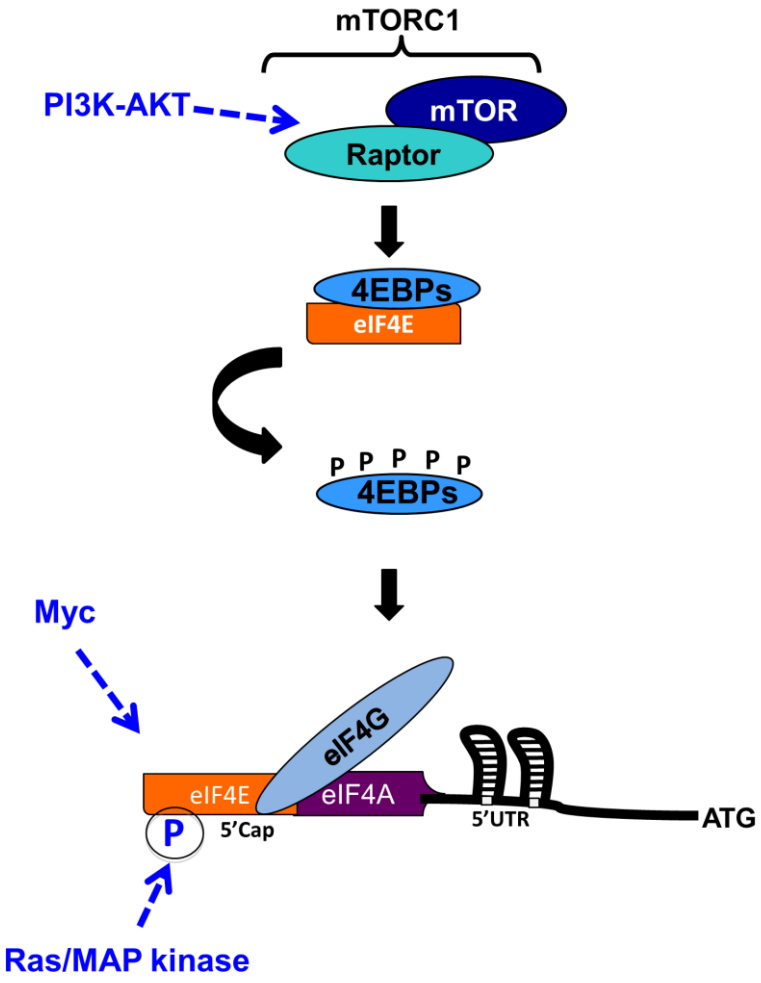
mTORC1
PI3K-AKT
mTOR
Raptor
4EBPs
eIF4E
P P P P P
4EBPs
Myc
eIF4G
eIF4E
eIF4A
P
5'Cap
5'UTR
ATG
Ras/MAP kinase

Chapter 2: Myc and mTOR converge on a common node in protein synthesis control that confers synthetic lethality in Myc-driven cancers

Background

The Myc transcription factor is one of the most frequently activated oncogenes in human tumors (Dang et al., 2006). Importantly, Myc overexpression also correlates with poor prognosis and decreased survival in a broad range of cancers (Barrans et al., 2010; Sato et al., 2006; Savage et al., 2009; Wolfer et al., 2010). However, therapeutic approaches to directly target Myc oncogenic activity are not currently available in the clinic (Prochownik and Vogt, 2010). An alternative approach for targeting Myc is to inhibit key downstream molecular pathways that are required for Myc-driven tumorigenesis. One of the major and immediate downstream effects of Myc activation is a dramatic increase in the protein synthetic capacity of the cell that results in increased cell survival, proliferation, and genome instability (Dai and Lu, 2008; Ruggero, 2009; van Riggelen et al., 2010). Importantly, genetically restoring enhanced protein synthesis to normal levels downstream of Myc suppresses tumor development (Barna et al., 2008), suggesting that modulating protein synthesis control may be a promising therapeutic approach (Chen et al., 2012; Graff et al., 2007; Lin et al., 2012). However, the components of the translation machinery that can be therapeutically targeted to exploit the addiction of Myc-driven cancer cells to augmented protein synthesis remain largely undefined.

Another master regulator of protein synthesis frequently found deregulated in cancer is the mammalian target of rapamycin (mTOR) kinase (Wang and Proud, 2006; Zoncu et al., 2011). mTOR also controls protein synthesis as part of a larger complex, mTOR complex 1 (mTORC1), at least in part, through direct phosphorylation of the tumor suppressor eukaryotic translation initiation factor 4E (eIF4E) binding protein 1 (4EBP1) and ribosomal protein p70S6 kinase (p70S6K1/2) (Bader et al., 2005; Brown et al., 1995; Gingras et al., 1998; Kim et al., 2002).

Although p70S6K is known to impinge on multiple aspects of mRNA translation, a major effect of mTOR-dependent protein synthesis control has been attributed to its regulation of 4EBP1 (Gingras et al., 2001b; Ruvinsky and Meyuhas, 2006). mTORC1-dependent phosphorylation of 4EBP1 blocks its ability to negatively regulate the translation initiation factor eIF4E, thus promoting eIF4E's ability to recruit the 40S ribosomal subunit to the 5′-cap of mRNAs and enhanced translation initiation (Sonenberg and Hinnebusch, 2009). Importantly, eIF4E hyperactivation alone is sufficient to act as a driving oncogenic event (Ruggero et al., 2004). Moreover, our laboratory and others have demonstrated that hyperactivation of eIF4E, through inhibition of 4EBP1, is critically required for mTOR-dependent tumorigenesis (Dumstorf et al., 2010; Hsieh et al., 2010). The recent development of mTOR ATP active site inhibitors capable of blocking mTOR-dependent phosphorylation of 4EBP1 has facilitated therapeutic targeting of this clinically relevant pathway (Feldman et al., 2009; Hsieh et al., 2010; Hsieh et al., 2012). In this regard, the mTOR–4EBP1 axis represents an attractive druggable node by which to target cancers addicted to enhanced protein synthesis. However, it remains an outstanding question whether Myc and mTOR converge on common translational nodes to regulate protein synthesis.

In this study, we uncover an unexpected and important link between Myc and mTOR-dependent 4EBP1 phosphorylation during Myc-driven tumorigenesis. To elucidate the functional consequences of 4EBP1 phosphorylation during Myc-driven tumorigenesis, we use a pharmacogenetic approach to target mTOR-dependent 4EBP1 phosphorylation in Myc-driven lymphoid cancer. In particular, we determine the therapeutic efficacy of the recently developed mTOR active site inhibitor MLN0128, which is uniquely capable of targeting 4EBP1 phosphorylation, in Myc-driven cancers. This reveals a remarkable requirement for the 4EBP1–eIF4E axis in conferring cell survival in Myc cancer cells, which is pharmacologically druggable. Finally, we explore the clinical potential of targeting mTOR-dependent 4EBP1 phosphorylation in human cancers driven by Myc hyperactivation.

Results

Myc and mTOR Signaling Converge on 4EBP1 Phosphorylation.

Myc's oncogenic activity depends directly on its capacity to increase protein synthesis (Barna et al., 2008). To explore the earliest events in tumorigenesis associated with the ability of Myc to drive increased protein synthesis, we analyzed key nodes of cap-dependent translation downstream of Myc oncogenic signaling in vivo. To this end, we used the ***Eμ-Myc***transgenic mouse model, a faithful model of human Burkitt's lymphoma in which constitutive overexpression of Myc in the B-cell compartment drives lymphomagenesis (Adams et al., 1985). Interestingly, we uncovered that primary B lymphocytes isolated from 4-wk-old ***Eμ-Myc*** mice show an unexpected and specific increase in mTOR-dependent phosphorylation of 4EBP1 at threonine 37/46 before tumor formation (Figure 2.1A). Surprisingly, another downstream effector of mTORC1 responsible for protein synthesis control, the ribosomal protein p70S6K, is on the contrary not altered in this pretumor setting. In line with this, there is no difference in mTOR phosphorylation at Ser2448, which has previously been shown to be a p70SK1 target (Figure S2.1) (Chiang and Abraham, 2005; Holz and Blenis, 2005). Moreover, phosphorylation of the mTORC2 substrate Akt was not enhanced in Myc-overexpressing B lymphocytes (Figure 2.1A). These data reveal that Myc overexpression results in 4EBP1 hyperphosphorylation and that only specific mTOR substrates are affected at the earliest steps of tumorigenesis.

Importantly, we find that 4EBP1 hyperphosphorylation is maintained during tumor progression in ***Eμ-Myc*** tumors (Figure S2.2). We next asked whether phosphorylation of 4EBP1 by mTOR is functionally required for Myc oncogenic activity. To address this question, we took advantage of the mTOR inhibitor MLN0128, a compound currently in early phase clinical trials. MLN0128 belongs to a new class of powerful mTOR active site inhibitors that exhibit enhanced

therapeutic potential compared with early allosteric inhibitors of mTOR such as rapamycin and its analogs (rapalogs). Our group and others have previously shown that, whereas rapalogs partially block the mTORC1 signaling pathway mainly by inhibiting p70S6K phosphorylation, mTOR active site inhibitors fully block mTORC1 activity including 4EBP1 phosphorylation as well as mTORC2 kinase activity . Moreover, the enhanced efficacy of mTOR active site inhibitors appears to be in large part due to their ability to block the 4EBP1–eIF4E axis (Feldman et al., 2009; Hsieh et al., 2010). We reasoned that by comparing the MLN0128 mTOR active site inhibitor with the rapalog RAD001, which fails to block 4EBP1 phosphorylation, we could pharmacologically dissect the relative functional importance of mTOR-dependent 4EBP1 phosphorylation downstream of oncogenic Myc signaling. To this end, wild-type and *Eμ-Myc* mice were treated with a single dose of either vehicle, RAD001, or MLN0128 and splenic B cells were analyzed for changes in cell cycle and programmed cell death. Strikingly, we find that, whereas both inhibitors cause cell cycle arrest, in line with previous preclinical data for RAD001 (Wall et al., 2013), only MLN0128 leads to a robust increase in apoptosis over vehicle in *Eμ-Myc* pretumor B cells (Figures 2.1B-C). Importantly, wild-type B-cell proliferation and survival is not affected by MLN0128 treatment (Figure S2.3). Thus, by comparing the efficacy of two pharmacological classes of mTOR inhibitors, our findings suggest a specific requirement for mTOR-dependent 4EBP1 phosphorylation in cell survival downstream of oncogenic Myc signaling, which can be selectively pharmacologically targeted by mTOR active site inhibitors.

mTOR-Dependent Phosphorylation of 4EBP1 as a Unique Therapeutic Target in Myc-Driven Tumors.

Despite the potential for significant clinical impact, therapeutic strategies for targeting Myc have remained elusive. Given our findings that mTOR-dependent phosphorylation of 4EBP1 is critically required for cell survival during the earliest stages of Myc tumorigenesis, we next explored the therapeutic potential of targeting mTOR in established Myc-driven tumors. We first asked if *Eμ-*

Myc tumors required mTOR signaling for tumor cell survival. *Eμ-Myc* mice with established tumors were treated with a single dose of vehicle, RAD001, or MLN0128 and tumors were analyzed. Strikingly, we find that MLN0128, but not RAD001, causes induction of programmed cell death in *Eμ-Myc* tumors within just 2 h of treatment, prior to any detectable changes in Myc oncogene levels (Figure 2.2A and S2.4). Moreover, we find that with just 3 d of MLN0128 treatment, tumor-bearing mice exhibit near complete resolution of lymphadenopathy (Figure 2.2B). Consistently, only treatment with MLN0128 is capable of inhibiting 4EBP1 phosphorylation and reducing tumor burden, measured as spleen weight (Figures 2.2C-D). Importantly, we find that the long-term treatment of *Eμ-Myc* tumors with MLN0128 significantly prolongs survival compared with vehicle and RAD001 (Figure 2.2E). Taken together, these data demonstrate the unexpected therapeutic potential of targeting Myc-driven tumors through the use of a recently developed class of mTOR active site inhibitors, which potently inhibit 4EBP1 phosphorylation.

Genetic Inactivation of mTOR-Dependent eIF4E Hyperactivation in Myc-Driven Lymphomagenesis.

To genetically determine the direct role of the mTOR-dependent phosphorylation of 4EBP1 in Myc-driven tumorigenesis and whether this parallels pharmacologic inhibition of mTOR, we genetically targeted eIF4E activity in vivo by using mouse models that express an inducible, dominant-negative 4EBP1 mutant (4EBP1^{m}). Importantly, 4EBP1^{m} is insensitive to mTOR signaling, as each of the mTOR-dependent phosphorylation sites has been mutated to alanine, allowing the 4EBP1^{m} protein to competitively bind and suppress eIF4E activity (Mothe-Satney et al., 2000). Previously, we have shown that 4EBP1^{m} is a powerful suppressor of eIF4E oncogenic activity in vivo (Hsieh et al., 2010). We therefore generated a unique transgenic mouse model that specifically expresses tetracycline-inducible 4EBP1^{m} in the B-cell compartment using a conditional rTTA allele [lox-stop-lox (LSL)-rTTA-internal ribosome entry site (IRES)-GFP] that concomitantly marks these cells with GFP (Figures 2.3A-B). Strikingly, we find that when

4EBP1^{m} is expressed in *Eμ-Myc* B cells (*Eμ-Myc;4EBP1m*), the number of circulating pretumor cells in the blood is dramatically reduced by more than 80% within 24 h of transgene induction (Figure 2.3C). In contrast, normal B cells are unaffected by expression of 4EBP1^{m} (Figure 2.3C). We next assessed if this marked reduction in *Eμ-Myc* pretumor B cells is caused by induction of programmed cell death. Indeed, we find that 4EBP1^{m} expression in *Eμ-Myc* mice leads to a robust induction of apoptosis in pretumor B cells (Figure 2.3D).

We next asked what effect genetically targeting eIF4E activity with the *4EBP1m* transgene would have on Myc-driven lymphomagenesis and tumor maintenance. To this end, we monitored *Eμ-Myc* mice for tumor development and survival upon induction of 4EBP1^{m}. Strikingly, *Eμ-Myc;4EBP1m* mice have significantly delayed lymphomagenesis compared with control *Eμ-Myc* mice (Figure 2.3E). Importantly, all of the tumors that develop in *Eμ-Myc;4EBP1m* mice are GFP negative, suggesting they arise from pretumor B cells that have failed to induce 4EBP1^{m} expression (Figure 2.3F). This is consistent with the fact that recombination of the LSL-rTTA-IRES-GFP locus by CD19-*Cre* does not occur in 100% of B cells. Finally, we asked whether established*Eμ-Myc;4EBP1m* tumors require 4EBP1–eIF4E hyperactivity for survival. Indeed, we find that tumor cells isolated from *Eμ-Myc;4EBP1m* mice undergo rapid apoptosis upon induction of 4EBP1^{m} (Figure S2.5). Altogether, these data demonstrate that 4EBP1-dependent inhibition of eIF4E activity impedes Myc-driven lymphomagenesis and tumor survival. Additionally, these genetic data strongly support that inhibition of mTOR-dependent phosphorylation of 4EBP1 is a key determinant of MLN0128 efficacy in Myc-driven lymphomas.

mTOR Active Site Inhibitor Efficacy in Myc-Driven Multiple Myeloma.

Myc is a dominant oncogenic driver in several hematologic malignancies. Therefore, we sought to extend our observations on the requirements for mTOR-dependent 4EBP1 phosphorylation to other Myc-driven cancers. Multiple myeloma (MM) is a plasma cell neoplasm with frequent Myc overexpression (Chng et al., 2011; Shou et al., 2000). In fact, Myc overexpression is associated

with poor survival in MM (Chng et al., 2011; Kanungo et al., 2006). Importantly, a transgenic mouse model that activates Myc in germinal center B cells (*Vk*MYC*) is able to fully recapitulate the clinical and pathologic features of the disease, demonstrating that Myc can in fact be a driving oncogenic event in MM (Chesi et al., 2008). We used this mouse model to examine the role of mTOR-dependent 4EBP1 phosphorylation in Myc-driven myeloma. We first asked if malignant plasma cells demonstrate increased mTOR activity. To this end, we isolated $CD138^+$ plasma cells and $CD138^-$ bone marrow mononuclear cells (BMMNCs) from *Vk*MYC* and wild-type mice and used a flow cytometry assay that we optimized to directly evaluate and quantify 4EBP1 phosphorylation. In line with our findings in MYC-driven lymphomas, we see that *Vk*MYC* malignant plasma cells display increased 4EBP1 phosphorylation compared with BMMNCs and wild-type plasma cells (Figure 2.4A). Importantly, these data suggest that cross-talk between the Myc and mTOR signaling pathways at the level of 4EBP1 phosphorylation may be a general feature of Myc-driven tumors.

We next examined the cellular effects of mTOR inhibition by MLN0128 in Myc-driven myeloma. *Vk*MYC* and wild-type mice were treated with a single dose of vehicle or MLN0128 and bone marrow was collected and analyzed. Importantly, we find that MLN0128 inhibition of mTOR induces apoptosis selectively in *Vk*MYC*$CD138^+$ plasma cells and not $CD138^-$ BMMNCs (Figure 2.4B). Moreover, wild-type $CD138^+$ plasma cells are unaffected by MLN0128 treatment. These findings demonstrate that Myc-driven myeloma requires mTOR-dependent signaling for tumor survival. Therefore, we next tested the efficacy of MLN0128 in Myc-driven MM in a preclinical trial. *Vk*MYC* were randomized for treatment with either vehicle or MLN0128 and monitored for therapeutic response as measured by changes from baseline monoclonal protein (M protein) production. Strikingly, we find that *Vk*MYC* mice treated with MLN0128 show significant preclinical responses as evidenced by decreases in M-protein production (Figure 2.4C). In fact, some *Vk*MYC* mice respond to mTOR inhibition with complete resolution of disease and full restoration of normal hematopoiesis (Figure 2.4D). Collectively, these results extend the

efficacy of mTOR active site inhibitors to Myc-driven MM and suggest that targeting mTOR-dependent phosphorylation of 4EBP1 could be a powerful therapeutic strategy for broadly targeting Myc-driven tumors.

Exploring the Clinical Relevance of mTOR-Dependent 4EBP1 Phosphorylation in Myc-Driven Human Lymphomas.

Myc overexpression is a common feature of human lymphoma and is associated with a poor response to standard chemotherapy (Barrans et al., 2010; Cuccuini et al., 2012; Johnson et al., 2012). We next sought to extend the relevance of our findings in mouse models of Myc-driven cancers to human lymphomas. We first asked if mTOR-dependent phosphorylation of 4EBP1 was required for the survival of human Myc-driven lymphomas. Therefore, we expressed an inducible $4EBP1^{m}$ vector in Raji cells, a human Burkitt's lymphoma cell line. We find that induction of $4EBP1^{m}$causes apoptosis in Raji cells that can be recapitulated by pharmacological treatment with the mTOR active site inhibitor MLN0128 (Figures 2.5A and S2.4A).

We next asked whether mTOR-dependent phosphorylation of 4EBP1 is a hallmark of Myc overexpression in human lymphomas. We addressed this question within the context of diffuse large B-cell lymphoma (DLBCL) because unlike Burkitt's lymphomas, where Myc is found translocated in 100% of cases, DLBCLs show Myc overexpression in a fraction of cases (29%) (Johnson et al., 2012). Therefore, the DLBCL model provides a unique opportunity to compare the status of 4EBP1 phosphorylation in human lymphomas that differentially express Myc. Importantly, Myc overexpression in DLBCL correlates with poor response to standard chemotherapy and shortened patient survival (Barrans et al., 2010; Johnson et al., 2012; Savage et al., 2009). Consequently, DLBCL is another cancer in which our findings may have strong therapeutic implications. Based on this rationale, we used a human tissue microarray (TMA) to determine the status of Myc overexpression and possible concomitant changes in 4EBP1 phosphorylation by immunohistochemistry (IHC). Importantly, we could confirm that high Myc

expression was correlated with expression of known Myc targets, such as eIF4E (Figure S2.6B) (Schmidt, 2004). Strikingly, we also find that significantly increased 4EBP1 phosphorylation in DLBCL cases correlates with high Myc expression (Figures 2.5B-C and Figures S2.6C). Moreover, only phosphorylation of 4EBP1 is affected, as there is no statistically significant difference in total 4EBP1 expression levels between low and high Myc DLBCL cases. Collectively, these findings show a strong correlation between high levels of Myc and 4EBP1 hyperphosphorylation in human lymphomas and demonstrate that mTOR-dependent inhibition of 4EBP1 is required for the survival of human tumors driven by oncogenic Myc signaling. Thus, mTOR-dependent phosphorylation of 4EBP1 may represent a highly relevant therapeutic target and biomarker that could be exploited for the treatment of a clinically important subset of human lymphomas driven by Myc.

Figures

Figure 2.1. Oncogenic Myc activity regulates mTOR-dependent phosphorylation of 4EBP1 at the earliest stages of tumorigenesis to promote cell survival. (*A*) Representative Western blot of mTOR signaling in wild-type B cells and Eμ-Myc pretumor cells from 4-wk-old mice and quantification of phosphoprotein levels relative to total protein levels in these cells (quantification is for four wild-type and four Eμ-Myc mice). Graph represents mean ± SD. (*B*) Cell cycle analysis of pretumor cells isolated from Eμ-Myc mice treated with vehicle, RAD001, or MLN0128 for 3 d (three to four mice per arm). (*C*) Analysis of apoptosis in pretumor cells isolated from Eμ-Myc mice treated with vehicle, RAD001, or MLN0128 (two mice per arm, representative of two experiments). Graph represents mean ± SD.

Figure 2.2. Therapeutic potential of the mTOR active site inhibitor MLN0128 compared with rapalogs in Myc-driven tumors. (*A*) Analysis of apoptosis in tumor cells isolated 2 h after a

single dose of vehicle, RAD001, or MLN0128 in mice with established Eμ-Myc tumor transplants (three mice per arm). Graph represents mean ± SD. (*B*) Response of primary Eμ-Myc tumor to 3 d of treatment with MLN0128. (*C*) Western blot of mTOR substrates in tumor cells isolated from mice with established Eμ-Myc tumor transplants after 3 d of treatment with vehicle (V), RAD001 (R), or MLN0128 (M). (*D*) Tumor burden as measured by spleen weight in mice with established Eμ-Myc tumor transplants after 3 d of treatment relative to WT mice (two to three mice per arm, representative of three separate transplanted tumors). Graph represents mean ± SD. (*E*) Kaplan–Meier curves from preclinical trial in Eμ-Myc transplant model. Day 0 indicates the first day of palpable tumor formation and the beginning of treatment (five mice per arm).

Figure 2.3. Genetic inhibition of mTOR-dependent 4EBP1–eIF4E activation blocks Myc-driven tumorigenesis. (*A*) Schematic of the system used to genetically target $4EBP1^{m}$ to the B-cell compartment. (*B*) Western blot for $4EBP1^{m}$ in B cells upon doxycycline administration. (*C*) Flow cytometry analysis of peripheral blood for $B220^{+}$, GFP^{+} B cells before and after induction of $4EBP1^{m}$ by i.p. injection of doxycycline (2 mice per arm). Graph represents mean ± SD. (*D*) Analysis of apoptosis in $B220^{+}$, GFP^{+} pretumor B cells upon induction of $4EBP1^{m}$ in Eμ-Myc;$4EBP^{m}$ mice (2 mice per arm). Graph represents mean ± SD. (*E*) Kaplan–Meier survival curve of Eμ-Myc;$4EBP1^{m}$ pretumor mice maintained on doxycycline water from weaning compared with Eμ-Myc littermate controls (8–10 mice per arm). (*F*) Representative flow cytometry plot showing the loss of GFP^{+} cells in tumors arising from Eμ-Myc;$4EBP1^{m}$ mice maintained on doxycycline (representative of eight tumors).

Figure 2.4. Efficacy of mTOR active site inhibitors in Myc-driven multiple myeloma. (*A*) Representative flow cytometry analysis of 4EBP1 phosphorylation in $CD138^{+}$ plasma cells and $CD138^{-}$ BMMNCs isolated from the bone marrow of wild-type and Vk*MYC mice. (*B*) Analysis of apoptosis in $CD138^{-}$ and $CD138^{+}$cells isolated from the bone marrow of wild-type and Vk*MYC mice treated with vehicle or MLN0128 (two mice per arm). Graph represents mean ±

SD. (*C*) Preclinical trial in Vk*MYC spontaneous tumors. Best response is measured as the change from baseline M protein after 8 wk of daily treatment with either vehicle or MLN0128. Bar represents mean. (*D*) Representative H&E staining of bone marrow from wild-type mice and Vk*MYC mice upon completion of the preclinical trial. Bone marrow of untreated Vk*MYC mice consists predominantly of malignant plasma cells. This is in contrast to Vk*MYC bone marrow after MLN0128 treatment, which demonstrates a mixed hematopoietic cell population with low frequency of plasma cells similar to wild-type bone marrow.

Figure 2.5. Clinical relevance of mTOR-dependent 4EBP1 phosphorylation in Myc-driven human lymphomas. (*A*) Analysis of apoptosis in the human Raji Burkitt's lymphoma cell line upon $4EBP1^{m}$ expression or MLN0128 treatment for 24 h. Graph represents mean ± SD. (*B*) Representative H&E, Myc staining, and phospho-4EBP1 staining in human diffuse large B-cell lymphoma (DLBCL). (*C*) Box and whisker plot of IHC intensity for total 4EBP1 and phospho-4EBP1 from a human DLBCL tissue microarray (TMA) consisting of 77 patients.

Figure 2.1

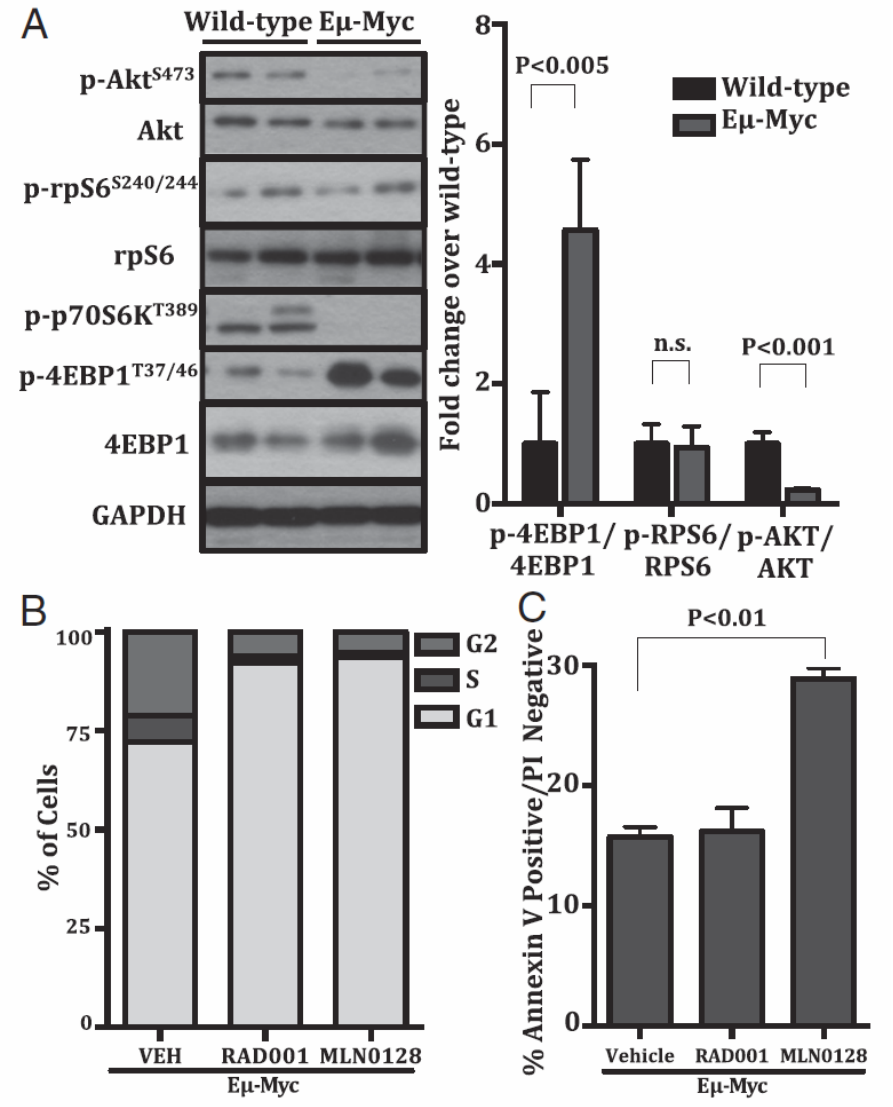
A
Wild-type
Eμ-Myc
p-Akt^{S473}
Akt
p-rpS6$^{S240/244}$
rpS6
p-p70S6K^{T389}
p-4EBP1$^{T37/46}$
4EBP1
GAPDH
Fold change over wild-type
P<0.005
n.s.
P<0.001
Wild-type
Eμ-Myc
p-4EBP1/ 4EBP1
p-RPS6/ RPS6
p-AKT/ AKT
B
% of Cells
G2
S
G1
VEH
RAD001
MLN0128
Eμ-Myc
C
% Annexin V Positive/PI Negative
P<0.01
Vehicle
RAD001
MLN0128
Eμ-Myc

Figure 2.2

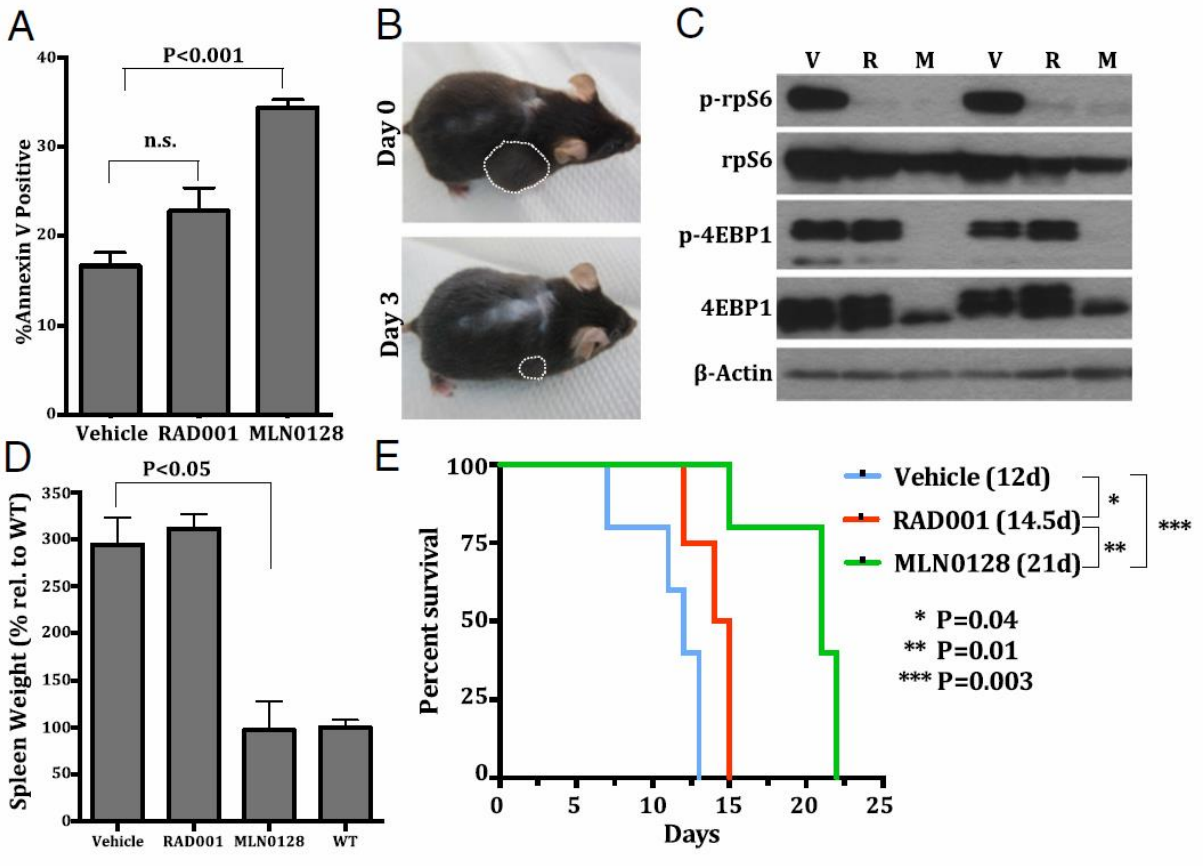
A
P<0.001
n.s.
%Annexin V Positive
Vehicle RAD001 MLN0128
B
Day 0
Day 3
C
V R M V R M
p-rpS6
rpS6
p-4EBP1
4EBP1
β-Actin
D
P<0.05
Spleen Weight (% rel. to WT)
Vehicle RAD001 MLN0128 WT
E
Percent survival
Days
Vehicle (12d)
RAD001 (14.5d)
MLN0128 (21d)
* P=0.04
** P=0.01
*** P=0.003

Figure 2.3

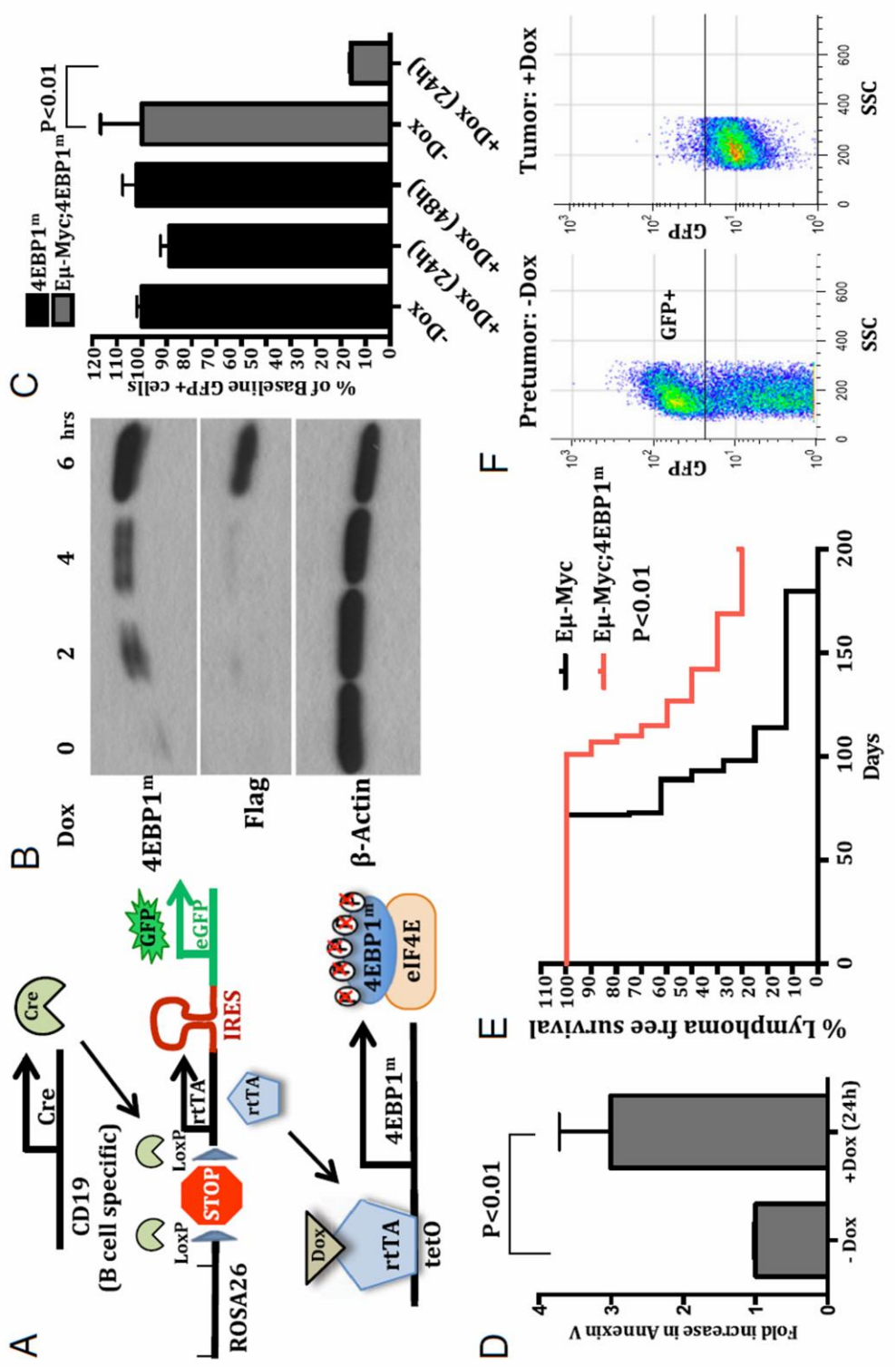
A
Cre
CD19
(B cell specific)
ROSA26
LoxP
STOP
LoxP
rtTA
IRES
GFP
eGFP
rtTA
Dox
rtTA
tetO
4EBP1m
eIF4E
B
Dox
0
2
4
6 hrs
4EBP1m
Flag
β-Actin
C
4EBP1m
Eμ-Myc;4EBP1m
P<0.01
% of Baseline GFP+ cells
-Dox
+Dox (24h)
+Dox (48h)
-Dox
+Dox (24h)
D
P<0.01
Fold increase in Annexin V
- Dox
+Dox (24h)
E
Eμ-Myc
Eμ-Myc;4EBP1m
P<0.01
% Lymphoma free survival
Days
F
Pretumor: -Dox
Tumor: +Dox
GFP+
GFP
SSC

Figure 2.4

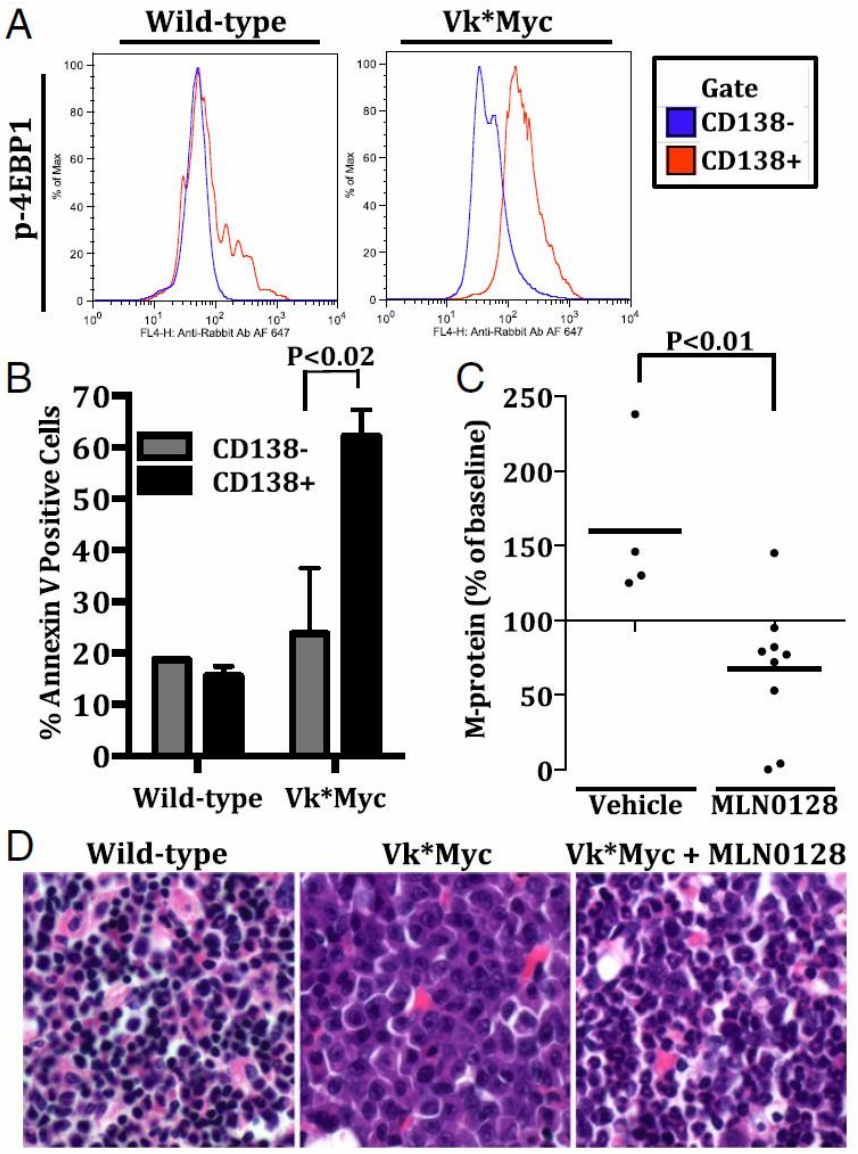
A
Wild-type
Vk*Myc
p-4EBP1
% of Max
FL4-H: Anti-Rabbit Ab AF 647
Gate
CD138-
CD138+
B
P<0.02
% Annexin V Positive Cells
CD138-
CD138+
Wild-type
Vk*Myc
C
P<0.01
M-protein (% of baseline)
Vehicle
MLN0128
D
Wild-type
Vk*Myc
Vk*Myc + MLN0128

Figure 2.5

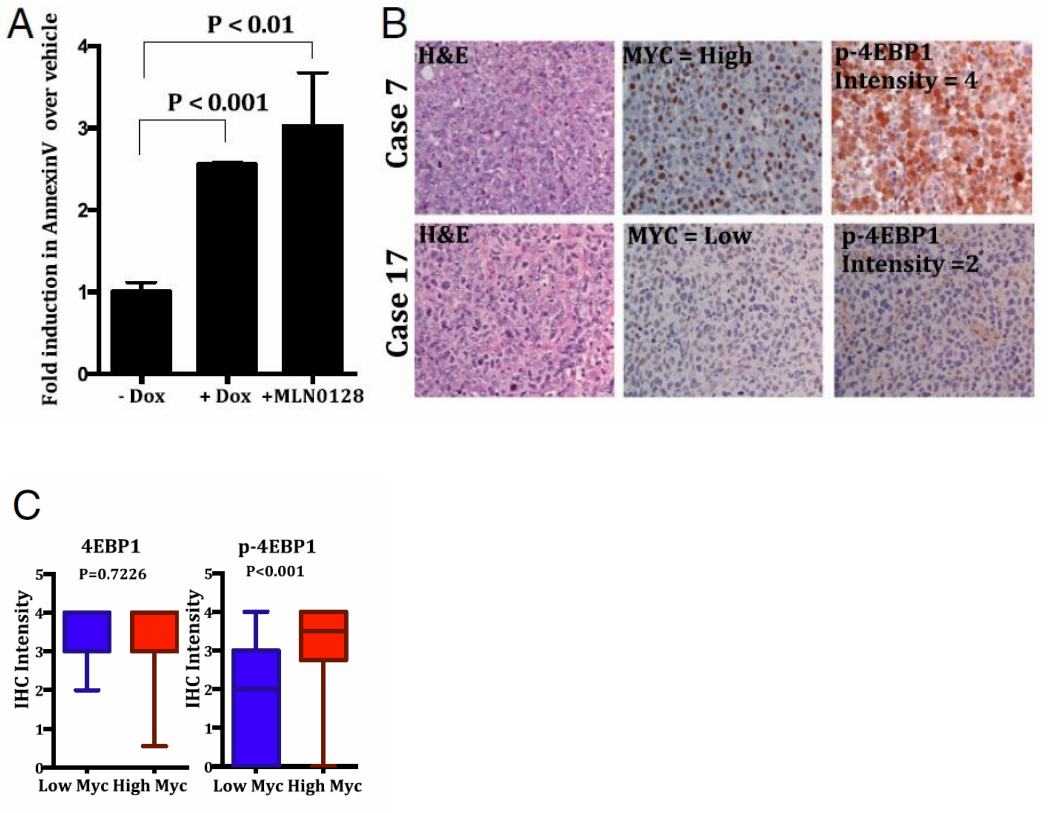
A
P < 0.01
P < 0.001
Fold induction in AnnexinV over vehicle
- Dox
+ Dox
+MLN0128
B
Case 7
H&E
MYC = High
p-4EBP1
Intensity = 4
Case 17
H&E
MYC = Low
p-4EBP1
Intensity =2
C
4EBP1
P=0.7226
p-4EBP1
P<0.001
IHC Intensity
Low Myc
High Myc

Supplemental Figure 2.1. Evaluation of mTOR activation in pretumor Eμ-Myc cells. Western blot comparing mTOR(S2448) phosphorylation in wild-type B cells and Eμ-Myc pretumor cells.

Supplemental Figure 2.2. mTOR-dependent phosphorylation of 4EBP1 is maintained throughout Myc tumorigenesis. Western blot comparing 4EBP1 phosphorylation in wildtype B cells, Eμ-Myc pretumor cells, and Eμ-Myc tumor cells.

Supplemental Figure 2.3. The effect of blocking mTOR-dependent 4EBP1 phosphorylation on normal B cells. Cell cycle analysis of B cells isolated from wild-type mice treated with vehicle, RAD001, or MLN0128 (two to four mice per arm).

Supplemental Figure 2.4. Inhibition of mTOR-dependent 4EBP1 phosphorylation demonstrates therapeutic efficacy without decreasing Myc protein levels. Western blot comparing Myc protein levels in Eμ-Myc tumor cells treated for 2 h in vitro with vehicle (V), rapamycin (R), or MLN0128 (M). Inhibition of 4EBP1 phosphorylation is also shown.

Supplemental Figure 2.5. 4EBP1–eukaryotic initiation factor 4E (eIF4E) activity is critically required for Myc tumor development and survival. Analysis of apoptosis in untreated Eμ-Myc;4EBP1m tumor cells upon administration of doxycycline in vitro. Graph represents mean ± SD (normalized to vehicle).

Supplemental Figure 2.6. Evaluation of 4EBP1–eIF4E activity in human Myc-driven lymphomas. (A) Western blot of 4EBP1m in the human Raji Burkitt's lymphoma cell line upon doxycycline induction. (B) Box and whisker plot of IHC intensity for eIF4E from the DLBCL TMA. (C) Box and whisker plot of percent of cells positive for phospo-4EBP1 in cases of Myc low (<40% cells Myc positive) vs. Myc high (>40%) from the DLBCL TMA.

Figure S2.1

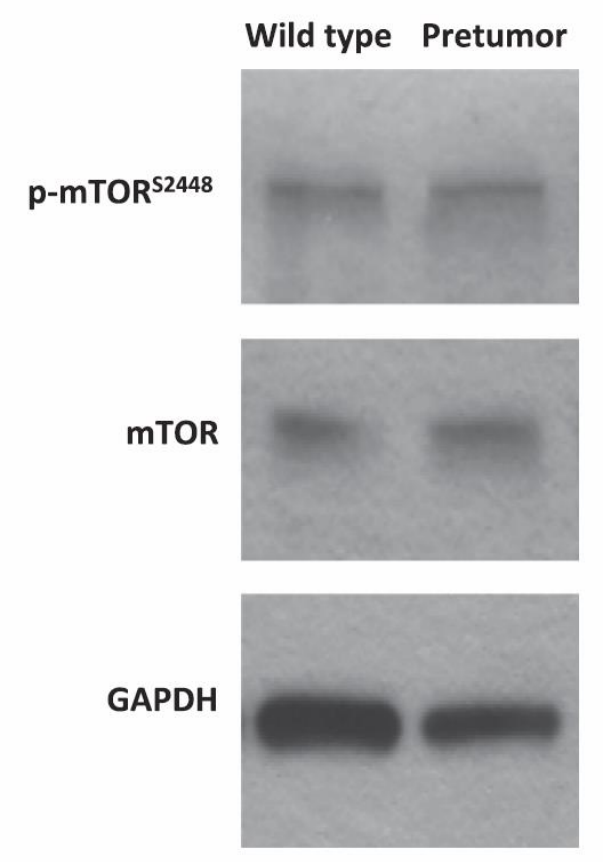

Figure S2.2

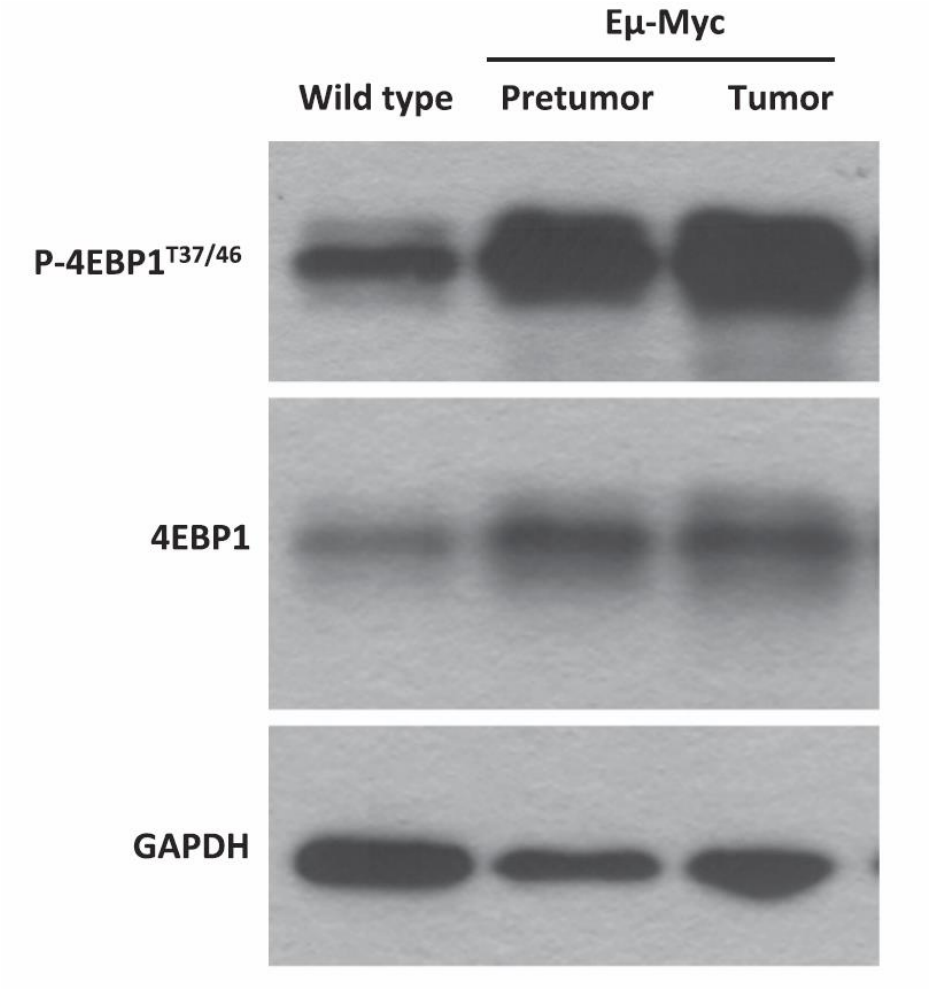

Figure S2.3

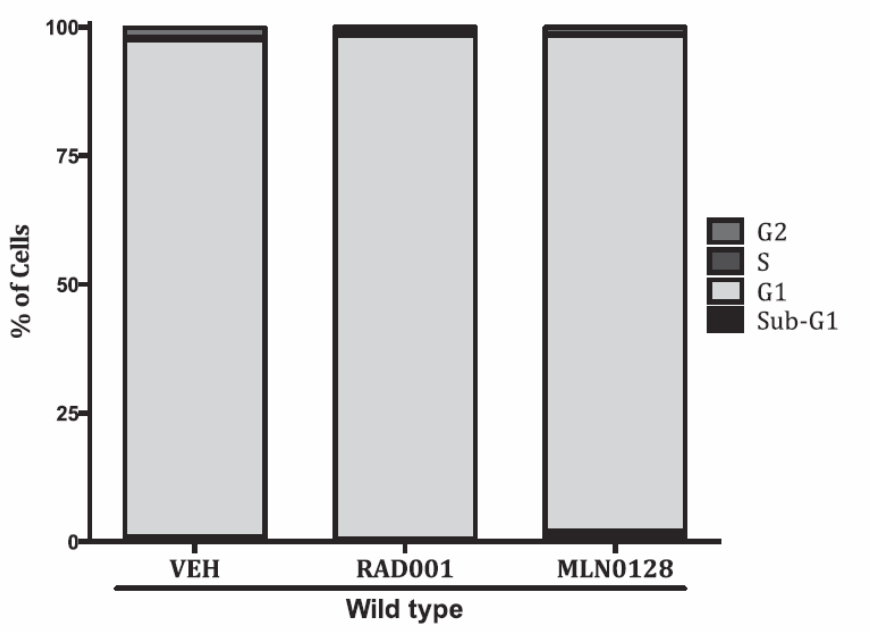
100
75
50
25
0
% of Cells
G2
S
G1
Sub-G1
VEH
RAD001
MLN0128
Wild type

Figure S2.4

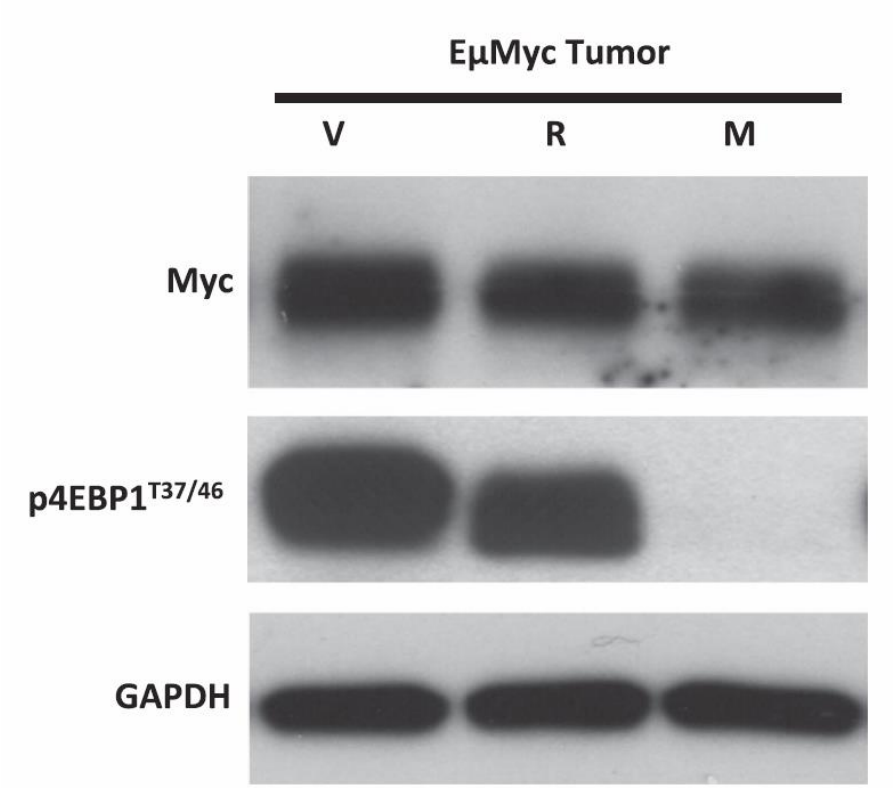

Figure S2.5

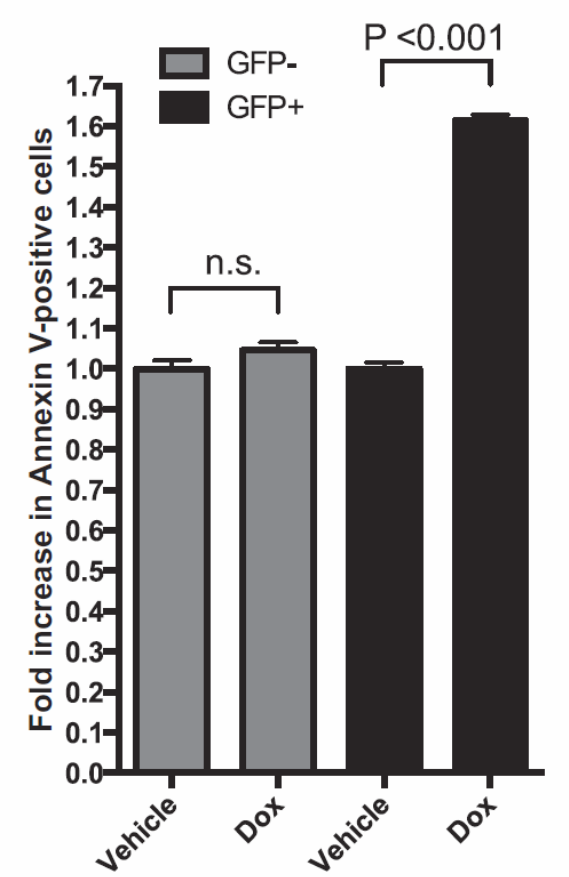
P <0.001
GFP-
GFP+
n.s.
Fold increase in Annexin V-positive cells
1.7
1.6
1.5
1.4
1.3
1.2
1.1
1.0
0.9
0.8
0.7
0.6
0.5
0.4
0.3
0.2
0.1
0.0
Vehicle
Dox
Vehicle
Dox

Figure S2.6

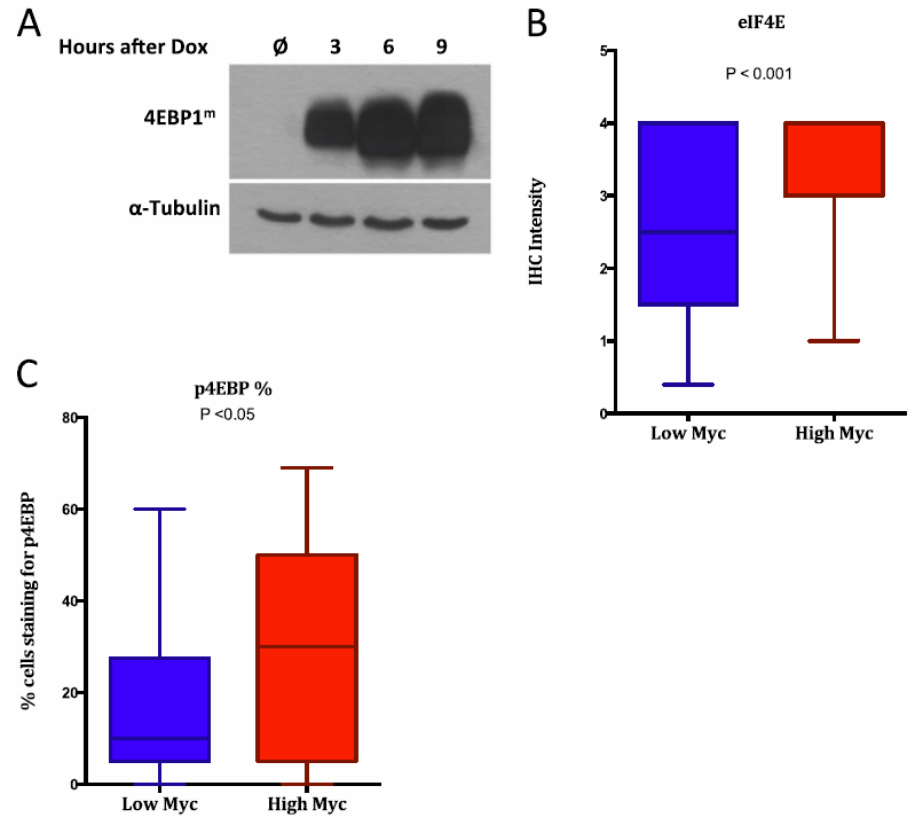
A
Hours after Dox
Ø
3
6
9
4EBP1m
α-Tubulin
B
eIF4E
P < 0.001
IHC Intensity
0
1
2
3
4
5
Low Myc
High Myc
C
p4EBP %
P <0.05
% cells staining for p4EBP
0
20
40
60
80
Low Myc
High Myc

Materials and Methods

Mouse Experiments.

The Eμ-Myc transgenic mouse model has been previously described (Adams et al., 1985). For pretumor and wild-type B-cell analysis, spleens were harvested from 4- to 5-wk-old Eμ-Myc mice and wild-type littermates. Spleens were dissociated over ice into single cell suspensions, depleted of red blood cells by ammonium–chloride–potassium (ACK) buffer treatment, and B cells were isolated using a B-cell isolation kit according to the manufacturer's protocol (Miltenyi Biotech; 130–090-862).

For pretumor drug studies, Eμ-Myc mice and wild-type littermates were randomized at 4 wk of age to receive vehicle, RAD001 (10 mg/kg; LC Laboratories), or MLN0128 (1 mg/kg; synthesized from commercially available starting materials as previously reported) (Hsieh et al., 2012) by oral gavage daily for 3 d. MLN0128 (formerly INK128), a highly selective and potent mammalian target of rapamycin (mTOR) active site inhibitor (1.4 nM inhibition constant), was administered based on previously published pharmacokinetic data that demonstrated 1 mg/kg daily dosing achieved maximal mTOR inhibition while minimizing off-target effects (Hsieh et al., 2012). Spleens were harvested from euthanized mice, dissociated over ice into single cell suspensions, depleted of red blood cells, and stained for B-cell–specific markers before being analyzed for cell cycle or apoptosis.

For Eμ-Myc tumor studies, unless otherwise noted, allograft mice were used. The Eμ-Myc allograft model was generated using spontaneous lymph node tumors from Eμ-Myc mice, which were dissociated in PBS and filtered through 40-mm nylon mesh (BD Biosciences). A total of 1×10^6 Eμ-Myc tumor cells were then injected into 8- to 12-wk-old C57/BL6 mice by tail vein. Mice were enrolled in drug studies at first detection of palpable tumors and randomized for treatment with vehicle, RAD001, and MLN001 as described above. To measure drug-induced apoptosis, mice were euthanized 2 h after a single round of drug treatment. Single cell suspensions of freshly

isolated lymph node tumors were stained with B-cell markers and analyzed for apoptosis. To evaluate treatment response and verify inhibition of mTOR substrate phosphorylation, mice were randomized and treated for 3 d with vehicle or drug. Two hours after the final dose, mice were euthanized, spleen weight was measured to analyze treatment response, and lymph node tumors were snap frozen for Western blot analysis of mTOR substrate phosphorylation. For preclinical trial, allograft mice were treated daily (6 d/wk) upon enrollment into the study and monitored for weight change and survival.

Tetracycline operator (TetO)-FLAG-4EBP1m mice were generated as previously described (Hsieh et al., 2010) using a 4EBP1 mutant construct in which all five mTOR-dependent 4EBP1 phosphorylation sites (T37, T46, S65, T70, and S82) were mutated to alanine (Mothe-Satney et al., 2000). ROSA26-lox-stop-lox (LSL)-rTTA-internal ribosome entry site (IRES)-GFP (Belteki et al., 2005) mice and CD19 Cre mice (Rickert et al., 1995; Rickert et al., 1997) were acquired from Jackson Laboratories. All mice were maintained in the C57/BL6 background. Mice were intercrossed to generate Eμ-Myc; CD19 Cre; ROSA26-LSL-rTTA-IRES-GFP; TetOFLAG-4EBP1m (referred to as Eμ-Myc;4EBP1m). For analysis of cellular effects of 4EBP1m expression, doxycycline (33 mg/kg) was administered once by i.p. injection. Peripheral blood was collected by tail bleed, depleted of red blood cells, and stained with anti-B220 APC (clone RA3-6B2) to mark B cells. Cells were assessed for GFP expression on a BD FACSCalibur flow cytometer and data were analyzed using FlowJo software. For survival studies, mice were put on continuous doxycycline (2 g/L in H2O) starting at weaning and compared with Eμ-MycCD19Cre control mice. Upon study completion, tumors were assessed for GFP expression by flow cytometry as described above.

Vk*MYC mice were obtained from Marta Chesi (Mayo Clinic) and have been previously described in detail (Chesi et al., 2008). Where noted, Vk*MYC allograft mice were generated for these studies by tail vein injecting 8- to 12-wk-old C57/BL6 mice with 1 × 106 freshly isolated bone marrow mononuclear cells freshly isolated from a diseased Vk*MYC mouse. For phospho-

flow cytometry experiments, allograft mice were analyzed. For all drug studies, Vk*MYC spontaneous and allograft mice were randomized and treated with vehicle or MLN0128 after they had developed significant monoclonal proteins (15g/L) as assessed by serum protein electrophoresis (SPEP) (Helena Laboratories QuickGel SPE kit; no. 3409). To measure drug induced apoptosis, wildtype and Vk*MYC allograft mice were treated daily for 3 d as described above. Mice were euthanized 2 h after the final dose. Single cell suspensions of freshly isolated bone marrow mononuclear cells were depleted of red blood cells and stained with plasma cell markers before being analyzed for apoptosis. For preclinical trial, spontaneous Vk*Myc mice with significant monoclonal protein levels were treated daily (6 d/wk) by oral gavage as described above for an 8-wk time course. Monoclonal protein levels were monitored weekly from baseline to end of trial by SPEP. At the end of the study, mice were euthanized and their sternums were fixed in formaldehyde, decalcified, and sectioned for H&E staining.

The University of California San Francisco Institutional Animal Care and Use Committee approved all studies involving live mice.

Cell Culture Studies.

Tumor cells were isolated from untreated Eμ-Myc;4EBP1m or Eμ-Myc mice and freshly plated on a feeder layer of irradiated mouse embryonic fibroblasts in RPMI supplement with 10% FBS for short-term culture. Eμ-Myc;4EBP1m tumor cells were treated with doxycycline (1 μg/mL final) to induce expression of 4EBP1m and were subsequently analyzed for apoptosis. Eμ-Myc tumors were treated in vitro with vehicle, rapamycin (50 nM; Cal Biochem) or MLN0128 (200 nM), and cells were collected for Western blot analysis.

A single vector tetracycline-inducible FLAG-4EBP1m expression system was developed in our laboratory by combining the TRE3g promoter (Clontech) and the TetOn3g transactivator (Clontech) into a lentiviral vector and subsequently inserting the FLAG-4EBP1m construct (discussed above) downstream of the TRE3g promoter. This vector was transduced into Raji cells

(obtained from ATCC) and FLAG-4EBP1m was induced by administering doxycycline (1 μg/mL final) to cultures. These cells were analyzed for apoptosis and compared with Raji cells treated with MLN0128 (200 nM).

Cell Cycle Analysis.

Single cell suspensions were stained with anti-CD19 FITC (clone 1D3) or anti-B220 FITC (clone RAD3.3/A1/6.1) B-cell–specific markers when required. Cells were fixed/ permeabilized in 90% methanol. After, RNaseH treatment, cells were stained with propidium iodide and run on a BD FACSCalibur flow cytometer to measure DNA content (at least 10,000 cells per sample were collected). Cell cycle data were analyzed using FlowJo software.

Apoptosis Analysis.

Single cell suspensions were stained with anti-CD19 FITC (clone 1D3) or anti-B220 FITC (clone RAD3.3/A1/6.1) B-cell–specific markers or anti-CD138 FITC (BD Pharmingen) or anti-CD138 PE (Stem Cell Technologies) plasma cell markers when required. Cells were stained with Annexin V APC (BD Pharmingen; 550475) and propidium iodide and run on a BD FACSCalibur flow cytometer to measure Annexin V positivity (at least 10,000 cells per sample were collected). Apoptosis data were analyzed using FlowJo software.

Phospho-Flow Cytometry.

Bone marrow mononuclear cells from Vk*MYC mice were depleted of red blood cells, stained for plasma cells with anti-CD138 PE (BD Pharmingen), fixed with 2% PFA, and permeabilized with 90% methanol. After rehydration in PBS, cells were stained with antiphospho-4EBP1 (Cell Signaling, 1:100). Secondary staining was performed with anti-rabbit IgG (H+L), F(ab′)2 fragment (Alexa Fluor 647 conjugate, Cell Signaling; 1:400). Samples were then run on a BD FACSCalibur flow cytometer to measure phospho-4EBP1 expression and data were analyzed using FlowJo software.

Western Assays.

Immunoblotting was performed using standard procedures. Commercial antibodies for pAKT(S473), p-p70S6K (T389), pS6(S234/236), mTOR(S2448), AKT1, rpS6, 4EBP1, and GAPDH were obtained from Cell Signaling. Alpha-tubulin antibody was obtained from Abcam. Anti-Flag and beta-actin antibodies were obtained from Sigma. Where noted, protein levels were quantified by analyzing optical density using ImageJ software.

Human DLBCL Tissue Microarray.

The tissue microarray (TMA) data represent 85 cases of diffuse large B-cell lymphoma (DLBCL) seen at Los Angeles County Hospital (LAC) and University of Southern California (USC) Medical Center between 2002 and 2012. DLBCL cases were identified by a database search and confirmed based on 2008 World Health Organization classification. Indolent lymphoma with subsequent transformation to DLBCL or arising from a known immune suppressed condition, such as HIV, was excluded. Samples were then selected based on the availability of sufficient nonfrozen, formalin-fixed material. The TMA consists of 2-mm cores taken in duplicate or triplicate. This study was approved by the LAC and USC institutional review boards.

Immunohistochemical staining was performed on 4-μm tissue sections using an automated immunostainer (Bond III; Leica Microsystems). Antibodies are as follows: 4EBP1 (Cell Signaling; 53H11 clone, 1:2,000 citrate buffer 20 min), phospho-4EBP1 (Cell Signaling; T37/46 clone, 1:200 EDTA 20 min), eIF4E (Cell Signaling, C46H6 clone, 1:200 EDTA 20 min), and Myc (Epitomics; Y69 clone,1:100 EDTA 20 min). A total of 77 cases were evaluable and scored by I.N.S. Myc staining intensity was scored as none, weak, moderate, or strong (0–3). Immunohistochemistry (IHC) scores of 0–4 were given for intensity of all other staining. Because there were no statistically significant difference for these stains between samples with undetectable Myc and low–moderate Myc, these groups were pooled into a single low Myc class

(0–2) and compared with cases with high Myc (score of 3). Percent of cells staining positive for Myc and phospho-4EBP1 was also noted.

Statistical Analysis.

All data presented as bar graphs refer to a mean value ± SD of the total number of animals analyzed across independent experiments. An unpaired, two-tailed t test was used to determine P values for Figs. 1, 2 A and D, 3 B and C, 4, and 5 and Figs. S3 and S4. Statistical analysis of lymphoma free survival and respective P values were determined using the log-rank (Mantel–Cox) test (Figs. 2 and 3).

Acknowledgments

We thank M. Barna for support, critical discussion, and reading the manuscript; M. Chesi, P. L. Bergsagel, and Cornell University for generously providing Vk*Myc mice; C. Stumpf for developing and providing the inducible 4EBP1^{m} lentiviral construct; M. McMahon and M. Moreno for technical assistance; and K. Tong for editing the manuscript. This work was supported by National Institutes of Health (NIH) Grants R01 CA154916 and R01 CA140456 (both to D.R.), the Waxman Foundation (K.M.S.), and the University of California San Francisco (UCSF)'s Stephen and Nancy Grand Multiple Myeloma Translational Initiative (D.R., K.M.S., and M.P.). M.P. is a recipient of the American Association for Cancer Research–Millennium Fellowship in Lymphoma Research. M.L.T. is supported in part by a UCSF Howard Hughes Medical Institute Graduate Education in Medical Sciences Fellowship. D.R. is a Leukemia and Lymphoma Society Scholar.

Chapter 3: eIF4E dose is critical for the oncogenic translation program but not mammalian development and protein synthesis

Background

For nearly 40 years, the major cap binding protein eukaryotic initiation factor 4E (eIF4E) has been recognized as the quantitatively rate-limiting factor for mRNA translation initiation of the eukaryotic genome (Duncan et al., 1987; Hiremath et al., 1985). eIF4E is a critical component of the eIF4F tertiary translation initiation complex, which recognizes the 5' 7-methyl guanosine cap of mRNAs and drives their translation. In addition to eIF4E, the eIF4F complex is comprised of the DEAD-box helicase eIF4A and eIF4G, a large protein scaffold that recruits the 40S ribosome subunit to mature mRNAs (Gingras et al., 1999b). Of the eIF4F complex components, eIF4E has been identified as the quantitatively rate-limiting initiation factor and thereby eIF4E expression levels are believed to be a critical determinant for translation of eukaryotic mRNAs (De Benedetti et al., 1991; Duncan et al., 1987; Hiremath et al., 1985). For example, eIF4E hyperactivation has been shown to drive not only global but also specific changes in mRNA translation, in particular for those mRNAs harboring structured 5'UTRs, that may rely more on eIF4E levels for their translation (Gkogkas et al., 2013; Hsieh et al., 2012; Koromilas et al., 1992; Nikolcheva et al., 2002; Polunovsky et al., 1996; Santini et al., 2013). As such, even small changes in eIF4E levels are believed to broadly impact mRNA translation and thus cellular and organismal function (Figure 3.1A). However, the normal physiological role and threshold for eIF4E dose in organismal development *in vivo* is essentially unknown. Moreover, the specific requirements for eIF4E dose in both global and specific translation of mRNAs genome-wide remain poorly defined.

In this study, we generate the first mouse model for *Eif4e* haploinsufficiency as a novel genetic tool to define the requirements for eIF4E dose *in vivo*. Surprisingly, we find that eIF4E

exists in excess for normal development and global protein synthesis but instead becomes limiting under specific conditions, such as oncogene induced cellular transformation. Our findings reveal a striking molecular program by which eIF4E dose is coupled to a specialized translational program underlying cellular transformation. As such, *Eif4e*$^{+/-}$ cells are remarkably resistant to oncogene-induced transformation consistent with the fact that eIF4E is a proto-oncogene (Ruggero et al., 2004). Employing unbiased genome-wide profiling to identify the translational landscape of mRNAs induced by oncogenic transformation, we delineate the "oncogenic translation program" comprised of hundreds of mRNAs. Several key nodes in this program, such as functional classes of mRNAs involved in redox balance, signaling and proteasome control, are exquisitely sensitive to eIF4E dose. In particular, we identify a novel functional class of translationally regulated genes involved in the regulation of and response to oxidative stress that includes the ferritin heavy chain (Fth1), the catalytic subunit of glutamate-cysteine ligase (Gclc), and lamin B1 (Lmnb1)(Cozzi et al., 2000; Deneke and Fanburg, 1989; Malhas et al., 2009; Pham et al., 2004). Moreover, as many as 26 mRNAs translationally controlled by eIF4E are responsible for both neutralizing and responding to intracellular ROS during oncogenic transformation.

One of the defining stress phenotypes that cancer cells encounter is the build-up of reactive oxygen species (ROS), and cancer cells typically generate more ROS than normal cells (Szatrowski and Nathan, 1991). Both oncogenic signaling and deregulated mitochondrial respiration of cancer cells can contribute to ROS generation and oncogenic stress (Irani et al., 1997; Sattler et al., 2000; Vafa et al., 2002; Wallace, 2012). The ability of cancer cells to distinguish between ROS as a survival or apoptotic signal is controlled by the dosage and duration of ROS production, such that modest levels are required for cancer cell survival whereas excessive levels promote cell death (Trachootham et al., 2006; Weinberg et al., 2010). Here, we show that the capacity to properly translationally control mRNAs regulating intracellular ROS levels is critical for tumor cell survival. We further demonstrate that reductions in eIF4E cause a toxic accumulation of ROS that renders, at least in part, *Eif4e* haploinsufficient mice remarkably

resistant to transformation. These studies thereby reveal a novel regulatory mechanism by which cancer cells respond to stress by regulating the translation of stress response transcripts, which is directly coupled to the dose of eIF4E in the cell. Collectively, these findings highlight that mammalian cells have evolved a surplus of eIF4E that exists above the threshold for normal development and physiology and instead plays a specialized role in regulating mRNA translation under specific conditions, which has been coopted by tumor cells to weather the stress of oncogenic transformation.

Results

In vivo requirements for a threshold of eIF4E

In order to address the *in vivo* requirements for a threshold of eIF4E, we generated the first eIF4E knock-out mouse (Figure S3.1A-B). We reasoned that in the context of *Eif4e* heterozygosity (*Eif4e*$^{+/-}$), the impact of 50% reductions in eIF4E levels could be assessed genetically at an organismal level to delineate the *in vivo* function of eIF4E dose. Surprisingly, *Eif4e*$^{+/-}$ mice are viable and indistinguishable from their WT littermates. For example, *Eif4e*$^{+/-}$ mice are born at normal Mendelian ratios (Table 3.1) and display normal body weight (Figure S3.1C) and survival (data not shown) within one year of age. In addition, *Eif4e*$^{+/-}$ embryos and adult mice show normal tissue architecture and development (Figure 3.1B, Figure S3.1D, and Figure S3.2A) with no obvious changes in cell size, cell survival, or cell proliferation (Figures S3.2B-E). Moreover, *Eif4e*$^{+/-}$ embryos show equal sensitivity to developmental defects induced by exposure to known teratogenic agents such as alcohol (Table 3.2).

To confirm that *Eif4e*$^{+/-}$ mice display reductions in eIF4E expression, we analyzed eIF4E mRNA and protein levels in these mice. We consistently observe a 50% reduction in eIF4E expression in virtually all cell and tissue types examined *in vivo* (Figures 3.1C-D and Figures S3.2F-G). We next asked if there might be compensation for eIF4E loss of function through known

translation initiation pathway regulators (Yanagiya et al., 2012). However, we find no evidence of compensation in *Eif4e*$^{+/-}$ mice either at the level of expression or phosphorylation of any other component of the eIF4F initiation complex or of the eIF4E inhibitor protein, eIF4E Binding Protein 1 (4EBP1), which blocks the interaction of eIF4E with eIF4G (Figure 3.2A) (Haghighat et al., 1995; Lin et al., 1994; Pause et al., 1994). In addition, eIF4E activity can be directly regulated by phosphorylation at Serine 209 by the Mnk kinases, however, we see no signs of compensation for reduced eIF4E levels through enhanced eIF4E phosphorylation (Fig. 2A-2B) (Waskiewicz et al., 1997). As expected, complete loss of function of eIF4E is not compatible with life and *Eif4e*$^{+/-}$ embryos die before E6.5 (data not shown). Together, these findings unexpectedly demonstrate that a 50% reduction of eIF4E is fully compatible with normal organismal development and physiology *in vivo*.

We next sought to determine the impact of a 50% reduction in eIF4E dose on protein synthesis control *in vivo*. Remarkably, we find that *Eif4e*$^{+/-}$ mice display normal levels of global protein synthesis as assessed by incorporation of ^{35}S labeled methionine (Figure 3.1E and Figure S3.2H). Interestingly, reductions of eIF4E in yeast have been shown to cause a dramatic redistribution of mRNA from actively translating poly-ribosomes to monosomes with minimal impacts on global protein synthesis rates (von der Haar and McCarthy, 2002). However, we find no evidence for globally altered polysome profiles in *Eif4e*$^{+/-}$ cells (Figure 3.1F and Figure S3.2I). Although the majority of cap-dependent translation is thought to rely on eIF4E activity, reductions in eIF4E could also affect internal ribosomal entry site (IRES)-mediated translation (Macejak and Sarnow, 1991; Pyronnet et al., 2000). To address this question, we employed a unique transgenic mouse that stably expresses a bicistronic luciferase reporter for cap- and IRES-mediated translation in all tissues (CMV-HCV-IRES^{T}) (Bellodi et al., 2010; Hsieh et al., 2010). By assaying Rluc and Fluc expression, we find that *Eif4e*$^{+/-}$ mice are not impaired in either cap- or IRES-mediated translation and further demonstrate that reductions in eIF4E do not induce a switch from cap- to IRES-dependent translation (Figure 3.1G).

Eif4e haploinsufficiency during cellular transformation

We next asked if eIF4E expression levels are critical during stress conditions that impinge on protein synthesis, such as during the early steps downstream of oncogenic signaling (Barna et al., 2008; Stefanovsky et al., 2001). Oncogenic signaling is known to increase expression and phosphorylation of eIF4E and also lead to hyperphosphorylation and inactivation of the eIF4E inhibitor protein, 4EBP1 (Figure 3.2A-B) (Aoki et al., 2001; Furic et al., 2010; Rajasekhar et al., 2003; Rosenwald et al., 1993). Modest overexpression of an eIF4E transgene under the control of the ubiquitous β-actin promoter results in the formation of multiple cancer types and phosphorylation of eIF4E, at Ser209, has been shown to be critically required for tumorigenesis (Furic et al., 2010; Lazaris-Karatzas et al., 1990; Ruggero et al., 2004). In addition, overexpression and hyperactivation of eIF4E is a common feature of many human cancers (De Benedetti and Graff, 2004). Yet, it remains an outstanding question how changes in the levels of eIF4E expression lead to cellular transformation and whether this is mediated through control of either global or transcript-specific mRNA translation.

We first tested the ability of specific oncogenic insults, such as Ras and Myc as well as Ras and E1A, to transform primary *Eif4e*$^{+/-}$ mouse embryonic fibroblasts (MEFs) under conditions where eIF4E is genetically reduced by 50%. Notably, *Eif4e*$^{+/-}$ MEFs show a consistent 50% reduction in eIF4E expression levels even upon oncogenic insult and, similar to steady state, no compensation is observed with respect to eIF4E phosphorylation, expression or phosphorylation of 4EBP1, or any other component of the eIF4F initiation complex (Figure 3.2A-B). Additionally, no differences are observed in cell size or in expression of the driving oncogenes in *Eif4e*$^{+/-}$ cells compared to WT (Figure 3.2C and Figure S3.3A). Strikingly, *Eif4e*$^{+/-}$ MEFs are dramatically resistant to cellular transformation as measured by soft agar colony formation (Figure 3.2D and Figure S3.3B). In addition, this transformation defect can be ascribed specifically to reductions in eIF4E dose as soft agar colony growth is fully rescued by restoring eIF4E expression back to WT

levels (Figure 3.2D and Figure S3.3C). Thereby, eIF4E dose becomes critical under specific cellular stress condition such as during cellular transformation.

Profiling the oncogenic translation program

In order to gain insight into the underlying mechanism by which *Eif4e*$^{+/-}$ cells are resistant to cellular transformation, we next asked if eIF4E dose is critical for global protein synthesis during oncogenic transformation. Remarkably, although oncogenic transformation leads to substantial increases in global protein synthesis relative to untransformed cells, *Eif4e*$^{+/-}$ MEFs show no difference in global protein synthesis rates in this setting (Figure S3.4A-B). We therefore asked whether eIF4E dose was important in regulating the expression of a specific subset of mRNAs integral to oncogenic transformation. We characterized the impact of oncogenic signaling on the translational landscape of gene expression by undertaking an unbiased translational profiling approach to monitor changes in poly-ribosomal associated mRNA and total transcript levels (Figure 3.3A and Table 3.3). By comparing the relative differences in the ratio of polysomal mRNA to total mRNA expression levels (termed translational efficiency), we identified 722 gene products that are translationally regulated by oncogenic transformation with Ras and Myc (Fold change >1.7, $p < 0.05$; Figure 3.3B and Appendix 1). Importantly, we find that the translation of a subset of 133 gene products is sensitive to eIF4E dose specifically during oncogenic transformation (Fold change >1.7, $p < 0.05$; Figure 3.3C, Figure S3.4C and Appendix 2). In order to better understand how eIF4E dose impacts expression of the translational program induced by oncogenic transformation, we next performed network analysis of the interactions of genes that were either translationally induced by transformation (Figure 3.3D and Figure S3.5A) or translationally repressed (Figure S3.5B). Strikingly, this analysis reveals that genes translationally regulated by transformation cluster into distinct associated nodes, including those involved in cell cycle control, signaling, cell-to-cell communication, cell adhesion, and protein homeostasis, and shows, moreover, that subsets of these mRNA become sensitive to eIF4E dose. Thus, employing

unbiased genome-wide translational profiling, this data demonstrates that eIF4E is required for a specific subset of mRNAs whose expression levels are translationally controlled upon oncogenic signaling, which we collectively term the 'oncogenic translational program'.

Since our network data analysis suggested that cellular transformation may promote the translation of distinct classes of mRNAs, we next performed gene set enrichment analysis (GSEA) to identify functional classes of genes whose translation is statistically enriched by cellular transformation and to evaluate their requirements for eIF4E dose (Mootha et al., 2003; Subramanian et al., 2005). This analysis revealed a large and diverse group of functional ontologies that were statistically enriched, including classes of genes known to be translationally regulated downstream of oncogenic signaling, such as cell cycle, apoptosis, ribosome biogenesis, and nucleotide biosynthesis (Appendices 3-4) (Cunningham et al., 2014; Hsieh et al., 2010; Hsieh et al., 2012; Stumpf et al., 2013). In line with our network interactome data, we find that eIF4E dose is critically required for the expression of a subset of functional classes of genes that are translationally induced by transformation. For example a 50% reduction of eIF4E significantly impacts the translation of genes involved in nucleotide biosynthesis, the proteasome, and cell signaling (Appendices 5-6).

Most strikingly, this analysis also revealed unexpected coordinate translational upregulation of genes involved in both the production of reactive oxygen species (ROS) and the regulation of ROS levels. Both oncogenic signaling and deregulated mitochondrial respiration of cancer cells can contribute to ROS generation and oncogenic stress (Irani et al., 1997; Sattler et al., 2000; Vafa et al., 2002; Wallace, 2012). The ability of cancer cells to modulate the dosage and duration of ROS production is vital for their growth and survival. Strikingly, mitochondrial oxidative phosphorylation, one of the main sources of cellular ROS (Balaban et al., 2005), is one of the functional classes most translationally enriched by transformation (Figure 3.4A, Figure S3.6A, and Appendix 7). Importantly, we also find enhanced translation of genes involved in detoxifying and regulating ROS levels, including glutathione metabolism genes, during cellular

transformation (Figure S3.6A-B, Appendix 8, and Appendix 9). Remarkably, eIF4E dose appears to be critical for select translation of mRNAs that control intracellular ROS levels during oncogenic transformation but not for mRNAs associated with oxidative phosphorylation (Appendices 5-6). In order to better understand the requirements for eIF4E in translational control of this novel class of genes, we next expanded our functional analysis to more broadly examine genes involved in the regulation and response to ROS and could identify 99 genes whose translation was induced upon oncogenic transformation (Figure 3.4B, Figure S3.6C, and Appendix 10). Strikingly, we observe that a large fraction, 26, of these genes are sensitive to eIF4E dose (Figure 3.4C, Figure S3.6D, and Appendix 11), including the ferritin heavy chain (Fth1), the catalytic subunit of glutamate-cysteine ligase (Gclc), and lamin B1 (Lmnb1) (Figure 3.4D-E) (Malhas et al., 2009; Pham et al., 2004; Shi et al., 2000). Moreover, we find that this class of genes is significantly reduced in *Eif4e*$^{+/-}$ cells only upon cellular transformation (Figure S6E-F). Thus, this analysis identifies groups of functional gene classes whose translation is induced by transformation in an eIF4E-dependent manner, including a novel class of mRNAs involved in the response to oxidative stress.

A Novel 5'UTR Signature of eIF4E-dependent mRNAs

It has been previously proposed that long 5'UTRs and complex secondary structures embedded within them, revealed by high GC content and low free energies, render certain transcripts sensitive to eIF4E activity (Koromilas et al., 1992; Pickering and Willis, 2005). Importantly, we observe that the 5'UTR activity of eIF4E target mRNAs, such as Fth1 and Lmnb1, are sensitive to reductions in eIF4E expression levels (Figures 3.5A-B). Surprisingly, however, we see no major differences in 5'UTR length, GC content, or free energy in eIF4E translational targets compared to the whole genome (Figure 3.5C). This suggests that additional features of specific 5'UTRs may sensitize them to changes in eIF4E expression levels. In order to identify potential cis-acting regulatory elements that may confer sensitivity to eIF4E dose during oncogenic transformation,

we performed an unbiased Multilpe Em for Motif Elicitation (MEME) search for the presence of sequence-specific motifs in the 5'UTRs of eIF4E sensitive mRNAs (Bailey and Elkan, 1994). This analysis identified a unique cytosine-rich 15-nucleotide motif that we have termed the Cytosine Enriched Regulator of Translation (CERT) domain (Figure 3.5D and Appendix 12). This motif is present in nearly 70% of eIF4E target mRNAs and is preferentially enriched (81%, $p<0.05$) in subsets of eIF4E targets increased by oncogenic transformation, including oxidative stress response genes like Fth1 (Figure 3.5D and Appendix 13). Notably, the CERT domain is located on average 143 nucleotides downstream of the 5'cap and 146 nucleotides upstream of the AUG start codon and can be present at multiple copies within the 5'UTR of target genes. Collectively, these data demonstrate remarkable translational reprogramming of genes involved in control of ROS upon oncogenic transformation that are sensitized to eIF4E dose and are marked by the presence of a unique 5'UTR cis-acting motif.

eIF4E dependent control of ROS during oncogenic transformation and *in vivo* tumorigenesis

Given the unexpected functional role for eIF4E in the expression of genes involved in the control of reactive oxygen species during oncogenic transformation, we next examined the ability of *Eif4e*$^{+/-}$ cells to regulate and respond to ROS. The ability to recognize and detoxify ROS is critical for the process of oncogenic transformation (DeNicola et al., 2011; Schafer et al., 2009). In particular, the accumulation of ROS is associated with the high proliferative capacity and altered mitochondrial respiration of cancer cells and needs to be detoxified in order to maintain tumor growth (Irani et al., 1997; Raj et al., 2011; Trachootham et al., 2006). Notably, in line with decreases in translation of ROS target genes, *Eif4e*$^{+/-}$ cells display elevated levels of intracellular reactive oxygen species during oncogenic insult driven by overexpression of Ras and Myc (Figure 3.6A). Importantly, we find that *Eif4e*$^{+/-}$ transformed cells are significantly more sensitive to the addition of exogenous ROS (Figure 3.6B). Indeed, they undergo programmed cell death under

anchorage independent growth conditions known to induce the accumulation of ROS (Figure 3.6C), suggesting that eIF4E is required to maintain accurate levels of ROS downstream of oncogenic signaling compatible with cancer cell survival. To extend these findings to specific genes that control ROS levels, we examined the role of Fth1 during the process of oncogenic transformation. Fth1 is one of the genes whose translation is most significantly enhanced by oncogenic signaling and is highly sensitized to eIF4E expression levels (Figures 3.4D-E). Fth1 is an iron storage protein that possesses an intrinsic ferroxidase activity, which allows it to neutralize toxic reactive oxygen species (Pham et al., 2004). We find that knockdown of Fth1 is sufficient to inhibit oncogenic transformation and mirrors the resistance to cellular transformation observed in *Eif4e*$^{+/-}$ cells (Figures 3.6C-D and Figures S3.7A-E). Therefore, we asked if the inability to regulate ROS underlies the transformation defect observed in *Eif4e*$^{+/-}$ cells. Remarkably, we demonstrate that addition of the antioxidant N-acetyl Cysteine (NAC) is able to significantly restore the tumorigenic potential of *Eif4e*$^{+/-}$ cells (Figure 3.6E and Figure S3.7F).

We next tested the requirements for eIF4E dose in the setting of *in vivo* tumorigenesis driven by endogenous expression of oncogenic KRas. Importantly, the ability to properly respond to and control ROS is critical for lung cancer driven by endogenous expression of oncogenic KRas (DeNicola et al., 2011; Raj et al., 2011; Sayin et al., 2014). Thus, we asked what effect genetically reducing eIF4E dose by 50% would have in the *KRas*^{LA2} model of lung cancer (Figure 3.7A) (Johnson et al., 2001). We find that limiting eIF4E levels has a dramatic effect on KRas-driven tumor initiation as revealed by a significant reduction in tumor number by 12 weeks of age in *Eif4e*$^{+/-}$ mice (Figure 3.7B). Strikingly, this manifests in a more than two-fold reduction in tumor burden in *Eif4e*$^{+/-}$ mice at one year of age (Figures 3.7C-D). Importantly, we find that reductions in tumor burden and tumor number are significantly correlated with markers of oxidative stress (Figure 3.7E). Moreover, we demonstrate that expression of eIF4E-dependent ROS target genes, such as Fth1 and Gclc, is significantly reduced in tumors of *Eif4e*$^{+/-}$ mice (Figure 3.7F), further revealing that eIF4E is critically required for the control of reactive oxygen species downstream

of cellular transformation *in vivo*. Together, these data reveal that *Eif4e* dose becomes critical during tumorigenesis and delineate a novel eIF4E-dependent translational program underlying regulation and response to ROS during cellular transformation.

Figures

Figure 3.1: A 50% reduction in eIF4E dose is compatible with normal *in vivo* development and protein synthesis. A) Cartoon demonstrating the current dogma of eIF4E as quantitatively limiting for protein synthesis. “7MG” denotes the 5’ 7-methylguanosine cap. “eIFs” denotes a group of eukaryotic initiation factors that promotes the association of eIF4E with the 40S ribosomal subunit. B) Gross morphology of WT and *Eif4e*$^{+/-}$ E15.5 embryos. C) Representative western blots for eIF4E protein levels in adult tissues of WT and *Eif4e*$^{+/-}$ mice. D) Quantitative polymerase chain reaction (qPCR) analysis of eIF4E mRNA levels in fetal (E11.5) and adult tissues. E) Global protein synthesis measured by ^{35}S methionine/cysteine incorporation in WT and *Eif4e*$^{+/-}$ MEFs. F) Polysome profiles of primary WT and *Eif4e*$^{+/-}$ MEFs. G) Cap and IRES dependent translation measured by luciferase activity in MEFs derived from the CMV-HCV-IRES^{T} dual luciferase reporter mouse. All results are representative of at least three independent experiments.

Figure 3.2: eIF4E is haploinsufficient for oncogenic transformation. A) Representative western blots for eIF4F complex members and regulators in WT and *Eif4e*$^{+/-}$ MEFs before and after overexpression of HRas^{G12D} and Myc. B) Quantification of eIF4E phosphorylation levels relative to total eIF4E in WT MEFs. C) Analysis of forward-scattered light (FSC) as a relative measurement of cell size in transformed WT and *Eif4e*$^{+/-}$ MEFs. D) Soft agar colony formation as a measure of oncogenic transformation by the overexpression of HRas^{G12D} and Myc in WT and *Eif4e*$^{+/-}$ MEFs with and without the rescue of eIF4E back to WT levels (average WT vector colony

number = 115). Asterisks indicate a statistically significant change (*= p<0.05, **= p<0.01). All results are representative of at least three independent experiments.

Figure 3.3: eIF4E is required for expression of the oncogenic translational program. A) Representative polysome profiles of transformed and untransformed WT and *Eif4e*$^{+/-}$ MEFs used for translational profiling by polysomal microarray. B) Changes in total RNA and polysome associated RNA in WT MEFs upon oncogenic transformation by HRas^{G12D} and Myc. Green points indicate genes with a fold change in translation efficiency (polysomal/total RNA) greater than 1.7 fold, p<0.05. C) Changes in translation efficiency induced by transformation in WT and *Eif4e*$^{+/-}$ MEFs. Red points indicate genes whose translation efficiency is reduced in *Eif4e*$^{+/-}$ MEFs relative to WT MEFs during oncogenic transformation (>1.7 fold decrease in TE, p<0.05). D) Interactome map of genes whose translation is increased upon transformation in WT MEFs. Pink nodes represent genes whose translation is sensitive to eIF4E dose.

Figure 3.4: eIF4E is critical for the translation of distinct functional classes of mRNAs induced by oncogenic transformation. A) GSEA analysis demonstrating enrichment for genes involved in oxidative phosphorylation (KEGG, FDR<0.01). B) GSEA analysis demonstrating enrichment for a broad class of genes involved in the regulation and response to oxidative stress, including subclasses such as glutathione metabolism (see Appendix 10) (FDR<0.01). C) GSEA analysis demonstrating *Eif4e*$^{+/-}$ MEFs are defective in a subset of translationally regulated genes involved in the regulation and response to oxidative stress (see Appendix 11) (FDR <0.01). Top 15 genes with the highest enrichment scores are shown for A, B, and C (red represents a relative increase and blue represents a relative decrease in a given gene). D) Western blot validation of genes involved in the regulation and response to oxidative stress. E) qPCR analysis of eIF4E target mRNA levels in untransformed and transformed WT and *Eif4e*$^{+/-}$ MEFs. Asterisks indicate a statistically significant change from WT samples (*= p<0.05, **= p<0.01). All results are

representative of experiments from at least three sets of independently isolated primary and transformed WT and *Eif4e*$^{+/-}$ cells.

Figure 3.5: The 5'UTR confers translational sensitivity to eIF4E target mRNAs. A) Diagram of the 5'UTR luciferase reporter assay. B) Requirements for eIF4E in 5'UTR mediated translation of target mRNAs (Fth1 and Lmnb1) and control mRNAs (Gapdh and B2M) by 5'UTR luciferase reporter assay in transformed MEFs. "pGL3" denotes the test vector lacking a 5'UTR. Results are normalized to 5'UTR reporter activity in transformed WT cells ± SEM. C) Comparison of canonical 5'UTR features between all mouse genes and the subset whose translation efficiency is reduced in *Eif4e*$^{+/-}$ during oncogenic transformation. D) Consensus sequence and enrichment value (E-value) of the Cytosine Enriched Regulator of Translation (CERT) motif identified by MEME analysis along with a diagram illustrating the frequency of eIF4E target mRNAs that contain a CERT. Asterisks indicate a statistically significant change (*= $p<0.05$, **= $p<0.01$). All results are representative of at least three independent experiments.

Figure 3.6: eIF4E-dependent control of reactive oxygen species is critical for cellular transformation. A) CM-H_2DCFDA fluorescence quantification by FACS as a relative measure of intracellular ROS levels in transformed WT and *Eif4e*$^{+/-}$ MEFs compared to transformed *Eif4e*$^{+/-}$ MEFs where eIF4E expression has been restored back to WT levels. (MFI = mean fluorescent intensity). B) Annexin V staining as a measure of apoptosis in response to the addition of exogenous ROS (2mM H_2O_2) to untransformed and transformed WT and *Eif4e*$^{+/-}$ MEFs. C) Apoptosis under adherent and non-adherent growth conditions (Poly-hema coated plates) in transformed WT and *Eif4e*$^{+/-}$ MEFs expressing either a non-targeting (n.t) shRNA or a Fth1 targeting shRNA. D) Quantification of soft agar colony formation as a measure of oncogenic transformation upon shRNA-mediated knock down of Fth1 (average WT n.t. shRNA colony number = 115). E) Restoration of oncogenic potential in *Eif4e*$^{+/-}$ MEFs upon addition of the antioxidant N-acetyl cysteine (NAC) as measured by soft agar colony formation (average WT

control colony number = 121). Asterisks indicate a statistically significant change from WT samples (*= p<0.05, **= p<0.01). All results are representative of at least three independent experiments.

Figure 3.7: eIF4E is required for lung tumorigenesis and regulation of the oxidative stress response *in vivo*. A) Cartoon outlining experimental mouse crosses used to test the requirements for eIF4E dose during *in vivo* lung tumorigenesis. B) Counts of superficial $KRas^{LA2}$ lung tumors in WT $KRas^{LA2}$ mice (n=11) and $Eif4e^{+/-}$ $KRas^{LA2}$ mice (n=10) at 12 weeks of age. C) Representative cross-section of lungs from 1 year old $KRas^{LA2}$ mice. D) Quantification of tumor burden (tumor area/ total lung area) in 1 year old $KRas^{LA2}$ mice (WT n=10 mice; $Eif4e^{+/-}$ n=5 mice). E) Quantification of the oxidative stress marker dityrosine in 12 week old lung tumors (WT n=3 tumors, $Eif4e^{+/-}$ n=3 tumors). F) Representative western blots of eIF4E ROS target gene expression and quantification in WT and $Eif4e^{+/-}$ $KRas^{LA2}$ tumors. Asterisks indicate a statistically significant change (*= p<0.05, **= p<0.01).

Figure 3.1

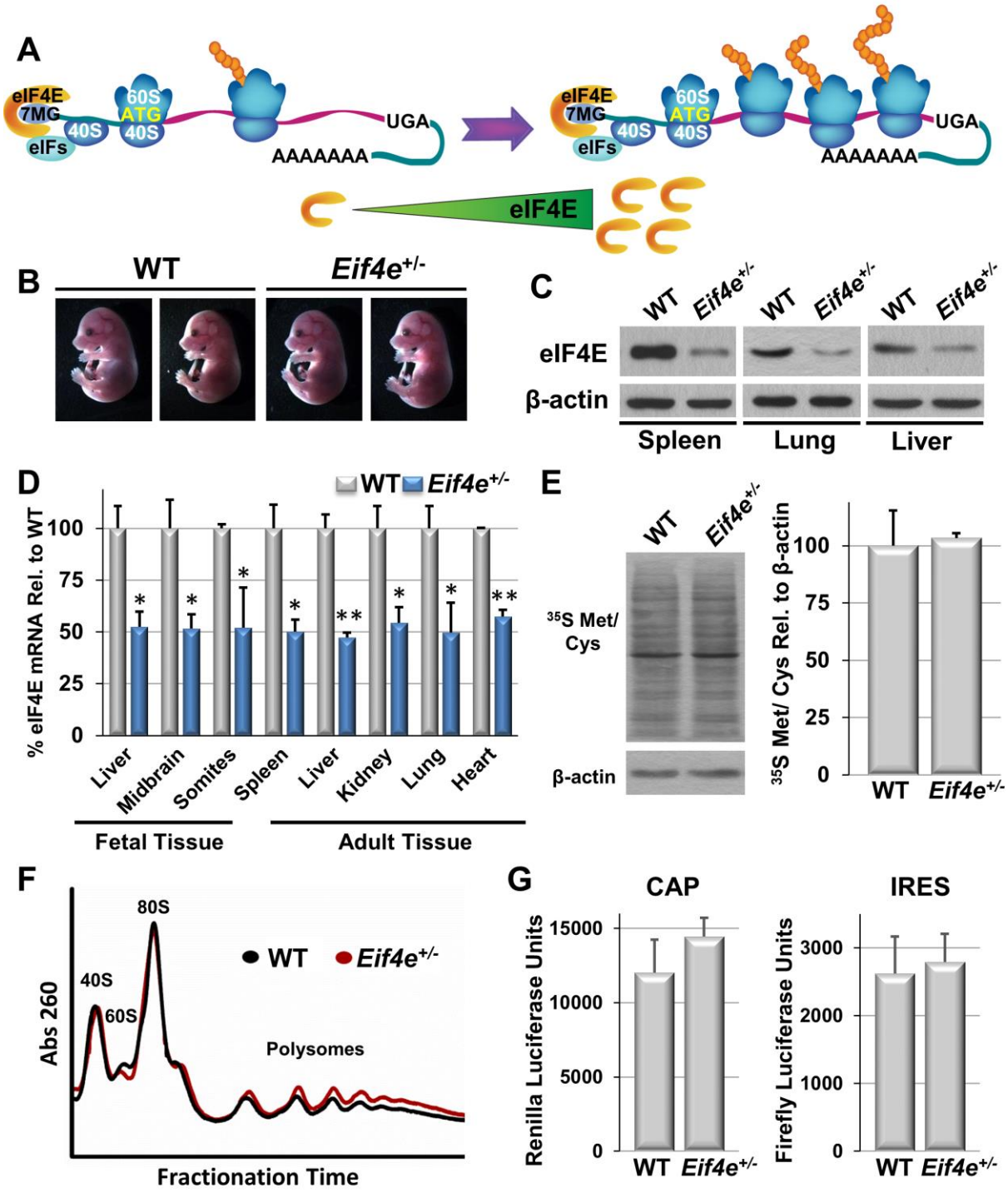
A
eIF4E
7MG
40S
eIFs
60S
ATG
40S
UGA
AAAAAAA
eIF4E
B
WT
Eif4e+/-
C
WT
Eif4e+/-
eIF4E
β-actin
Spleen
Lung
Liver
D
WT
Eif4e+/-
% eIF4E mRNA Rel. to WT
100
75
50
25
0
Liver
Midbrain
Somites
Spleen
Liver
Kidney
Lung
Heart
Fetal Tissue
Adult Tissue
E
WT
Eif4e+/-
35S Met/ Cys
β-actin
35S Met/ Cys Rel. to β-actin
F
80S
40S
60S
WT
Eif4e+/-
Polysomes
Abs 260
Fractionation Time
G
CAP
IRES
Renilla Luciferase Units
15000
10000
5000
0
Firefly Luciferase Units
3000
2000
1000
0
WT
Eif4e+/-

Figure 3.2

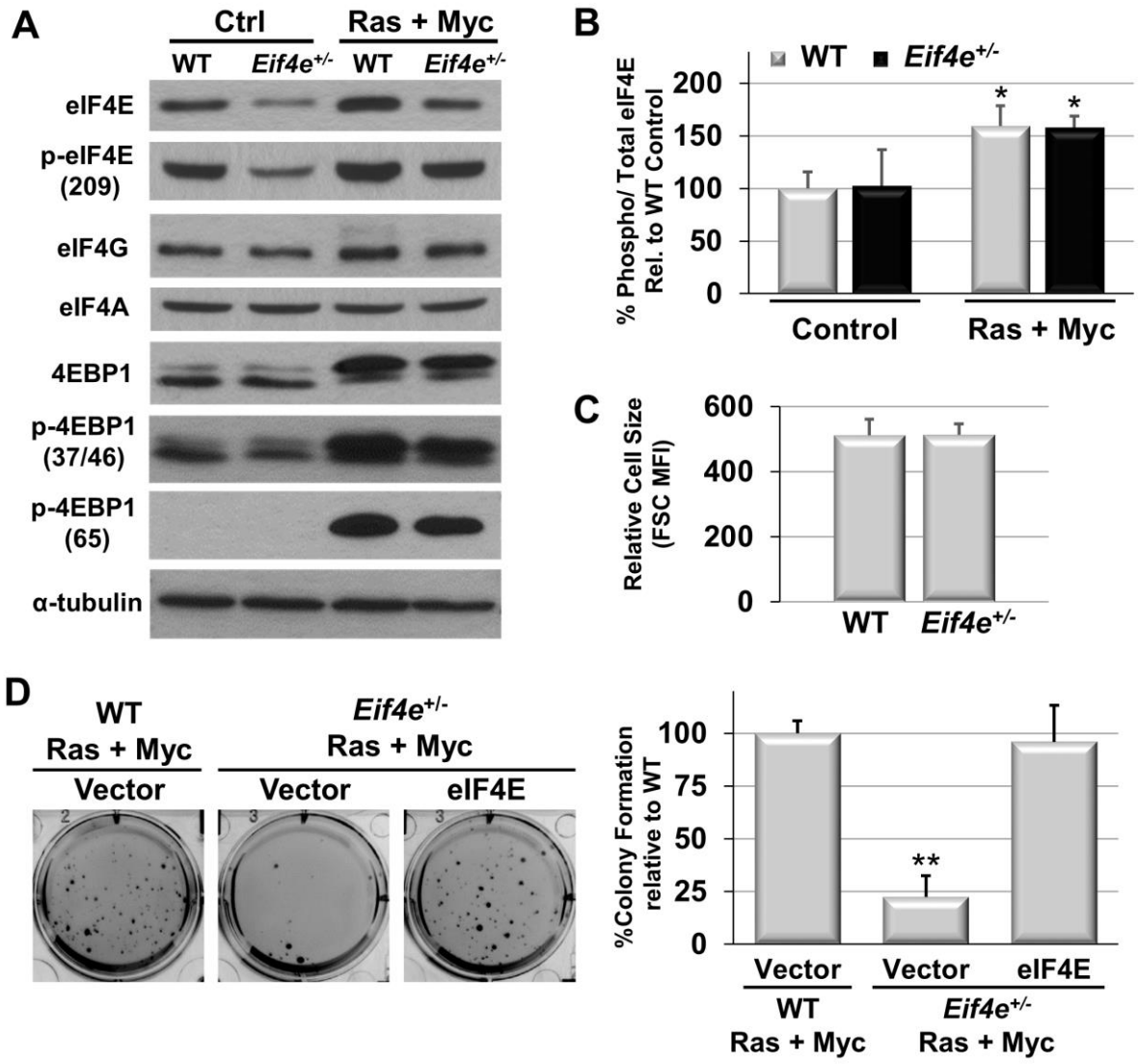
A
Ctrl
Ras + Myc
WT
Eif4e+/-
WT
Eif4e+/-
eIF4E
p-eIF4E (209)
eIF4G
eIF4A
4EBP1
p-4EBP1 (37/46)
p-4EBP1 (65)
α-tubulin
B
WT
Eif4e+/-
% Phospho/ Total eIF4E Rel. to WT Control
200
150
100
50
0
*
*
Control
Ras + Myc
C
Relative Cell Size (FSC MFI)
600
400
200
0
WT
Eif4e+/-
D
WT
Ras + Myc
Eif4e+/-
Ras + Myc
Vector
Vector
eIF4E
%Colony Formation relative to WT
100
75
50
25
0
**
Vector
Vector
eIF4E
WT
Ras + Myc
Eif4e+/-
Ras + Myc

Figure 3.3

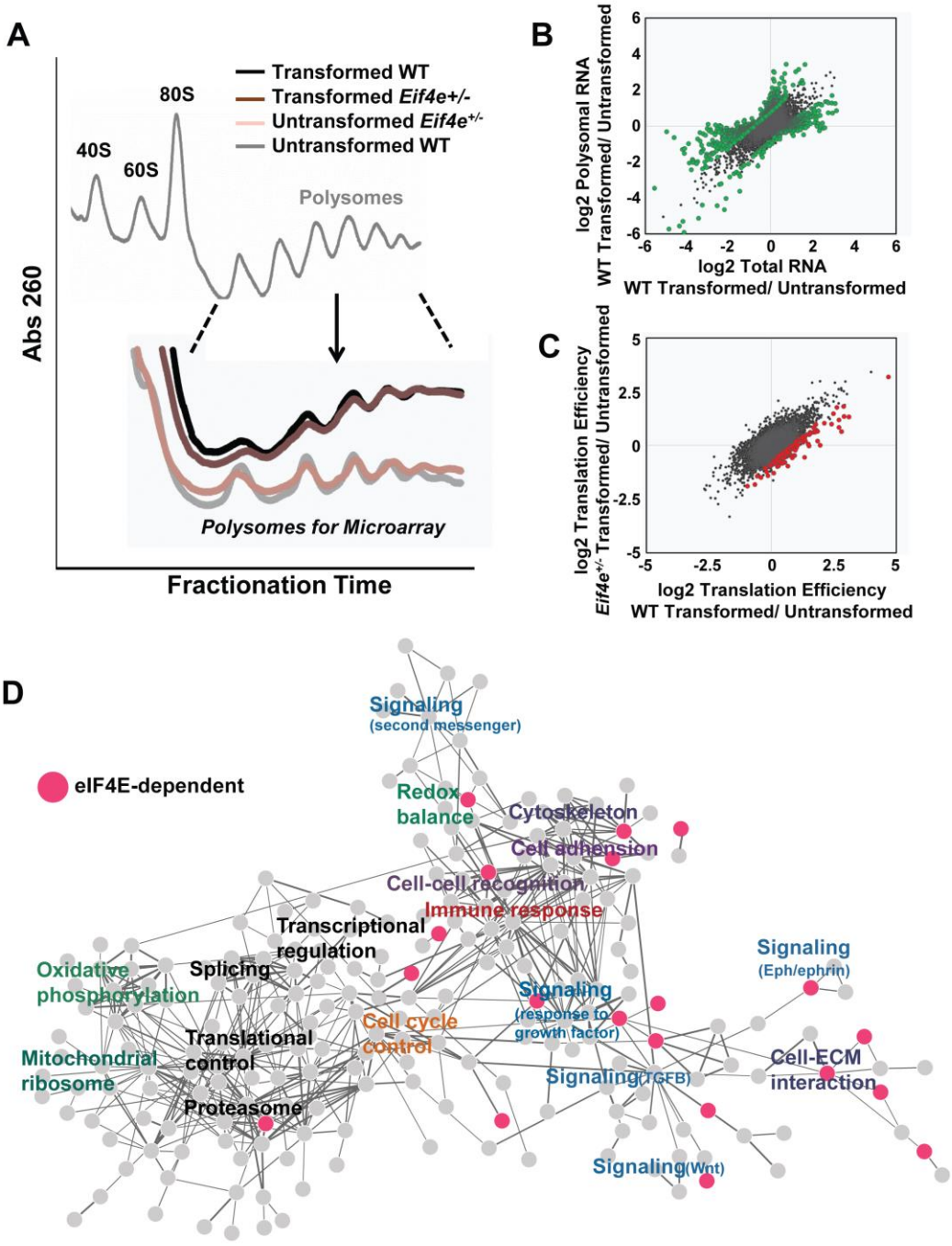
A
Transformed WT
Transformed Eif4e+/-
Untransformed Eif4e+/-
Untransformed WT
80S
40S
60S
Polysomes
Abs 260
Polysomes for Microarray
Fractionation Time
B
log2 Polysomal RNA
WT Transformed/ Untransformed
log2 Total RNA
WT Transformed/ Untransformed
C
log2 Translation Efficiency
Eif4e+/- Transformed/ Untransformed
log2 Translation Efficiency
WT Transformed/ Untransformed
D
eIF4E-dependent
Signaling
(second messenger)
Redox
balance
Cytoskeleton
Cell adhesion
Cell-cell recognition
Immune response
Transcriptional
regulation
Oxidative
phosphorylation
Splicing
Translational
control
Mitochondrial
ribosome
Proteasome
Cell cycle
control
Signaling
(response to
growth factor)
Signaling
(Eph/ephrin)
Cell-ECM
interaction
Signaling(TGFB)
Signaling(Wnt)

Figure 3.4

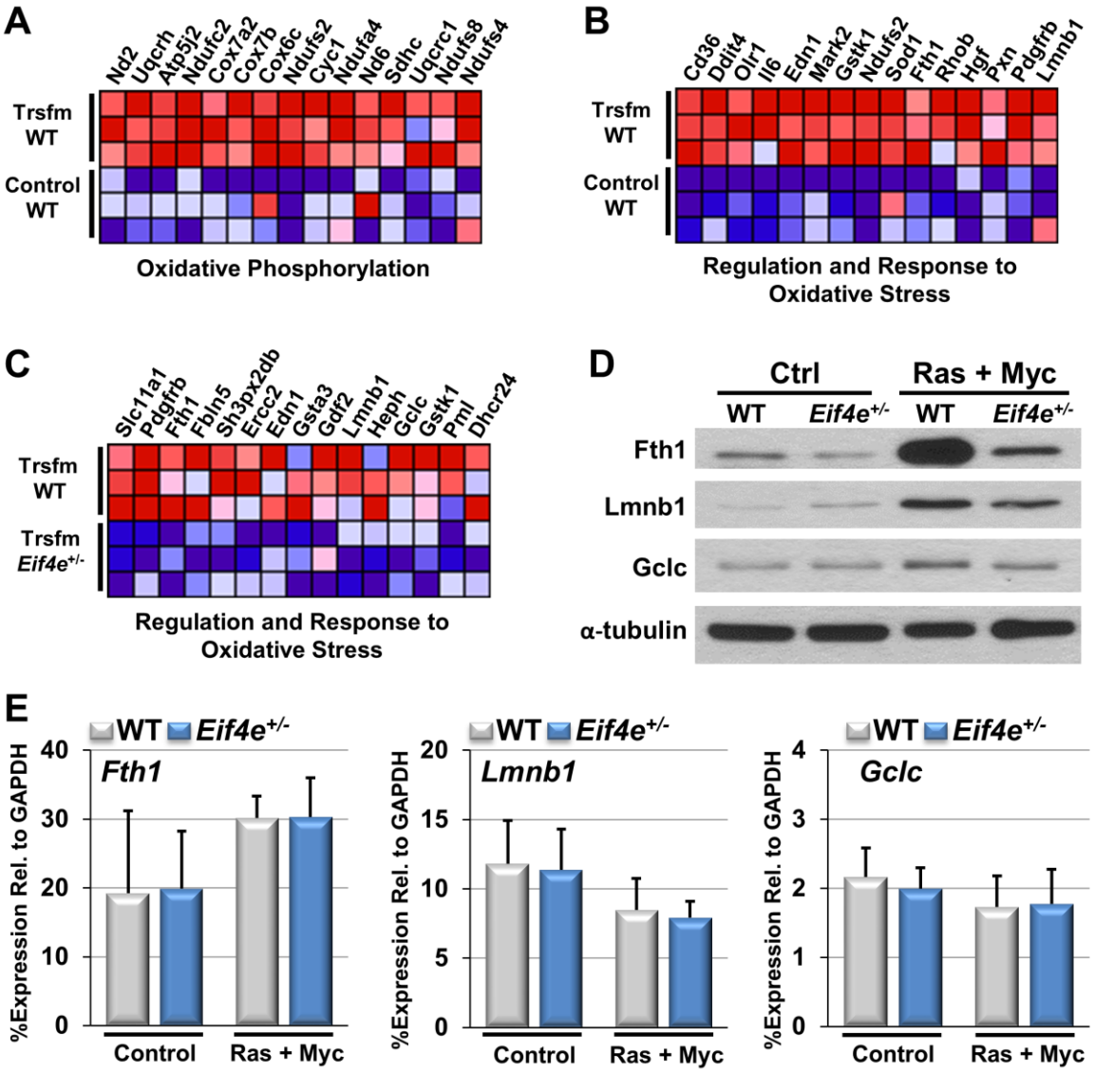
A
Nd2 Uqcrh Atp5j2 Ndufc2 Cox7a2 Cox7b Cox6c Ndufs2 Cyc1 Ndufa4 Nd6 Sdhc Uqcrc1 Ndufs8 Ndufs4
Trsfm WT
Control WT
Oxidative Phosphorylation
B
Cd36 Ddit4 Olr1 Il6 Edn1 Mark2 Gstk1 Ndufs2 Sod1 Fth1 Rhob Hgf Pxn Pdgfrb Lmnb1
Trsfm WT
Control WT
Regulation and Response to Oxidative Stress
C
Slc11a1 Pdgfrb Fth1 Fbln5 Sh3px2db Ercc2 Edn1 Gsta3 Gdf2 Lmnb1 Heph Gclc Gstk1 Pml Dhcr24
Trsfm WT
Trsfm Eif4e+/-
Regulation and Response to Oxidative Stress
D
Ctrl
Ras + Myc
WT
Eif4e+/-
WT
Eif4e+/-
Fth1
Lmnb1
Gclc
α-tubulin
E
WT Eif4e+/-
Fth1
%Expression Rel. to GAPDH
0 10 20 30 40
Control
Ras + Myc
WT Eif4e+/-
Lmnb1
%Expression Rel. to GAPDH
0 5 10 15 20
Control
Ras + Myc
WT Eif4e+/-
Gclc
%Expression Rel. to GAPDH
0 1 2 3 4
Control
Ras + Myc

Figure 3.5

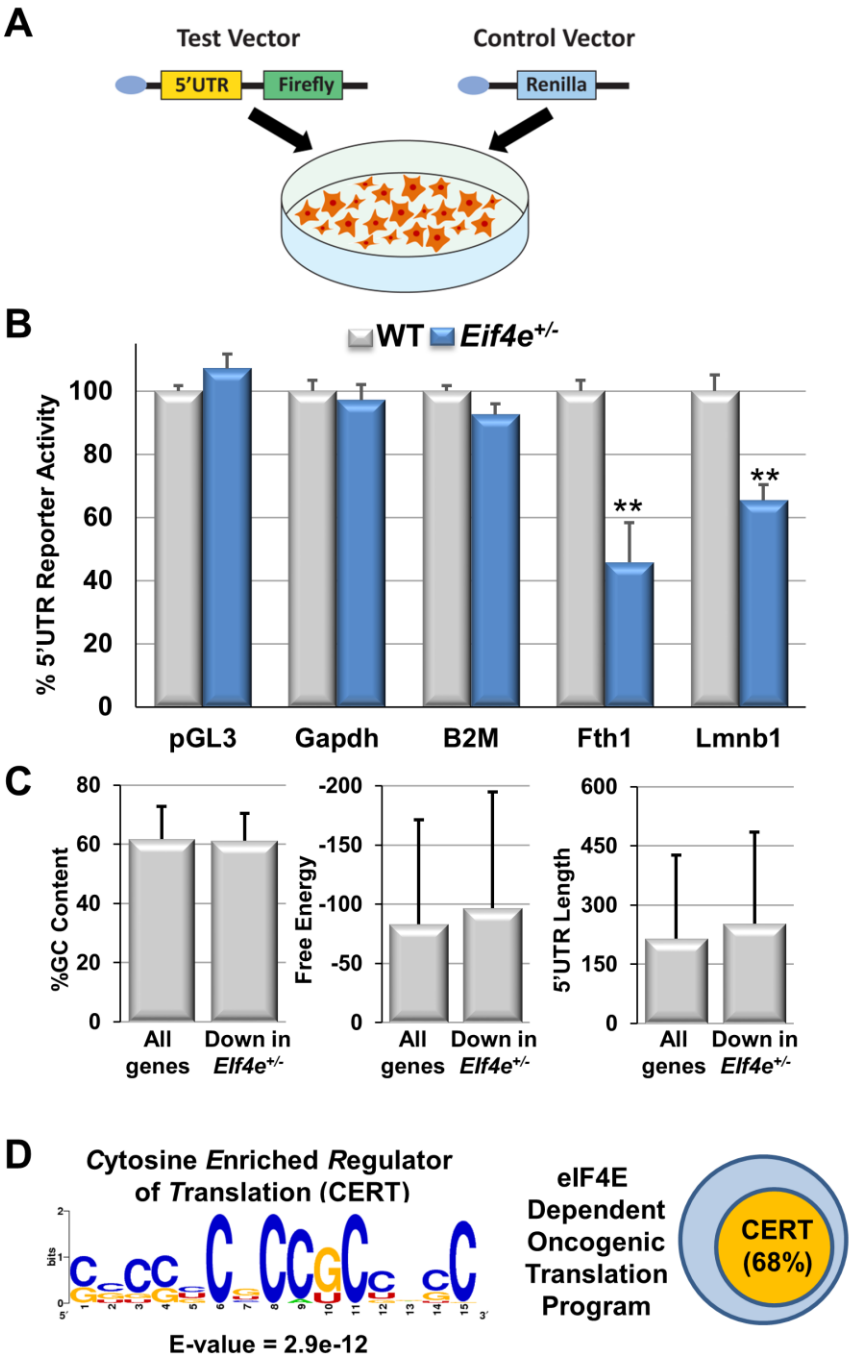
A
Test Vector
Control Vector
5'UTR
Firefly
Renilla
B
WT
Eif4e+/-
% 5'UTR Reporter Activity
100
80
60
40
20
0
**
**
pGL3
Gapdh
B2M
Fth1
Lmnb1
C
%GC Content
80
60
40
20
0
All genes
Down in Elf4e+/-
Free Energy
-200
-150
-100
-50
0
All genes
Down in Elf4e+/-
5'UTR Length
600
450
300
150
0
All genes
Down in Elf4e+/-
D
Cytosine Enriched Regulator of Translation (CERT)
bits
E-value = 2.9e-12
eIF4E Dependent Oncogenic Translation Program
CERT (68%)

Figure 3.6

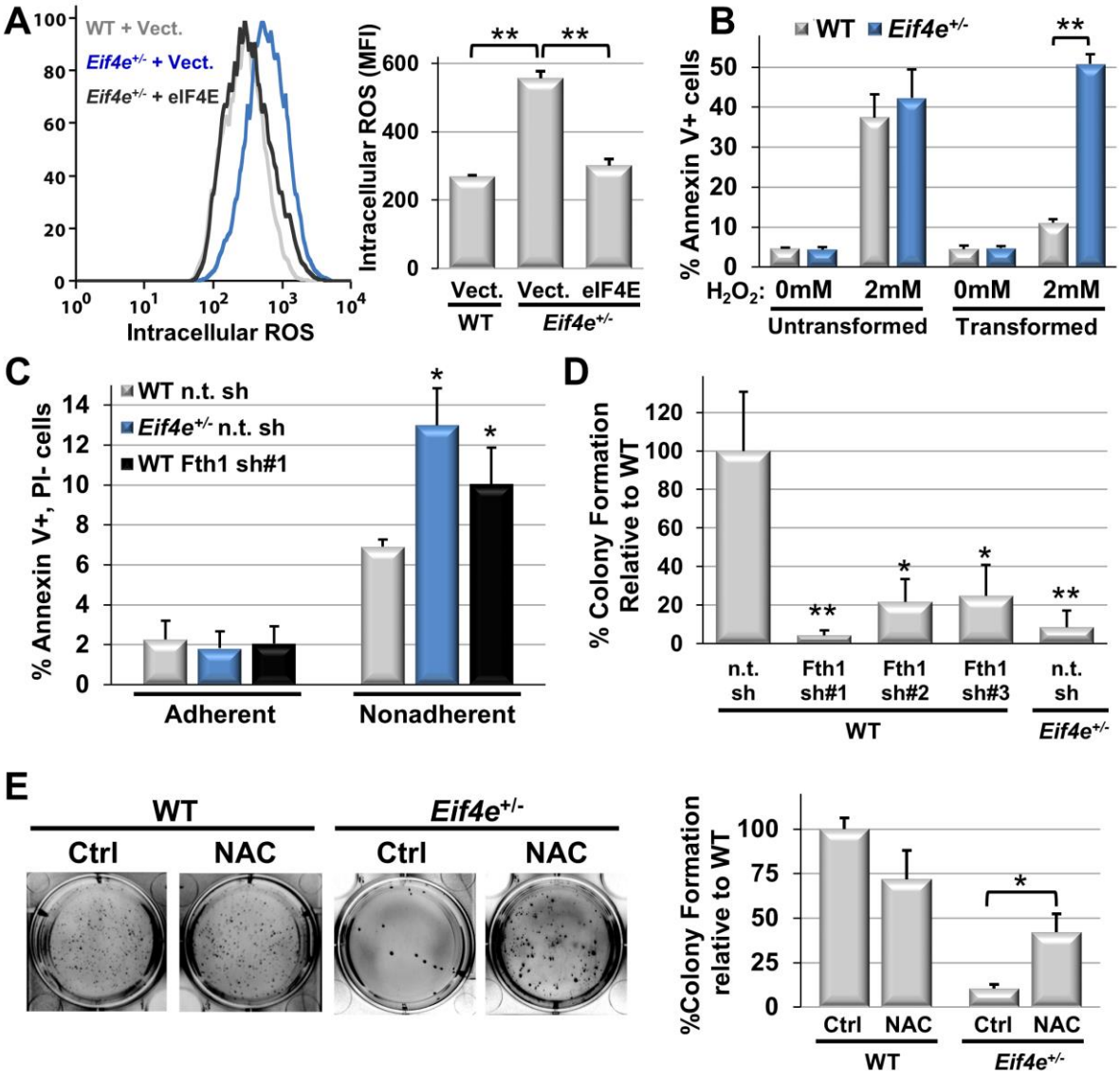
A
WT + Vect.
Eif4e+/- + Vect.
Eif4e+/- + eIF4E
Intracellular ROS
Intracellular ROS (MFI)
Vect.
Vect. eIF4E
WT
Eif4e+/-
B
WT
Eif4e+/-
% Annexin V+ cells
H2O2: 0mM 2mM 0mM 2mM
Untransformed
Transformed
C
WT n.t. sh
Eif4e+/- n.t. sh
WT Fth1 sh#1
% Annexin V+, PI- cells
Adherent
Nonadherent
D
% Colony Formation Relative to WT
n.t. sh
Fth1 sh#1
Fth1 sh#2
Fth1 sh#3
n.t. sh
WT
Eif4e+/-
E
WT
Eif4e+/-
Ctrl
NAC
Ctrl
NAC
%Colony Formation relative to WT
Ctrl
NAC
Ctrl
NAC
WT
Eif4e+/-

Figure 3.7

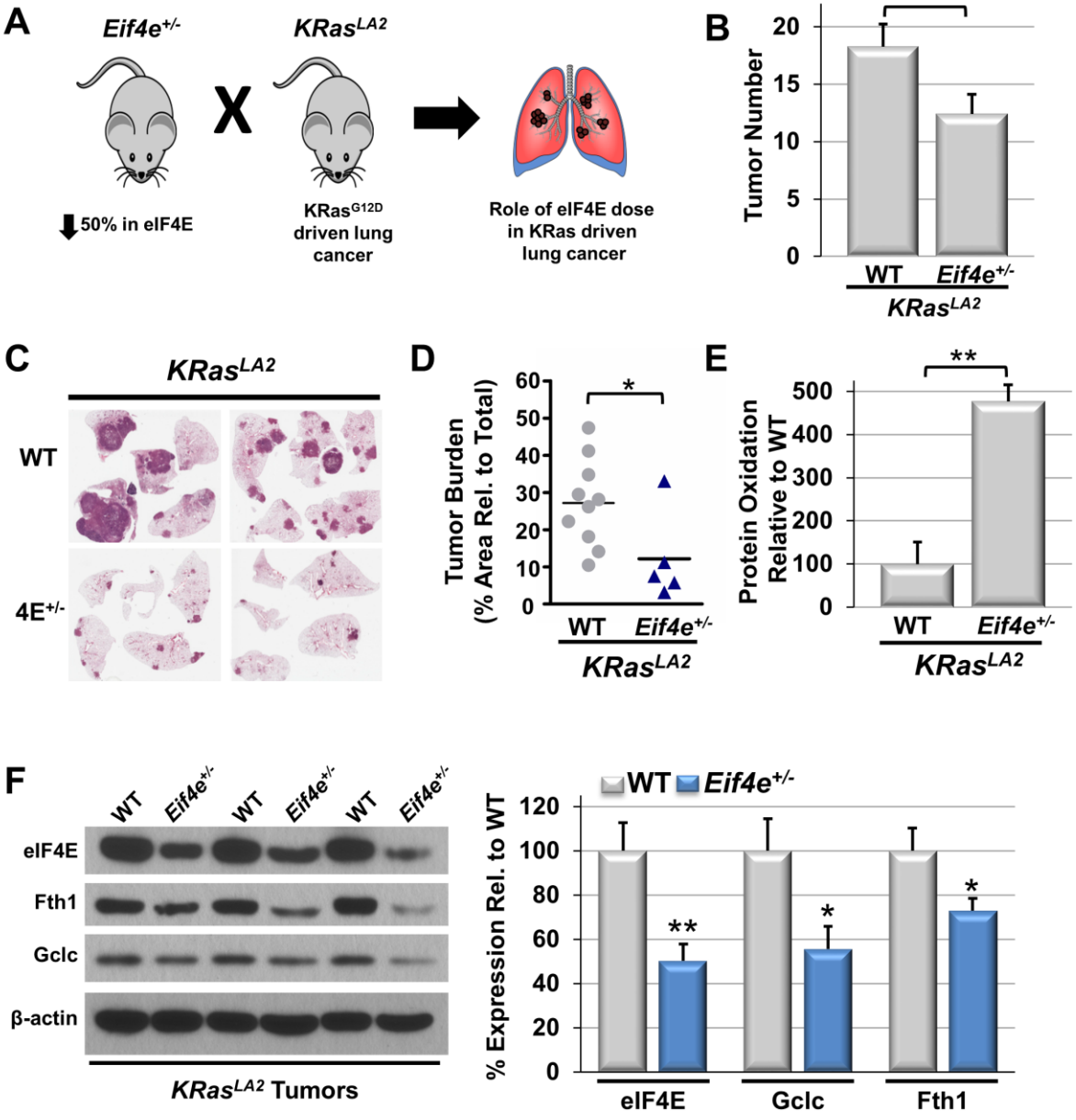
A
Eif4e+/-
KRasLA2
X
50% in eIF4E
KRasG12D driven lung cancer
Role of eIF4E dose in KRas driven lung cancer
B
Tumor Number
20
15
10
5
0
*
WT
Eif4e+/-
KRasLA2
C
KRasLA2
WT
4E+/-
D
Tumor Burden (% Area Rel. to Total)
60
50
40
30
20
10
0
*
WT
Eif4e+/-
KRasLA2
E
Protein Oxidation Relative to WT
500
400
300
200
100
0
**
WT
Eif4e+/-
KRasLA2
F
WT
Eif4e+/-
WT
Eif4e+/-
WT
Eif4e+/-
eIF4E
Fth1
Gclc
β-actin
KRasLA2 Tumors
WT
Eif4e+/-
% Expression Rel. to WT
120
100
80
60
40
20
0
**
*
*
eIF4E
Gclc
Fth1

Supplemental Figure 3.1: Generation of *Eif4e* haploinsufficient mice. A) Diagrams of the wild-type *Eif4e* genetic locus, Gene Trap targeting vector, and *Eif4e* knock out (KO) allele. "EV" denotes EcoRV restriction sites used for southern blot validation of the Gene Trap insertion. B) Southern blot validation of the Gene Trap insertion using a probe against the region highlighted in panel A. C) Time-course comparing the average weight of WT and *Eif4e*$^{+/-}$ mice. D) Representative FACS plots showing immune cell populations (T-cells: CD3, CD4, CD8; B-cells: B220; and granulocytes/macrophages: CD11b, Gr1) in lymphoid organs of WT and *Elf4e*$^{+/-}$mice are identical.

Supplemental Figure 3.2: A 50% reduction in eIF4E protein levels is compatible with normal cellular function and protein synthesis rates A) H&E staining of adult tissues from WT and *Eif4E*$^{+/-}$ mice. B) FACS analysis of forward-scattered light (FSC) as a relative measurement of WT and *Elf4e*$^{+/-}$ MEF cell size. C) Annexin V staining as a measure of apoptosis in primary MEFs and B-cells from WT and *Eif4e*$^{+/-}$ mice. D) Cellular proliferation of primary WT and *Eif4e*$^{+/-}$ MEFs. E) Cell cycle analysis of primary B-cells from WT and *Eif4e*$^{+/-}$ mice. F) Western blot analysis and quantification of eIF4E protein levels in primary MEFs. G) Representative western blots for eIF4E protein levels in adult tissues. H) Global protein synthesis measured by ^{35}S methionine/cysteine incorporation in primary WT and *Eif4e*$^{+/-}$ B-cells. I) Polysome profiles of WT and *Eif4e*$^{+/-}$ primary B-cells. Asterisks indicate a statistically significant change from WT samples (*= $p<0.05$). All results are representative of at least three independent experiments.

Supplemental Figure 3.3: eIF4E dose is critical for cellular transformation. A) Representative western blots for Ras and Myc expression in WT and *Eif4e*$^{+/-}$ MEFs before and after overexpression of HRas^{G12D} and Myc. B) Soft agar growth of WT and *Eif4e*$^{+/-}$ MEFs upon overexpression of HRas^{G12D} and E1A (average WT colony number = 19). C) Western blot analysis of eIF4E rescue. Asterisks indicate a statistically significant change (*= $p<0.05$, **= $p<0.01$). All results are representative of at least three independent experiments.

Supplemental Figure 3.4: Translational requirements for eIF4E during cellular transformation. A) Global protein synthesis measured by ^{35}S methionine/cysteine incorporation in WT and *Eif4e*$^{+/-}$ MEFs transformed by the combination of HRas^{G12D} and Myc overexpression. B) Relative Cap and IRES luciferase activity in MEFs derived from the CMV-HCV-IRES^{T} dual luciferase reporter mouse upon the overexpression of HRas^{G12D} and Myc. C) Differences in total mRNA and polysome associated mRNA between primary WT and *Eif4e*$^{+/-}$ MEFs. Orange points indicate the two genes (A130049A11Rik and Olfr1487) whose translation is impaired in primary *Eif4e*$^{+/-}$ MEFs (>1.9 fold decrease in TE, $p<0.05$). Asterisks indicate a statistically significant change from WT samples (*= $p<0.05$).

Supplemental Figure 3.5: Network analysis of the oncogenic translation program. A) Interactome map with gene labels of mRNAs whose translation is increased upon transformation in WT MEFs (Corresponds to Figure 3.3D). Pink nodes represent genes whose translation is sensitive to eIF4E dose. B) Interactome map with gene labels of mRNAs whose translation is decreased upon transformation in WT MEFs.

Supplemental Figure 3.6: eIF4E dose is critical for translation of distinct functional classes of mRNAs. A) Enrichment scores for functional groups identified by GSEA analysis of mRNAs translationally induced by oncogenic transformation (corresponds to Figure 3.4A and Figure S3.6B). B) GSEA analysis demonstrating enrichment for distinct functional classes in genes whose translation is enhanced by oncogenic transformation (Glutathione metabolism, KEGG, FDR=0.044; Response to oxidative stress, GO biological process, FDR=0.043). Red represents a relative increase and blue represents a relative decrease in a given gene. Top 15 genes with the highest enrichment scores (ES) are shown. C) Enrichment scores for the group of genes involved in the regulation and response to oxidative stress during oncogenic transformation (corresponds to Figure 3.4B). D) Enrichment scores for the effect of eIF4E on the subset of translationally controlled genes involved in the regulation and response to oxidative stress

(corresponds to Figure 3.4F). E) Heatmaps of average translational efficiencies for transformed and untransformed WT and *Eif4e*$^{+/-}$ MEFs demonstrating that a 50% reduction in eIF4E does not impact the translation of the subset of genes involved in oxidative phosphorylation (corresponds to Figure 3.4A). F) Heatmaps of average translational efficiencies for transformed and untransformed WT and *Elf4e*$^{+/-}$ MEFs demonstrating that eIF4E is required for translation of genes involved in the regulation and response to oxidative stress specifically during oncogenic transformation (corresponds to Figure 3.4C).

Supplemental Figure 3.7: Functional requirements for translational control of ROS. A) Effect of Fth1 knock down on proliferation of untransformed WT MEFs. B) Effect of Fth1 knock down on cell-cycle distribution of transformed WT MEFs under steady-state growth conditions. C) Western blot analysis of Fth1 knock down using three independent shRNA constructs. D) Representative images of soft agar colony formation as a measure of oncogenic transformation upon shRNA-mediated knock down of Fth1 (corresponds to Figure 3.6D). E) Effect of rescuing Fth1 knock down on soft agar colony growth by overexpressing a shRNA resistant Fth1 mutant (average WT n.t. shRNA + vector colony number = 29). F) Western blot analysis of Fth1 upon treatment of WT and *Eif4e*$^{+/-}$ MEFs with 1mM NAC. Asterisks indicate a statistically significant change from WT samples (*= $p<0.05$, **= $p<0.01$). All results are representative of at least three independent experiments.

Figure S3.1

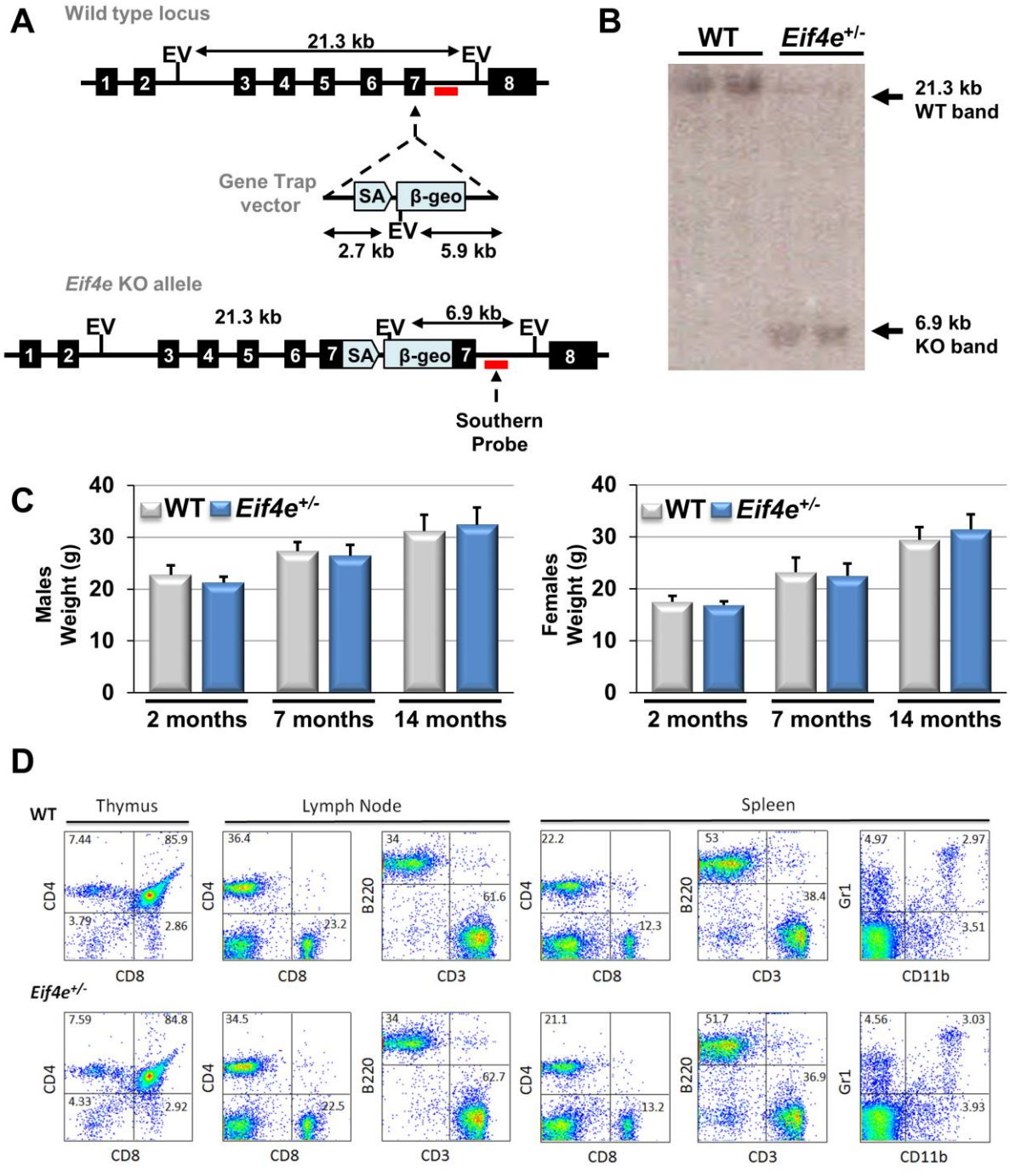
A
Wild type locus
EV
21.3 kb
EV
1 2 3 4 5 6 7 8
Gene Trap vector
SA β-geo
EV
2.7 kb
5.9 kb
Eif4e KO allele
EV
21.3 kb
EV
6.9 kb
EV
1 2 3 4 5 6 7 SA β-geo 7 8
Southern Probe
B
WT
Eif4e+/-
21.3 kb WT band
6.9 kb KO band
C
WT Eif4e+/-
Males Weight (g)
40
30
20
10
0
2 months
7 months
14 months
WT Eif4e+/-
Females Weight (g)
40
30
20
10
0
2 months
7 months
14 months
D
WT
Thymus
Lymph Node
Spleen
7.44
85.9
3.79
2.86
CD4
CD8
36.4
23.2
CD4
CD8
34
61.6
B220
CD3
22.2
12.3
CD4
CD8
53
38.4
B220
CD3
4.97
2.97
3.51
Gr1
CD11b
Eif4e+/-
7.59
84.8
4.33
2.92
CD4
CD8
34.5
22.5
CD4
CD8
34
62.7
B220
CD3
21.1
13.2
CD4
CD8
51.7
36.9
B220
CD3
4.56
3.03
3.93
Gr1
CD11b

Figure S3.2

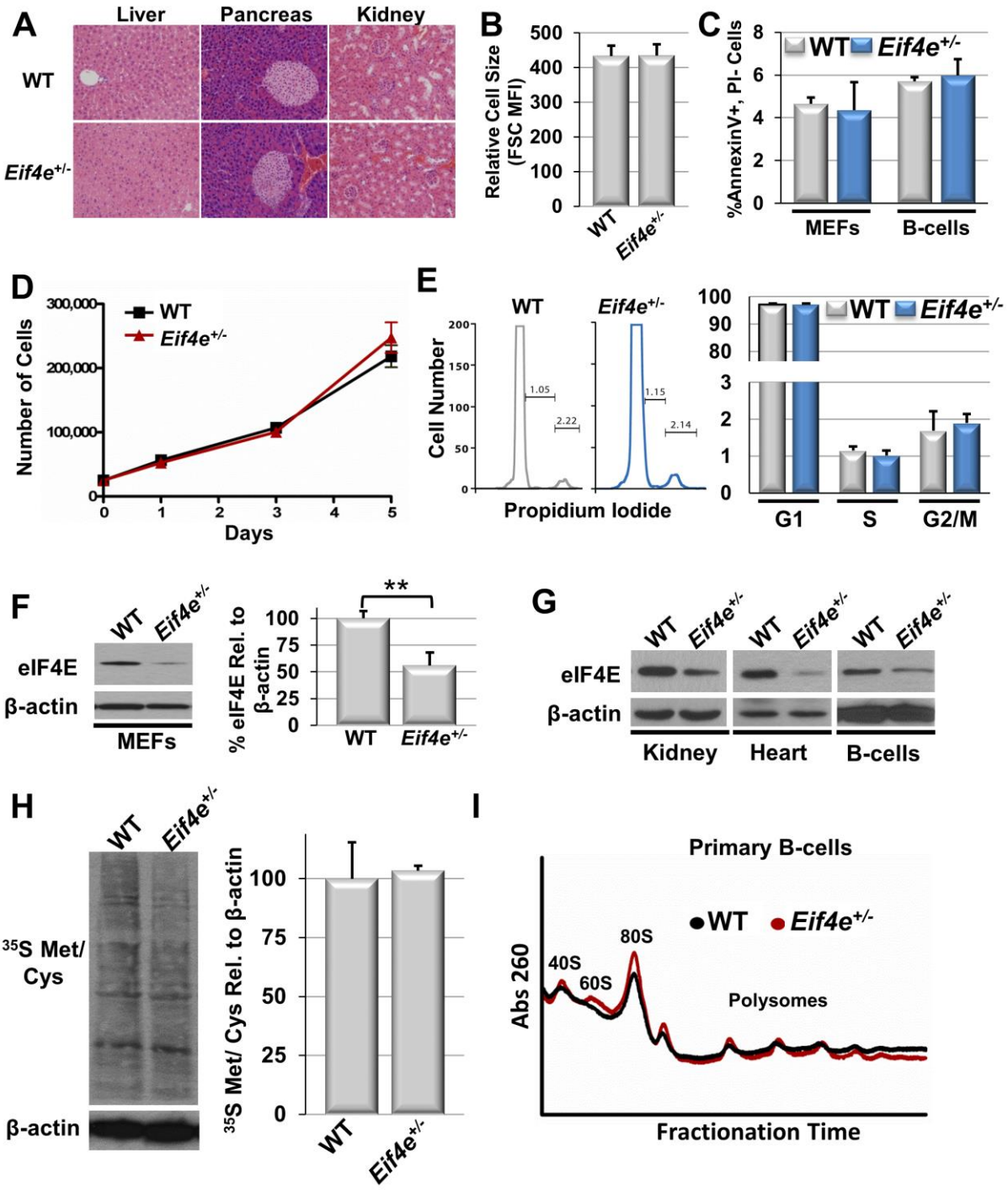
A
Liver
Pancreas
Kidney
WT
Eif4e+/-
B
Relative Cell Size (FSC MFI)
500
400
300
200
100
0
WT
Eif4e+/-
C
%AnnexinV+, PI- Cells
8
6
4
2
0
WT
Eif4e+/-
MEFs
B-cells
D
Number of Cells
300,000
200,000
100,000
0
WT
Eif4e+/-
0
1
2
3
4
5
Days
E
WT
Eif4e+/-
Cell Number
200
150
100
50
0
1.05
2.22
1.15
2.14
Propidium Iodide
100
90
80
3
2
1
0
WT
Eif4e+/-
G1
S
G2/M
F
WT
Eif4e+/-
eIF4E
β-actin
MEFs
% eIF4E Rel. to β-actin
100
75
50
25
0
**
WT
Eif4e+/-
G
WT
Eif4e+/-
WT
Eif4e+/-
WT
Eif4e+/-
eIF4E
β-actin
Kidney
Heart
B-cells
H
WT
Eif4e+/-
35S Met/ Cys
β-actin
35S Met/ Cys Rel. to β-actin
100
75
50
25
0
WT
Eif4e+/-
I
Primary B-cells
WT
Eif4e+/-
Abs 260
40S
60S
80S
Polysomes
Fractionation Time

Figure S3.3

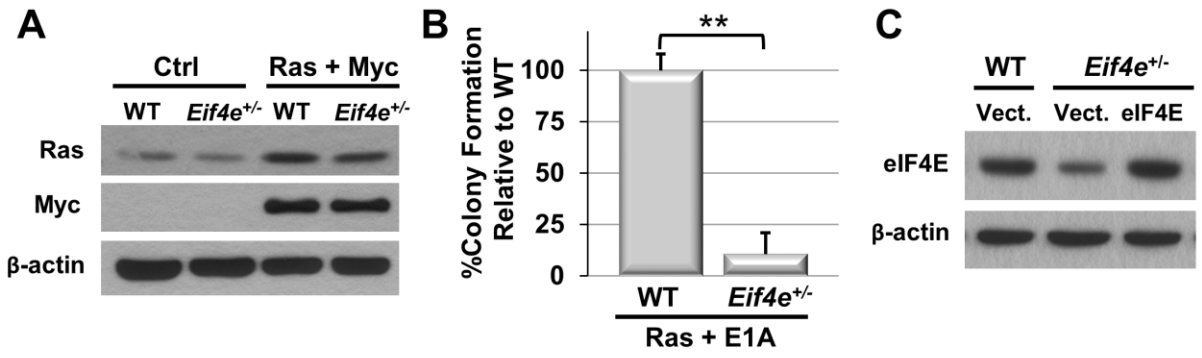
A
Ctrl
Ras + Myc
WT
Eif4e+/-
WT
Eif4e+/-
Ras
Myc
β-actin
B
**
%Colony Formation Relative to WT
100
75
50
25
0
WT
Eif4e+/-
Ras + E1A
C
WT
Eif4e+/-
Vect.
Vect.
eIF4E
eIF4E
β-actin

Figure S3.4

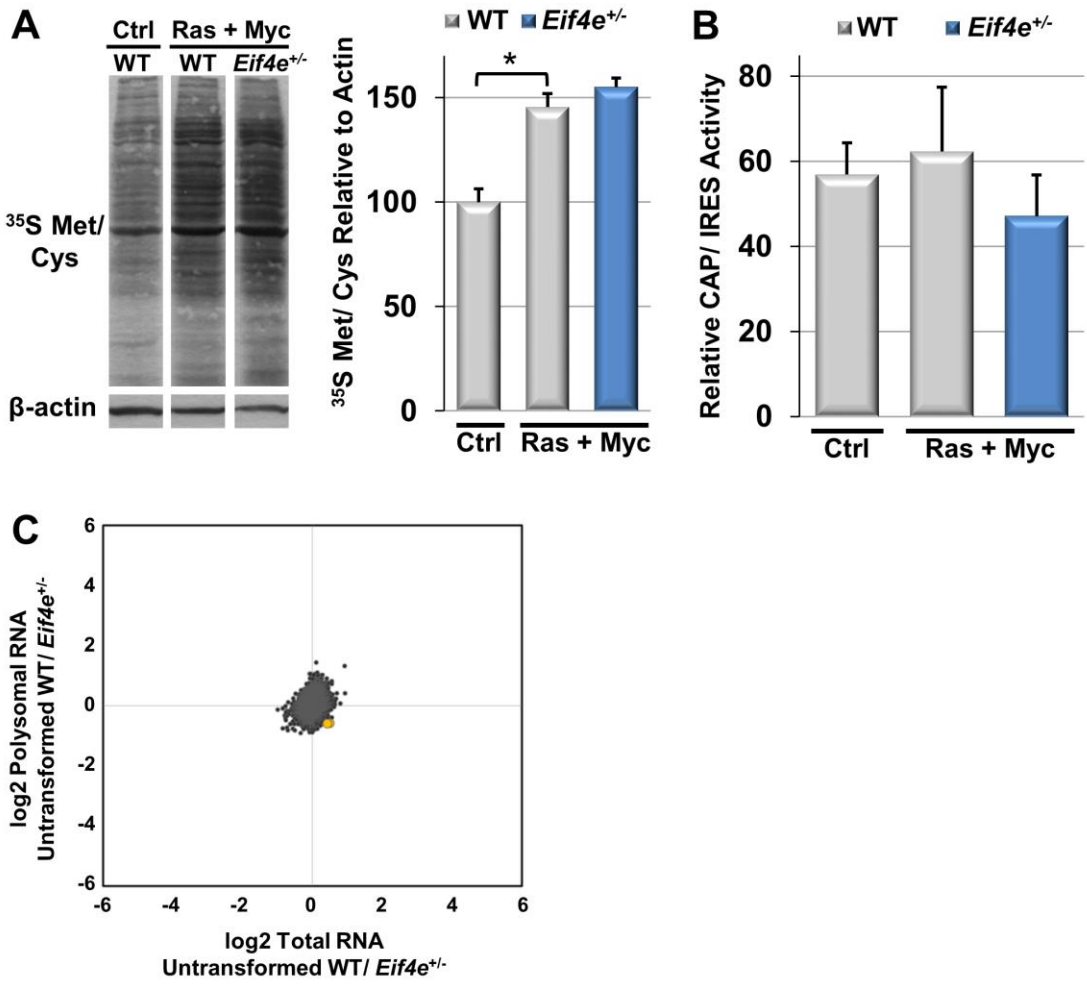
A
Ctrl
Ras + Myc
WT
WT
Eif4e+/-
35S Met/ Cys
β-actin
WT
Eif4e+/-
35S Met/ Cys Relative to Actin
150
100
50
0
*
Ctrl
Ras + Myc
B
WT
Eif4e+/-
Relative CAP/ IRES Activity
80
60
40
20
0
Ctrl
Ras + Myc
C
log2 Polysomal RNA Untransformed WT/ Eif4e+/-
6
4
2
0
-2
-4
-6
-6
-4
-2
0
2
4
6
log2 Total RNA Untransformed WT/ Eif4e+/-

Figure S3.5

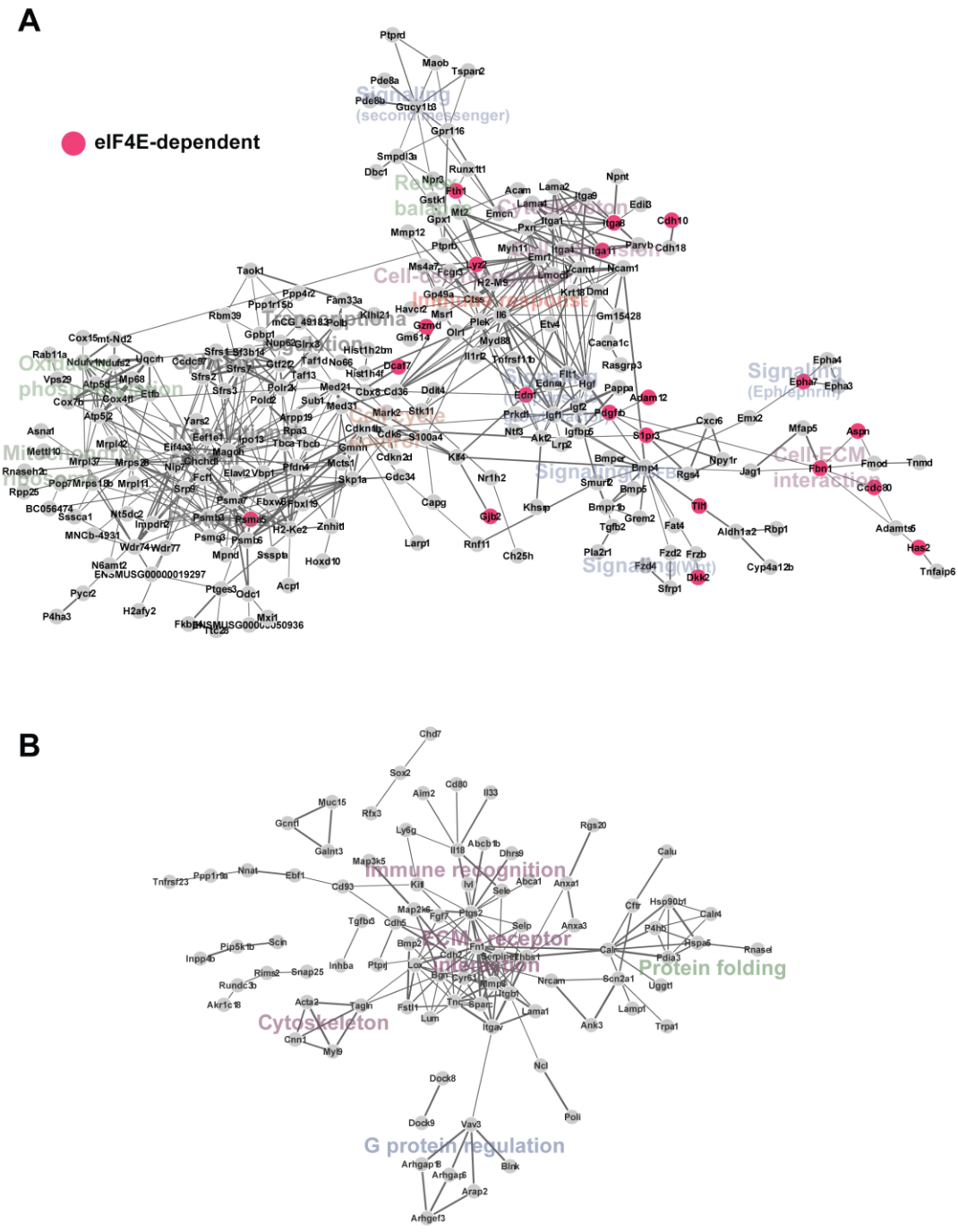
A
eIF4E-dependent
Immune recognition
ECM receptor interaction
Protein folding
Cytoskeleton
G protein regulation
B

Figure S3.6

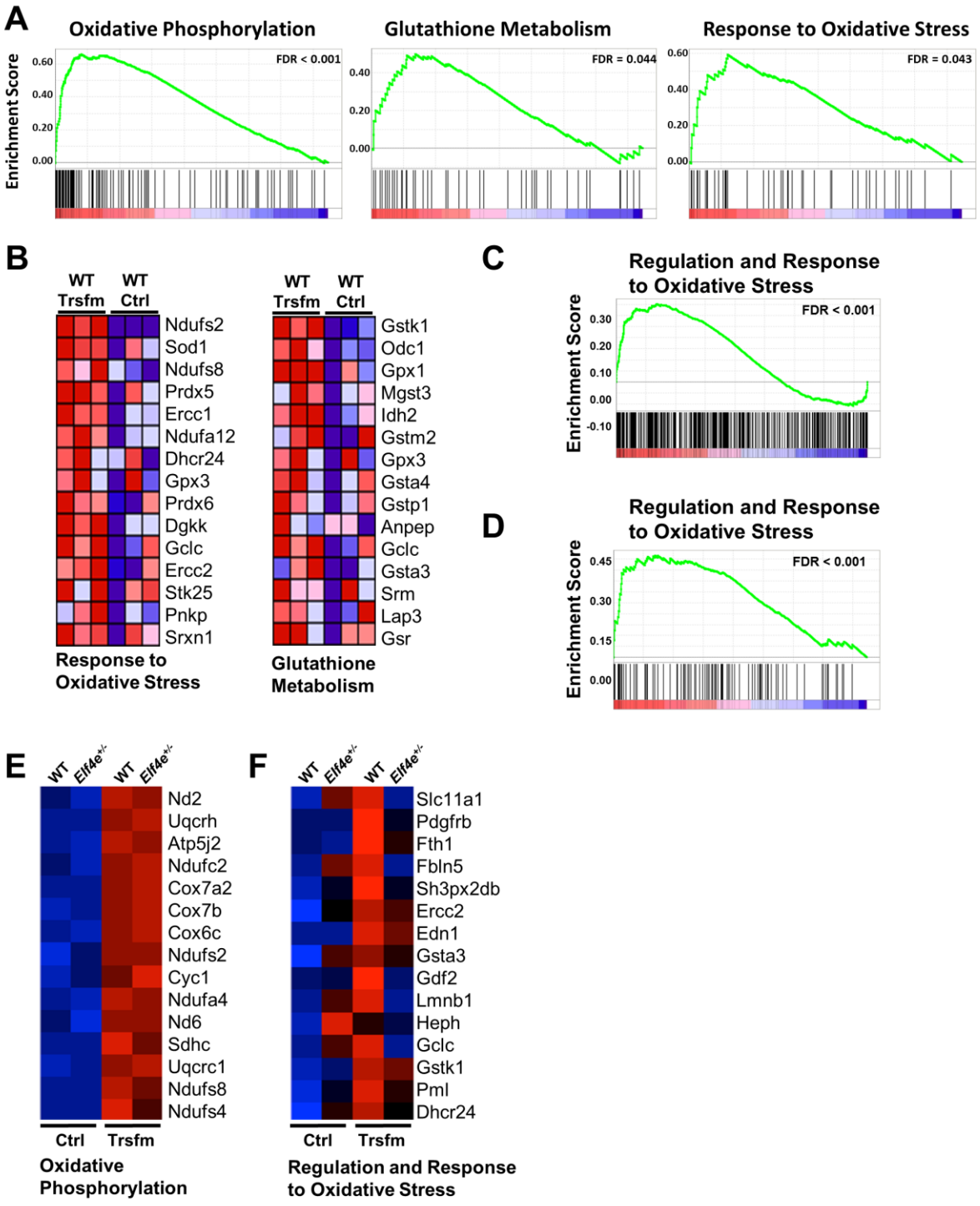
A
Oxidative Phosphorylation
Glutathione Metabolism
Response to Oxidative Stress
Enrichment Score
FDR < 0.001
FDR = 0.044
FDR = 0.043
B
WT Trsfm
WT Ctrl
Ndufs2
Sod1
Ndufs8
Prdx5
Ercc1
Ndufa12
Dhcr24
Gpx3
Prdx6
Dgkk
Gclc
Ercc2
Stk25
Pnkp
Srxn1
Response to Oxidative Stress
Gstk1
Odc1
Gpx1
Mgst3
Idh2
Gstm2
Gpx3
Gsta4
Gstp1
Anpep
Gclc
Gsta3
Srm
Lap3
Gsr
Glutathione Metabolism
C
Regulation and Response to Oxidative Stress
FDR < 0.001
D
Regulation and Response to Oxidative Stress
FDR < 0.001
E
WT
Elf4e+/-
Nd2
Uqcrh
Atp5j2
Ndufc2
Cox7a2
Cox7b
Cox6c
Ndufs2
Cyc1
Ndufa4
Nd6
Sdhc
Uqcrc1
Ndufs8
Ndufs4
Ctrl
Trsfm
Oxidative Phosphorylation
F
Slc11a1
Pdgfrb
Fth1
Fbln5
Sh3px2db
Ercc2
Edn1
Gsta3
Gdf2
Lmnb1
Heph
Gclc
Gstk1
Pml
Dhcr24
Regulation and Response to Oxidative Stress

Figure S3.7

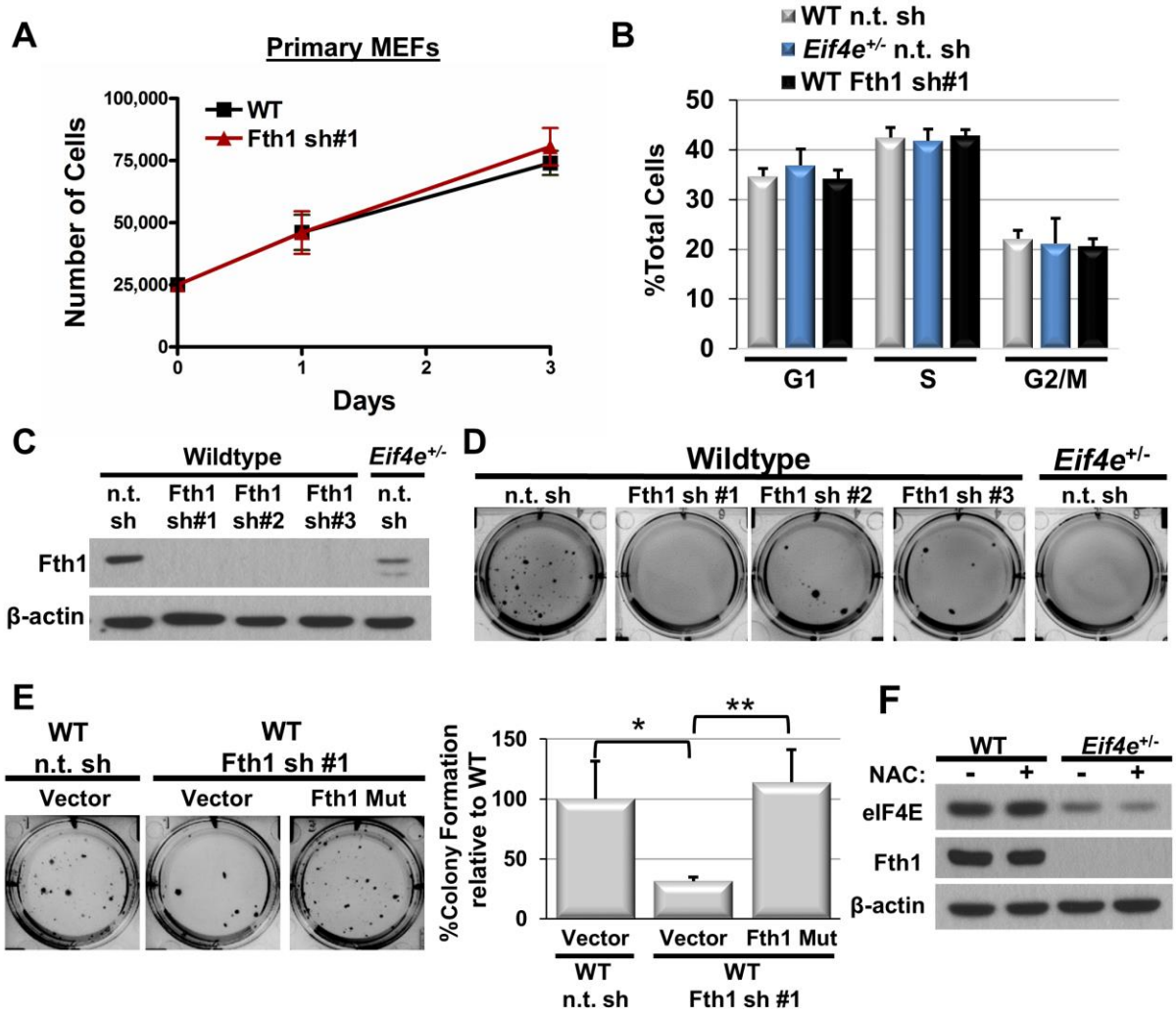
A
Primary MEFs
Number of Cells
100,000
75,000
50,000
25,000
0
WT
Fth1 sh#1
0
1
2
3
Days
B
WT n.t. sh
Eif4e+/- n.t. sh
WT Fth1 sh#1
%Total Cells
50
40
30
20
10
0
G1
S
G2/M
C
Wildtype
Eif4e+/-
n.t. sh
Fth1 sh#1
Fth1 sh#2
Fth1 sh#3
n.t. sh
Fth1
β-actin
D
Wildtype
Eif4e+/-
n.t. sh
Fth1 sh #1
Fth1 sh #2
Fth1 sh #3
n.t. sh
E
WT n.t. sh
WT Fth1 sh #1
Vector
Vector
Fth1 Mut
%Colony Formation relative to WT
150
100
50
0
*
**
Vector
Vector
Fth1 Mut
WT n.t. sh
WT Fth1 sh #1
F
WT
Eif4e+/-
NAC:
-
+
-
+
eIF4E
Fth1
β-actin

Tables

Table 3.1: *Eif4e*$^{+/-}$ mice are born at a normal frequency. Numbers and frequencies of mice born from mating *Eif4e*$^{+/-}$ mice to WT mice. Frequencies are noted in parentheses.

Table 3.2: Teratogenic effects of alcohol in *Eif4e*$^{+/-}$ embryos. Numbers, frequencies, and weights of WT and *Eif4e*$^{+/-}$ fetuses with limb and head birth defects upon exposure to alcohol at gestational day E9. Frequencies are noted in parentheses.

Table 3.3: Variance of microarray data. Quantile and mean gene variances for each group of samples in the polysomal microarray.

Table 3.1

	WT (*Eif4e*$^{+/+}$)	*Eif4e*$^{+/-}$	Total
Males	52 (23.3)	51 (22.9)	103 (46.2)
Females	62 (27.8)	58 (26.0)	120 (53.8)
Total	114 (51.1)	109 (48.9)	223 (100)

Table 3.2

	No. of Fetuses (%)	% Fetuses with head defects	%Fetuses with limb defects	Mean fetal wt. g+/-S.D.
WT	27 (45.8)	14.8	7.4	1.08+/-0.23
Eif4e$^{+/-}$	32 (54.2)	12.5	6.3	1.00+/-0.12
Total	59 (100)	13.6	6.8	1.03+/-0.18

Table 3.3

Quantile	WT Untrsfm	*Eif4e*$^{+/-}$ Untrsfm	WT Trsfm	*Eif4e*$^{+/-}$ Trsfm
0%	2.10E-06	9.02E-06	1.06E-05	8.43E-07
25%	2.99E-02	1.81E-02	2.25E-02	2.19E-02
50%	7.88E-02	4.44E-02	5.76E-02	5.40E-02
75%	1.87E-01	9.35E-02	1.31E-01	1.16E-01
100%	8.20E+00	1.03E+01	9.26E+00	7.98E+00
Mean	0.159636	0.074142	0.114173	0.095406
Variance				

Materials and Methods

Mice

Transgenic mice stably expressing a bicistronic luciferase reporter for cap- and IRES-mediated translation (CMV-HCV-IRES^{T}) have been previously described (Bellodi et al., 2010; Hsieh et al., 2010). *Eif4e* genetic loss-of-function mice were generated using embryonic stem cells obtained from BayGenomics (line RRO036), now maintained by the Mutant Mouse Regional Resources Center. RRO036 ES cells were propagated in 1X GMEM medium supplemented with 2mM glutamine, 1mM sodium pyruvate, and 1X nonessential amino acids, 10% fetal bovine serum, 500 units/ml of leukocyte inhibitory factor, and a 1:1,000 dilution of β-mercaptoethanol. ES cells were microinjected into blastocysts collected from super-ovulated female mice and implanted into recipient females. Founder lines were generated and crossed with WT C57BL/6J mice (Jackson Laboratories). Gene-trap insertion and germ-line transmission were validated by PCR and by Southern blot analysis of genomic DNA digested with EcoRV and probed with a PCR product specific to eIF4E (see Figure S3.1A-B). *Eif4e*$^{+/-}$ mice were maintained on a C57BL/6J background and crossed with *KRas*^{LA2} mice maintained on an FVB/n background for *in vivo* lung tumorigenesis experiments. All mice were maintained under specific pathogen-free conditions. Experiments were performed in compliance with guidelines approved by the Institutional Animal Care and Use Committee of UCSF.

In vivo tumor analysis

C57BL/6J *Elf4e*$^{+/-}$ mice were crossed to FVB/n *KRas*^{LA2} mice and the resulting F1 litters were evaluated for *in vivo* lung tumorigenesis. Tumor initiation was measured by counting superficial lung tumors on perfused lung specimens under a dissecting microscope. Tumor burden analysis was performed on all 5 lobes of the lung from serial sectioned formalin-fixed paraffin embedded tissue. Sections were Haematoxylin and Eosin stained and scanned using an Aperio Digital

Pathology Slide Scanner. Total tumor area and total lung area were measured using Aperio ImageScope software and tumor burden was calculated as tumor area relative to total lung area in the largest cross section of lung tissue.

Cell Culture and Reagents

Primary mouse embryonic fibroblasts were isolated from E13.5 embryos and cultured in Dulbecco's Modified Eagle Medium supplemented with 10% Fetal Bovine Serum and Penicillin/ Streptomycin (DMEM, 10% FBS, P/S). 293T cells were obtained from ATCC and maintained in DMEM, 10% FBS, P/S. Retroviral and lentiviral particles were produced by transfecting 293T cells with the appropriate expression and packaging plasmids using PolyFect Transfection Reagent (Qiagen) and filtering cultured supernatants through a 0.22 μM filter. Early passage MEFs (P4 or earlier) were transformed by retroviral infection with human $HRas^{V12D}$ and human c-Myc or E1A expression vectors followed by appropriate selection with puromycin (2 μg/ml), hygromycin (100 μg/ml), or blasticidin (5 μg/ml). shRNA-mediated knock down of Fth1 was obtained by infecting transformed MEFs with pLKO.1 lentiviral vectors and selection with puromycin.

Soft Agar Colony Forming Assays

Transformed MEFs were plated in 6-well plates at 300-1,000 cells per well in DMEM, 10% FBS, P/S with 0.3% agar over a base layer of 0.6% agar. Colonies were allowed to form over the course of 2-3 weeks and cultures were fed every three days. Where indicated, the antioxidant N-acetyl cysteine (Sigma) was added to cultures at a concentration of 1mM to inhibit reactive oxygen species.

Western Blot Analysis

Western blot analysis was performed on samples lysed in RIPA buffer (50 mM Tris pH8, 150 mM NaCl, 0.5% Na deoxycholate, 0.5 mM EDTA, 0.5% TritoxX-100) with the addition of PhosSTOP and Complete Mini proteasome inhibitors (Roche) using standard procedures with commercial

antibodies for eIF4E (BD Biosciences), phospho-eIF4E^{S209} (Cell Signaling), eIF4G (Cell Signaling), eIF4A (Cell Signaling), 4EBP1 (Cell Signaling), 4EBP2 (Cell Signaling), phospho-4EBP1$^{T37/46}$ (Cell Signaling), phospho-4EBP1^{S65} (Cell Signaling), Fth1 (Cell Signaling), Lmnb1 (Cell Signaling), Gclc (Proteintech), Ras (Cell Signaling), Myc (Cell Signaling), Dityrosine (Genox), α-tubulin (Sigma), and β-actin (Sigma). Where mentioned, protein levels were quantified using ImageJ software to analyze optical density of western blots normalized to loading control.

Analysis of Global Protein Synthesis

Primary B-cell, primary MEFs, or transformed MEFs were methionine starved for 45 minutes by incubation in labeling media (methionine-free media supplement with 10% dialyzed FBS). 30 μCi of ^{35}S labeled methionine/cysteine was then added to the media and incubated for 1hour. For all analyses, cell lysates were prepared using standard procedures and equal amounts of total protein were separated out on a 10% SDS polyacrylamide gel and transferred to PVDF membrane. Membranes were exposed to autoradiography film for 12-48 hours and then developed. ^{35}S methionine/cysteine incorporation was quantified using ImageJ software to analyze optical density and normalized to β-actin levels.

Bicistronic CAP/IRES Luciferase Reporter Assays

WT and *Eif4e*$^{+/-}$ MEFs expressing a bicistronic transgenic luciferase reporter for cap- and IRES-mediated translation (CMV-HCV-IRES^{T}) were isolated from E13.5 embryos. Equal numbers of primary or transformed MEFs were analyzed directly for Firefly and *Renilla* luciferase expression using a Dual Luciferase Assay kit (Promega) measured on a Glomax 96-well plate luminometer (Promega).

Polysome Fractionation and Isolation of Polysome Associated RNA for Microarray

Primary MEFs, transformed MEFs, and LPS-stimulated B-cells were treated with 100 μg/ml cyclohexamide (Sigma) on ice in PBS for 10 minutes and then pelleted. Cell pellets were lysed in

10mM Tris-HCl pH8, 140 mM NaCl, 1.5mM $MgCl_2$, 0.25% NP-40, 0.1% Triton-X 100, 50mM DTT in the presence of 150μg/ml cyclohexamide and 640U/ml Rnasin for 20 minutes. Lysates were spun down for 5 minutes at 9,300g and supernatants were loaded onto a 10-50% sucrose gradient. Samples were spun at 37,000 rpm for 2.5 hours at 4 degrees Celcius in a Beckman L8-70M ultracentrifuge. Samples were then separated on a gradient fractionation system (ISCO) to evaluate polysome profiles and collect polysome fractions. For polysome microarrays, three sets of independently isolated primary and matched transformed WT and *Eif4e*$^{+/-}$ MEFs were prepared as above and RNA was isolated from high MW polysome fractions (fractions 10-13) using TRIzol Reagent (Invitrogen) and the Pure Link RNA mini kit (Invitrogen). RNA was Dnase-treated with Pure Link Dnase (Invitrogen) and RNA purity was evaluated by BioAnalyzer (Agilent). Samples were amplified and hybridized to Affymetrix Mouse Gene 1.0 ST arrays by the UCSF Gladstone Genomics core.

Analysis of Microarray Data Set

Affymetrix Mouse Gene 1.0 ST data from 24 arrays were preprocessed by RMA (background correction, quantile normalization, probeset summarization) using the aroma.affymetrix R package with default settings. Polysomal and Total RNA datasets were quantile normalized separately. Probe sets annotated as being in the main design and not cross-hybridizing were retained (Affymetrix NetAffx version 30). The difference in log2 intensity between polysomal RNA and total RNA (matched for MEFs derived from the same embryo) was taken to quantify translational efficiency (TE). These data are grouped by two binary factors, eIF4E status (WT / Eif4e+/-) and transformation status (Transformed / Untransformed), forming a 2x2 factorial design with three replicates in each combination. The limma R package was used to assess the two and four level comparisons reported in the main text (Figure 3.3B-C, Figure S3.4C, and Appenices 1-2). The fold change and p-value for each array probeset that passed a filtering step were determined. Limma incorporates a linear modeling framework for microarray data. Testing is

based on moderated t-statistics to stabilize variance estimates in the small sample size setting. This has led to superior performance in this context for identifying differentially expressed genes(Jeanmougin et al., 2010).

Interaction Network Analysis

Protein interaction networks were retrieved from STRING v9.1 database (Franceschini et al., 2013) and imported into Cytoscape for visualization. Each node represents a gene and edge shows protein-protein association with width proportional to the association score. Genes with related functions were clustered together and disconnected nodes were removed from the plot for simplicity.

Gene Set Enrichment Analysis

Gene set enrichment analysis (GSEA) was performed using version 2.0.12 of the GSEA desktop application (downloaded from the Broad Institute). Log2 values of translational efficiency (TE) were calculated for transformed and untransformed WT cells and input into GSEA. Gene set enrichment in transformed WT samples over untransformed WT samples was analyzed by collapsing the data into gene symbols and running 1000 permutations of the gene set using a weighted enrichment statistic. Gene sets were filtered for a minimum of 15 and a maximum of 500 genes and genes were ranked by signal to noise ratios for both Kyoto Encyclopedia of Genes and Genomes (c2.cp.kegg.v3.1.symbols.gmt) and Gene Ontology Biological Process (c5.bp.v3.1.symbols.gmt) gene set collections. Genes whose translation efficiency was enhanced by transformation based on core enrichment were then evaluated for requirements for eIF4E dose. Fold changes in the Log2 values of TE mRNA between transformed and untransformed states were calculated for both WT and *Eif4e*$^{+/-}$ cells and input into GSEA for analysis of enrichment in WT samples over *Eif4e*$^{+/-}$ samples. In order to broadly evaluate the impact of transformation on the regulation and response to ROS a user-defined gene list based on current GO classifications for response to oxidative stress (GO:0006979), reactive oxygen species

metabolic process (GO:0072593), response to reactive oxygen species (GO:0000302), iron ion homeostasis (GO:0055072), and glutathione metabolic process (GO:0006749) was created (Appendix 10). GSEA analysis for enrichment in transformed WT samples over untransformed WT samples in this set identified 99 genes whose translation efficiency was enhanced by transformation based on core enrichment. In order to evaluate the requirements for eIF4E in translation of this gene set, fold changes in the Log2 values of TE mRNA between transformed and untransformed states were calculated for both WT and *Eif4e*$^{+/-}$ cells and input into GSEA for analysis of enrichment in WT samples over *Eif4e*$^{+/-}$ samples.

Analysis of General 5'UTR Features

5'UTRs were obtained from the UCSC Genome Browser (GRCm38/mm10) for all genes present on the microarray. The longest 5'UTR sequence of each RefSeq annotated mRNAs was selected for analysis. The 133 mRNAs whose translational was dependent on eIF4E (Appendix 2) were compared to all genes for 5'UTR %G+C content, length, and Gibbs free energy.

5' UTR Luciferase Reporter Assays

5'UTRs were amplified from MEF cDNA and cloned in the pGL3-T7 vector between the T7 promoter and the firefly luciferase open reading using HindIII and NcoI. Plasmids were linearized with ClaI and *in vitro* transcribed using the Ambion T7 Megascript kit (Life Technologies). A control *Renilla* reporter (pRL) was linearized using BamHI and was *in vitro* transcribed in a similar fashion. RNA was capped using the vaccinia RNA capping system (New England Biolabs) and then purified. Transformed WT and *Eif4e*$^{+/-}$ MEFs were cotransfected with pGL3-T7 5'UTR reporter RNA and pRL control RNA at a ratio of 20:1 using the TransIT mRNA transfection kit (Mirus Bio). Cells were harvested 4hrs later and luciferase activity was measured using a Dual Luciferase Assay kit (Promega). Firefly luciferase activity was normalized to *Renilla* activity and presented as values relative to transformed WT MEFs.

Motif analysis

Multiple Em for Motif Elicitation (MEME) was performed using version 4.9.1 of the MEME browser application. Annotated probe sets with a greater than 1.407 fold decrease in translational efficiency ($p<0.05$) in transformed Eif4e+/- relative to WT were obtained by filtering the output from limma (described above). 5'UTRs were called from the UCSC Genome Browser (GRCm38/mm10) and RefSeq annotated mRNAs with known 5'UTRs were selected for further analysis. The longest 5'UTR for each gene was compiled for input into MEME as a training set (see Appendix 12 for full list of genes used in this training set). The CERT motif was identified using search parameters for a 6-15 nucleotide sequence with any number of repeats. The 116 eIF4E targets with RefSeq annotated mRNAs containing known 5'UTRs (out of 133 total targets) were evaluated for the presence of the consensus CERT motif using Find Individual Motif Occurrences (FIMO). The subset of eIF4E targets whose translational efficiency was also increase during transformation (ie. also present in Apendix 1) were analyzed for enrichment of a CERT domain relative to all genes with annotated 5'UTRs by Chi-squared analysis with a Yates' correction.

Analysis of Reactive Oxygen Species Levels

Transformed WT and *Eif4e*$^{+/-}$ MEFs were harvested and resuspended in PBS containing 10μM CM-H_2DCFDA (Life Technologies). Cells were incubated at 37 degrees Celsius in the dark for 30 minutes, washed with PBS, and then immediately collected on a BD FACSCalibur flow cytometer to measure fluorescence of CM-H_2DCFDA as a measure of reactive oxygen species levels. At least 10,000 events were recorded and analyzed using FlowJo software.

Apoptosis analysis

Single cell suspensions in BD binding buffer were stained for Annexin V (BD Pharmingen) and propidium iodide. Data was collected using a BD FACSCalibur flow cytometer to measure

Annexin V and propidium iodide levels. At least 10,000 events were recorded and analyzed using FlowJo software.

Quantitative Polymerase Chain Reaction (qPCR)

RNA was isolated using TRIzol Reagent (Invitrogen) and the Pure Link RNA mini kit (Invitrogen) according to the manufacturer's protocol. RNA was Dnase-treated with Pure Link Dnase (Invitrogen) and reverse-transcribed to cDNA using a High Capacity cDNA Reverse Transcription kit (Applied Biosystems). cDNA samples were diluted 1:20 and 1ul of template was used in a SYBR green detection qPCR assay (Biorad) run on a MyiQ2 Real-Time PCR Detection System (Biorad).

Statistical Analysis

All data are presented as the average mean of values with error bars representing the standard deviation of at least three independent biological experiments. Unless otherwise noted p-values indicate statistical significance in an unpaired, two-tailed t test denoted by *= $p<0.05$, **= $p<0.01$.

Teratogenic studies

Ethanol induced teratogenicity was evaluated in *Eif4e*$^{+/-}$ mice by dosing pregnant females in the C57BL/6J background with two doses of 2.9g/kg of ethanol spaced four hours apart on gestational day 9. Pregnant females were euthanized at gestational day 18 and embryos were genotyped and evaluated for the presence of limb and head defects.

Cell Cycle Analysis

Single cell suspensions were prepared and fixed/permeabilized with 90% ice-cold methanol. Cells were treated with RNaseH and stained with propidium iodide to measure DNA content. Data was collected using a BD FACSCalibur flow cytometer. At least 10,000 events were recorded and analyzed using FlowJo software.

FACS Analysis of Immune Cells

Single cell suspension of thymus, spleen, and lymph nodes were prepared and depleted of red blood cells by treatment with ACK buffer. Cell were incubated with Fc block for 30minutes and then stained with T-cell, B-cell, and granulocyte/macrophage specific antibodies conjugated to Fitc, PE, or APC fluorophores (T-cells: CD3, CD4, CD8; B-cells: B220; and granulocytes/macrophages: CD11b, Gr1; all antibodies from BD BioSciences).

Proliferation Assays

Single cell suspensions of primary MEFs were plated in 6-well plates at a concentration of 25,000 cells per well. Cell viability was checked by trypan-blue staining and cells were counted on days 1, 3, and 5 by measuring events great than 8 μM in sized on a BD Coulter Counter.

B-cell isolations

Spleens were harvested from WT and *Eif4e*$^{+/-}$ littermates and disassociated over ice into single cell suspensions. Red blood cells were depleted by treatment with ACK buffer and B-cells were isolated using a B-cell isolation kit (Miltenyi Biotech) by following the manufacturer's recommended protocol.

Plasmids

Retroviral vectors were obtained from Addgene: pBabe puro H-RasV12 (9051), pWZL hygro Myc (1875), pWZL hygro H-RasV12 (18749), pWZL blasticidin Myc (10674), pWZL hygro E1A (18748), and pMSCV eIF4E IRES GFP (18761). Flag-Fth1 was amplified by PCR from WT MEF cDNA and cloned into pMSCV puro (Clontech). Lentiviral shRNA vectors were made by cloning a non-targeting sequence (CAACAAGATGAAGAGCACCAA), Fth1- specific targeting sequence sh#1 (GACTTCATTGAGACGTATTAT), sh#2 (CTATCTGTCTATGTCTTGTTA), and sh#3 (GAGACGTATTATCTGAGTGAA) into the pLKO.1 puro shRNA construct (Addgene 8453). For Flag-Fth1 knock down resistant plasmids, mutagenesis was performed using the QuikChange II

site-directed mutagenesis kit (Stratagene). The pGL3-T7 and pRL vectors used in the 5'UTR luciferase reporter assay were purchased from Promega. All plasmids were validated by sequencing through Quintara Biosciences.

Oligonucleotides

Oligonucleotides for qPCR were as follows: eIF4E forward 5'-CCCACCTGCAGAAGAGGAA-3', reverse 5'- ATCGAAGGTTTGCTTGCCA-3'; β-actin forward 5′-CTAAGGCCAACCGTGAAAAG-3′, reverse 5′-ACCAGAGGCATACAGGGACA-3′; GAPDH forward 5'-CAATGAATACGGCTACAGCAA-3', reverse 5'- AGGGAGATGCTCAGTGTTGG-3'; Fth1 forward 5'- CCATCAACCGCCAGATCAACCT-3', reverse 5'- GCATGCTCCCTCTCCTCATGAG-3'; Lmnb1 forward 5'-TCTCAGTGGAGCCCAGATCA-3', reverse 5'-GGATGCTTCTAGCTGGGCAA-3'; and Gclc forward 5'- GGTTTAAGCCTCCTCCTCCA-3', reverse 5'- CCCTAGTGAGCAGTACCACGA-3'.

Acknowlegements

We thank members of the Ruggero lab for critical discussion and Adam Olshen for reading the manuscript. This work was supported by National Institutes of Health (NIH) Director's New Innovator Award, 1DP2OD008509 (M.B.), NIH P30CA82103 (T.T.), NIH 1F32CA189696 (C.S.C.), NIH R01CA140456 (D.R.), and NIH R01CA154916 (D.R.). M.L.T. is in part supported by the UCSF HHMI GEMS fellowship. D.R. is a Leukemia & Lymphoma Society Scholar. M.B. is a Pew Scholar and Alfred P. Sloan Research Fellow.

Chapter 4: Conclusions and Future Directions

Myc and mTOR converge on a common node in protein synthesis control that confers synthetic lethality in Myc-driven cancers

In Chapter 2, we discovered that a previously unknown function of the Myc oncogenic program is to regulate the activity of the 4EBP1 tumor suppressor at the earliest stage of tumor initiation. We used a genetic approach to uncover that mTOR-dependent 4EBP1 phosphorylation is essential for cancer cell survival throughout Myc tumor development, from tumor initiation to maintenance. Furthermore, we find that hyperactivation of 4EBP1 renders Myc-driven lymphomas and myelomas druggable by a potent new class of mTOR active site inhibitors that are capable of blocking 4EBP1 phosphorylation. Importantly, we observed that the efficacy of the mTOR active site inhibitor MLN0128 is superior to RAD001, an allosteric inhibitor of mTOR that ineffectively blocks 4EBP1 phosphorylation and has modest therapeutic effects in the clinic. Finally, we provide evidence that mTOR active site inhibitors may have therapeutic efficacy across a broad range of hematologic malignancies that are characterized by the overexpression of Myc.

A key function of Myc is to directly regulate the protein synthesis machinery. This function has historically been attributed to Myc's transcriptional activity in activating target genes such as ribosomal proteins, translation initiation factors, and ribosomal DNA (van Riggelen et al., 2010). For example, Myc is known to transcriptionally activate the eIF4E oncogene (Schmidt, 2004), a finding we validated at the protein level in human DLBCL, and eIF4E overexpression has been shown to promote Myc tumorigenesis (Wendel et al., 2004). Our study further suggests that Myc enhances protein synthesis during tumorigenesis not only through transcriptional control but also by activating mTOR-dependent phosphorylation of 4EBP1, offering a unique window of opportunity for pharmacological intervention. This is further substantiated by our genetic data demonstrating that Myc-overexpressing B cells become addicted to mTOR-dependent

phosphorylation of 4EBP1. Importantly, the programmed cell death observed upon the inhibition of 4EBP1 phosphorylation cannot be attributed to decreases in Myc protein levels. Moreover, normal B-cell survival is not dependent on 4EBP1 phosphorylation, thus inhibiting this node of translation control in the context of Myc overexpression is synthetically lethal. These data strongly support pharmacologic targeting of mTOR with active site inhibitors as a clinically attractive therapeutic approach to Myc-driven cancers.

The substrate specificity of mTOR is dictated by its interaction with other proteins as part of either the mTORC1 or mTORC2 complex. Our observation that Myc modulates mTORC1 specificity toward 4EBP1 without an increase in p70S6K phosphorylation cannot be explained by upstream activation of mTOR through tuberous sclerosis complex 1/2 or AKT-dependent regulation. In line with this, we do not find increased activation of mTOR at the Ser2448 phosphorylation site, a p70SK1 target (Chiang and Abraham, 2005; Holz and Blenis, 2005). Therefore, this finding reveals an aspect of mTOR biology that was previously unknown. One potential explanation for how Myc may direct mTOR substrate specificity is through allosteric structural changes of mTORC1 through a yet unidentified protein. In principle, this may resemble the allosteric interaction of mTOR with rapalogs, which affects the phosphorylation of only a subset of mTORC1 substrates. Future studies addressing the molecular basis for Myc-dependent regulation of 4EBP1 through mTORC1 may provide important insights into how mTOR function is regulated under normal and pathological cellular conditions. Together, these findings highlight a unique function of the Myc oncogenic program that converges on regulation of mTOR-dependent protein synthesis, which can be pharmacologically exploited as a synthetic lethal interaction to specifically target Myc-driven malignancies.

eIF4E dose is critical for the oncogenic translation program but not mammalian development and protein synthesis

In Chapter 3, we unexpectedly uncover that eIF4E expression levels can be maintained at half of the normal genetic dosage without apparent consequences to normal organismal development and global mRNA translation. This finding is consistent with previous cell based observations showing that depletion of eIF4E by 80-90% in rabbit reticulocyte extracts has only a moderate effect on protein synthesis (Rau et al., 1996). Although we cannot formally exclude the potential for unknown compensatory mechanisms arising from reductions in eIF4E levels, mammalian cells appear to have evolved surplus levels of eIF4E. Therefore, it remains an outstanding question what benefit an excess of eIF4E might convey at the organismal level. While it is possible that additional translation-independent eIF4E functions, such as mRNA transport (Topisirovic et al., 2011; von der Haar et al., 2004), could require higher levels of eIF4E, our data suggest that eIF4E dose may predominately be required to buffer against stress conditions, for example during the oncogene induced cellular stress response underlying transformation.

Deregulated translation control is a hallmark of human cancers and is critical for tumorigenesis downstream of multiple oncogenic signaling pathways (Barna et al., 2008; Hsieh et al., 2010). However, the full repertoire of mRNAs translationally altered by oncogenic signaling and the underlying molecular mechanisms that direct their translational control remain poorly understood. Employing unbiased genome-wide profiling we have uncovered an oncogenic translational program comprised of hundreds of mRNAs and find that a specific subset of transcripts within this group is exquisitely sensitized to eIF4E dose. Moreover, we demonstrate that translational changes induced by transformation affect many functional gene classes, such as those involved in cell signaling, apoptosis, ribosome biogenesis, the proteasome, nucleotide biosynthesis, oxidative phosphorylation, and the oxidative stress response, which may in concert, act to promote tumorigenesis. This data further suggests that translational control of mRNAs comprising multiple cellular functions are likely to underlie the remarkable resistance to transformation in *Eif4e*$^{+/-}$ cells and mice. In this regard, we have functionally delineated the impact of translation control of at least one of these functional classes, a novel group of mRNAs involved

in the regulation and response to ROS, towards cellular transformation. In particular, we show that key eIF4E-dependent ROS targets, such as Fth1, are critically required for cellular transformation and, moreover, demonstrate that antioxidant suppression of ROS in *Eif4e*$^{+/-}$ cells rescues to a large extent the cellular transformation capacity of these cells. Future studies will be needed to further validate the role of other eIF4E-dependent functional gene classes during tumorigenesis and to elucidate specific conditions where eIF4E-dependent translation of these mRNAs becomes important.

Oxidative stress is one of the defining stress phenotypes encountered during tumorigenesis and cancer cells have been shown to typically generate more ROS than normal cells (Szatrowski and Nathan, 1991). In this regard, it has been historically thought that ROS plays a distinctly pro-tumorigenic role. Recent studies have also shown that physiological expression of oncogenes may drive down intracellular ROS levels, suggesting that complex regulation of ROS levels may occur during different stages of *in vivo* tumorigenesis as well as downstream of progressive genomic aberrations, such as oncogene amplification. Thereby, our understanding of the key molecular mechanisms responsible for intricately maintaining ROS levels compatible with tumor cell survival is incomplete. Here, we find that genes regulating ROS are under exquisite translational regulation during oncogenic transformation and are sensitized to eIF4E dose, revealing a very unexpected post-transcriptional circuitry regulating ROS levels. For example, Fth1, an iron-storage protein that protects against the formation of hydroxyl radicals, and Gclc, the rate-limiting enzyme for the synthesis of glutathione used to neutralize ROS, are translationally induced by cellular transformation in an eIF4E-dependent manner. Importantly, we show that reduction in eIF4E dose lead to significant increases in intracellular ROS downstream of ectopic oncogene expression, sensitizing tumor cells to ROS induced apoptosis and blocking cellular transformation. In addition, we demonstrate that eIF4E is required for proper expression of the ROS response and control of intratumoral oxidative stress underlying *in vivo* lung tumorigenesis driven by endogenous expression of KRas. Thereby, our data suggest that the

regulation of ROS levels through eIF4E-mediated translational control may provide a molecular rheostat that fine-tunes the levels of oxidative species that are selectively required to maintain cancer cell survival.

Precisely how distinct subsets of mRNAs become sensitized to eIF4E dose during oncogenic transformation remains an important area of investigation. Classically, long, structured 5'UTRs with high GC content and low free energy have been thought to be the only features that confer sensitivity to eIF4E dose. Interestingly, these 5'UTR features were not significantly enriched in the subset of eIF4E-dependent genes translationally activated by transformation, suggesting that alternative modes of translational control may also be important. Recently, there has been an emerging appreciation for the role of shorter, sequence-specific elements embedded within the 5'UTR in directing mRNA translation (Hsieh et al., 2012; Thoreen et al., 2012; Wolfe et al., 2014). Along these lines, we find that the majority of eIF4E-dependent mRNAs induced by transformation are marked by the presence of a novel sequence-specific CERT motif within their 5'UTRs, suggesting that this motif may have broader impacts towards eIF4E-dependent translation. Further studies will be required to address the functional requirement for the CERT motif and whether this signature simply demarcates eIF4E sensitized mRNAs or has a more functional role in coupling eIF4E dose to translational control of these subsets of mRNAs. Thereby, our data surprisingly show that the long held dogma that eIF4E dose is critically required for translating the mammalian genome needs to be revisited. Maintaining eIF4E dose at 50% normal levels does not appear to be detrimental for normal mammalian development and even more strikingly global protein synthesis control. Our findings further point to the possibility that cancer cells have specifically usurped excess eIF4E levels to promote their growth and survival. The fact that reducing eIF4E expression is not detrimental for normal mammalian physiology reveals a potent therapeutic window for targeting the eIF4E-dependent oncogenic translational

program, which may be greatly enhanced in combination with drugs that exploit the sensitivity of cancer cells to ROS.

References

Adams, J.M., Harris, A.W., Pinkert, C.A., Corcoran, L.M., Alexander, W.S., Cory, S., Palmiter, R.D., and Brinster, R.L. (1985). The c-myc oncogene driven by immunoglobulin enhancers induces lymphoid malignancy in transgenic mice. Nature *318*, 533-538.

Altmann, M., Schmitz, N., Berset, C., and Trachsel, H. (1997). A novel inhibitor of cap-dependent translation initiation in yeast: p20 competes with eIF4G for binding to eIF4E. The EMBO journal *16*, 1114-1121.

Aoki, M., Blazek, E., and Vogt, P.K. (2001). A role of the kinase mTOR in cellular transformation induced by the oncoproteins P3k and Akt. Proceedings of the National Academy of Sciences of the United States of America *98*, 136-141.

Assouline, S., Culjkovic, B., Cocolakis, E., Rousseau, C., Beslu, N., Amri, A., Caplan, S., Leber, B., Roy, D.C., Miller, W.H., Jr*., et al.* (2009). Molecular targeting of the oncogene eIF4E in acute myeloid leukemia (AML): a proof-of-principle clinical trial with ribavirin. Blood *114*, 257-260.

Avdulov, S., Li, S., Michalek, V., Burrichter, D., Peterson, M., Perlman, D.M., Manivel, J.C., Sonenberg, N., Yee, D., Bitterman, P.B*., et al.* (2004). Activation of translation complex eIF4F is essential for the genesis and maintenance of the malignant phenotype in human mammary epithelial cells. Cancer cell *5*, 553-563.

Avni, D., Biberman, Y., and Meyuhas, O. (1997). The 5' terminal oligopyrimidine tract confers translational control on TOP mRNAs in a cell type- and sequence context-dependent manner. Nucleic acids research *25*, 995-1001.

Avni, D., Shama, S., Loreni, F., and Meyuhas, O. (1994). Vertebrate mRNAs with a 5'-terminal pyrimidine tract are candidates for translational repression in quiescent cells: characterization of the translational cis-regulatory element. Molecular and cellular biology *14*, 3822-3833.

Bader, A.G., Kang, S., Zhao, L., and Vogt, P.K. (2005). Oncogenic PI3K deregulates transcription and translation. Nat Rev Cancer *5*, 921-929.

Bailey, T.L., and Elkan, C. (1994). Fitting a mixture model by expectation maximization to discover motifs in biopolymers. Proceedings / International Conference on Intelligent Systems for Molecular Biology ; ISMB International Conference on Intelligent Systems for Molecular Biology *2*, 28-36.

Balaban, R.S., Nemoto, S., and Finkel, T. (2005). Mitochondria, oxidants, and aging. Cell *120*, 483-495.

Barna, M., Pusic, A., Zollo, O., Costa, M., Kondrashov, N., Rego, E., Rao, P.H., and Ruggero, D. (2008). Suppression of Myc oncogenic activity by ribosomal protein haploinsufficiency. Nature *456*, 971-975.

Barrans, S., Crouch, S., Smith, A., Turner, K., Owen, R., Patmore, R., Roman, E., and Jack, A. (2010). Rearrangement of MYC is associated with poor prognosis in patients with diffuse large B-cell lymphoma treated in the era of rituximab. Journal of clinical oncology : official journal of the American Society of Clinical Oncology *28*, 3360-3365.

Bellodi, C., Kopmar, N., and Ruggero, D. (2010). Deregulation of oncogene-induced senescence and p53 translational control in X-linked dyskeratosis congenita. The EMBO journal *29*, 1865-1876.

Belteki, G., Haigh, J., Kabacs, N., Haigh, K., Sison, K., Costantini, F., Whitsett, J., Quaggin, S.E., and Nagy, A. (2005). Conditional and inducible transgene expression in mice through the combinatorial use of Cre-mediated recombination and tetracycline induction. Nucleic acids research *33*, e51.

Boussemart, L., Malka-Mahieu, H., Girault, I., Allard, D., Hemmingsson, O., Tomasic, G., Thomas, M., Basmadjian, C., Ribeiro, N., Thuaud, F.*, et al.* (2014). eIF4F is a nexus of resistance to anti-BRAF and anti-MEK cancer therapies. Nature *513*, 105-109.

Braunstein, S., Karpisheva, K., Pola, C., Goldberg, J., Hochman, T., Yee, H., Cangiarella, J., Arju, R., Formenti, S.C., and Schneider, R.J. (2007). A hypoxia-controlled cap-dependent to cap-independent translation switch in breast cancer. Molecular cell *28*, 501-512.

Brown, E.J., Beal, P.A., Keith, C.T., Chen, J., Shin, T.B., and Schreiber, S.L. (1995). Control of p70 s6 kinase by kinase activity of FRAP in vivo. Nature *377*, 441-446.

Chen, L., Aktas, B.H., Wang, Y., He, X., Sahoo, R., Zhang, N., Denoyelle, S., Kabha, E., Yang, H., Freedman, R.Y.*, et al.* (2012). Tumor suppression by small molecule inhibitors of translation initiation. Oncotarget *3*, 869-881.

Chesi, M., Robbiani, D.F., Sebag, M., Chng, W.J., Affer, M., Tiedemann, R., Valdez, R., Palmer, S.E., Haas, S.S., Stewart, A.K.*, et al.* (2008). AID-dependent activation of a MYC transgene induces multiple myeloma in a conditional mouse model of post-germinal center malignancies. Cancer cell *13*, 167-180.

Chiang, G.G., and Abraham, R.T. (2005). Phosphorylation of mammalian target of rapamycin (mTOR) at Ser-2448 is mediated by p70S6 kinase. The Journal of biological chemistry *280*, 25485-25490.

Chng, W.J., Huang, G.F., Chung, T.H., Ng, S.B., Gonzalez-Paz, N., Troska-Price, T., Mulligan, G., Chesi, M., Bergsagel, P.L., and Fonseca, R. (2011). Clinical and biological implications of MYC activation: a common difference between MGUS and newly diagnosed multiple myeloma. Leukemia *25*, 1026-1035.

Choo, A.Y., Yoon, S.O., Kim, S.G., Roux, P.P., and Blenis, J. (2008). Rapamycin differentially inhibits S6Ks and 4E-BP1 to mediate cell-type-specific repression of mRNA translation. Proceedings of the National Academy of Sciences of the United States of America *105*, 17414-17419.

Cozzi, A., Corsi, B., Levi, S., Santambrogio, P., Albertini, A., and Arosio, P. (2000). Overexpression of wild type and mutated human ferritin H-chain in HeLa cells: in vivo role of ferritin ferroxidase activity. The Journal of biological chemistry *275*, 25122-25129.

Cuccuini, W., Briere, J., Mounier, N., Voelker, H.U., Rosenwald, A., Sundstrom, C., Cogliatti, S., Hirchaud, E., Ysebaert, L., Bron, D.*, et al.* (2012). MYC+ diffuse large B-cell lymphoma is not salvaged by classical R-ICE or R-DHAP followed by BEAM plus autologous stem cell transplantation. Blood *119*, 4619-4624.

Cunningham, J.T., Moreno, M.V., Lodi, A., Ronen, S.M., and Ruggero, D. (2014). Protein and nucleotide biosynthesis are coupled by a single rate-limiting enzyme, PRPS2, to drive cancer. Cell *157*, 1088-1103.

Dai, M.S., and Lu, H. (2008). Crosstalk between c-Myc and ribosome in ribosomal biogenesis and cancer. Journal of cellular biochemistry *105*, 670-677.

Dang, C.V., O'Donnell, K.A., Zeller, K.I., Nguyen, T., Osthus, R.C., and Li, F. (2006). The c-Myc target gene network. Seminars in cancer biology *16*, 253-264.

De Benedetti, A., and Graff, J.R. (2004). eIF-4E expression and its role in malignancies and metastases. Oncogene *23*, 3189-3199.

De Benedetti, A., Joshi-Barve, S., Rinker-Schaeffer, C., and Rhoads, R.E. (1991). Expression of antisense RNA against initiation factor eIF-4E mRNA in HeLa cells results in lengthened cell division times, diminished translation rates, and reduced levels of both eIF-4E and the p220 component of eIF-4F. Molecular and cellular biology *11*, 5435-5445.

Deneke, S.M., and Fanburg, B.L. (1989). Regulation of cellular glutathione. Am J Physiol *257*, L163-173.

DeNicola, G.M., Karreth, F.A., Humpton, T.J., Gopinathan, A., Wei, C., Frese, K., Mangal, D., Yu, K.H., Yeo, C.J., Calhoun, E.S.*, et al.* (2011). Oncogene-induced Nrf2 transcription promotes ROS detoxification and tumorigenesis. Nature *475*, 106-109.

Dumstorf, C.A., Konicek, B.W., McNulty, A.M., Parsons, S.H., Furic, L., Sonenberg, N., and Graff, J.R. (2010). Modulation of 4E-BP1 function as a critical determinant of enzastaurin-induced apoptosis. Molecular cancer therapeutics *9*, 3158-3163.

Duncan, R., Milburn, S.C., and Hershey, J.W. (1987). Regulated phosphorylation and low abundance of HeLa cell initiation factor eIF-4F suggest a role in translational control. Heat shock effects on eIF-4F. The Journal of biological chemistry *262*, 380-388.

Emanuilov, I., Sabatini, D.D., Lake, J.A., and Freienstein, C. (1978). Localization of eukaryotic initiation factor 3 on native small ribosomal subunits. Proceedings of the National Academy of Sciences of the United States of America *75*, 1389-1393.

Fan, S., Li, Y., Yue, P., Khuri, F.R., and Sun, S.Y. (2010). The eIF4E/eIF4G interaction inhibitor 4EGI-1 augments TRAIL-mediated apoptosis through c-FLIP Down-regulation and DR5 induction independent of inhibition of cap-dependent protein translation. Neoplasia *12*, 346-356.

Feldman, M.E., Apsel, B., Uotila, A., Loewith, R., Knight, Z.A., Ruggero, D., and Shokat, K.M. (2009). Active-site inhibitors of mTOR target rapamycin-resistant outputs of mTORC1 and mTORC2. PLoS biology *7*, e38.

Flowers, A., Chu, Q.D., Panu, L., Meschonat, C., Caldito, G., Lowery-Nordberg, M., and Li, B.D. (2009). Eukaryotic initiation factor 4E overexpression in triple-negative breast cancer predicts a worse outcome. Surgery *146*, 220-226.

Franceschini, A., Szklarczyk, D., Frankild, S., Kuhn, M., Simonovic, M., Roth, A., Lin, J., Minguez, P., Bork, P., von Mering, C.*, et al.* (2013). STRING v9.1: protein-protein interaction networks, with increased coverage and integration. Nucleic acids research *41*, D808-815.

Furic, L., Rong, L., Larsson, O., Koumakpayi, I.H., Yoshida, K., Brueschke, A., Petroulakis, E., Robichaud, N., Pollak, M., Gaboury, L.A.*, et al.* (2010). eIF4E phosphorylation promotes tumorigenesis and is associated with prostate cancer progression. Proceedings of the National Academy of Sciences of the United States of America *107*, 14134-14139.

Gingras, A.C., Gygi, S.P., Raught, B., Polakiewicz, R.D., Abraham, R.T., Hoekstra, M.F., Aebersold, R., and Sonenberg, N. (1999a). Regulation of 4E-BP1 phosphorylation: a novel two-step mechanism. Genes & development *13*, 1422-1437.

Gingras, A.C., Kennedy, S.G., O'Leary, M.A., Sonenberg, N., and Hay, N. (1998). 4E-BP1, a repressor of mRNA translation, is phosphorylated and inactivated by the Akt(PKB) signaling pathway. Genes & development *12*, 502-513.

Gingras, A.C., Raught, B., Gygi, S.P., Niedzwiecka, A., Miron, M., Burley, S.K., Polakiewicz, R.D., Wyslouch-Cieszynska, A., Aebersold, R., and Sonenberg, N. (2001a). Hierarchical phosphorylation of the translation inhibitor 4E-BP1. Genes & development *15*, 2852-2864.

Gingras, A.C., Raught, B., and Sonenberg, N. (1999b). eIF4 initiation factors: effectors of mRNA recruitment to ribosomes and regulators of translation. Annual review of biochemistry *68*, 913-963.

Gingras, A.C., Raught, B., and Sonenberg, N. (2001b). Regulation of translation initiation by FRAP/mTOR. Genes & development *15*, 807-826.

Gkogkas, C.G., Khoutorsky, A., Ran, I., Rampakakis, E., Nevarko, T., Weatherill, D.B., Vasuta, C., Yee, S., Truitt, M., Dallaire, P.*, et al.* (2013). Autism-related deficits via dysregulated eIF4E-dependent translational control. Nature *493*, 371-377.

Graff, J.R., Konicek, B.W., Lynch, R.L., Dumstorf, C.A., Dowless, M.S., McNulty, A.M., Parsons, S.H., Brail, L.H., Colligan, B.M., Koop, J.W.*, et al.* (2009). eIF4E activation is commonly elevated in advanced human prostate cancers and significantly related to reduced patient survival. Cancer research *69*, 3866-3873.

Graff, J.R., Konicek, B.W., Vincent, T.M., Lynch, R.L., Monteith, D., Weir, S.N., Schwier, P., Capen, A., Goode, R.L., Dowless, M.S.*, et al.* (2007). Therapeutic suppression of translation initiation factor eIF4E expression reduces tumor growth without toxicity. The Journal of clinical investigation *117*, 2638-2648.

Haghighat, A., Mader, S., Pause, A., and Sonenberg, N. (1995). Repression of cap-dependent translation by 4E-binding protein 1: competition with p220 for binding to eukaryotic initiation factor-4E. The EMBO journal *14*, 5701-5709.

Haghighat, A., and Sonenberg, N. (1997). eIF4G dramatically enhances the binding of eIF4E to the mRNA 5'-cap structure. The Journal of biological chemistry *272*, 21677-21680.

Hannan, K.M., Brandenburger, Y., Jenkins, A., Sharkey, K., Cavanaugh, A., Rothblum, L., Moss, T., Poortinga, G., McArthur, G.A., Pearson, R.B.*, et al.* (2003). mTOR-dependent regulation of

ribosomal gene transcription requires S6K1 and is mediated by phosphorylation of the carboxy-terminal activation domain of the nucleolar transcription factor UBF. Molecular and cellular biology *23*, 8862-8877.

Hiremath, L.S., Webb, N.R., and Rhoads, R.E. (1985). Immunological detection of the messenger RNA cap-binding protein. The Journal of biological chemistry *260*, 7843-7849.

Holz, M.K., and Blenis, J. (2005). Identification of S6 kinase 1 as a novel mammalian target of rapamycin (mTOR)-phosphorylating kinase. The Journal of biological chemistry *280*, 26089-26093.

Hsieh, A.C., Costa, M., Zollo, O., Davis, C., Feldman, M.E., Testa, J.R., Meyuhas, O., Shokat, K.M., and Ruggero, D. (2010). Genetic dissection of the oncogenic mTOR pathway reveals druggable addiction to translational control via 4EBP-eIF4E. Cancer cell *17*, 249-261.

Hsieh, A.C., Liu, Y., Edlind, M.P., Ingolia, N.T., Janes, M.R., Sher, A., Shi, E.Y., Stumpf, C.R., Christensen, C., Bonham, M.J.*, et al.* (2012). The translational landscape of mTOR signalling steers cancer initiation and metastasis. Nature *485*, 55-61.

Irani, K., Xia, Y., Zweier, J.L., Sollott, S.J., Der, C.J., Fearon, E.R., Sundaresan, M., Finkel, T., and Goldschmidt-Clermont, P.J. (1997). Mitogenic signaling mediated by oxidants in Ras-transformed fibroblasts. Science *275*, 1649-1652.

Jeanmougin, M., de Reynies, A., Marisa, L., Paccard, C., Nuel, G., and Guedj, M. (2010). Should we abandon the t-test in the analysis of gene expression microarray data: a comparison of variance modeling strategies. PloS one *5*, e12336.

Johnson, L., Mercer, K., Greenbaum, D., Bronson, R.T., Crowley, D., Tuveson, D.A., and Jacks, T. (2001). Somatic activation of the K-ras oncogene causes early onset lung cancer in mice. Nature *410*, 1111-1116.

Johnson, N.A., Slack, G.W., Savage, K.J., Connors, J.M., Ben-Neriah, S., Rogic, S., Scott, D.W., Tan, K.L., Steidl, C., Sehn, L.H.*, et al.* (2012). Concurrent expression of MYC and BCL2 in diffuse large B-cell lymphoma treated with rituximab plus cyclophosphamide, doxorubicin, vincristine, and prednisone. Journal of clinical oncology : official journal of the American Society of Clinical Oncology *30*, 3452-3459.

Jones, R.M., Branda, J., Johnston, K.A., Polymenis, M., Gadd, M., Rustgi, A., Callanan, L., and Schmidt, E.V. (1996). An essential E box in the promoter of the gene encoding the mRNA cap-binding protein (eukaryotic initiation factor 4E) is a target for activation by c-myc. Molecular and cellular biology *16*, 4754-4764.

Kanungo, A., Medeiros, L.J., Abruzzo, L.V., and Lin, P. (2006). Lymphoid neoplasms associated with concurrent t(14;18) and 8q24/c-MYC translocation generally have a poor prognosis. Modern pathology : an official journal of the United States and Canadian Academy of Pathology, Inc *19*, 25-33.

Kentsis, A., Topisirovic, I., Culjkovic, B., Shao, L., and Borden, K.L. (2004). Ribavirin suppresses eIF4E-mediated oncogenic transformation by physical mimicry of the 7-methyl guanosine mRNA cap. Proceedings of the National Academy of Sciences of the United States of America *101*, 18105-18110.

Kim, D.H., Sarbassov, D.D., Ali, S.M., King, J.E., Latek, R.R., Erdjument-Bromage, H., Tempst, P., and Sabatini, D.M. (2002). mTOR interacts with raptor to form a nutrient-sensitive complex that signals to the cell growth machinery. Cell *110*, 163-175.

Konicek, B.W., Stephens, J.R., McNulty, A.M., Robichaud, N., Peery, R.B., Dumstorf, C.A., Dowless, M.S., Iversen, P.W., Parsons, S., Ellis, K.E.*, et al.* (2011). Therapeutic inhibition of MAP kinase interacting kinase blocks eukaryotic initiation factor 4E phosphorylation and suppresses outgrowth of experimental lung metastases. Cancer research *71*, 1849-1857.

Koromilas, A.E., Lazaris-Karatzas, A., and Sonenberg, N. (1992). mRNAs containing extensive secondary structure in their 5' non-coding region translate efficiently in cells overexpressing initiation factor eIF-4E. The EMBO journal *11*, 4153-4158.

Kullmann, M., Gopfert, U., Siewe, B., and Hengst, L. (2002). ELAV/Hu proteins inhibit p27 translation via an IRES element in the p27 5'UTR. Genes & development *16*, 3087-3099.

Larsson, O., Perlman, D.M., Fan, D., Reilly, C.S., Peterson, M., Dahlgren, C., Liang, Z., Li, S., Polunovsky, V.A., Wahlestedt, C.*, et al.* (2006). Apoptosis resistance downstream of eIF4E: posttranscriptional activation of an anti-apoptotic transcript carrying a consensus hairpin structure. Nucleic acids research *34*, 4375-4386.

Lazaris-Karatzas, A., Montine, K.S., and Sonenberg, N. (1990). Malignant transformation by a eukaryotic initiation factor subunit that binds to mRNA 5' cap. Nature *345*, 544-547.

Levy, S., Avni, D., Hariharan, N., Perry, R.P., and Meyuhas, O. (1991). Oligopyrimidine tract at the 5' end of mammalian ribosomal protein mRNAs is required for their translational control. Proceedings of the National Academy of Sciences of the United States of America *88*, 3319-3323.

Lin, C.J., Nasr, Z., Premsrirut, P.K., Porco, J.A., Jr., Hippo, Y., Lowe, S.W., and Pelletier, J. (2012). Targeting synthetic lethal interactions between Myc and the eIF4F complex impedes tumorigenesis. Cell reports *1*, 325-333.

Lin, T.A., Kong, X., Haystead, T.A., Pause, A., Belsham, G., Sonenberg, N., and Lawrence, J.C., Jr. (1994). PHAS-I as a link between mitogen-activated protein kinase and translation initiation. Science *266*, 653-656.

Macejak, D.G., and Sarnow, P. (1991). Internal initiation of translation mediated by the 5' leader of a cellular mRNA. Nature *353*, 90-94.

Malhas, A.N., Lee, C.F., and Vaux, D.J. (2009). Lamin B1 controls oxidative stress responses via Oct-1. The Journal of cell biology *184*, 45-55.

Mamane, Y., Petroulakis, E., Martineau, Y., Sato, T.A., Larsson, O., Rajasekhar, V.K., and Sonenberg, N. (2007). Epigenetic activation of a subset of mRNAs by eIF4E explains its effects on cell proliferation. PloS one *2*, e242.

Manzella, J.M., and Blackshear, P.J. (1990). Regulation of rat ornithine decarboxylase mRNA translation by its 5'-untranslated region. The Journal of biological chemistry *265*, 11817-11822.

Martin, D.E., Soulard, A., and Hall, M.N. (2004). TOR regulates ribosomal protein gene expression via PKA and the Forkhead transcription factor FHL1. Cell *119*, 969-979.

Mayer, C., Zhao, J., Yuan, X., and Grummt, I. (2004). mTOR-dependent activation of the transcription factor TIF-IA links rRNA synthesis to nutrient availability. Genes & development *18*, 423-434.

McMahon, R., Zaborowska, I., and Walsh, D. (2011). Noncytotoxic inhibition of viral infection through eIF4F-independent suppression of translation by 4EGi-1. Journal of virology *85*, 853-864.

Mills, J.R., Hippo, Y., Robert, F., Chen, S.M., Malina, A., Lin, C.J., Trojahn, U., Wendel, H.G., Charest, A., Bronson, R.T.*, et al.* (2008). mTORC1 promotes survival through translational control of Mcl-1. Proceedings of the National Academy of Sciences of the United States of America *105*, 10853-10858.

Miskimins, W.K., Wang, G., Hawkinson, M., and Miskimins, R. (2001). Control of cyclin-dependent kinase inhibitor p27 expression by cap-independent translation. Molecular and cellular biology *21*, 4960-4967.

Moerke, N.J., Aktas, H., Chen, H., Cantel, S., Reibarkh, M.Y., Fahmy, A., Gross, J.D., Degterev, A., Yuan, J., Chorev, M.*, et al.* (2007). Small-molecule inhibition of the interaction between the translation initiation factors eIF4E and eIF4G. Cell *128*, 257-267.

Mootha, V.K., Lindgren, C.M., Eriksson, K.F., Subramanian, A., Sihag, S., Lehar, J., Puigserver, P., Carlsson, E., Ridderstrale, M., Laurila, E.*, et al.* (2003). PGC-1alpha-responsive genes involved in oxidative phosphorylation are coordinately downregulated in human diabetes. Nature genetics *34*, 267-273.

Mothe-Satney, I., Yang, D., Fadden, P., Haystead, T.A., and Lawrence, J.C., Jr. (2000). Multiple mechanisms control phosphorylation of PHAS-I in five (S/T)P sites that govern translational repression. Molecular and cellular biology *20*, 3558-3567.

Nikolcheva, T., Pyronnet, S., Chou, S.Y., Sonenberg, N., Song, A., Clayberger, C., and Krensky, A.M. (2002). A translational rheostat for RFLAT-1 regulates RANTES expression in T lymphocytes. The Journal of clinical investigation *110*, 119-126.

Pause, A., Belsham, G.J., Gingras, A.C., Donze, O., Lin, T.A., Lawrence, J.C., Jr., and Sonenberg, N. (1994). Insulin-dependent stimulation of protein synthesis by phosphorylation of a regulator of 5'-cap function. Nature *371*, 762-767.

Pham, C.G., Bubici, C., Zazzeroni, F., Papa, S., Jones, J., Alvarez, K., Jayawardena, S., De Smaele, E., Cong, R., Beaumont, C.*, et al.* (2004). Ferritin heavy chain upregulation by NF-kappaB inhibits TNFalpha-induced apoptosis by suppressing reactive oxygen species. Cell *119*, 529-542.

Pickering, B.M., and Willis, A.E. (2005). The implications of structured 5' untranslated regions on translation and disease. Seminars in cell & developmental biology *16*, 39-47.

Polunovsky, V.A., Rosenwald, I.B., Tan, A.T., White, J., Chiang, L., Sonenberg, N., and Bitterman, P.B. (1996). Translational control of programmed cell death: eukaryotic translation initiation factor 4E blocks apoptosis in growth-factor-restricted fibroblasts with physiologically expressed or deregulated Myc. Molecular and cellular biology *16*, 6573-6581.

Prochownik, E.V., and Vogt, P.K. (2010). Therapeutic Targeting of Myc. Genes & cancer *1*, 650-659.

Pyronnet, S., Pradayrol, L., and Sonenberg, N. (2000). A cell cycle-dependent internal ribosome entry site. Molecular cell *5*, 607-616.

Raj, L., Ide, T., Gurkar, A.U., Foley, M., Schenone, M., Li, X., Tolliday, N.J., Golub, T.R., Carr, S.A., Shamji, A.F.*, et al.* (2011). Selective killing of cancer cells by a small molecule targeting the stress response to ROS. Nature *475*, 231-234.

Rajasekhar, V.K., Viale, A., Socci, N.D., Wiedmann, M., Hu, X., and Holland, E.C. (2003). Oncogenic Ras and Akt signaling contribute to glioblastoma formation by differential recruitment of existing mRNAs to polysomes. Molecular cell *12*, 889-901.

Rau, M., Ohlmann, T., Morley, S.J., and Pain, V.M. (1996). A reevaluation of the cap-binding protein, eIF4E, as a rate-limiting factor for initiation of translation in reticulocyte lysate. The Journal of biological chemistry *271*, 8983-8990.

Rickert, R.C., Rajewsky, K., and Roes, J. (1995). Impairment of T-cell-dependent B-cell responses and B-1 cell development in CD19-deficient mice. Nature *376*, 352-355.

Rickert, R.C., Roes, J., and Rajewsky, K. (1997). B lymphocyte-specific, Cre-mediated mutagenesis in mice. Nucleic acids research *25*, 1317-1318.

Rogers, G.W., Jr., Richter, N.J., and Merrick, W.C. (1999). Biochemical and kinetic characterization of the RNA helicase activity of eukaryotic initiation factor 4A. The Journal of biological chemistry *274*, 12236-12244.

Rosenwald, I.B., Rhoads, D.B., Callanan, L.D., Isselbacher, K.J., and Schmidt, E.V. (1993). Increased expression of eukaryotic translation initiation factors eIF-4E and eIF-2 alpha in response to growth induction by c-myc. Proceedings of the National Academy of Sciences of the United States of America *90*, 6175-6178.

Rousseau, D., Kaspar, R., Rosenwald, I., Gehrke, L., and Sonenberg, N. (1996). Translation initiation of ornithine decarboxylase and nucleocytoplasmic transport of cyclin D1 mRNA are increased in cells overexpressing eukaryotic initiation factor 4E. Proceedings of the National Academy of Sciences of the United States of America *93*, 1065-1070.

Ruggero, D. (2009). The role of Myc-induced protein synthesis in cancer. Cancer research *69*, 8839-8843.

Ruggero, D., Montanaro, L., Ma, L., Xu, W., Londei, P., Cordon-Cardo, C., and Pandolfi, P.P. (2004). The translation factor eIF-4E promotes tumor formation and cooperates with c-Myc in lymphomagenesis. Nature medicine *10*, 484-486.

Ruvinsky, I., and Meyuhas, O. (2006). Ribosomal protein S6 phosphorylation: from protein synthesis to cell size. Trends in biochemical sciences *31*, 342-348.

Santini, E., Huynh, T.N., MacAskill, A.F., Carter, A.G., Pierre, P., Ruggero, D., Kaphzan, H., and Klann, E. (2013). Exaggerated translation causes synaptic and behavioural aberrations associated with autism. Nature *493*, 411-415.

Sato, H., Minei, S., Hachiya, T., Yoshida, T., and Takimoto, Y. (2006). Fluorescence in situ hybridization analysis of c-myc amplification in stage TNM prostate cancer in Japanese patients. International journal of urology : official journal of the Japanese Urological Association *13*, 761-766.

Sattler, M., Verma, S., Shrikhande, G., Byrne, C.H., Pride, Y.B., Winkler, T., Greenfield, E.A., Salgia, R., and Griffin, J.D. (2000). The BCR/ABL tyrosine kinase induces production of reactive oxygen species in hematopoietic cells. The Journal of biological chemistry *275*, 24273-24278.

Savage, K.J., Johnson, N.A., Ben-Neriah, S., Connors, J.M., Sehn, L.H., Farinha, P., Horsman, D.E., and Gascoyne, R.D. (2009). MYC gene rearrangements are associated with a poor prognosis in diffuse large B-cell lymphoma patients treated with R-CHOP chemotherapy. Blood *114*, 3533-3537.

Sayin, V.I., Ibrahim, M.X., Larsson, E., Nilsson, J.A., Lindahl, P., and Bergo, M.O. (2014). Antioxidants accelerate lung cancer progression in mice. Science translational medicine *6*, 221ra215.

Schafer, Z.T., Grassian, A.R., Song, L., Jiang, Z., Gerhart-Hines, Z., Irie, H.Y., Gao, S., Puigserver, P., and Brugge, J.S. (2009). Antioxidant and oncogene rescue of metabolic defects caused by loss of matrix attachment. Nature *461*, 109-113.

Scheper, G.C., Morrice, N.A., Kleijn, M., and Proud, C.G. (2001). The mitogen-activated protein kinase signal-integrating kinase Mnk2 is a eukaryotic initiation factor 4E kinase with high levels of basal activity in mammalian cells. Molecular and cellular biology *21*, 743-754.

Schmidt, E.V. (2004). The role of c-myc in regulation of translation initiation. Oncogene *23*, 3217-3221.

She, Q.B., Halilovic, E., Ye, Q., Zhen, W., Shirasawa, S., Sasazuki, T., Solit, D.B., and Rosen, N. (2010). 4E-BP1 is a key effector of the oncogenic activation of the AKT and ERK signaling pathways that integrates their function in tumors. Cancer cell *18*, 39-51.

Shi, Z.Z., Osei-Frimpong, J., Kala, G., Kala, S.V., Barrios, R.J., Habib, G.M., Lukin, D.J., Danney, C.M., Matzuk, M.M., and Lieberman, M.W. (2000). Glutathione synthesis is essential for mouse development but not for cell growth in culture. Proceedings of the National Academy of Sciences of the United States of America *97*, 5101-5106.

Shou, Y., Martelli, M.L., Gabrea, A., Qi, Y., Brents, L.A., Roschke, A., Dewald, G., Kirsch, I.R., Bergsagel, P.L., and Kuehl, W.M. (2000). Diverse karyotypic abnormalities of the c-myc locus associated with c-myc dysregulation and tumor progression in multiple myeloma. Proceedings of the National Academy of Sciences of the United States of America *97*, 228-233.

Sonenberg, N., and Hinnebusch, A.G. (2009). Regulation of translation initiation in eukaryotes: mechanisms and biological targets. Cell *136*, 731-745.

Stefanovsky, V.Y., Pelletier, G., Hannan, R., Gagnon-Kugler, T., Rothblum, L.I., and Moss, T. (2001). An immediate response of ribosomal transcription to growth factor stimulation in mammals is mediated by ERK phosphorylation of UBF. Molecular cell *8*, 1063-1073.

Stumpf, C.R., Moreno, M.V., Olshen, A.B., Taylor, B.S., and Ruggero, D. (2013). The translational landscape of the mammalian cell cycle. Molecular cell *52*, 574-582.

Subramanian, A., Tamayo, P., Mootha, V.K., Mukherjee, S., Ebert, B.L., Gillette, M.A., Paulovich, A., Pomeroy, S.L., Golub, T.R., Lander, E.S.*, et al.* (2005). Gene set enrichment analysis: a knowledge-based approach for interpreting genome-wide expression profiles. Proceedings of the National Academy of Sciences of the United States of America *102*, 15545-15550.

Szatrowski, T.P., and Nathan, C.F. (1991). Production of large amounts of hydrogen peroxide by human tumor cells. Cancer research *51*, 794-798.

Thoreen, C.C., Chantranupong, L., Keys, H.R., Wang, T., Gray, N.S., and Sabatini, D.M. (2012). A unifying model for mTORC1-mediated regulation of mRNA translation. Nature *485*, 109-113.

Thoreen, C.C., Kang, S.A., Chang, J.W., Liu, Q., Zhang, J., Gao, Y., Reichling, L.J., Sim, T., Sabatini, D.M., and Gray, N.S. (2009). An ATP-competitive mammalian target of rapamycin inhibitor reveals rapamycin-resistant functions of mTORC1. The Journal of biological chemistry *284*, 8023-8032.

Topisirovic, I., Ruiz-Gutierrez, M., and Borden, K.L. (2004). Phosphorylation of the eukaryotic translation initiation factor eIF4E contributes to its transformation and mRNA transport activities. Cancer research *64*, 8639-8642.

Topisirovic, I., Svitkin, Y.V., Sonenberg, N., and Shatkin, A.J. (2011). Cap and cap-binding proteins in the control of gene expression. Wiley interdisciplinary reviews RNA *2*, 277-298.

Trachootham, D., Zhou, Y., Zhang, H., Demizu, Y., Chen, Z., Pelicano, H., Chiao, P.J., Achanta, G., Arlinghaus, R.B., Liu, J.*, et al.* (2006). Selective killing of oncogenically transformed cells through a ROS-mediated mechanism by beta-phenylethyl isothiocyanate. Cancer cell *10*, 241-252.

Ueda, T., Sasaki, M., Elia, A.J., Chio, II, Hamada, K., Fukunaga, R., and Mak, T.W. (2010). Combined deficiency for MAP kinase-interacting kinase 1 and 2 (Mnk1 and Mnk2) delays tumor development. Proceedings of the National Academy of Sciences of the United States of America *107*, 13984-13990.

Vafa, O., Wade, M., Kern, S., Beeche, M., Pandita, T.K., Hampton, G.M., and Wahl, G.M. (2002). c-Myc can induce DNA damage, increase reactive oxygen species, and mitigate p53 function: a mechanism for oncogene-induced genetic instability. Molecular cell *9*, 1031-1044.

van Riggelen, J., Yetil, A., and Felsher, D.W. (2010). MYC as a regulator of ribosome biogenesis and protein synthesis. Nat Rev Cancer *10*, 301-309.

von der Haar, T., Gross, J.D., Wagner, G., and McCarthy, J.E. (2004). The mRNA cap-binding protein eIF4E in post-transcriptional gene expression. Nature structural & molecular biology *11*, 503-511.

von der Haar, T., and McCarthy, J.E. (2002). Intracellular translation initiation factor levels in Saccharomyces cerevisiae and their role in cap-complex function. Molecular microbiology *46*, 531-544.

von Manteuffel, S.R., Dennis, P.B., Pullen, N., Gingras, A.C., Sonenberg, N., and Thomas, G. (1997). The insulin-induced signalling pathway leading to S6 and initiation factor 4E binding protein 1 phosphorylation bifurcates at a rapamycin-sensitive point immediately upstream of p70s6k. Molecular and cellular biology *17*, 5426-5436.

Wall, M., Poortinga, G., Stanley, K.L., Lindemann, R.K., Bots, M., Chan, C.J., Bywater, M.J., Kinross, K.M., Astle, M.V., Waldeck, K.*, et al.* (2013). The mTORC1 inhibitor everolimus prevents and treats Emu-Myc lymphoma by restoring oncogene-induced senescence. Cancer discovery *3*, 82-95.

Wallace, D.C. (2012). Mitochondria and cancer. Nat Rev Cancer *12*, 685-698.

Wang, R., Geng, J., Wang, J.H., Chu, X.Y., Geng, H.C., and Chen, L.B. (2009). Overexpression of eukaryotic initiation factor 4E (eIF4E) and its clinical significance in lung adenocarcinoma. Lung cancer *66*, 237-244.

Wang, X., Li, W., Williams, M., Terada, N., Alessi, D.R., and Proud, C.G. (2001). Regulation of elongation factor 2 kinase by p90(RSK1) and p70 S6 kinase. The EMBO journal *20*, 4370-4379.

Wang, X., and Proud, C.G. (2006). The mTOR pathway in the control of protein synthesis. Physiology *21*, 362-369.

Waskiewicz, A.J., Flynn, A., Proud, C.G., and Cooper, J.A. (1997). Mitogen-activated protein kinases activate the serine/threonine kinases Mnk1 and Mnk2. The EMBO journal *16*, 1909-1920.

Weinberg, F., Hamanaka, R., Wheaton, W.W., Weinberg, S., Joseph, J., Lopez, M., Kalyanaraman, B., Mutlu, G.M., Budinger, G.R., and Chandel, N.S. (2010). Mitochondrial metabolism and ROS generation are essential for Kras-mediated tumorigenicity. Proceedings of the National Academy of Sciences of the United States of America *107*, 8788-8793.

Wendel, H.G., De Stanchina, E., Fridman, J.S., Malina, A., Ray, S., Kogan, S., Cordon-Cardo, C., Pelletier, J., and Lowe, S.W. (2004). Survival signalling by Akt and eIF4E in oncogenesis and cancer therapy. Nature *428*, 332-337.

Westman, B., Beeren, L., Grudzien, E., Stepinski, J., Worch, R., Zuberek, J., Jemielity, J., Stolarski, R., Darzynkiewicz, E., Rhoads, R.E.*, et al.* (2005). The antiviral drug ribavirin does not mimic the 7-methylguanosine moiety of the mRNA cap structure in vitro. Rna *11*, 1505-1513.

Wolfe, A.L., Singh, K., Zhong, Y., Drewe, P., Rajasekhar, V.K., Sanghvi, V.R., Mavrakis, K.J., Jiang, M., Roderick, J.E., Van der Meulen, J.*, et al.* (2014). RNA G-quadruplexes cause eIF4A-dependent oncogene translation in cancer. Nature *513*, 65-70.

Wolfer, A., Wittner, B.S., Irimia, D., Flavin, R.J., Lupien, M., Gunawardane, R.N., Meyer, C.A., Lightcap, E.S., Tamayo, P., Mesirov, J.P.*, et al.* (2010). MYC regulation of a "poor-prognosis" metastatic cancer cell state. Proceedings of the National Academy of Sciences of the United States of America *107*, 3698-3703.

Yan, Y., Svitkin, Y., Lee, J.M., Bisaillon, M., and Pelletier, J. (2005). Ribavirin is not a functional mimic of the 7-methyl guanosine mRNA cap. Rna *11*, 1238-1244.

Yanagiya, A., Suyama, E., Adachi, H., Svitkin, Y.V., Aza-Blanc, P., Imataka, H., Mikami, S., Martineau, Y., Ronai, Z.A., and Sonenberg, N. (2012). Translational homeostasis via the mRNA cap-binding protein, eIF4E. Molecular cell *46*, 847-858.

Zoncu, R., Efeyan, A., and Sabatini, D.M. (2011). mTOR: from growth signal integration to cancer, diabetes and ageing. Nature reviews Molecular cell biology *12*, 21-35.

Appendices

Appendix 1: List of genes whose translation is altered by oncogenic transformation. 880 probes corresponding to 722 annotated genes whose translational efficiency is changed (472 increased, 250 decreased) upon oncogenic transformation in WT cells (fold change>1.7, p<0.05). NA = not annotated.

Appendix 2: List of genes whose translation is limited by eIF4E during oncogenic transformation. 154 probes corresponding to 133 annotated genes whose translational efficiency is decreased upon oncogenic transformation in *Eif4e*$^{+/-}$ cells (fold change<1.7, p<0.05). NA = not annotated.

Appendix 3: KEGG pathways enriched in genes translationally induced by oncogenic transformation. Top 35 KEGG pathways identified by GSEA analysis of changes in translational efficiency induced by oncogenic transformation.

Appendix 4: Biological processes enriched in genes translationally induced by oncogenic transformation. Top 35 gene ontology biological processes identified by GSEA analysis of changes in translational efficiency induced by oncogenic transformation.

Appendix 5: KEGG pathways induced by transformation in an eIF4E-dependent manner. KEGG pathways identified by GSEA analysis of changes in translational efficiency induced by oncogenic transformation (see Appenix 3) whose translation is significantly reduced in transformed *Eif4e*$^{+/-}$ cells (FDR < 0.15).

Appendix 6: Biological processes induced by transformation in an eIF4E-dependent manner. Biological processes identified by GSEA analysis of changes in translational efficiency induced by oncogenic transformation (see Appendix 4) whose translation is significantly reduced in transformed *Eif4e*$^{+/-}$ cells (FDR < 0.15).

Appendix 7: Translation of the oxidative phosphorylation pathway is induced during oncogenic transformation. GSEA analysis of the KEGG “Oxidative Phosphorylation” pathway for genes whose translational efficiency is induced by transformation.

Appendix 8: Translation of the response to oxidative stress is induced during transformation. GSEA analysis of the gene ontology biological process “Response to Oxidative Stress” for genes whose translational efficiency is induced by transformation.

Appendix 9: Translation of the glutathione metabolism pathway is induced during oncogenic transformation. GSEA analysis of the KEGG “Glutathione Metabolism” pathway for genes whose translational efficiency is induced by transformation.

Appendix 10: Translationally controlled genes involved in the regulation and response to oxidative stress during oncogenic transformation. GSEA analysis for a defined class of genes broadly involved in the regulation and response to oxidative stress (see Experimental Procedures).

Appendix 11: eIF4E-dependent genes involved in the regulation and response to oxidative stress. GSEA analysis for the subset of translationally controlled genes involved in the regulation and response to oxidative stress.

Appendix 12: Training set used for motif analysis. List of genes symbols, UCSC known gene IDs, and 5’UTR lengths for 5’UTRs retrieved from the UCSC genome browser and used for identification of the CERT motif through MEME.

Appendix 13: eIF4E targets are enriched for the presence of the cis-acting CERT motif. List CERT locations in 79 eIF4E targets containing a CERT motif ($p<10^{-3}$) out of the 116 eIF4E target genes with UCSC annotated 5’UTRs. All 5’UTR sequences with significant homology to the CERT motif and their respective locations are listed. *denotes use of NCBI RefSeq annotated 5’UTR.

Appendix 1:

Affymetrix ID	GeneName	Fold Change	t-score	p-value
10513774	NA	4.68195	19.6412	1.70E-07
10536667	Ptprz1	3.99018	12.4172	4.17E-06
10398360	NA	3.10131	5.57717	0.000770198
10440258	Epha3	3.02465	11.7597	6.06E-06
10601648	Tnmd	2.96449	11.4565	7.25E-06
10344674	Fam150a	2.93333	9.70467	2.23E-05
10398366	NA	2.90159	7.13759	0.000167528
10598034	ND2	2.89413	10.6465	1.19E-05
10423243	Cdh10	2.88212	10.3445	1.45E-05
10398362	Rian	2.80696	4.65384	0.00219051
10430723	Slc25a17	2.80529	7.24748	0.00015195
10542953	Tfpi2	2.7895	8.00179	8.01E-05
10398364	NA	2.70394	4.5453	0.00249657
10398368	NA	2.69896	7.38941	0.000134183
10474096	Lrrc4c	2.6933	9.88	1.98E-05
10598075	NA	2.68747	10.6357	1.20E-05
10372648	Lyz2	2.61822	9.0743	3.50E-05
10520452	Il6	2.60974	5.79207	0.000613813
10346878	Zdbf2	2.53934	7.15916	0.000164334
10513957	Ptprd	2.49136	10.3536	1.44E-05
10477813	Rbm39	2.48631	4.06223	0.00456359
10402604	NA	2.47517	8.84582	4.14E-05
10420274	Gzmd	2.39889	4.94367	0.00155783
10398326	Meg3	2.33989	5.83309	0.000588177
10456721	NA	2.31035	8.53646	5.24E-05
10488060	Jag1	2.27835	5.15539	0.00122361
10598064	NA	2.2428	7.66028	0.000106386
10548385	Olr1	2.24177	8.05599	7.67E-05
10496359	Emcn	2.18652	7.63308	0.000108863
10601421	A630033H20Rik	2.16006	3.54852	0.00900538
10543114	Rpa3	2.15197	4.78893	0.00186594
10528207	Cd36	2.13686	9.06955	3.51E-05
10578880	Tll1	2.11392	6.96995	0.00019487
10443459	Sfrs3	2.0576	4.86494	0.00170692
10368409	Lama2	2.02647	5.69343	0.000680708
10436727	ORF63	2.00994	8.1566	7.07E-05
10398358	NA	2.00555	7.41554	0.000131172
10398354	NA	1.9979	7.98763	8.11E-05
10494271	Ctss	1.99215	8.44627	5.62E-05

10483081	Fap	1.97444	5.06973	0.00134818
10428707	Has2	1.95175	5.58831	0.000761082
10353674	Lsm5	1.94605	6.68498	0.000253631
10485711	Fibin	1.93915	7.30088	0.000144972
10490818	Stmn2	1.91405	7.1615	0.000163991
10453049	Cdc42ep3	1.8905	5.27864	0.00106618
10522324	Gabrb1	1.88914	7.20379	0.00015794
10494821	Tspan2	1.86285	5.63874	0.000721278
10606016	Il2rg	1.86121	4.2739	0.00348865
10420362	Gjb2	1.84332	7.44894	0.000127435
10405047	Aspn	1.84331	5.57123	0.000775107
10466676	1110059E24Rik	1.83541	3.79183	0.00649491
10598073	NA	1.82593	7.68251	0.000104409
10582821	NA	1.82485	5.52344	0.000815915
10598032	NA	1.81575	6.4064	0.000330913
10377982	Kif1c	1.80331	5.21737	0.00114144
10480090	Itga8	1.8014	6.34332	0.000351875
10428604	Tnfrsf11b	1.79932	7.01787	0.000186574
10505489	Pappa	1.79432	6.24294	0.000388362
10363082	Lilrb4	1.77908	5.99793	0.000496538
10468517	Mxi1	1.77786	4.68943	0.00209935
10404783	Edn1	1.76886	6.63597	0.000265617
10473779	Cugbp1	1.76632	4.14913	0.00408382
10447649	Fndc1	1.7511	6.78638	0.000230704
10398380	NA	1.73372	5.10236	0.00129915
10604694	Mtap7d3	1.73266	6.11314	0.000441969
10601569	Pcdh11x	1.71663	5.74908	0.000642021
10423742	Polr2k	1.71053	4.5241	0.00256165
10385716	0610009B22Rik	1.70564	2.57967	0.0357624
10353102	Cpa6	1.70542	6.07323	0.000460078
10461402	Fth1	1.70174	6.71626	0.000246297
10360920	Tgfb2	1.69623	5.49787	0.00083873
10587616	Prss35	1.6921	5.60624	0.000746657
10600604	Dmd	1.68648	6.15106	0.0004255
10503659	Epha7	1.68537	7.00205	0.000189268
10360415	Grem2	1.68268	7.27555	0.000148236
10541496	Mfap5	1.67852	3.3004	0.0126779
10478943	Pfdn4	1.67314	4.99426	0.00146964
10587231	Bmp5	1.6598	6.38897	0.000336562
10355893	Epha4	1.65877	6.40307	0.000331986
10407122	NA	1.65793	5.44301	0.000890101
10536635	A430107O13Rik	1.63708	6.78936	0.000230066
10498935	Gucy1b3	1.63105	5.27548	0.00106993

10502552	Clca1	1.62925	4.39126	0.00301464
10357833	Atp2b4	1.61975	5.8388	0.000584701
10542750	Med21	1.61159	3.53213	0.00920869
10539433	Mobkl1b	1.61094	6.90208	0.000207335
10351043	NA	1.60441	5.68936	0.000683641
10483439	Lrp2	1.59186	5.23849	0.00111486
10578241	A730069N07Rik	1.58673	6.65008	0.000262103
10358583	Hmcn1	1.577	6.53744	0.000291689
10375137	Kcnmb1	1.57227	4.62829	0.00225864
10394770	Odc1	1.55637	5.36341	0.000970978
10467110	AI747699	1.55001	6.1037	0.000446178
10346882	Adam23	1.54804	6.20813	0.000401987
10358666	Hmcn1	1.54081	5.73647	0.000650573
10423287	Cdh18	1.53855	5.61881	0.000736719
10355500	Igfbp5	1.53504	6.13923	0.000430562
10413014	Chchd1	1.5338	4.11357	0.00427312
10523021	Slc4a4	1.52999	5.48594	0.000849616
10423080	C1qtnf3	1.52551	4.88648	0.00166462
10412298	Itga1	1.52036	6.10143	0.000447196
10507152	Cyp4a12b	1.51916	5.77252	0.000626469
10491732	Fat4	1.51693	6.21975	0.000397381
10404024	Hist1h4h	1.5168	4.77989	0.00188592
10435961	Gm10808	1.51282	6.07254	0.000460396
10408197	Hist1h2bh	1.50024	6.39957	0.000333115
10586079	Itga11	1.4999	4.04945	0.00463922
10530832	2610024G14Rik	1.49509	4.9803	0.00149341
10375443	Havcr2	1.48523	2.86172	0.0236731
10598027	NA	1.48325	4.30766	0.00334445
10424555	NA	1.47476	3.59966	0.00840158
10435948	Ccdc80	1.47006	4.12307	0.00422163
10446619	Myom1	1.46814	5.57504	0.000771954
10408762	Eef1e1	1.46535	2.76916	0.0270833
10399820	Acp1	1.45744	4.97006	0.00151112
10502565	Clca2	1.45703	5.09095	0.00131607
10599335	Mcts1	1.44527	4.39475	0.00300167
10559790	Zim1	1.44222	4.7778	0.00189058
10540283	Ppp4r2	1.44005	4.18981	0.00387837
10367100	Ptges3	1.43577	2.58869	0.0352898
10456545	Ccdc68	1.42999	4.14531	0.00410371
10349947	Fmod	1.42899	5.83478	0.000587145
10507653	NA	1.42476	6.13472	0.000432508
10572070	Npy1r	1.42392	5.95474	0.000518906
10427796	Npr3	1.4194	3.08028	0.0172922

10406710	Tbca	1.4173	2.74077	0.0282293
10600524	Vbp1	1.4164	3.20097	0.0145747
10519998	Lrrc17	1.41622	5.72696	0.0006571
10376956	Hs3st3a1	1.40812	5.06804	0.00135078
10366476	Ptprb	1.40765	5.05299	0.00137414
10438904	Lrrc15	1.39887	4.49291	0.00266088
10515164	Cmpk1	1.39105	3.92072	0.00548184
10423274	Cdh18	1.38785	5.7508	0.000640866
10604226	C1galt1c1	1.38306	3.8822	0.00576526
10599736	Fhl1	1.38163	4.42285	0.00289947
10467136	Ch25h	1.38063	4.33929	0.00321521
10506736	Magoh	1.37274	3.23124	0.0139672
10555323	P4ha3	1.36893	5.16208	0.00121444
10571399	Zdhhc2	1.3672	4.23987	0.00364094
10358668	Hmcn1	1.36606	3.71579	0.00718659
10601942	Nrk	1.3596	4.6236	0.00227142
10537712	Gstk1	1.3559	5.22195	0.00113562
10405179	S1pr3	1.35342	4.106	0.00431468
10502451	Bmpr1b	1.34741	4.96557	0.00151895
10558454	Glrx3	1.34463	2.82348	0.0250237
10407337	Hcn1	1.32987	5.44802	0.000885266
10568668	Adam12	1.32918	4.85575	0.00172532
10567297	Itpripl2	1.32912	4.52728	0.00255177
10521759	Slit2	1.32677	5.00942	0.00144432
10601659	Srpx2	1.32552	3.99006	0.00500897
10451838	Slc5a7	1.31994	5.24909	0.00110177
10403943	Hist1h2bm	1.31799	4.0436	0.00467427
10408225	Hist1h4c	1.31752	5.25205	0.00109814
10423109	Adamts12	1.3112	5.67198	0.000696313
10441811	NA	1.30774	4.61608	0.00229202
10372988	Slc16a7	1.30553	5.52289	0.000816402
10450784	H2-M9	1.30421	4.29043	0.00341722
10436493	NA	1.29899	4.1683	0.00398555
10404700	Ubxn2a	1.29736	3.77861	0.00660976
10412082	Gpbp1	1.29464	2.61925	0.0337363
10428081	Hrsp12	1.29269	2.72767	0.0287752
10439500	Upk1b	1.28663	4.37949	0.00305884
10479973	Gm10115	1.28516	5.38818	0.000944964
10519886	Sema3c	1.28405	3.05278	0.0179838
10358577	Hmcn1	1.28165	4.06723	0.0045344
10578264	Msr1	1.27781	5.39993	0.0009329
10590031	Itga9	1.27337	4.16459	0.00400437
10444713	Bat4	1.26854	4.41423	0.0029304

10578324	Mtus1	1.26366	4.48173	0.00269747
10421911	Pcdh20	1.26011	5.08781	0.00132077
10437885	Myh11	1.2576	4.99984	0.00146026
10594480	Rab11a	1.25636	3.36631	0.0115672
10460626	Rnaseh2c	1.24877	3.67748	0.00756492
10399202	Macc1	1.24593	5.35075	0.000984577
10354472	Gls	1.24561	2.56395	0.0366015
10385770	Olfr1372-ps1	1.24452	3.45266	0.0102671
10392464	Fam20a	1.24436	4.91568	0.00160912
10498018	Pcdh18	1.2431	5.12697	0.00126347
10593293	Ncam1	1.24274	3.75356	0.00683354
10405211	Gadd45g	1.24001	3.81772	0.00627614
10368495	Rspo3	1.23823	4.60675	0.00231791
10575144	Nip7	1.23816	4.59045	0.00236388
10351013	Rc3h1	1.22315	4.89206	0.00165385
10376312	Larp1	1.21836	3.97155	0.00513068
10363231	Smpdl3a	1.21772	4.45254	0.00279561
10446965	Rasgrp3	1.21767	2.55501	0.0370877
10456046	Pdgfrb	1.21619	5.26144	0.00108674
10377851	Psmb6	1.21318	3.54882	0.00900174
10517421	Pnrc2	1.21181	2.60943	0.0342276
10519857	Hgf	1.20973	4.89457	0.00164902
10459225	NA	1.20961	5.06717	0.00135212
10353032	Rpa3	1.20873	3.55403	0.00893821
10351037	Gas5	1.20796	3.70127	0.00732758
10408200	Hist1h4f	1.20563	4.41226	0.00293754
10358565	Hmcn1	1.20534	4.55964	0.00245354
10574023	Mt2	1.20061	4.15968	0.00402943
10530421	Gabra4	1.19751	5.07489	0.0013403
10450814	Ppp1r11	1.19671	3.97775	0.00508956
10388154	Med31	1.19372	4.50748	0.00261401
10563570	Tph1	1.19019	3.2025	0.0145433
10380210	Sfrs1	1.18879	3.42493	0.0106666
10462507	Papss2	1.18737	4.38184	0.00304997
10384032	Pold2	1.1855	4.48516	0.00268617
10525381	Vps29	1.1841	3.11734	0.0164047
10398356	NA	1.18379	4.39153	0.00301365
10535095	Zfand2a	1.18199	3.5302	0.00923296
10358664	Hmcn1	1.17881	2.92224	0.0216892
10401172	Vti1b	1.17815	2.61621	0.0338877
10505512	Trim32	1.17529	3.96972	0.00514288
10459335	Fam38b	1.1712	3.69419	0.00739731
10359908	Rgs4	1.17109	4.78634	0.00187164

10595402	Fam46a	1.16925	3.91714	0.00550747
10375501	NA	1.16406	3.01129	0.019083
10464400	E330013P04Rik	1.16246	3.59687	0.00843342
10440534	Adamts5	1.15453	4.02825	0.0047677
10566993	Galntl4	1.15034	3.83252	0.00615469
10588899	Gpx1	1.15026	3.61554	0.00822312
10446282	Emr1	1.149	4.65945	0.00217586
10545629	Htra2	1.14717	4.28975	0.00342013
10461164	Wdr74	1.14333	4.67136	0.00214511
10369290	Ddit4	1.14309	4.18809	0.00388683
10421932	Pcdh9	1.14273	3.60299	0.00836374
10369842	NA	1.14178	4.68104	0.00212047
10496519	Unc5c	1.13975	4.76818	0.00191216
10568593	Mettl10	1.13825	4.46365	0.00275778
10458052	Epb4.1l4a	1.1367	4.37111	0.00309073
10601846	2900062L11Rik	1.13617	4.52054	0.00257278
10403076	NA	1.13574	3.60679	0.00832094
10605986	Slc7a3	1.13239	3.77827	0.00661272
10352393	Srp9	1.12585	3.35944	0.0116779
10592420	AW551984	1.12102	3.11795	0.0163906
10548038	Ntf3	1.11855	4.44721	0.00281394
10591118	Fat3	1.11614	4.20951	0.00378299
10595614	2810026P18Rik	1.11409	3.28851	0.0128902
10603567	Dynlt3	1.11233	3.33993	0.0119987
10580300	Asna1	1.11141	3.94138	0.00533606
10482968	Pla2r1	1.10363	4.76289	0.00192414
10480139	C1ql3	1.1036	4.32203	0.00328505
10362186	Moxd1	1.09638	4.12082	0.00423376
10380815	Psmb3	1.09606	3.85232	0.00599612
10478692	Slc2a10	1.09434	3.29324	0.0128053
10435991	Gm5406	1.0897	3.26455	0.0133296
10585180	Ncam1	1.08562	4.34276	0.00320137
10459768	NA	1.08356	4.64388	0.00221681
10576029	Cox4i1	1.08136	2.7874	0.0263726
10397277	Fcf1	1.08071	2.71817	0.0291779
10362487	Tspyl1	1.07918	3.79848	0.00643789
10574427	Impdh2	1.0776	2.76593	0.0272112
10598067	NA	1.07559	2.56236	0.0366872
10407841	Hecw1	1.07229	2.77729	0.0267639
10513208	Svep1	1.07122	3.92199	0.00547273
10393047	Galk1	1.06618	3.92582	0.0054454
10495279	Psma5	1.06536	2.91979	0.0217663
10507238	Lrrc41	1.06489	3.74364	0.0069244

10421924	Pcdh9	1.06332	3.72686	0.00708111
10546432	Adamts9	1.06275	2.427	0.0448267
10404132	Cmah	1.06124	3.92018	0.00548568
10601356	Cox7b	1.05964	3.26752	0.0132742
10365559	Igf1	1.05578	4.10954	0.00429518
10466200	Ms4a7	1.05209	4.17101	0.0039719
10450055	H2-Ke2	1.04982	3.16803	0.0152682
10474915	Gchfr	1.04603	4.31778	0.0033025
10476106	NA	1.04492	4.40133	0.00297739
10531177	Adamts3	1.04267	3.89217	0.00569038
10372078	D10Ertd322e	1.04231	3.55246	0.00895731
10577641	1810011O10Rik	1.04109	3.72838	0.00706675
10503382	Runx1t1	1.0402	3.83741	0.0061151
10420268	Gzme	1.03657	3.9345	0.00538407
10515253	Uqcrh	1.03636	3.80947	0.00634496
10358670	Hmcn1	1.0351	3.68171	0.00752217
10369481	H2afy2	1.03501	3.0919	0.0170086
10375031	Snrnp25	1.03092	2.74671	0.0279853
10603583	Srpx	1.03077	3.01129	0.0190831
10487476	1500011K16Rik	1.02863	2.63949	0.0327469
10484389	Tfpi	1.02576	2.53532	0.0381818
10524312	Ttc28	1.02464	3.71691	0.00717582
10571567	Sorbs2	1.02411	3.78596	0.0065456
10362538	Lama4	1.02314	3.4757	0.00994736
10573578	BC056474	1.02308	3.59425	0.00846335
10398442	NA	1.02145	3.45888	0.0101797
10401527	Ltbp2	1.02084	3.60141	0.00838167
10358585	Hmcn1	1.01841	3.22732	0.0140443
10604333	Decaf12l1	1.01795	4.34485	0.00319308
10388682	Taok1	1.01683	3.74348	0.00692591
10522208	Uchl1	1.01395	3.32526	0.0122461
10570957	Sfrp1	1.01378	4.10436	0.00432373
10495111	Wdr77	1.01149	2.81582	0.0253039
10569014	Ifitm2	1.01066	2.81771	0.0252345
10552418	Etfb	1.00763	3.68615	0.00747747
10501734	Palmd	1.00702	3.69635	0.00737599
10402752	2010107E04Rik	1.00702	3.19521	0.0146935
10559270	Tssc4	1.00687	4.24313	0.00362604
10408223	Hist1h2bc	1.00519	4.26449	0.00353006
10560530	Bloc1s3	1.0051	3.77654	0.00662794
10534654	Znhit1	1.00416	2.61989	0.0337045
10531261	Rassf6	1.00388	2.95673	0.0206379
10349868	Ppp1r15b	1.00348	2.75114	0.0278047

10489299	NA	1.00116	3.60808	0.00830635
10364683	Stk11	1.00053	2.85484	0.0239104
10393395	Sfrs2	1.0003	3.84715	0.00603707
10346150	Tmeff2	0.997808	3.72564	0.00709268
10391490	Etv4	0.997286	3.68898	0.00744921
10473125	Itga4	0.997281	2.94685	0.0209336
10455948	Chsy3	0.992034	3.79706	0.00644999
10601878	Tceal1	0.990342	3.6377	0.00798076
10382010	Dcaf7	0.990063	3.94401	0.0053178
10351026	Gas5	0.989241	3.81908	0.00626488
10400896	2810055F11Rik	0.989084	2.64441	0.0325112
10591544	Yipf2	0.987793	4.14739	0.00409288
10552311	Gm15470	0.987407	3.12748	0.0161704
10366043	Dusp6	0.98733	2.46328	0.042478
10490370	Psma7	0.987037	2.74066	0.0282338
10558515	Inpp5a	0.984043	2.93619	0.0212574
10476321	Prnd	0.983123	2.81198	0.0254455
10456719	NA	0.980383	3.49539	0.00968266
10414355	Mapk1ip1l	0.979594	3.47109	0.0100105
10583297	Taf1d	0.978707	3.59746	0.0084266
10358581	Hmcn1	0.977283	3.12195	0.0162976
10487021	Slc30a4	0.975625	3.89958	0.00563545
10465649	Mark2	0.974084	3.40626	0.0109449
10393642	Eif4a3	0.972658	3.64256	0.00792871
10351039	Gas5	0.972129	2.57312	0.0361094
10395733	Npas3	0.969539	3.58023	0.00862572
10395659	Coch	0.969445	4.11937	0.00424163
10583870	Bmper	0.969283	4.17967	0.00392851
10420385	N6amt2	0.965773	2.69254	0.0302936
10347792	NA	0.961164	3.22953	0.0140006
10345777	Il1rl2	0.960705	3.99699	0.0049642
10398378	NA	0.95969	3.97366	0.00511666
10461150	NA	0.95773	2.78033	0.0266455
10479228	Etohi1	0.957575	3.39582	0.0111041
10553773	Gabrb3	0.956792	3.64743	0.00787688
10358549	Hmcn1	0.955565	3.89657	0.00565771
10597136	Ptpn23	0.954248	3.19475	0.0147032
10505182	Gng10	0.952652	2.91127	0.0220354
10379989	Fam33a	0.950148	3.98782	0.00502357
10356712	Kif1a	0.948964	3.84615	0.0060451
10604523	Rap2c	0.948015	3.16174	0.0154044
10508721	Snora44	0.945693	3.51683	0.00940306
10452228	Khsrp	0.945364	2.98276	0.0198801

10475625	Eid1	0.945085	2.68935	0.0304357
10360058	Tomm40l	0.944757	3.46964	0.0100305
10358652	Hmcn1	0.944215	3.06278	0.0177289
10539135	Capg	0.94297	3.60205	0.00837446
10583314	Taf1d	0.942579	2.55676	0.0369918
10453102	Sfrs7	0.941358	2.60784	0.0343079
10439980	Pcnp	0.939369	3.13778	0.0159359
10427807	Sub1	0.938858	2.82454	0.0249852
10546450	Adamts9	0.938402	2.95383	0.0207242
10360076	Ndufs2	0.938177	4.03326	0.00473697
10586448	2810417H13Rik	0.937404	3.31833	0.0123649
10400170	Prkd1	0.937157	4.04927	0.00464029
10499062	Fhdc1	0.936319	3.20034	0.0145877
10472958	Hoxd10	0.934577	3.75823	0.00679119
10598029	ND1	0.930336	3.36062	0.0116587
10513805	Dbc1	0.929945	3.31366	0.0124455
10561854	Tbcb	0.928606	2.88898	0.0227567
10546430	Adamts9	0.928495	2.71447	0.0293361
10408321	Gmnn	0.928228	2.88963	0.0227354
10590623	Cxcr6	0.927952	3.97769	0.00508994
10514185	NA	0.927916	3.77654	0.00662796
10484307	Frzb	0.927288	3.19673	0.0146621
10502240	Npnt	0.926543	2.65678	0.0319257
10354205	Gm5100	0.926418	2.86691	0.0234956
10513008	Klf4	0.924797	2.98608	0.0197855
10606600	Pcdh19	0.923887	3.84635	0.00604351
10360040	Fcgr3	0.923583	3.92645	0.00544093
10350123	Lmod1	0.921979	3.22391	0.0141117
10593316	NA	0.921967	3.82559	0.00621122
10565255	9930013L23Rik	0.921297	3.85773	0.00595363
10497209	Mrps28	0.921217	2.69412	0.0302238
10515536	Ipo13	0.920355	3.75965	0.00677842
10404422	Serpinb6b	0.918383	2.4525	0.0431622
10394353	0610009D07Rik	0.917024	3.07064	0.0175315
10499504	Mtx1	0.916885	2.61162	0.0341176
10579812	Ednra	0.91663	3.58706	0.00854615
10372177	Tmtc2	0.91646	3.32551	0.0122418
10542317	Cdkn1b	0.914318	3.67602	0.00757982
10465220	Sssca1	0.912509	3.29475	0.0127782
10375380	Gm12164	0.911619	2.68861	0.0304688
10546454	Adamts9	0.911104	3.4663	0.0100765
10581499	Chtf8	0.905653	3.34553	0.0119056
10592237	Ei24	0.905486	2.46815	0.0421724

10601768	Armcx4	0.905368	3.87349	0.00583158
10392259	Smurf2	0.904854	2.73724	0.0283753
10460544	Yif1a	0.903954	3.09824	0.0168559
10557742	Fbxl19	0.903749	3.42655	0.0106428
10451421	Klhdc3	0.903315	2.67164	0.0312364
10551393	Akt2	0.901741	3.30884	0.0125295
10519945	Tmem60	0.899104	2.72816	0.0287544
10473874	Arfgap2	0.898659	3.61291	0.0082523
10358658	Hmcn1	0.896974	2.98838	0.0197204
10480714	Uap1l1	0.896459	3.82031	0.00625471
10567589	Usp31	0.896294	3.16413	0.0153526
10598020	NA	0.895897	2.94791	0.0209018
10371432	D10Wsu52e	0.895398	2.6365	0.0328913
10487040	Fbn1	0.895091	2.59979	0.0347174
10397143	2410016O06Rik	0.891765	3.25341	0.0135393
10415377	2610027L16Rik	0.891327	3.3899	0.0111954
10425852	Parvb	0.891281	3.38011	0.0113481
10544452	Fam115c	0.889073	2.88119	0.0230149
10474229	Cd59a	0.888733	3.16825	0.0152634
10455826	Megf10	0.888606	3.07336	0.0174635
10404051	Hist1h4d	0.88787	3.26754	0.0132738
10531175	Adamts3	0.886902	2.70968	0.0295426
10598482	Timm17b	0.883803	3.68274	0.00751176
10381603	Fzd2	0.882003	3.02537	0.0187024
10434802	Lpp	0.880968	3.05771	0.0178576
10563110	Snord34	0.880288	2.76054	0.0274261
10398352	NA	0.879953	3.14126	0.0158575
10496125	Dkk2	0.879278	2.896	0.0225271
10364455	Cdc34	0.879088	3.04531	0.0181765
10415411	BC030046	0.878507	2.9981	0.0194472
10445496	Yipf3	0.878479	3.1751	0.0151165
10420198	Ripk3	0.877121	2.47782	0.0415724
10587104	Arpp19	0.876966	2.9604	0.0205294
10600205	Dusp9	0.87677	3.5518	0.00896536
10597648	Myd88	0.876129	3.58637	0.00855424
10404178	BC005537	0.875922	2.66236	0.0316648
10424392	9930014A18Rik	0.875215	2.85318	0.0239677
10445268	Gpr116	0.874913	2.6382	0.0328091
10588037	Rbp1	0.873921	3.08923	0.0170733
10393614	Cbx8	0.87346	3.50298	0.00958262
10603746	Maob	0.87015	3.3864	0.0112496
10554521	Pde8a	0.86658	3.13888	0.015911
10566326	Trim12	0.865762	2.49747	0.0403802

10577544	Polb	0.865452	3.28085	0.0130289
10477169	Id1	0.862368	2.76054	0.0274258
10535807	Flt1	0.862349	3.11609	0.0164337
10431486	Sbf1	0.862239	3.60758	0.00831197
10434743	NA	0.857933	3.62928	0.00807187
10438911	Atp13a3	0.857794	2.95029	0.0208301
10495340	Taf13	0.856456	3.70135	0.00732673
10533050	Hspb8	0.853906	3.19571	0.0146833
10558948	Cd151	0.853497	2.81833	0.0252118
10503989	2010003O02Rik	0.852533	2.76148	0.0273884
10585438	Crabp1	0.851475	3.06166	0.0177573
10400321	1110002B05Rik	0.851402	3.05142	0.0180188
10554808	Fzd4	0.846384	3.60533	0.00833733
10548194	Fkbp4	0.846247	2.87061	0.0233701
10455108	Pcdhb16	0.843841	3.36158	0.0116433
10411459	Tmem171	0.843834	2.80096	0.025857
10391572	Lsm12	0.843231	2.47442	0.0417828
10584561	9030425E11Rik	0.8424	3.19497	0.0146985
10453692	Vps24	0.84238	2.77834	0.026723
10404063	Hist1h2ab	0.839809	3.24175	0.0137625
10524310	Ttc28	0.838966	3.58687	0.00854839
10515072	Rnf11	0.838124	2.58092	0.0356964
10346562	Cflar	0.837858	3.48318	0.00984595
10404731	Tmem14c	0.837329	3.32428	0.0122628
10475514	Spata5l1	0.836597	3.37833	0.0113761
10358272	Lhx9	0.836256	3.03161	0.0185361
10468519	Smndc1	0.835187	3.01851	0.0188867
10572024	Spock3	0.834606	3.1529	0.0155984
10502778	Lphn2	0.834594	3.43182	0.0105657
10550527	Irf2bp1	0.832814	3.4146	0.0108197
10446013	Mpnd	0.831742	2.80145	0.0258384
10491414	Usp13	0.830864	3.50387	0.00957101
10583056	Mmp12	0.830793	3.29478	0.0127777
10591517	Cdkn2d	0.830363	2.5842	0.0355239
10404069	Hist1h1a	0.829911	2.92541	0.0215903
10490931	Ythdf3	0.829288	2.39255	0.0471793
10566767	St5	0.829005	3.1149	0.0164615
10413710	Nt5dc2	0.828908	3.41599	0.010799
10497994	Pabpc4l	0.828365	2.41826	0.045412
10351574	Dedd	0.827024	3.00414	0.0192797
10514352	Elavl2	0.826782	3.38065	0.0113395
10427075	Krt18	0.826709	2.81178	0.0254531
10433904	Yars2	0.824964	2.648	0.0323399

10562576	Plekhf1	0.823616	3.09811	0.016859
10547322	Cacna1c	0.82353	3.50598	0.00954349
10352306	Pycr2	0.822088	3.53119	0.00922058
10578986	Psd3	0.821645	3.13299	0.0160444
10434291	B3gnt5	0.821377	2.73975	0.0282713
10376482	2310033P09Rik	0.82108	2.52441	0.0388027
10524703	Pxn	0.821067	2.8914	0.0226775
10562847	Nr1h2	0.82028	2.62107	0.0336462
10421661	Gtf2f2	0.820182	3.06999	0.0175477
10552740	Nup62	0.819742	3.28154	0.0130163
10470316	NA	0.819741	3.43712	0.010489
10503958	1700009N14Rik	0.819583	2.67775	0.030958
10396656	Gm70	0.818639	3.4318	0.0105661
10586865	Aldh1a2	0.81863	2.73176	0.0286035
10454198	Rnf125	0.817899	3.49871	0.00963879
10587488	4930486G11Rik	0.817396	2.68393	0.0306786
10358656	Hmcn1	0.815842	2.36179	0.0493867
10403951	Hist1h2bp	0.814748	2.5449	0.0376451
10533095	Fbxw8	0.81339	3.39354	0.011139
10561078	Ccdc97	0.81307	3.31476	0.0124265
10514884	Mrpl37	0.812501	3.46513	0.0100928
10493812	S100a4	0.811679	2.74076	0.0282297
10590842	Gm10708	0.811178	2.58078	0.0357038
10501608	Vcam1	0.810538	2.68912	0.0304458
10490544	Ythdf1	0.810209	2.87217	0.0233173
10510624	Klhl21	0.809351	3.18328	0.0149429
10445235	Gm9753	0.808112	3.1949	0.0147
10384458	Plek	0.807464	2.96158	0.0204944
10472050	Tnfaip6	0.806113	2.41921	0.0453475
10358662	Hmcn1	0.803805	2.96275	0.0204601
10594800	B230380D07Rik	0.802358	3.30318	0.0126288
10535647	Atp5j2	0.802144	3.25947	0.0134247
10565612	1810020D17Rik	0.801783	3.10944	0.0165898
10367335	NA	0.800069	3.40985	0.0108908
10460492	Mrpl11	0.799558	2.38939	0.0474018
10380620	NA	0.79906	2.35484	0.0498998
10519324	Cdk6	0.796378	2.40597	0.046248
10580452	Siah1a	0.794999	3.07704	0.0173723
10464391	Emx2	0.793441	2.35795	0.0496694
10464572	Ndufv1	0.792681	3.33803	0.0120303
10385511	Psme2	0.790454	2.67111	0.031261
10488589	Fam110a	0.789404	2.60701	0.03435
10411171	Pde8b	0.787233	2.66957	0.0313317

10534839	Pop7	0.786854	2.89189	0.0226614
10585703	Rpp25	0.786822	2.77756	0.0267535
10353783	Ccdc115	0.786646	3.37965	0.0113553
10567086	Cyp2r1	0.786618	3.03002	0.0185783
10409278	Nfil3	0.785903	2.59716	0.0348519
10456492	D18Ertd653e	0.785899	2.47316	0.0418607
10486710	Lcmt2	0.785883	2.61703	0.033847
10450640	Mrps18b	0.784211	2.83592	0.0245758
10499612	Zbtb7b	0.783278	3.13965	0.0158937
10375935	Skp1a	0.779345	3.14431	0.0157891
10358982	Mr1	0.778027	2.79965	0.0259063
10556576	1110004F10Rik	0.777313	2.6311	0.0331535
10563407	Kcnj14	0.776574	3.00418	0.0192784
10437590	Carhsp1	0.775567	2.52728	0.0386382
10415604	Gjb2	0.775361	2.96436	0.0204128
10406504	Edil3	0.775269	3.22832	0.0140245
10419261	Bmp4	0.774607	3.08331	0.0172178
10494407	Hist2h2bb	0.773588	2.91818	0.0218167
10535184	Psmg3	0.772533	2.86411	0.023591
10569344	Igf2	0.772114	3.27369	0.0131601
10456378	Chmp1b	0.770322	2.37224	0.0486252
10351738	Pex19	0.770113	2.53828	0.0380152
10467859	Cox15	0.770009	2.41804	0.0454263
10568115	Mvp	0.768317	3.24245	0.0137489
10485198	Tspan18	0.767672	3.31438	0.0124331
10377416	2310047M10Rik	0.767577	2.77787	0.0267414
10483023	Rbms1	0.766736	2.82169	0.0250891
10461093	Pla2g16	0.766479	2.92351	0.0216498
10364696	Atp5d	0.766326	2.72022	0.0290903
10372383	Zdhhc17	0.765784	2.42843	0.0447316
10378855	Ssh2	-0.767097	-2.47041	0.0420318
10506108	NA	-0.767106	-2.58448	0.0355093
10580219	Calr	-0.769229	-3.0807	0.0172819
10371482	Hsp90b1	-0.770678	-3.21893	0.014211
10398615	Gm10158	-0.770805	-3.00186	0.0193427
10405576	Fbxl21	-0.77153	-2.48146	0.0413488
10543791	Podxl	-0.772902	-2.37191	0.0486491
10430929	Tbrg3	-0.773461	-2.51768	0.0391909
10370544	2610008E11Rik	-0.776731	-2.53469	0.0382173
10473281	Itgav	-0.777157	-3.05424	0.0179465
10519951	Pion	-0.779774	-2.9438	0.0210258
10512949	Abca1	-0.780509	-3.16938	0.0152391
10476297	NA	-0.780771	-2.4432	0.043762

10393823	P4hb	-0.780901	-3.14405	0.0157951
10459655	Poli	-0.781739	-3.32338	0.0122782
10383212	NA	-0.782288	-2.8414	0.0243809
10462140	Dock8	-0.782331	-3.23806	0.0138339
10497501	Naaladl2	-0.783912	-2.7086	0.0295892
10416725	Tdrd3	-0.784239	-2.54487	0.0376468
10383198	NA	-0.785474	-2.99404	0.0195609
10426368	Lrrk2	-0.785685	-3.18385	0.0149309
10396950	NA	-0.786128	-3.09831	0.0168542
10593668	Dmxl2	-0.786631	-3.29108	0.012844
10403743	Inhba	-0.787064	-2.91631	0.0218757
10605357	Gab3	-0.787123	-2.70367	0.0298038
10423796	NA	-0.791851	-2.58975	0.0352345
10396608	Syne2	-0.792177	-2.51029	0.0396214
10421970	NA	-0.793267	-2.36795	0.0489363
10574572	2210023G05Rik	-0.793848	-3.06128	0.0177669
10484894	Ptprj	-0.794828	-3.22113	0.0141669
10585381	Slc35f2	-0.796111	-3.2379	0.0138371
10593671	Dmxl2	-0.800288	-2.90444	0.0222539
10365344	Tcp11l2	-0.802011	-2.72722	0.028794
10386058	Sparc	-0.803873	-3.42611	0.0106493
10579047	Lzts1	-0.805573	-3.15599	0.0155304
10361191	Syt14	-0.805847	-2.94798	0.0208994
10504656	NA	-0.809949	-3.26616	0.0132995
10551998	NA	-0.810692	-3.04116	0.0182848
10531288	NA	-0.815605	-3.51711	0.00939939
10572178	LOC674930	-0.815832	-2.53224	0.0383561
10476512	Snap25	-0.816745	-2.35422	0.0499457
10399478	Lpin1	-0.817222	-3.49415	0.00969908
10582839	Gm9909	-0.818497	-2.65343	0.0320832
10479884	Gm13199	-0.818563	-2.67251	0.0311968
10447557	Ldhal6b	-0.818671	-3.14822	0.015702
10420216	Sdr39u1	-0.822659	-2.66452	0.0315647
10532085	Tgfbr3	-0.822747	-3.25642	0.0134822
10428308	G930009F23Rik	-0.823835	-2.88842	0.0227755
10413280	NA	-0.825784	-2.7111	0.0294814
10603206	BC022960	-0.827302	-2.81622	0.0252894
10591200	Gm6495	-0.827458	-3.29847	0.012712
10505643	4930473A06Rik	-0.830395	-3.27712	0.0130971
10522696	Arl9	-0.831085	-2.55738	0.0369581
10488382	Cd93	-0.831714	-2.54263	0.0377718
10369176	D630037F22Rik	-0.831982	-3.48791	0.00978233
10413419	Arhgef3	-0.833131	-3.40867	0.0109086

10499113	Gm1019	-0.833194	-3.2825	0.0129989
10352097	1700016C15Rik	-0.835478	-3.15838	0.015478
10570344	Lamp1	-0.835693	-3.33944	0.0120068
10530841	Igfbp7	-0.837718	-3.51098	0.00947845
10446769	NA	-0.837983	-2.51986	0.0390645
10407281	Esm1	-0.838693	-2.95432	0.0207097
10383200	NA	-0.83988	-3.44438	0.0103847
10574438	Cdh5	-0.840708	-3.07441	0.0174374
10593460	4833427G06Rik	-0.841744	-2.79958	0.0259088
10549473	Caprin2	-0.843333	-3.42862	0.0106124
10375358	Ebf1	-0.844051	-3.12222	0.0162915
10349333	3110009E18Rik	-0.844322	-3.39287	0.0111494
10540227	Kbtbd8	-0.84452	-2.9119	0.0220154
10477920	Myl9	-0.845839	-3.1602	0.0154381
10523451	Anxa3	-0.846684	-2.74398	0.0280973
10574145	Nlrc5	-0.847211	-3.62352	0.00813495
10498998	D930015E06Rik	-0.847475	-3.40682	0.0109365
10383152	NA	-0.84837	-3.59392	0.00846716
10480145	Rsu1	-0.848422	-3.08745	0.0171166
10457644	Cdh2	-0.848456	-3.20902	0.0144105
10506170	Efcab7	-0.849658	-3.50734	0.00952569
10596381	NA	-0.857711	-3.1613	0.0154142
10432471	NA	-0.858055	-3.41182	0.0108612
10536805	Fam71f1	-0.860171	-3.14258	0.015828
10431697	Abcd2	-0.863565	-3.3469	0.0118831
10445338	Enpp5	-0.864956	-3.55019	0.00898502
10513739	Tnc	-0.865974	-2.93702	0.021232
10579066	Gm3365	-0.866344	-3.45513	0.0102323
10524327	Mn1	-0.868646	-3.15047	0.015652
10351400	Fam78b	-0.869162	-3.4747	0.0099611
10383214	Rnf213	-0.869164	-3.05124	0.0180233
10400072	Scin	-0.874197	-2.67003	0.0313107
10519555	Abcb1b	-0.877655	-3.71763	0.00716896
10504664	NA	-0.879275	-3.57729	0.00866021
10555848	Trim6	-0.882842	-3.62463	0.00812275
10362630	NA	-0.883115	-2.3651	0.0491445
10530029	Lgi2	-0.885612	-3.11164	0.0165381
10586920	Rfx7	-0.888821	-2.89447	0.0225769
10407211	Ppap2a	-0.889429	-3.68186	0.00752061
10601312	Gm10454	-0.889539	-3.2268	0.0140545
10580953	NA	-0.889566	-2.98252	0.0198871
10409579	Cxcl14	-0.891448	-2.73276	0.0285619
10446473	Lama1	-0.893571	-2.38157	0.0479554

10561351	NA	-0.894979	-2.95155	0.0207923
10503161	Chd7	-0.896803	-3.7644	0.0067357
10356403	Kcnj13	-0.896918	-2.71803	0.0291838
10531256	AU017193	-0.897084	-2.37228	0.0486223
10392796	Cd300lb	-0.898297	-3.76718	0.00671087
10513266	Olfr267	-0.899064	-3.84731	0.00603583
10513004	Gm10588	-0.899742	-2.94948	0.0208545
10422537	Nalcn	-0.900801	-2.75772	0.0275391
10403081	Wdr60	-0.901294	-3.63974	0.00795881
10475910	NA	-0.902427	-2.87629	0.0231785
10500140	Anxa9	-0.902931	-3.86079	0.00592972
10350742	Rnasel	-0.903703	-3.30649	0.0125707
10477986	Nnat	-0.904019	-3.62503	0.00811832
10410776	NA	-0.904649	-3.46328	0.0101184
10471880	NA	-0.907228	-2.73583	0.0284338
10408613	Tubb2b	-0.912841	-3.89628	0.00565982
10367434	ENSMUSG00000065996	-0.913744	-3.23153	0.0139615
10504672	Tdrd7	-0.914964	-2.62215	0.0335931
10502284	Tet2	-0.916092	-3.39316	0.0111449
10352957	Rgs20	-0.916183	-3.85193	0.00599924
10523903	NA	-0.916668	-3.24761	0.0136498
10434745	NA	-0.918609	-2.45317	0.0431195
10499904	Ivl	-0.919031	-3.01238	0.0190534
10604616	Plac1	-0.922096	-3.94568	0.00530621
10401320	Adam4	-0.922471	-3.43722	0.0104875
10357164	Epb4.1l5	-0.923407	-3.63933	0.00796328
10574415	1700047G07Rik	-0.924325	-2.83285	0.0246854
10423855	Rims2	-0.924812	-3.60608	0.00832892
10504658	NA	-0.928976	-3.6189	0.00818582
10466865	Rfx3	-0.932062	-3.75782	0.00679488
10475335	Pdia3	-0.93309	-3.30488	0.0125988
10450872	Olfr99	-0.933536	-2.91625	0.0218776
10471586	Hspa5	-0.933643	-3.61511	0.00822787
10527959	NA	-0.934519	-3.55911	0.00887668
10598757	Gpr82	-0.943354	-2.45418	0.0430553
10396511	Syne2	-0.943863	-3.51571	0.00941743
10383168	NA	-0.944322	-3.22664	0.0140577
10544148	Jhdm1d	-0.944784	-3.82112	0.00624802
10472400	Scn2a1	-0.951697	-2.54584	0.0375931
10606163	4930519F16Rik	-0.958403	-3.45938	0.0101728
10473058	Osbpl6	-0.958454	-4.13172	0.00417534
10384229	NA	-0.959642	-3.19633	0.0146703
10473219	NA	-0.959709	-3.38983	0.0111963

10396485	Syne2	-0.960078	-3.84809	0.00602967
10383192	NA	-0.96269	-2.73784	0.0283504
10497463	Cpb1	-0.96291	-3.77833	0.00661218
10475890	Mertk	-0.963463	-3.4613	0.010146
10401317	Gm4787	-0.966169	-3.62532	0.00811513
10395273	Gdap10	-0.9702	-3.06452	0.0176851
10435802	2610015P09Rik	-0.970348	-3.70258	0.00731472
10488430	Gm10750	-0.97225	-3.61519	0.00822696
10556640	6330503K22Rik	-0.974382	-3.88707	0.00572855
10356995	NA	-0.975219	-3.14302	0.0158181
10396079	Klhdc1	-0.977507	-4.18393	0.00390736
10601610	LOC100044428	-0.980062	-3.15031	0.0156556
10546832	NA	-0.987763	-3.26857	0.0132547
10495416	Vav3	-0.987895	-3.34521	0.011911
10569504	Tnfrsf23	-0.988562	-3.90725	0.00557915
10513145	Ptpn3	-0.991473	-3.01773	0.0189079
10415787	Kcnrg	-0.998346	-3.06261	0.0177333
10471878	NA	-0.99944	-3.32977	0.0121695
10395457	Etv1	-0.999699	-3.22935	0.0140042
10488322	A230067G21Rik	-1.00185	-4.10318	0.00433027
10586591	Car12	-1.00938	-3.46178	0.0101392
10357658	NA	-1.00988	-3.51069	0.00948217
10353803	Uggt1	-1.013	-3.52427	0.00930803
10417068	NA	-1.01409	-2.58086	0.0356995
10550169	Phf20	-1.01609	-4.34736	0.00318316
10396730	NA	-1.01935	-2.95534	0.0206791
10585194	Il18	-1.01946	-2.61018	0.0341901
10603878	Uxt	-1.02748	-3.64396	0.00791368
10402061	Eml5	-1.02863	-3.10385	0.0167221
10591614	Dock6	-1.03026	-3.02146	0.0188072
10502655	Cyr61	-1.0336	-3.89901	0.00563968
10348299	5830472F04Rik	-1.03392	-3.45641	0.0102144
10353989	NA	-1.03506	-2.66423	0.031578
10556528	Pde3b	-1.04151	-3.33991	0.0119989
10422436	Dock9	-1.04161	-3.87969	0.00578431
10595081	Tinag	-1.04232	-3.39174	0.0111669
10557357	D430042O09Rik	-1.04675	-3.37213	0.0114742
10580955	NA	-1.0491	-3.24206	0.0137565
10469672	Gad2	-1.05618	-3.46133	0.0101455
10522666	2310040G07Rik	-1.05894	-2.79854	0.0259481
10472538	Dhrs9	-1.06063	-2.6696	0.0313304
10603182	Arhgap6	-1.06093	-3.88186	0.00576788
10504662	NA	-1.06236	-4.42061	0.00290747

10416181	Stc1	-1.06258	-4.11635	0.00425801
10383202	NA	-1.06442	-3.02882	0.0186101
10400155	Nova1	-1.06474	-3.04847	0.0180948
10354267	A530098C11Rik	-1.0662	-3.32881	0.0121857
10503200	Chd7	-1.07141	-4.62349	0.00227171
10530100	Arap2	-1.07255	-3.79795	0.00644245
10504660	NA	-1.07515	-4.64169	0.00222262
10366645	1700006J14Rik	-1.07579	-2.74907	0.0278891
10363786	Ank3	-1.07768	-4.02837	0.00476693
10593123	Tagln	-1.08187	-3.11396	0.0164835
10560408	Psg17	-1.08381	-4.50302	0.00262825
10356329	Ncl	-1.086	-3.1344	0.0160124
10494978	Ptpn22	-1.08772	-3.06079	0.0177794
10370007	Gstt4	-1.08866	-4.65297	0.0021928
10491477	Sox2	-1.09395	-3.88163	0.00576959
10501629	Cdc14a	-1.09539	-4.64862	0.00220426
10517609	Cda	-1.09941	-2.89311	0.0226212
10536297	Ppp1r9a	-1.10238	-3.94668	0.00529929
10466606	Anxa1	-1.10432	-2.35914	0.0495814
10554129	B130024G19Rik	-1.10569	-3.92826	0.00542814
10541034	Anubl1	-1.10586	-4.63399	0.00224326
10458894	Lox	-1.10823	-3.28892	0.0128828
10402020	Eml5	-1.10976	-4.41178	0.00293926
10435641	Fstl1	-1.10977	-4.12138	0.00423077
10530156	Tmem156	-1.11163	-4.12926	0.00418847
10549377	1700034J05Rik	-1.12298	-3.9599	0.00520898
10450038	Angptl4	-1.12339	-3.75174	0.00685008
10530319	Atp8a1	-1.12709	-4.13179	0.00417495
10520388	Prr8	-1.12889	-2.53591	0.0381487
10374840	NA	-1.13304	-3.35591	0.0117352
10365845	Fgd6	-1.13535	-4.89194	0.00165409
10356997	NA	-1.14022	-4.16553	0.00399958
10376577	NA	-1.14119	-4.88921	0.00165934
10412258	NA	-1.14588	-4.33923	0.00321545
10574163	Nlrc5	-1.14764	-4.90857	0.00162245
10369171	9530009G21Rik	-1.14985	-4.63452	0.00224183
10383204	NA	-1.1531	-3.63643	0.00799441
10417998	NA	-1.15917	-4.29338	0.00340464
10450930	Crisp1	-1.16122	-3.44598	0.0103619
10598071	NA	-1.16345	-4.72164	0.00202045
10536818	Calu	-1.16536	-4.87746	0.00168219
10362097	Raet1b	-1.16554	-2.59006	0.0352187
10357553	Il24	-1.16722	-3.83265	0.00615358

10601583	Mthfd2l	-1.16965	-4.23168	0.0036787
10427908	Gm9948	-1.17429	-3.27144	0.0132015
10503206	Chd7	-1.17725	-4.8432	0.00175082
10583809	Cnn1	-1.18264	-4.24312	0.00362608
10599192	Lonrf3	-1.18328	-4.76942	0.00190935
10503202	Chd7	-1.18775	-3.18923	0.014818
10351206	Selp	-1.19648	-2.69624	0.0301301
10584315	NA	-1.19776	-3.80159	0.00641148
10503168	Chd7	-1.19787	-4.2799	0.00346254
10531009	Tmprss11b	-1.20326	-4.16293	0.00401284
10483249	Galnt3	-1.23051	-3.20568	0.0144784
10531274	Btc	-1.23072	-4.93356	0.00157614
10437195	Igsf5	-1.23104	-4.66406	0.00216389
10422244	Slitrk6	-1.2395	-2.68027	0.0308434
10467508	Blnk	-1.2423	-5.34257	0.000993471
10424683	Ly6g	-1.24753	-4.5285	0.00254799
10396606	Syne2	-1.25017	-3.72688	0.00708093
10583071	Mmp3	-1.25644	-3.1786	0.015042
10372342	Nav3	-1.25717	-4.99913	0.00146145
10351477	Sh2d1b1	-1.26126	-4.11694	0.00425479
10578796	4930431L04Rik	-1.26197	-4.85867	0.00171945
10406334	Mctp1	-1.26995	-3.21398	0.0143102
10532574	Myo18b	-1.27068	-2.82625	0.0249235
10532586	Myo18b	-1.27362	-2.40939	0.0460138
10585186	1600029D21Rik	-1.27427	-4.64036	0.00222617
10462818	Hhex	-1.27587	-2.6467	0.0324016
10588091	Cep70	-1.27784	-4.96034	0.00152814
10503186	Chd7	-1.27846	-4.36654	0.00310829
10466521	Gcnt1	-1.2806	-5.35964	0.000974998
10536563	Cftr	-1.2832	-3.66521	0.00769064
10544150	Jhdm1d	-1.29292	-4.3527	0.0031621
10519607	4930420K17Rik	-1.30084	-4.9019	0.00163506
10503178	Chd7	-1.30733	-3.90222	0.00561598
10366052	Kitl	-1.31162	-3.61482	0.00823109
10428536	Trps1	-1.31354	-3.53878	0.00912563
10376096	Acsl6	-1.31428	-5.12686	0.00126363
10576661	Itgb1	-1.32073	-5.10267	0.0012987
10475643	Fgf7	-1.32097	-4.57248	0.00241572
10349634	NA	-1.32655	-3.91292	0.00553794
10479747	NA	-1.32873	-3.5737	0.00870242
10456171	Spink10	-1.32999	-4.60139	0.00233291
10503166	Chd7	-1.34129	-2.84277	0.0243325
10361926	Map3k5	-1.34977	-3.96199	0.0051948

10532576	Myo18b	-1.35705	-3.22345	0.0141208
10431659	Kif21a	-1.35885	-4.44353	0.00282669
10383206	NA	-1.36095	-3.02619	0.0186804
10488010	Hao1	-1.37025	-5.29951	0.00104181
10441787	Airn	-1.37832	-4.0567	0.00459617
10503170	Chd7	-1.38004	-4.71658	0.00203264
10503222	Chd7	-1.39441	-5.89245	0.000553167
10421100	Nefm	-1.39863	-4.54358	0.00250178
10503196	Chd7	-1.40293	-4.6222	0.00227522
10561008	Ceacam1	-1.40481	-3.20008	0.0145931
10424582	NA	-1.40615	-5.28793	0.00105526
10590962	1700012B09Rik	-1.42795	-4.52385	0.00256245
10362294	Arhgap18	-1.43104	-4.92123	0.0015988
10528090	Rundc3b	-1.44015	-5.7128	0.000666957
10428594	Samd12	-1.4435	-5.21332	0.00114663
10495120	Ovgp1	-1.44768	-3.6054	0.00833659
10503218	Chd7	-1.45225	-4.82849	0.00178122
10476395	Bmp2	-1.45545	-5.03379	0.00140459
10485633	Gm10796	-1.45748	-3.20983	0.014394
10395553	Nrcam	-1.48001	-4.69587	0.00208332
10603809	Gm14636	-1.48754	-6.40052	0.000332807
10595768	Pls1	-1.4882	-5.46973	0.000864656
10349943	NA	-1.4965	-3.58517	0.00856809
10416505	Kctd4	-1.51124	-5.32722	0.00101041
10365983	Lum	-1.52525	-3.33124	0.0121445
10351182	Sele	-1.52882	-4.77447	0.00189802
10466779	Pip5k1b	-1.53595	-5.6054	0.000747319
10382300	Map2k6	-1.53637	-6.39968	0.000333079
10503208	Chd7	-1.55242	-6.18874	0.000409809
10586971	Prtg	-1.55588	-5.321	0.00101737
10503214	Chd7	-1.5761	-5.48853	0.00084724
10548497	Klra6	-1.59638	-4.69792	0.00207823
10500845	A130049A11Rik	-1.60919	-3.50733	0.00952581
10355403	Fn1	-1.61074	-3.68375	0.00750156
10435712	Cd80	-1.64096	-3.93917	0.00535142
10606333	Fndc3c1	-1.65055	-7.11673	0.000170683
10388958	Evi2a	-1.66317	-7.1057	0.000172378
10467124	Acta2	-1.66336	-6.73329	0.000242404
10474467	Muc15	-1.66983	-4.42103	0.00290596
10353221	Trpa1	-1.67361	-2.69131	0.0303483
10351867	Aim2	-1.70863	-5.31078	0.00102891
10503194	Chd7	-1.70892	-4.83235	0.00177319
10554814	Prss23	-1.75837	-5.58323	0.00076522

10503184	Chd7	-1.76978	-5.9433	0.000525013
10503188	Chd7	-1.77198	-5.54524	0.000797012
10474522	Olfr1317	-1.77525	-4.19167	0.00386927
10506929	Calr4	-1.77877	-5.63918	0.000720942
10503212	Chd7	-1.82332	-7.23266	0.000153952
10407435	Akr1c18	-1.82898	-6.15224	0.000424996
10534667	Serpine1	-1.849	-6.37695	0.00034052
10600169	Bgn	-1.88043	-4.72143	0.00202096
10503174	Chd7	-1.94135	-4.56761	0.00243001
10573082	Inpp4b	-2.01847	-7.68467	0.00010422
10389699	NA	-2.05887	-5.6926	0.000681304
10503172	Chd7	-2.12581	-5.69193	0.00068179
10350516	Ptgs2	-2.13441	-7.30019	0.00014506
10354003	Mgat4a	-2.13499	-9.20035	3.19E-05
10529890	4930435H24Rik	-2.23671	-7.35426	0.000138354
10351873	Pyhin1	-2.24672	-9.5127	2.55E-05
10530998	Tmprss11f	-2.2889	-6.22714	0.000394483
10462442	Il33	-2.31421	-5.46735	0.000866885
10548552	Klra2	-2.31471	-6.09237	0.000451289
10474700	Thbs1	-2.42502	-9.29325	2.98E-05
10503198	Chd7	-2.4672	-9.8635	2.00E-05
10503180	Chd7	-2.59383	-5.44825	0.000885045
10503182	Chd7	-2.64118	-7.64332	0.000107923
10503176	Chd7	-2.67636	-6.88556	0.000210504

Appendix 2:

Affymetrix ID	GeneName	Fold Change	t-score	p-value
10398362	Rian	-4.4706	-2.83909	0.0183
10428707	Has2	-3.8385	-4.48669	0.0013
10521759	Slit2	-3.6798	-3.92411	0.0031
10398364	NA	-3.6492	-2.57462	0.0286
10398360	NA	-3.4131	-2.44055	0.0358
10405047	Aspn	-3.1289	-3.91974	0.0031
10461158	Snhg1	-3.0979	-2.8395	0.0183
10398366	NA	-2.9408	-2.81456	0.0191
10586079	Itga11	-2.8803	-3.36059	0.0077
10398368	NA	-2.8502	-3.10091	0.0118
10513774	NA	-2.8203	-3.06862	0.0125
10420274	Gzmd	-2.6609	-2.40987	0.0377
10502778	Lphn2	-2.6561	-2.70783	0.0228
10435948	Ccdc80	-2.6531	-2.90385	0.0164
10514185	NA	-2.6328	-3.28099	0.0088
10492021	Postn	-2.6051	-2.54983	0.0298
10487040	Fbn1	-2.5674	-3.26561	0.0090
10344981	Pi15	-2.5173	-3.31413	0.0083
10458999	Fbn2	-2.4047	-3.53726	0.0057
10414065	Anxa8	-2.4025	-2.51349	0.0317
10446771	Lclat1	-2.3787	-3.78623	0.0038
10485622	Qser1	-2.3688	-2.411	0.0376
10598381	Gpkow	-2.3374	-2.96189	0.0149
10420362	Gjb2	-2.2817	-2.85657	0.0178
10543709	Tmem209	-2.2734	-2.65987	0.0247
10502780	Lphn2	-2.2638	-4.42836	0.0014
10358549	Hmcn1	-2.2522	-2.50182	0.0323
10571252	Tex15	-2.2342	-3.02306	0.0134
10498584	Rarres1	-2.2271	-3.88912	0.0033
10405179	S1pr3	-2.1980	-2.92108	0.0159
10447649	Fndc1	-2.1822	-2.33652	0.0426
10354205	Gm5100	-2.1644	-2.96868	0.0147
10382010	Dcaf7	-2.1574	-3.71421	0.0043
10374777	Efemp1	-2.1559	-2.68833	0.0236
10489299	NA	-2.1439	-2.65315	0.0250
10458340	Hbegf	-2.1432	-2.94259	0.0154
10480090	Itga8	-2.1378	-3.10008	0.0118
10567010	Dkk3	-2.1240	-3.01005	0.0137
10498018	Pcdh18	-2.1154	-4.01173	0.0027
10578880	Tll1	-2.1146	-2.87475	0.0172
10602692	Rragb	-2.1052	-2.91511	0.0161

10503659	Epha7	-2.1010	-3.30067	0.0085
10423243	Cdh10	-2.0974	-2.59972	0.0274
10496125	Dkk2	-2.0864	-2.7828	0.0201
10463355	Scd2	-2.0765	-3.53356	0.0058
10427862	Cdh6	-2.0714	-2.40156	0.0382
10515712	BC059842	-2.0711	-3.81291	0.0037
10522749	Lphn3	-2.0695	-2.49773	0.0325
10515702	BC059842	-2.0649	-3.60722	0.0051
10431915	Slc38a4	-2.0647	-3.10152	0.0118
10495279	Psma5	-2.0585	-2.28951	0.0461
10459866	Slc14a1	-2.0517	-2.36852	0.0404
10455813	Lmnb1	-2.0502	-2.70905	0.0228
10597136	Ptpn23	-2.0457	-2.96638	0.0148
10537831	Olfr47	-2.0332	-2.8622	0.0176
10453057	Cyp1b1	-2.0281	-2.90363	0.0164
10442373	Dcpp2	-2.0217	-2.46956	0.0341
10439832	NA	-2.0199	-2.70929	0.0228
10418002	Gm6128	-2.0172	-2.46242	0.0345
10435961	Gm10808	-2.0057	-3.54049	0.0057
10402604	NA	-2.0046	-3.03223	0.0132
10358666	Hmcn1	-1.9995	-2.65659	0.0249
10606235	Zdhhc15	-1.9982	-2.77116	0.0205
10568668	Adam12	-1.9914	-2.84893	0.0180
10445141	Olfr111	-1.9820	-2.72372	0.0222
10607962	Ube1y1	-1.9618	-3.1747	0.0104
10423593	Laptm4b	-1.9502	-3.66154	0.0047
10386703	Gm12271	-1.9491	-2.2712	0.0476
10445528	BC040756	-1.9469	-3.03803	0.0131
10514933	Cpt2	-1.9361	-2.31926	0.0439
10356520	Col6a3	-1.9355	-2.33348	0.0429
10467110	AI747699	-1.9196	-2.95803	0.0150
10403052	LOC638798	-1.9188	-2.85737	0.0177
10368647	Dse	-1.9188	-2.96966	0.0147
10593937	Mpi	-1.9188	-2.74005	0.0216
10493809	S100a2	-1.9182	-2.26577	0.0480
10456046	Pdgfrb	-1.9138	-3.41729	0.0070
10555870	Olfr651	-1.9086	-2.92753	0.0158
10473058	Osbpl6	-1.9074	-2.57849	0.0284
10473874	Arfgap2	-1.9068	-2.64746	0.0253
10547943	Ncapd2	-1.9065	-2.71623	0.0225
10529154	Nrbp1	-1.9029	-3.25955	0.0091
10471036	Dolpp1	-1.8932	-3.07507	0.0123
10410287	Zfp458	-1.8874	-2.603	0.0272
10519998	Lrrc17	-1.8871	-3.14572	0.0110
10360806	Capn2	-1.8860	-2.51391	0.0316

10419296	Wdhd1	-1.8738	-2.35359	0.0414
10588077	2410012M07Rik	-1.8726	-3.46955	0.0064
10526772	Cnpy4	-1.8656	-2.66971	0.0243
10576873	Elavl1	-1.8603	-2.43045	0.0364
10375065	Sh3pxd2b	-1.8580	-2.7353	0.0218
10412981	Sec24c	-1.8572	-2.49572	0.0326
10416974	Gpc6	-1.8564	-2.39372	0.0387
10428955	Gsdmc2	-1.8514	-2.58622	0.0280
10586448	2810417H13Rik	-1.8502	-2.24857	0.0494
10455108	Pcdhb16	-1.8499	-2.50191	0.0323
10553895	NA	-1.8413	-2.75639	0.0210
10455050	Pcdhb2	-1.8331	-2.54477	0.0300
10480139	C1ql3	-1.8244	-2.55656	0.0294
10461402	Fth1	-1.8238	-2.99326	0.0141
10355534	Tns1	-1.8235	-2.80055	0.0195
10587616	Prss35	-1.8214	-2.26115	0.0484
10402211	Fbln5	-1.8210	-2.69598	0.0233
10356880	St8sia4	-1.8163	-2.7588	0.0209
10536220	Col1a2	-1.8112	-2.60078	0.0273
10444713	Bat4	-1.8104	-2.38483	0.0393
10593988	Clk3	-1.8100	-2.46957	0.0341
10421309	Slc39a14	-1.8084	-2.28668	0.0463
10351013	Rc3h1	-1.8083	-2.26918	0.0477
10454235	Asxl3	-1.8032	-2.53229	0.0307
10551405	C030039L03Rik	-1.8019	-2.67121	0.0243
10372648	Lyz2	-1.8006	-2.32357	0.0436
10545450	Tgoln1	-1.7953	-2.96216	0.0149
10363455	Pcbd1	-1.7951	-2.62872	0.0261
10420268	Gzme	-1.7932	-2.53581	0.0305
10430474	Baiap2l2	-1.7902	-2.62926	0.0260
10482030	Stom	-1.7899	-2.40209	0.0382
10459768	NA	-1.7886	-3.04016	0.0131
10476582	Macrod2	-1.7873	-2.7069	0.0229
10364280	Pttg1ip	-1.7844	-2.48169	0.0334
10358599	Hmcn1	-1.7819	-2.56489	0.0290
10435383	Ptplb	-1.7816	-2.9913	0.0142
10569198	Cd151	-1.7809	-2.30438	0.0450
10506870	Txndc12	-1.7729	-2.76487	0.0207
10466947	Ermp1	-1.7729	-2.69277	0.0234
10454198	Rnf125	-1.7719	-3.17979	0.0103
10389701	Akap1	-1.7705	-2.59129	0.0278
10573344	NA	-1.7700	-2.81275	0.0191
10473384	Slc43a3	-1.7695	-2.7993	0.0196
10355341	NA	-1.7635	-2.73753	0.0217
10425985	NA	-1.7618	-2.64313	0.0254

10398727	Klc1	-1.7554	-2.25293	0.0490
10404783	Edn1	-1.7480	-2.49764	0.0325
10604169	Rhox12	-1.7450	-2.72942	0.0220
10376532	Olfr225	-1.7443	-2.50026	0.0324
10362186	Moxd1	-1.7442	-2.6188	0.0265
10473592	Olfr1183	-1.7440	-2.47172	0.0340
10587266	Gclc	-1.7433	-2.38722	0.0392
10414355	Mapk1ip1l	-1.7431	-2.41625	0.0373
10456891	Atp5a1	-1.7422	-2.55008	0.0298
10557951	Armc5	-1.7417	-2.66208	0.0246
10566593	NA	-1.7347	-2.96957	0.0147
10583363	NA	-1.7335	-3.03048	0.0133
10582310	Mvd	-1.7331	-2.94786	0.0152
10562005	Wbp7	-1.7326	-2.74787	0.0213
10369210	Serinc1	-1.7284	-2.83263	0.0185
10454632	Camk4	-1.7280	-2.91988	0.0160
10567219	Arl6ip1	-1.7213	-2.54055	0.0302
10559964	Zik1	-1.7196	-2.51037	0.0318
10551207	NA	-1.7182	-2.61541	0.0267
10521537	Cytl1	-1.7155	-2.51754	0.0314
10592330	Nrgn	-1.7128	-2.77262	0.0205
10534862	Pcolce	-1.7110	-2.88894	0.0168
10414433	6720456H20Rik	-1.7064	-2.56927	0.0288

Appendix 3:

Gene Set	Size	FDR q-val
KEGG SYSTEMIC LUPUS ERYTHEMATOSUS	64	0
KEGG OXIDATIVE PHOSPHORYLATION	100	0
KEGG PARKINSONS DISEASE	98	0
KEGG HUNTINGTONS DISEASE	142	0
KEGG PROTEASOME	42	0
KEGG ALZHEIMERS DISEASE	138	0
KEGG CELL CYCLE	110	0.001125389
KEGG CHRONIC MYELOID LEUKEMIA	70	0.001123257
KEGG SPLICEOSOME	98	0.002315087
KEGG ARGININE AND PROLINE METABOLISM	47	0.012494632
KEGG RNA POLYMERASE	26	0.012544655
KEGG HYPERTROPHIC CARDIOMYOPATHY HCM	81	0.012461762
KEGG RIBOSOME	32	0.019167677
KEGG OOCYTE MEIOSIS	100	0.017888179
KEGG GLIOMA	60	0.017406158
KEGG RENAL CELL CARCINOMA	68	0.019247126
KEGG AXON GUIDANCE	125	0.024434771
KEGG CITRATE CYCLE TCA CYCLE	27	0.026893122
KEGG PURINE METABOLISM	151	0.025477694
KEGG NON SMALL CELL LUNG CANCER	51	0.03168244
KEGG DNA REPLICATION	34	0.03085226
KEGG UBIQUITIN MEDIATED PROTEOLYSIS	122	0.04253078
KEGG BASAL TRANSCRIPTION FACTORS	33	0.04458054
KEGG GLUTATHIONE METABOLISM	44	0.04436181
KEGG DILATED CARDIOMYOPATHY	87	0.047109563
KEGG NEUROTROPHIN SIGNALING PATHWAY	118	0.04614926
KEGG CARDIAC MUSCLE CONTRACTION	67	0.04877423
KEGG PANCREATIC CANCER	69	0.049678884
KEGG MTOR SIGNALING PATHWAY	50	0.050188206
KEGG NUCLEOTIDE EXCISION REPAIR	42	0.050542273
KEGG PHENYLALANINE METABOLISM	16	0.05174342
KEGG ARRHYTHMOGENIC RIGHT VENTRICULAR CARDIOMYOPATHY ARVC	71	0.060537565
KEGG WNT SIGNALING PATHWAY	138	0.06234247
KEGG BASE EXCISION REPAIR	31	0.067242615
KEGG TGF BETA SIGNALING PATHWAY	84	0.08229815

Appendix 4:

Gene Set	Size	FDR q-val
INTERPHASE	65	0.09522871
MITOCHONDRION ORGANIZATION AND BIOGENESIS	41	0.054587618
INTERPHASE OF MITOTIC CELL CYCLE	59	0.05055552
RESPONSE TO OXIDATIVE STRESS	43	0.042850938
NEGATIVE REGULATION OF MAP KINASE ACTIVITY	15	0.042388722
PROTEIN AMINO ACID DEPHOSPHORYLATION	62	0.06340121
CELLULAR BIOSYNTHETIC PROCESS	269	0.060720213
DEPHOSPHORYLATION	69	0.060573004
INDUCTION OF APOPTOSIS BY INTRACELLULAR SIGNALS	20	0.07735149
REGULATION OF CELL CYCLE	165	0.07007759
RIBOSOME BIOGENESIS AND ASSEMBLY	18	0.07534616
RRNA METABOLIC PROCESS	16	0.07122221
RRNA PROCESSING	15	0.06853415
REGULATION OF CYCLIN DEPENDENT PROTEIN KINASE ACTIVITY	40	0.0771385
NITROGEN COMPOUND BIOSYNTHETIC PROCESS	21	0.08543029
RIBONUCLEOPROTEIN COMPLEX BIOGENESIS AND ASSEMBLY	71	0.085171945
NUCLEOTIDE BIOSYNTHETIC PROCESS	17	0.08474893
CELLULAR RESPIRATION	18	0.083551235
NEGATIVE REGULATION OF CELL CYCLE	70	0.086013295
MACROMOLECULAR COMPLEX ASSEMBLY	254	0.08588677
MITOTIC CELL CYCLE	145	0.08224452
COENZYME METABOLIC PROCESS	35	0.08011086
CELL CYCLE GO 0007049	286	0.07976671
RESPONSE TO DRUG	17	0.08513009
CELLULAR PROTEIN COMPLEX ASSEMBLY	32	0.08474605
TRANSLATIONAL INITIATION	35	0.08605239
CELLULAR COMPONENT ASSEMBLY	271	0.085346945
CELL CYCLE ARREST GO 0007050	51	0.08596166
NEGATIVE REGULATION OF CELLULAR METABOLIC PROCESS	220	0.09443352
REGULATION OF DNA BINDING	44	0.09179682
COFACTOR METABOLIC PROCESS	50	0.095516376
NUCLEOTIDE METABOLIC PROCESS	39	0.09723977
NEGATIVE REGULATION OF METABOLIC PROCESS	222	0.09569606
PROTEIN RNA COMPLEX ASSEMBLY	52	0.09392731
MAPKKK CASCADE GO 0000165	94	0.09178534

Appendix 5:

Gene Set
KEGG HUNTINGTONS DISEASE
KEGG PROTEASOME
KEGG ALZHEIMERS DISEASE
KEGG CELL CYCLE
KEGG SPLICEOSOME
KEGG ARGININE AND PROLINE METABOLISM
KEGG HYPERTROPHIC CARDIOMYOPATHY HCM
KEGG OOCYTE MEIOSIS
KEGG GLIOMA
KEGG RENAL CELL CARCINOMA
KEGG AXON GUIDANCE
KEGG CITRATE CYCLE TCA CYCLE
KEGG GLUTATHIONE METABOLISM
KEGG DILATED CARDIOMYOPATHY
KEGG NEUROTROPHIN SIGNALING PATHWAY
KEGG CARDIAC MUSCLE CONTRACTION
KEGG PHENYLALANINE METABOLISM
KEGG ARRHYTHMOGENIC RIGHT VENTRICULAR CARDIOMYOPATHY ARVC
KEGG WNT SIGNALING PATHWAY
KEGG TGF BETA SIGNALING PATHWAY

Appendix 6:

Gene Set
RESPONSE TO OXIDATIVE STRESS
CELLULAR BIOSYNTHETIC PROCESS
REGULATION OF CELL CYCLE
NUCLEOTIDE BIOSYNTHETIC PROCESS
NEGATIVE REGULATION OF CELL CYCLE
MACROMOLECULAR COMPLEX ASSEMBLY
MITOTIC CELL CYCLE
COENZYME METABOLIC PROCESS
CELL CYCLE GO 0007049
RESPONSE TO DRUG
CELLULAR COMPONENT ASSEMBLY
COFACTOR METABOLIC PROCESS

Appendix 7:

GENE SYMBOL	RANK METRIC SCORE	RUNNING ES	CORE ENRICHMENT
ND2	1.266602755	0.038279053	Yes
UQCRH	1.12375927	0.072850935	Yes
ATP5J2	1.052620292	0.10510322	Yes
NDUFC2	0.925483644	0.13257249	Yes
COX7A2	0.874625325	0.15906864	Yes
COX7B	0.866518795	0.18607107	Yes
COX6C	0.853266418	0.21242164	Yes
NDUFS2	0.800621808	0.23541646	Yes
CYC1	0.646903336	0.24994786	Yes
NDUFA4	0.624139309	0.26851597	Yes
ND6	0.596562862	0.2849396	Yes
SDHC	0.58931154	0.30289343	Yes
UQCRC1	0.584037244	0.3207773	Yes
NDUFS8	0.576855838	0.33829415	Yes
NDUFS4	0.568206668	0.35501817	Yes
COX4I1	0.563366175	0.37225562	Yes
ATP5B	0.561034858	0.38965762	Yes
NDUFV1	0.555339158	0.4064066	Yes
ATP5G3	0.531497478	0.41984585	Yes
ATP5D	0.526997745	0.43570855	Yes
NDUFA10	0.525252581	0.45180163	Yes
SDHB	0.505333066	0.464945	Yes
UQCRFS1	0.486477852	0.47806856	Yes
ATP5A1	0.475600272	0.49051955	Yes
COX15	0.448188454	0.49969158	Yes
ND1	0.446091741	0.51340413	Yes
NDUFA9	0.440991312	0.5261499	Yes
NDUFB9	0.425663471	0.5356147	Yes
COX17	0.410314322	0.5441247	Yes
PPA1	0.398960829	0.55370426	Yes
NDUFA5	0.390954584	0.5636982	Yes
ATP5J	0.377916127	0.57081515	Yes
PPA2	0.373564422	0.58093005	Yes
NDUFV2	0.369241148	0.5910997	Yes
CYTB	0.364747375	0.60074896	Yes
NDUFB7	0.356677681	0.60957605	Yes
NDUFB8	0.352619916	0.6186086	Yes
SDHD	0.34792763	0.6275894	Yes
NDUFS6	0.341334462	0.63512945	Yes
COX6A1	0.325045407	0.6387886	Yes
NDUFB10	0.308788002	0.6410371	Yes

ATP5C1	0.298504323	0.64524335	Yes
ATP4B	0.298388392	0.65457445	Yes
COX6B1	0.288188845	0.65774584	Yes
NDUFA3	0.242117569	0.6358286	No
NDUFS7	0.231061429	0.63417447	No
COX10	0.228697464	0.6392843	No
COX11	0.225119948	0.6425728	No
NDUFA7	0.209884435	0.636505	No
ATP5F1	0.206695408	0.6400721	No
ATP6V0B	0.201212898	0.6414733	No
NDUFB6	0.199986145	0.64658755	No
NDUFA11	0.198333398	0.6512702	No
NDUFA8	0.191900373	0.65052825	No
ATP6V0D1	0.186654299	0.6502871	No
NDUFS5	0.181594938	0.65003014	No
NDUFB2	0.176245689	0.64908355	No
NDUFV3	0.163237825	0.63932526	No
NDUFA2	0.154988706	0.6342475	No
ATP6V1H	0.140621543	0.61860603	No
NDUFA1	0.135946199	0.61511713	No
NDUFB3	0.130368322	0.6104566	No
UQCRQ	0.118124731	0.5940166	No
NDUFA6	0.116205715	0.5949913	No
ATP5E	0.107700482	0.5846834	No
NDUFA4L2	0.097198047	0.5704382	No
ATP6V1G3	0.089875646	0.55981034	No
COX5A	0.084503114	0.5517686	No
NDUFC1	0.084104136	0.5535439	No
ATP6V1C1	0.081287853	0.5517173	No
NDUFS1	0.079296902	0.5504931	No
ATP6V1C2	0.075266533	0.5460564	No
TCIRG1	0.063569933	0.52582103	No
ATP6V1E1	0.046047207	0.49368864	No
ATP6V1A	0.018893115	0.4376291	No
COX7A1	0.001796493	0.3983197	No
ATP6V0A4	-0.005872103	0.3816934	No
ATP4A	-0.033924568	0.32140285	No
ATP6V1E2	-0.042431898	0.30430532	No
COX8C	-0.048781324	0.29115772	No
COX7A2L	-0.058424875	0.2727084	No
NDUFB5	-0.061467011	0.26836246	No
ATP5O	-0.078283101	0.23291697	No
ATP6V1D	-0.086378567	0.21975796	No
SDHA	-0.089249641	0.21666071	No
ATP12A	-0.095960043	0.2052259	No

ATP6V1B1	-0.112864383	0.17860197	No
COX8A	-0.11548268	0.1768949	No
ATP6V0E2	-0.117574036	0.17596552	No
COX6B2	-0.137584165	0.14607833	No
ATP6V0A1	-0.14564772	0.13842915	No
COX6A2	-0.153388098	0.1324466	No
ATP6V1G2	-0.167424142	0.11731088	No
ATP6V0A2	-0.190598533	0.09221559	No
UQCRC2	-0.198017508	0.08929066	No
ATP6V1B2	-0.204004437	0.08897472	No
COX7B2	-0.219266012	0.07982886	No
COX4I2	-0.299375504	0.032540433	No
ATP6AP1	-0.316685647	0.035225876	No
ATP6V0D2	-0.486181527	0.013723135	No

Appendix 8:

GENE SYMBOL	RANK METRIC SCORE	RUNNING ES	CORE ENRICHMENT
NDUFS2	0.800621808	0.079041176	Yes
SOD1	0.710364759	0.15327941	Yes
NDUFS8	0.576855838	0.20803776	Yes
PRDX5	0.486397028	0.24925755	Yes
ERCC1	0.485981137	0.30184543	Yes
NDUFA12	0.480219871	0.3525307	Yes
DHCR24	0.437145323	0.39220473	Yes
GPX3	0.368789673	0.41140473	Yes
PRDX6	0.353683323	0.44407564	Yes
DGKK	0.349298239	0.48024964	Yes
GCLC	0.290542871	0.4845817	Yes
ERCC2	0.268579751	0.50050545	Yes
STK25	0.243328065	0.5095268	Yes
PNKP	0.234438822	0.5282881	Yes
SRXN1	0.230517775	0.5500346	Yes
OXSR1	0.226563022	0.5709738	Yes
RNF7	0.223803088	0.59256124	Yes
NUDT1	0.155385688	0.5375494	No
NDUFA6	0.116205715	0.49022812	No
PRDX2	0.103854127	0.4818703	No
ERCC3	0.092400678	0.47217724	No
IPCEF1	0.078520596	0.4544929	No
DUSP1	0.074829794	0.45686725	No
SOD2	0.065033801	0.44515735	No
PRNP	0.064279273	0.45041436	No
GLRX2	0.057262711	0.44283533	No
GCLM	0.039422389	0.4108766	No
ATOX1	0.03654949	0.40995735	No
SEPP1	0.017476056	0.37164366	No
SCARA3	-0.008734356	0.31391376	No
CYGB	-0.011763306	0.3087472	No
APTX	-0.046259768	0.23850647	No
ANGPTL7	-0.055306401	0.22455905	No
PDLIM1	-0.069539584	0.20116627	No
GSS	-0.074868716	0.1972463	No
MSRA	-0.086267002	0.18347919	No
APOA4	-0.101541862	0.16336305	No
ERCC6	-0.123938553	0.13624851	No
MPO	-0.132056653	0.1372911	No
TXNRD2	-0.151875213	0.123384155	No
ERCC8	-0.16139999	0.12732069	No

CCL5	-0.199545532	0.097834215	No
SGK2	-0.341549754	0.0404431	No

Appendix 9:

GENE SYMBOL	RANK METRIC SCORE	RUNNING ES	CORE ENRICHMENT
GSTK1	0.819810569	0.072465666	Yes
ODC1	0.777224481	0.14653097	Yes
GPX1	0.61903888	0.2003741	Yes
MGST3	0.47937125	0.23029758	Yes
IDH2	0.431552351	0.2632075	Yes
GSTM2	0.392126262	0.29020926	Yes
GPX3	0.368789673	0.31774154	Yes
GSTA4	0.353747785	0.3464669	Yes
GSTP1	0.322213858	0.3640823	Yes
ANPEP	0.310313523	0.38887867	Yes
GCLC	0.290542871	0.40721074	Yes
GSTA3	0.261050731	0.41453618	Yes
SRM	0.258345008	0.43808034	Yes
LAP3	0.238762751	0.44722202	Yes
GSR	0.237214357	0.46876386	Yes
GSTM1	0.234934881	0.48980042	Yes
PGD	0.206607103	0.4852144	Yes
GSTM3	0.198811248	0.49758476	Yes
GGT7	0.173242852	0.48526323	No
OPLAH	0.160565078	0.4856357	No
GSTM5	0.150138661	0.4861808	No
RRM2	0.114866532	0.4436644	No
GPX5	0.110155016	0.44681934	No
MGST2	0.086257838	0.41327307	No
GGCT	0.070757329	0.39295214	No
TXNDC12	0.045354858	0.34790808	No
GCLM	0.039422389	0.33804512	No
GSTO1	-0.002006373	0.24906144	No
GGT1	-0.025533197	0.19996347	No
MGST1	-0.03314342	0.18726555	No
GSTT2	-0.04314772	0.16952336	No
GPX7	-0.047899306	0.16389258	No
GSTO2	-0.050449319	0.16239265	No
GSTT1	-0.069487251	0.12811947	No
GSS	-0.074868716	0.12330506	No
GPX6	-0.104189858	0.07468554	No
RRM2B	-0.126762405	0.04587337	No
GSTZ1	-0.146764711	0.028331306	No
IDH1	-0.155764148	0.03074815	No
GPX2	-0.254551977	-0.05367685	No
GGT6	-0.258175343	-0.03100163	No

GGT5	-0.303122103	-0.027788464	No
RRM1	-0.367845774	-0.014887155	No
GSTM4	-0.49426654	0.012408255	No

Appendix 10:

GENE SYMBOL	RANK METRIC SCORE	RUNNING ES	CORE ENRICHMENT
CD36	1.470462799	0.017031047	Yes
DDIT4	1.33265245	0.032643598	Yes
OLR1	1.150194764	0.045866564	Yes
IL6	1.093556046	0.058648396	Yes
EDN1	0.943031788	0.068509966	Yes
MARK2	0.860973835	0.07728717	Yes
GSTK1	0.819810569	0.085472405	Yes
NDUFS2	0.800621808	0.094534434	Yes
SOD1	0.710364759	0.100342184	Yes
FTH1	0.707865655	0.10867271	Yes
RHOB	0.690630853	0.116410375	Yes
HGF	0.664190829	0.12344435	Yes
PXN	0.656448662	0.13086677	Yes
PDGFRB	0.652569711	0.13853149	Yes
LMNB1	0.652317584	0.14638585	Yes
GPX1	0.61903888	0.15224998	Yes
PLA2R1	0.614936829	0.1591244	Yes
NDFIP1	0.610210478	0.16623093	Yes
RELA	0.588312447	0.1715806	Yes
NDUFS8	0.576855838	0.17765933	Yes
NDUFS4	0.568206668	0.18344125	Yes
ETV5	0.538250387	0.18655045	Yes
ATPIF1	0.529092073	0.19152424	Yes
CDKN1A	0.520207405	0.19639105	Yes
PRDX1	0.516137838	0.20212403	Yes
APEX1	0.508813381	0.20738348	Yes
FOSL1	0.505089641	0.2127426	Yes
SH3PXD2B	0.504281163	0.21876632	Yes
CCS	0.489038795	0.22296883	Yes
PRDX5	0.486397028	0.22863272	Yes
ERCC1	0.485981137	0.23443611	Yes
PRKD1	0.485060304	0.24003573	Yes
SLC8A1	0.483250588	0.2454209	Yes
NDUFA12	0.480219871	0.25062507	Yes
MGST3	0.47937125	0.2563007	Yes
JUN	0.477163911	0.26170892	Yes
IER3	0.473255098	0.26663655	Yes
NDUFA13	0.467636853	0.27130386	Yes
DHCR24	0.437145323	0.2711245	Yes
AGAP3	0.436499417	0.2761876	Yes
DIABLO	0.420798302	0.27691925	Yes

CYBB	0.414715767	0.28037137	Yes
CRYAB	0.411943227	0.28431994	Yes
GSTM2	0.392126262	0.28364667	Yes
MGMT	0.387959063	0.28672844	Yes
CYBA	0.379563451	0.28807145	Yes
GPX3	0.368789673	0.2890439	Yes
NUBP1	0.366054863	0.2923436	Yes
EGLN1	0.364575267	0.29615533	Yes
HIF1A	0.354104698	0.29685462	Yes
GSTA4	0.353747785	0.30082497	Yes
PRDX6	0.353683323	0.30508357	Yes
MPV17	0.353620917	0.3093414	Yes
DGKK	0.349298239	0.31190953	Yes
PSMB5	0.346052706	0.3147757	Yes
BAK1	0.342279971	0.31711483	Yes
MYC	0.341907799	0.32079813	Yes
PPP2CB	0.332257479	0.32080084	Yes
SELK	0.326980233	0.32305205	Yes
MAP2K1	0.324194402	0.32570323	Yes
GSTP1	0.322213858	0.32823423	Yes
FBLN5	0.321981966	0.33191845	Yes
FXN	0.301373005	0.32639542	Yes
BAD	0.290546089	0.32392105	Yes
GCLC	0.290542871	0.3274194	Yes
HEPH	0.281652421	0.32536778	Yes
PLK3	0.277970374	0.32649904	Yes
ERCC2	0.268579751	0.32409737	Yes
SFXN3	0.266429812	0.32610118	Yes
GSTA3	0.261050731	0.32563186	Yes
JAK2	0.248914793	0.32058504	Yes
STK25	0.243328065	0.31889084	Yes
TXNRD1	0.24024494	0.31961602	Yes
FPR1	0.239922658	0.32236037	Yes
UCP2	0.238485754	0.32412404	Yes
PML	0.238114417	0.32650942	Yes
GSR	0.237214357	0.32883582	Yes
GSTM1	0.234934881	0.3298824	Yes
PNKP	0.234438822	0.33246437	Yes
CLN8	0.23413901	0.33499455	Yes
SRXN1	0.230517775	0.33483195	Yes
OXSR1	0.226563022	0.33389923	Yes
PDK3	0.224867865	0.33472827	Yes
RNF7	0.223803088	0.33665234	Yes
CYB5R4	0.222701967	0.33846682	Yes
FOXM1	0.222330719	0.34095114	Yes

PRDX3	0.222196177	0.3435302	Yes
GDF2	0.218538627	0.34269354	Yes
SLC11A1	0.216697827	0.3437132	Yes
UCP3	0.211888805	0.34231478	Yes
LONP1	0.210922375	0.34418008	Yes
CDK2	0.208769113	0.34520063	Yes
EPHX2	0.205007076	0.343623	Yes
SRI	0.204760939	0.34594396	Yes
FKBP1B	0.203703716	0.34777054	Yes
EPAS1	0.203036383	0.34973356	Yes
ATP6V0B	0.201212898	0.3505186	Yes
GSTM3	0.198811248	0.3507449	Yes
PARK7	0.197600946	0.35187182	Yes
SLC23A2	0.192350462	0.34831145	No
ATP6V0D1	0.186654299	0.34415266	No
GADD45A	0.185438558	0.34537396	No
PTGS1	0.185160846	0.34736258	No
ROMO1	0.184663847	0.3490562	No
SDC1	0.182016328	0.34782794	No
BDH2	0.180384859	0.3474952	No
MAPK14	0.176462382	0.34523672	No
BNIP3	0.174636245	0.34512377	No
GGT7	0.173242852	0.3459092	No
PNPT1	0.172581449	0.34721655	No
FOS	0.171329901	0.34783444	No
NOX1	0.168238819	0.3461513	No
FABP1	0.163203359	0.34238446	No
OPLAH	0.160565078	0.34070525	No
SH3PXD2A	0.159068495	0.34083834	No
NUDT1	0.155385688	0.33875957	No
GSTM5	0.150138661	0.3321381	No
CST3	0.145361543	0.3274821	No
CNDP2	0.144887775	0.3289858	No
RNF41	0.143692181	0.3290783	No
PRKCD	0.14210549	0.3289108	No
ATP6V1H	0.140621543	0.3285328	No
CYP1A1	0.140327469	0.32959625	No
COQ7	0.138532236	0.32837424	No
PPP1R15B	0.138451532	0.32994497	No
STX3	0.128771722	0.31598562	No
PRG3	0.126635313	0.31413868	No
ADA	0.125473067	0.3138191	No
GRB2	0.125091925	0.3147473	No
SLC11A2	0.122635379	0.3128522	No
PSIP1	0.122187443	0.31355277	No

MAPK7	0.117505617	0.3062975	No
NDUFA6	0.116205715	0.30591452	No
SFXN1	0.113775454	0.3032384	No
IREB2	0.113262638	0.30373514	No
MON1A	0.110892609	0.30140966	No
TGFBR2	0.110741854	0.30235773	No
GPX5	0.110155016	0.3030579	No
TSPO	0.103932656	0.29438686	No
PRDX2	0.103854127	0.29549286	No
PLEKHA1	0.101334319	0.2927151	No
STEAP3	0.10009297	0.29194543	No
STK24	0.098162562	0.289852	No
TRPM2	0.094693214	0.2848268	No
NFE2L2	0.094491705	0.28557917	No
ETS1	0.093741924	0.28564823	No
MFI2	0.093511008	0.2862443	No
ALS2	0.093408257	0.28717634	No
ERCC3	0.092400678	0.28621772	No
VNN1	0.090705559	0.28393817	No
ATP6V1G3	0.089875646	0.28338265	No
PDK2	0.089693397	0.28412545	No
KLF2	0.088829651	0.283461	No
STEAP1	0.087665193	0.28234902	No
ATRN	0.087559283	0.28316247	No
MGST2	0.086257838	0.28160003	No
AATF	0.084536001	0.27919802	No
ABCB6	0.083582729	0.27813324	No
ATP6V1C1	0.081287853	0.27578846	No
PKD2	0.081216715	0.27667004	No
ACE2	0.080789909	0.27667946	No
PRODH	0.080213554	0.27697095	No
ZC3H12A	0.079311542	0.27614373	No
NDUFS1	0.079296902	0.27705035	No
IPCEF1	0.078520596	0.27655077	No
ATP6V1C2	0.075266533	0.2720623	No
DUSP1	0.074829794	0.27257797	No
CHUK	0.072592422	0.26921332	No
GGCT	0.070757329	0.26683807	No
STC2	0.069288693	0.26454148	No
NOX4	0.065295637	0.25762093	No
SOD2	0.065033801	0.25782597	No
PRNP	0.064279273	0.25686592	No
TCIRG1	0.063569933	0.25642717	No
TGFB1	0.059344869	0.2495313	No
AGT	0.059179854	0.24995485	No

HFE	0.058630444	0.2496493	No
GLRX2	0.057262711	0.2466299	No
DHRS2	0.056918427	0.2467854	No
COL1A1	0.054571416	0.2427221	No
PNKD	0.052296817	0.23959473	No
ARG1	0.05203161	0.23973955	No
ADNP2	0.049898885	0.2360535	No
OGG1	0.048901491	0.23510094	No
ETFDH	0.048038743	0.23413801	No
ATP6V1E1	0.046047207	0.2306464	No
MYCN	0.045777123	0.2306196	No
NFKB1	0.042096041	0.2228417	No
HYAL2	0.03983831	0.21773396	No
GCLM	0.039422389	0.2172453	No
F2RL1	0.039421674	0.21771996	No
GNAO1	0.039366465	0.21790496	No
MBL2	0.038616214	0.21731025	No
ADIPOQ	0.037598837	0.21626978	No
ATOX1	0.03654949	0.21478316	No
PAX2	0.033978023	0.21008655	No
SIRT1	0.031642538	0.20608434	No
NCF1	0.031323794	0.20597982	No
PDGFB	0.030899053	0.2055812	No
FTMT	0.029819012	0.20372455	No
DUOX2	0.029027425	0.2023882	No
TACR1	0.02715903	0.19924718	No
LPO	0.025860224	0.19700569	No
FECH	0.025304912	0.19562452	No
SFTPC	0.024968907	0.19505815	No
HAGH	0.024443494	0.19438913	No
UACA	0.023981297	0.19357003	No
ABCG2	0.023869943	0.19361661	No
KRT1	0.023205167	0.19235466	No
IL18BP	0.0223253	0.19122662	No
DPEP1	0.019366583	0.18495724	No
ATP6V1A	0.018893115	0.18407688	No
SEPP1	0.017476056	0.18028942	No
BIRC3	0.017196888	0.1800148	No
NOXA1	0.013298976	0.170975	No
SYK	0.012286803	0.1688109	No
HMOX2	0.010201097	0.16344267	No
MB	0.00877841	0.16036934	No
BMP7	0.008399849	0.15989247	No
MT3	0.007994216	0.15941072	No
SLC40A1	0.007854268	0.15921628	No

TMPRSS6	0.007746	0.1589242	No
DUOXA1	0.004634777	0.15185127	No
SLC46A1	0.003643273	0.14992027	No
ALOX12	0.002918296	0.14875123	No
CAT	0.002727825	0.1484469	No
CHRNA4	0.001109957	0.14479956	No
GATM	9.71E-04	0.14452225	No
CCR7	-3.57E-04	0.14134751	No
ALDH3B1	-0.00168259	0.13857408	No
STEAP2	-0.003018986	0.13547955	No
GAB1	-0.003774706	0.13403182	No
SLC22A17	-0.004586733	0.13273837	No
FANCC	-0.004707712	0.13250604	No
ATP6V0A4	-0.005872103	0.12992755	No
SCARA3	-0.008734356	0.12338564	No
UCN	-0.010424075	0.120043114	No
HAGHL	-0.010473941	0.11988022	No
LTC4S	-0.010503072	0.11995852	No
DUOX1	-0.011577858	0.1180749	No
CYGB	-0.011763306	0.117686704	No
SLC7A11	-0.012950674	0.11601228	No
APOE	-0.01411848	0.11319591	No
LIG1	-0.016215215	0.108092755	No
RAC2	-0.020049145	0.09971222	No
ACO1	-0.020200081	0.099714614	No
ALOX5AP	-0.020678882	0.09909659	No
GGT1	-0.025533197	0.08861457	No
AQP1	-0.026333565	0.08710129	No
LIAS	-0.029243991	0.08123983	No
RIPK1	-0.029333377	0.08135219	No
PREX1	-0.029675653	0.08117966	No
PTPRN	-0.03028712	0.08019566	No
F2	-0.030310446	0.08056062	No
MGST1	-0.03314342	0.07522779	No
GPX8	-0.037148181	0.0663788	No
P2RX7	-0.037609477	0.06577197	No
PPIF	-0.037815258	0.06584195	No
ABCB7	-0.038281135	0.064809695	No
PON2	-0.041205883	0.059862945	No
SLC25A37	-0.041416701	0.06002446	No
CYP11A1	-0.041543368	0.0601875	No
TXN2	-0.041703377	0.06049697	No
ATP6V1E2	-0.042431898	0.059466526	No
APTX	-0.046259768	0.05120892	No
RAC1	-0.046676144	0.051241096	No

GPX7	-0.047899306	0.04897597	No
NGF	-0.04845567	0.048114393	No
SFXN4	-0.050412375	0.043760166	No
ANGPTL7	-0.055306401	0.034118306	No
NNT	-0.058807909	0.027601307	No
ALDH5A1	-0.060584892	0.024766417	No
NQO1	-0.062484369	0.021424556	No
PYCR1	-0.062537991	0.022033056	No
VRK2	-0.063003361	0.02173198	No
PRKAA1	-0.065748289	0.016743567	No
TPO	-0.065845236	0.01734372	No
GSTT1	-0.069487251	0.009173121	No
PDLIM1	-0.069539584	0.010010426	No
GSS	-0.074868716	-0.001322581	No
LTF	-0.07919541	-0.009472621	No
WNT16	-0.08406689	-0.018912688	No
NEO1	-0.084701806	-0.019097	No
ADAM9	-0.08504533	-0.0185065	No
APOD	-0.086207584	-0.019395191	No
MSRA	-0.086267002	-0.018500978	No
ATP6V1D	-0.086378567	-0.017460922	No
XPA	-0.088891543	-0.021689001	No
NOS2	-0.09220051	-0.0281411	No
HPX	-0.094449453	-0.031338915	No
NAPRT1	-0.097758166	-0.037435092	No
PMAIP1	-0.097982951	-0.03654431	No
TRAP1	-0.098852672	-0.03689541	No
CBS	-0.099853091	-0.037330795	No
GLS2	-0.101529285	-0.03928735	No
APOA4	-0.101541862	-0.03816105	No
SLC25A28	-0.102343589	-0.03818111	No
GPX6	-0.104189858	-0.04010563	No
SCARA5	-0.105817214	-0.041480716	No
ATP6V1B1	-0.112864383	-0.052548897	No
PPARGC1B	-0.115440845	-0.05640914	No
PSEN1	-0.116100147	-0.056215394	No
ATP6V0E2	-0.117574036	-0.058364097	No
RGS14	-0.117675468	-0.057188038	No
TAT	-0.119048618	-0.059126318	No
ERCC6	-0.123938553	-0.065292604	No
HMOX1	-0.125166446	-0.0657122	No
SOD3	-0.126690343	-0.06698046	No
PTPRK	-0.126753226	-0.0655506	No
RRM2B	-0.126762405	-0.06412063	No
HDAC6	-0.126958042	-0.062784635	No

CYP2E1	-0.130514503	-0.06670421	No
AOX1	-0.131341115	-0.06613429	No
MPO	-0.132056653	-0.066085584	No
SIN3A	-0.137802973	-0.074830465	No
WRN	-0.138812482	-0.07474859	No
ARNT	-0.143165037	-0.07943102	No
NCF2	-0.143631294	-0.07799061	No
FBXL5	-0.144537389	-0.07764713	No
BCL2	-0.144697696	-0.07619387	No
ATP6V0A1	-0.14564772	-0.07593335	No
LCK	-0.146603554	-0.07561316	No
GSTZ1	-0.146764711	-0.074038684	No
NEIL1	-0.149474859	-0.07614045	No
CYBRD1	-0.150456712	-0.07538853	No
MCOLN1	-0.1510095	-0.07462995	No
TXNRD2	-0.151875213	-0.07357194	No
CTNS	-0.15275456	-0.073225856	No
ECT2	-0.154316142	-0.073342636	No
IDH1	-0.155764148	-0.07382733	No
HAMP	-0.160342962	-0.07801392	No
ERCC8	-0.16139999	-0.077708244	No
SFXN5	-0.164521858	-0.08054401	No
EPX	-0.16689992	-0.08147262	No
ATP6V1G2	-0.167424142	-0.08070906	No
FOXO1	-0.16788815	-0.07965092	No
MPV17L	-0.168443695	-0.07800808	No
CRYAA	-0.171485096	-0.080182	No
PTK2B	-0.173646584	-0.08122204	No
STAR	-0.173797488	-0.07937024	No
ATP7A	-0.174869478	-0.07880604	No
HP	-0.175270423	-0.076791994	No
HYAL1	-0.180924639	-0.082561135	No
MTF1	-0.183947712	-0.084584996	No
CYP1A2	-0.184152573	-0.082753	No
SFXN2	-0.184577808	-0.08086773	No
HTT	-0.190103456	-0.08561117	No
ATP6V0A2	-0.190598533	-0.08370157	No
TPM4	-0.191872671	-0.08273997	No
SFTPD	-0.19850564	-0.08887543	No
NOXO1	-0.20395121	-0.09239245	No
ATP6V1B2	-0.204004437	-0.090032436	No
PXDN	-0.213282838	-0.09733865	No
TFRC	-0.213544413	-0.094911925	No
NET1	-0.214185327	-0.093055494	No
SNCA	-0.214523539	-0.09090599	No

NOX3	-0.215233773	-0.089036934	No
CASP3	-0.222039431	-0.09267333	No
OXR1	-0.223773122	-0.091231294	No
PDK1	-0.226529256	-0.090671256	No
HNF1A	-0.235517219	-0.096553735	No
TMEM161A	-0.242329597	-0.09960865	No
PDK4	-0.243831724	-0.097876936	No
CRYGD	-0.248633355	-0.09868843	No
GPX2	-0.254551977	-0.10000666	No
GGT6	-0.258175343	-0.09930642	No
CD38	-0.269919902	-0.10371499	No
HFE2	-0.270770162	-0.101032734	No
MET	-0.271234602	-0.098007716	No
MMP14	-0.277681172	-0.09866212	No
DRD5	-0.278389245	-0.095695466	No
PARK2	-0.300313652	-0.10441029	No
PPARGC1A	-0.302305609	-0.10149283	No
SCGB1A1	-0.302719831	-0.09804054	No
GGT5	-0.303122103	-0.09453525	No
CP	-0.305301666	-0.091967046	No
STEAP4	-0.327381611	-0.09756226	No
BCO2	-0.33926478	-0.09761966	No
SGK2	-0.341549754	-0.094277844	No
ALAS2	-0.341682702	-0.09021191	No
POU2F1	-0.351683855	-0.08853026	No
APP	-0.359250218	-0.0864685	No
TPM1	-0.376210868	-0.08723706	No
TXNIP	-0.391041577	-0.08570769	No
CTGF	-0.410472274	-0.084618695	No
LCN2	-0.438023061	-0.0830053	No
ANXA1	-0.447937101	-0.07915318	No
XDH	-0.467330158	-0.07636807	No
ATP6V0D2	-0.486181527	-0.07200729	No
GSTM4	-0.49426654	-0.06730833	No
LRRK2	-0.599362671	-0.065871656	No
IL18	-0.636775672	-0.059456788	No
CYR61	-0.64619565	-0.05177248	No
MAP3K5	-0.694724441	-0.0446117	No
TRPA1	-0.759079099	-0.03667604	No
HAO1	-1.03902328	-0.026044006	No
PTGS2	-1.045087934	-0.013460425	No
THBS1	-1.185952306	4.34E-04	No

Appendix 11:

GENE SYMBOL	RANK METRIC SCORE	RUNNING ES	CORE ENRICHMENT
SLC11A1	3.181774139	0.0811868	Yes
PDGFRB	1.80320406	0.12402745	Yes
FTH1	1.705875397	0.16688529	Yes
FBLN5	1.208094597	0.1861812	Yes
SH3PXD2B	1.148617864	0.21192694	Yes
ERCC2	1.101492643	0.23788698	Yes
EDN1	1.082759261	0.2651703	Yes
GSTA3	1.053350925	0.29017898	Yes
GDF2	1.013752103	0.31269872	Yes
LMNB1	0.989409626	0.33611283	Yes
HEPH	0.980635166	0.36053616	Yes
GCLC	0.976197004	0.38536784	Yes
GSTK1	0.895933867	0.40125322	Yes
PML	0.813556015	0.4122216	Yes
DHCR24	0.710214496	0.41241652	Yes
GSTM3	0.650471985	0.41568306	Yes
DGKK	0.628231585	0.42559597	Yes
UCP3	0.622840643	0.44035617	Yes
SRI	0.603137553	0.45019445	Yes
NDUFS2	0.514754713	0.43273926	Yes
PRKD1	0.507505357	0.44306564	Yes
EPAS1	0.496974379	0.4513172	Yes
APEX1	0.489394695	0.46037126	Yes
DDIT4	0.451914668	0.45231846	Yes
ETV5	0.446796864	0.46165562	Yes
PRDX6	0.432892501	0.46564996	Yes
HIF1A	0.413600504	0.46511278	No
MAP2K1	0.380288631	0.45370114	No
RHOB	0.33886534	0.43633494	No
TXNRD1	0.337273508	0.44418904	No
MYC	0.336570352	0.452215	No
SOD1	0.298505247	0.4339548	No
FOSL1	0.294661134	0.43800804	No
EGLN1	0.276488751	0.43195546	No
MPV17	0.274692804	0.43744272	No
PLA2R1	0.263195366	0.43451506	No
OXSR1	0.260833293	0.4391241	No
JUN	0.256211728	0.4423324	No
NDUFS4	0.245090991	0.43784767	No
GSR	0.240249291	0.4393165	No
NDUFS8	0.230456844	0.4373525	No

PXN	0.216499254	0.42980686	No
CDK2	0.212268591	0.4309845	No
CD36	0.194867283	0.41984442	No
CCS	0.18510896	0.41391432	No
ERCC1	0.174322158	0.4077547	No
IL6	0.168195054	0.40571123	No
AGAP3	0.163723469	0.40540478	No
GSTM2	0.157802045	0.40323687	No
CYBA	0.14813669	0.39687964	No
PARK7	0.146517992	0.39917028	No
GSTM1	0.139579892	0.39615455	No
STK25	0.135372087	0.39493012	No
PDK3	0.132312834	0.3953365	No
PLK3	0.124965236	0.39113826	No
SLC8A1	0.114635922	0.38287607	No
NDUFA13	0.113016866	0.38383156	No
PRDX3	0.111839689	0.38556403	No
BAD	0.110064298	0.38658616	No
FKBP1B	0.107871778	0.38726708	No
FXN	0.106554307	0.38862643	No
SRXN1	0.090477981	0.3738084	No
DIABLO	0.086889371	0.37176627	No
NUBP1	0.082963467	0.3698607	No
EPHX2	0.073512614	0.36149213	No
FOXM1	0.063787334	0.35296878	No
GSTP1	0.0450195	0.3358438	No
GPX1	0.008708655	0.29860306	No
NDUFA12	-0.004810794	0.28391176	No
ATPIF1	-0.015675321	0.27405792	No
MGMT	-0.026483925	0.26348448	No
SELK	-0.032999109	0.25815907	No
NDFIP1	-0.037402228	0.2549885	No
PRDX5	-0.039353475	0.25386235	No
SFXN3	-0.043845672	0.25061986	No
PRDX1	-0.058319896	0.23801498	No
CRYAB	-0.058380142	0.23946671	No
HGF	-0.066157177	0.23290356	No
GSTA4	-0.067189135	0.2334419	No
RELA	-0.080838434	0.22274484	No
OLR1	-0.100695223	0.20586254	No
GPX3	-0.101791903	0.20757441	No
ATP6V0B	-0.107428774	0.20487264	No
MARK2	-0.108251482	0.20694032	No
LONP1	-0.131162986	0.19122031	No
BAK1	-0.146790117	0.18027009	No

CDKN1A	-0.195635021	0.14403102	No
JAK2	-0.234622061	0.121423714	No
PSMB5	-0.342370301	0.058895875	No
CYBB	-0.350975484	0.06268588	No
PNKP	-0.365389168	0.06371213	No
CLN8	-0.379861951	0.065822296	No
PPP2CB	-0.381056964	0.07508566	No
IER3	-0.384382963	0.083864644	No
UCP2	-0.460898697	0.062224906	No
MGST3	-0.472490638	0.070797384	No
RNF7	-0.532708943	0.0651518	No
FPR1	-0.55302906	0.073085986	No
CYB5R4	-0.687478304	0.05883185	No

Appendix 12:

Gene Symbol	UCSC Gene ID	5' UTR Length
1110008L16Rik	uc007nop.2	1271
2310035C23Rik	uc007cgk.2	247
2410012M07Rik	uc012gyw.1	228
2610301B20Rik	uc012dam.1	117
4931431F19Rik	uc012frf.1	208
5730590G19Rik	uc009hyp.1	144
6720456H20Rik	uc007tjo.2	104
A930038C07Rik	uc009cei.1	492
Acer2	uc008tmf.2	75
Adam12	uc009kdp.2	220
Ahcyl2	uc009bek.2	127
Ahi1	uc007eod.2	364
Akap11	uc007usi.2	201
Aldh1l2	uc007gkh.2	126
Aldh9a1	uc007dkx.1	245
Aldoc	uc007kix.1	204
Anxa8	uc007taj.1	66
Arfgap2	uc008kvr.2	218
Arl11	uc007ufu.1	288
Armcx4	uc029xmw.1	583
Aspm	uc007cwh.1	159
Aspn	uc007qjm.2	298
Asxl1	uc008nhs.1	195
Asxl3	uc008efm.2	405
Atxn1l	uc009njh.1	348
B3gnt5	uc012acn.1	1151
Baiap2l2	uc007wtb.1	121
Bcs1l	uc007bmq.1	200
Bdp1	uc007rqc.1	232
Blm	uc009iaw.2	343
Bmpr1b	uc008roi.1	348
Cacna1c	uc009dlt.2	214
Camk4	uc008ejq.2	355
Capn2	uc007dye.2	129
Capn5	uc009ikd.1	180
Carhsp1	uc007yct.1	48
Casc5	uc008lta.1	121
Ccdc80	uc007zig.1	408
Ccl24	uc008zyn.1	71
Ccl25	uc009ktw.2	118
Cdh10	uc007vil.1	486

Cdh11	uc009mzu.1	506
Cdh6	uc007vif.1	259
Cluap1	uc007xzb.1	123
Cntnap1	uc007lnt.1	141
Crebbp	uc007xzl.1	181
Crisp1	uc008coh.2	55
Ctcf	uc009ndm.2	309
Cx3cr1	uc009sbz.1	87
Cyp1b1	uc008dqc.1	356
Dcaf7	uc007lxz.1	252
Ddx51	uc008yre.2	37
Ddx52	uc007kpz.2	88
Dkk2	uc008rjw.2	741
Dkk3	uc009jgj.1	115
Dnajb6	uc008wuo.2	245
Dnajc18	uc008emq.2	79
Dock8	uc008hba.1	122
E430025E21Rik	uc007vxt.1	232
Edn1	uc007qfl.2	625
Elavl1	uc009kts.1	231
Epha7	uc008sen.2	239
Esco2	uc007ujp.2	181
Fam110c	uc007nhb.1	73
Fam20a	uc007mcw.1	541
Fanci	uc009hyh.1	73
Fap	uc008jvk.1	170
Fat4	uc008pbf.1	20
Fbn1	uc008mco.1	286
Fbn2	uc008ezn.1	121
Fbxl12	uc009oiz.1	2009
Fhl1	uc009tgn.1	295
Fibin	uc008lmv.1	198
Fpgs	uc008jgm.2	49
Fth1	uc008got.1	502
Fzd3	uc007ujb.2	463
Fzd9	uc008zya.2	18
Gabrb2	uc007imi.1	427
Gbp1	uc008rox.1	79
Gclc	uc009qtm.2	275
Gcnt4	uc007rno.2	378
Gjb2	uc007ucx.2	256
Gm14137	uc008lth.2	453
Gm2016	uc007ojn.1	491
Gm5662	uc007ojs.3	488
Gpkow	uc009sma.1	92

Gpm6b	uc009uwq.2	468
Grb10	uc007iba.2	334
Guf1	uc008xqm.1	113
Gzmd	uc007ubp.1	71
Has2	uc007vsl.2	553
Hbq1a	uc007ijn.1	49
Hdx	uc009udb.1	113
Herc4	uc007fkd.2	476
Hist2h2be	uc008qmj.1	45
Hmcn1	uc007cyj.1	384
Hmgn5	uc009ucs.1	114
Inha	uc007bps.1	171
Ints4	uc009iji.2	141
Itga11	uc009qal.2	90
Itga8	uc008ijk.1	138
Kbtbd7	uc007usy.1	219
Kcnip1	uc007ikq.2	395
Kcnj15	uc008abs.1	470
Klf10	uc007vnr.1	113
Klf6	uc007pjw.1	150
Klhl24	uc007yph.1	242
Lag3	uc009dsl.2	354
Larp1	uc007jah.2	129
Larp4	uc007xql.1	193
Lclat1	uc008dnh.2	197
Ldlrap1	uc012dmx.1	104
Lgr6	uc007csq.1	136
Lipo1	uc008hfv.1	571
Lmnb1	uc012bdd.2	300
Lphn2	uc008rsb.1	100
Lphn3	uc008xwp.1	513
Ltn1	uc007zug.1	139
Lypd6b	uc008jpz.1	456
Lyzl6	uc007lvl.1	188
Mapk1ip1l	uc007thy.1	96
Mcm7	uc009aeu.1	106
Mecom	uc008oup.2	852
Mmp16	uc008sbw.2	239
Moxd1	uc007equ.1	87
Mtr	uc007plh.2	257
Nat6	uc009rmb.1	1927
Nudt10	uc009skw.2	156
Nudt11	uc009sku.1	404
Nup54	uc008ydk.1	129
Olfr651	uc009iwm.2	37

Osbpl1a	uc008ecp.2	865
Pank3	uc007ilf.1	425
Pappa	uc008thm.1	368
Pcdh18	uc012cph.1	452
Pcdhb16	uc008eqb.1	221
Pcdhb20	uc008eqf.2	159
Pddc1	uc012fwy.1	60
Pdgfrb	uc008fbl.2	429
Pdk1	uc008kbj.2	98
Pdp1	uc008sab.1	193
Pdpk1	uc012amc.1	134
Pi15	uc007ake.2	144
Postn	uc008pfj.2	36
Ppp1r3f	uc009slj.1	64
Prrx1	uc007dhk.1	1015
Prss35	uc012gxu.1	195
Psmb8	uc012apv.1	204
Psmc6	uc007tgn.1	24
Ptgdr	uc007ter.1	122
Ptgir	uc009fim.2	295
Ptpn23	uc009rty.1	93
Qser1	uc008lkg.2	206
Rbm10	uc009stf.2	704
Rev1	uc007asr.1	211
Rraga	uc008tlw.2	246
Rragb	uc012hqx.1	526
Runx1t1	uc008saw.2	534
S1pr1	uc008rbo.2	518
S1pr3	uc007qmf.2	471
Sdc2	uc007vkx.1	523
Seh1l	uc008fmx.1	134
Sfrp1	uc009lev.2	283
Sgpl1	uc007ffk.2	190
Slc14a1	uc008fsd.2	243
Slc16a1	uc008qui.1	204
Slc1a3	uc007vey.2	566
Slc25a35	uc007jop.1	532
Slc39a14	uc007unu.1	258
Slit2	uc008xjo.2	1885
Slitrk6	uc007uyd.2	546
Snx19	uc009oqy.1	239
St5	uc009jdv.1	115
St8sia4	uc011wpu.1	333
Svep1	uc008syr.1	220
Tha1	uc007moh.2	127

Tll1	uc009lut.1	610
Tmem176b	uc009bvu.2	636
Tmem209	uc009bfj.1	19
Tmem37	uc007cjd.1	48
Tmem44	uc007ywq.1	79
Tmod2	uc009qsk.1	433
Trpa1	uc007ajc.1	27
Trps1	uc011zss.1	440
Tstd2	uc008stg.2	139
Ttc30a1	uc008kew.2	230
Ube1y1	uc009uyx.1	102
Ube2v1	uc008oaa.1	44
Ublcp1	uc007ing.2	164
Ubr1	uc008lxb.1	113
Uhmk1	uc007dma.1	153
Usp26	uc009tec.1	695
Usp28	uc009pir.1	96
Wbscr16	uc008zvc.2	53
Wdhd1	uc007thu.2	260
Wfs1	uc008xff.1	122
Yipf2	uc009olx.2	273
Zcchc5	uc009ubw.1	374
Zdhhc15	uc009uaj.2	265
Zfp146	uc009gdn.1	682
Zfp36l1	uc007oal.1	138
Zfp459	uc007rat.2	80
Zfp516	uc008fuf.2	269
Zfp54	uc008aqu.1	397
Zfp72	uc007rff.1	97
Zfp828	uc009kyq.2	217
Zik1	uc009fdf.1	246

Appendix 13:

Gene Symbol	CERT Distance from 5'cap	p-value	q-value
Fth1*	153	2.71E-09	4.11E-05
Elavl1	112	1.12E-08	4.26E-05
Elavl1	115	1.12E-08	4.26E-05
Elavl1	118	1.12E-08	4.26E-05
Elavl1	121	3.45E-08	0.000105
Elavl1	163	4.23E-08	0.000107
Gjb2	186	1.95E-07	0.000423
Dcaf7	147	2.60E-07	0.000457
Fth1*	150	2.90E-07	0.000457
Elavl1	80	3.02E-07	0.000457
Capn2	79	3.55E-07	0.000485
Qser1	42	4.68E-07	0.000544
Wdhd1	76	5.02E-07	0.000544
Tll1	278	5.84E-07	0.00059
Qser1	45	6.99E-07	0.000662
Zdhhc15	193	8.29E-07	0.000739
Lmnb1	285	9.34E-07	0.000787
Lmnb1	6	1.63E-06	0.00124
Akap1	2	1.68E-06	0.00124
Elavl1	127	1.72E-06	0.00124
Lmnb1	228	1.92E-06	0.00132
Laptm4b	144	2.11E-06	0.00139
Itga11	75	2.85E-06	0.0018
Lipo1	263	3.23E-06	0.00196
Fbn2	79	3.73E-06	0.00217
Osbpl6	12	4.33E-06	0.00243
Hbegf	269	5.19E-06	0.0028
Pdgfrb	188	5.35E-06	0.0028
Laptm4b	29	6.61E-06	0.00334
Gjb2	17	7.51E-06	0.0035
Gzmd	36	8.04E-06	0.0035
Lclat1	53	8.28E-06	0.0035
Lmnb1	222	8.31E-06	0.0035
Scd2	362	8.49E-06	0.0035
Lmnb1	225	8.52E-06	0.0035
Dse	101	8.71E-06	0.0035
Osbpl6	6	8.77E-06	0.0035
Dse	353	9.11E-06	0.00354
Zdhhc15	196	1.05E-05	0.00399
Pdgfrb	205	1.26E-05	0.00433
Dcaf7	238	1.34E-05	0.00433

Laptm4b	20	1.34E-05	0.00433
Qser1	39	1.41E-05	0.00433
Slit2	263	1.45E-05	0.00433
Elavl1	50	1.46E-05	0.00433
Elavl1	56	1.46E-05	0.00433
Elavl1	62	1.46E-05	0.00433
Elavl1	68	1.46E-05	0.00433
Elavl1	74	1.46E-05	0.00433
Lmnb1	13	1.49E-05	0.00434
Zdhhc15	173	1.56E-05	0.00446
Dkk2	122	1.68E-05	0.00471
6720456H20Rik	53	1.78E-05	0.00487
Lmnb1	30	1.80E-05	0.00487
Pcbd1	40	1.86E-05	0.00495
Lmnb1	93	1.99E-05	0.00515
Hbegf	266	2.02E-05	0.00515
2410012M07Rik	149	2.07E-05	0.00515
Elavl1	109	2.07E-05	0.00515
Fbln5	207	2.25E-05	0.00549
Dse	291	2.38E-05	0.00573
Zdhhc15	185	2.46E-05	0.00584
Scd2	482	2.58E-05	0.00597
Qser1	9	2.60E-05	0.00597
Dcaf7	150	2.67E-05	0.00604
Camk4	189	2.80E-05	0.00604
Fbln5	204	2.80E-05	0.00604
Arfgap2	170	2.84E-05	0.00604
Laptm4b	99	2.85E-05	0.00604
Laptm4b	96	2.89E-05	0.00604
Fth1*	75	2.93E-05	0.00604
Capn2	46	2.95E-05	0.00604
Fth1*	143	3.05E-05	0.00617
Sh3pxd2b	44	3.21E-05	0.00632
Osbpl6	66	3.39E-05	0.00647
Lmnb1	16	3.43E-05	0.00647
Camk4	199	3.45E-05	0.00647
Gclc	214	3.50E-05	0.00647
Gjb2	193	3.50E-05	0.00647
Mapk1ip1l	45	3.55E-05	0.00647
Arfgap2	147	3.62E-05	0.00651
Fbln5	202	3.69E-05	0.00651
Tll1	388	3.76E-05	0.00651
Qser1	12	3.80E-05	0.00651
Fbn1	63	3.82E-05	0.00651
Laptm4b	91	3.82E-05	0.00651

Klc1	16	4.06E-05	0.00668
Zdhhc15	221	4.06E-05	0.00668
Fbln5	280	4.13E-05	0.00668
Dse	201	4.14E-05	0.00668
Lmnb1	219	4.29E-05	0.00685
Qser1	36	4.38E-05	0.00691
Dcaf7	227	4.50E-05	0.00704
Osbpl6	63	4.62E-05	0.0071
Gpank1	89	4.64E-05	0.0071
6720456H20Rik	29	4.78E-05	0.00725
Dcaf7	155	4.83E-05	0.00725
Lclat1	45	5.05E-05	0.0075
Slit2	1314	5.12E-05	0.00754
Gpc6	479	5.18E-05	0.00755
Elavl1	53	5.47E-05	0.00767
Elavl1	59	5.47E-05	0.00767
Elavl1	65	5.47E-05	0.00767
Elavl1	71	5.47E-05	0.00767
Gjb2	189	5.59E-05	0.00778
Pcdh18	206	5.65E-05	0.00779
Laptm4b	115	6.13E-05	0.00837
Armc5	690	6.28E-05	0.00841
Dcaf7	235	6.28E-05	0.00841
Rragb	275	6.44E-05	0.00841
Lmnb1	110	6.47E-05	0.00841
Lmnb1	23	6.49E-05	0.00841
Lmnb1	122	6.69E-05	0.00859
Hbegf	9	7.19E-05	0.00904
Hbegf	237	7.21E-05	0.00904
Hmcn1	29	7.21E-05	0.00904
Osbpl6	78	7.32E-05	0.00904
Gclc	90	7.37E-05	0.00904
Klc1	108	7.40E-05	0.00904
Hmcn1	151	7.50E-05	0.0091
St8sia4	211	7.76E-05	0.00928
Moxd1	36	7.78E-05	0.00928
Scd2	475	7.87E-05	0.00928
Fbln5	221	7.90E-05	0.00928
Clk3	276	8.04E-05	0.00937
Hmcn1	70	8.18E-05	0.00946
Camk4	130	8.27E-05	0.00946
Cd151	16	8.30E-05	0.00946
Pcbd1	43	8.45E-05	0.00956
Lrrc17	87	8.76E-05	0.00971
Dse	247	8.78E-05	0.00971

Zik1	168	8.78E-05	0.00971
2410012M07Rik	164	8.88E-05	0.00971
Klc1	136	8.91E-05	0.00971
Dse	278	9.19E-05	0.00995
Camk4	268	9.29E-05	0.00999
Slit2	1431	9.39E-05	0.01
Edn1	423	9.46E-05	0.01
Hmcn1	91	9.69E-05	0.0102
Edn1	387	9.96E-05	0.0104
Elavl1	86	0.000101	0.0105
Rarres1	3	0.000103	0.0106
Dkk2	112	0.000106	0.0108
Tll1	271	0.000106	0.0108
Cpt2	77	0.000107	0.0108
2410012M07Rik	196	0.000108	0.0108
Adam12	138	0.000108	0.0108
Lipo1	377	0.000112	0.0111
Gpc6	476	0.000115	0.0113
Tll1	89	0.000115	0.0113
Adam12	79	0.000117	0.0114
Osbpl6	55	0.000118	0.0114
Cnpy4	4	0.00012	0.0115
Camk4	302	0.000122	0.0115
Dcaf7	185	0.000123	0.0115
Dse	284	0.000123	0.0115
Lmnb1	83	0.000123	0.0115
Gclc	26	0.000124	0.0115
Osbpl6	58	0.000127	0.0117
Itga11	70	0.000128	0.0118
Fbln5	277	0.000129	0.0118
Fth1*	148	0.00013	0.0118
Armc5	697	0.000132	0.0119
6720456H20Rik	34	0.000133	0.012
Tll1	582	0.000134	0.012
Aspn	258	0.000136	0.012
Capn2	76	0.000137	0.012
Elavl1	41	0.000137	0.012
Lmnb1	129	0.000138	0.012
Dkk3	29	0.00014	0.0121
Dse	309	0.000142	0.0122
Osbpl6	121	0.000142	0.0122
Lclat1	48	0.000145	0.0123
Clk3	272	0.000152	0.0129
Clk3	269	0.000158	0.0132
Pdgfrb	202	0.000158	0.0132

Gzmd	33	0.000159	0.0132
Gjb2	66	0.000162	0.0134
Laptm4b	22	0.000162	0.0134
6720456H20Rik	31	0.000164	0.0134
Capn2	74	0.000168	0.0137
Fth1*	85	0.00017	0.0138
Fbn2	86	0.000174	0.0139
Slit2	413	0.000174	0.0139
St8sia4	209	0.000174	0.0139
Gjb2	19	0.000175	0.0139
Capn2	19	0.000176	0.0139
Fbn1	32	0.000177	0.0139
Lphn3	86	0.000182	0.0141
Clk3	292	0.000183	0.0141
Pcbd1	37	0.000184	0.0141
Camk4	197	0.000185	0.0141
Lmnb1	125	0.000185	0.0141
Tll1	174	0.000185	0.0141
Psma5	54	0.000186	0.0141
Gjb2	10	0.000187	0.0141
Fth1*	138	0.00019	0.0142
Pcbd1	24	0.00019	0.0142
Dse	280	0.000192	0.0142
Dse	344	0.000193	0.0142
Elavl1	106	0.000193	0.0142
Wdhd1	68	0.000193	0.0142
Laptm4b	98	0.000197	0.0144
Pcdh18	228	0.000198	0.0144
Psma5	327	0.000201	0.0145
Dcaf7	144	0.000202	0.0145
Fth1*	145	0.000204	0.0146
Camk4	270	0.000207	0.0146
Dse	218	0.000207	0.0146
Arl6ip1	41	0.000208	0.0146
Capn2	43	0.000209	0.0146
Gpc6	468	0.00021	0.0146
Fbln5	213	0.00022	0.0153
Clk3	290	0.000223	0.0153
Edn1	406	0.000223	0.0153
Clk3	32	0.000225	0.0153
Dcaf7	153	0.000225	0.0153
Lipo1	270	0.000226	0.0154
Lyz2	9	0.000228	0.0154
Ccdc80	193	0.000232	0.0156
Elavl1	167	0.000232	0.0156

Hmcn1	40	0.000234	0.0156
Qser1	6	0.000239	0.0159
Lipo1	170	0.000246	0.0163
Nrgn	147	0.000248	0.0163
Gpank1	39	0.000249	0.0163
Lmnb1	197	0.000249	0.0163
Capn2	51	0.000252	0.0163
Slit2	1270	0.000252	0.0163
Fth1*	82	0.000255	0.0164
Dcaf7	202	0.000257	0.0164
Osbpl6	82	0.000257	0.0164
Lipo1	292	0.000263	0.0166
Capn2	54	0.000266	0.0167
Lmnb1	194	0.000268	0.0168
Macrod2	152	0.000271	0.0168
Gclc	212	0.000272	0.0168
Zik1	185	0.000276	0.017
2410012M07Rik	158	0.00028	0.0171
Klc1	19	0.00028	0.0171
Osbpl6	44	0.000281	0.0171
Nrgn	140	0.000282	0.0171
Wdhd1	73	0.000283	0.0171
Osbpl6	9	0.000288	0.0173
Rarres1	86	0.000289	0.0173
Fth1*	78	0.00029	0.0173
Lmnb1	136	0.000296	0.0174
Mapk1ip1l	48	0.000296	0.0174
Wdhd1	59	0.000297	0.0174
Zdhhc15	188	0.000297	0.0174
Edn1	53	0.000298	0.0174
Lclat1	123	0.000298	0.0174
Elavl1	124	0.000299	0.0174
Tll1	150	0.000302	0.0175
Pttg1ip	32	0.000305	0.0176
Slit2	1588	0.000307	0.0176
Itga8	77	0.00031	0.0177
Osbpl6	1	0.000311	0.0177
Dcaf7	206	0.000314	0.0178
Fth1*	68	0.000322	0.0181
Tll1	184	0.000324	0.0182
Elavl1	44	0.000327	0.0183
S1pr3	92	0.000328	0.0183
Elavl1	166	0.000332	0.0184
Efemp1	60	0.000334	0.0184
Osbpl6	69	0.000335	0.0184

Dse	194	0.000336	0.0184
Col1a2	64	0.000346	0.0188
Dse	270	0.000346	0.0188
Adam12	173	0.000347	0.0188
Psma5	324	0.000348	0.0188
Pcbd1	46	0.000349	0.0188
Qser1	3	0.000354	0.019
Lipo1	172	0.000357	0.0191
6720456H20Rik	87	0.000358	0.0191
Macrod2	51	0.00036	0.0191
Cyp1b1	304	0.000361	0.0191
Klc1	22	0.000364	0.0192
Rc3h1	219	0.00037	0.0195
2410012M07Rik	199	0.000373	0.0195
Pcdhb16	93	0.000378	0.0197
Dcaf7	141	0.000379	0.0197
Adam12	178	0.000381	0.0198
Gjb2	82	0.000382	0.0198
Fbln5	224	0.000389	0.0199
Lmnb1	27	0.000389	0.0199
Edn1	418	0.00039	0.0199
Gpc6	230	0.00039	0.0199
2410012M07Rik	176	0.000394	0.02
Dse	398	0.000394	0.02
Gjb2	26	0.000395	0.02
Gclc	217	0.000398	0.02
Gpc6	198	0.000398	0.02
Dse	425	0.0004	0.02
Itga11	41	0.000401	0.02
Wdhd1	79	0.000402	0.02
Lmnb1	1	0.000408	0.0202
Rarres1	90	0.00041	0.0202
Efemp1	105	0.000412	0.0203
Klc1	14	0.000415	0.0204
Gclc	72	0.000421	0.0206
Dse	215	0.000426	0.0207
Fbn1	235	0.000426	0.0207
Slit2	1277	0.000427	0.0207
Pcbd1	1	0.000434	0.0209
Cyp1b1	8	0.000437	0.021
Zik1	163	0.000441	0.021
Elavl1	158	0.000442	0.021
Psma5	318	0.000445	0.021
Tll1	579	0.000445	0.021
Fbln5	216	0.000446	0.021

Edn1	411	0.000447	0.021
Edn1	414	0.000448	0.021
Elavl1	77	0.000448	0.021
Fbn1	66	0.000454	0.0212
2410012M07Rik	153	0.000457	0.0213
Pcdh18	136	0.000458	0.0213
Baiap2l2	64	0.000459	0.0213
Dse	288	0.000463	0.0213
Tll1	281	0.000463	0.0213
Gpc6	54	0.000465	0.0213
Gpc6	524	0.000466	0.0213
Hbegf	263	0.000467	0.0213
Clk3	320	0.00047	0.0214
Cyp1b1	222	0.000478	0.0217
Dcaf7	224	0.000482	0.0217
Dcaf7	212	0.000484	0.0217
Dse	210	0.000484	0.0217
Armc5	693	0.000486	0.0217
Gpc6	337	0.000488	0.0217
Lclat1	131	0.000488	0.0217
Qser1	48	0.000488	0.0217
Lmnb1	282	0.00049	0.0217
Lipo1	459	0.000491	0.0217
Capn2	48	0.000496	0.0218
Gjb2	69	0.000499	0.0218
Psma5	13	0.000503	0.0218
2410012M07Rik	188	0.000504	0.0218
Slit2	1267	0.000504	0.0218
Tll1	395	0.000504	0.0218
Lmnb1	24	0.000506	0.0218
Camk4	149	0.000508	0.0218
Clk3	34	0.000509	0.0218
St8sia4	95	0.000512	0.0218
Fbln5	211	0.000513	0.0218
Fbn1	22	0.000517	0.0218
Lmnb1	3	0.000518	0.0218
Adam12	145	0.000519	0.0218
Osbpl6	15	0.000519	0.0218
Pcbd1	34	0.000521	0.0218
Fth1*	65	0.000523	0.0218
Hbegf	4	0.000527	0.0218
Fbn1	238	0.00053	0.0218
Fbn1	241	0.00053	0.0218
Fbn1	244	0.00053	0.0218
Fbn1	247	0.00053	0.0218

Rc3h1	209	0.00053	0.0218
Slit2	104	0.00053	0.0218
Gjb2	85	0.000533	0.0218
Rhox12	235	0.000539	0.022
Hbegf	201	0.000552	0.0224
Adam12	143	0.000554	0.0224
Qser1	5	0.000555	0.0224
Fth1*	146	0.00056	0.0226
Dse	273	0.000561	0.0226
2410012M07Rik	183	0.00057	0.0228
Has2	494	0.000571	0.0228
Itga11	67	0.000571	0.0228
Itga11	64	0.000573	0.0228
Slit2	1434	0.000574	0.0228
Slc14a1	154	0.000575	0.0228
S1pr3	346	0.000577	0.0228
Dkk2	119	0.000584	0.023
Fbln5	218	0.000586	0.023
Baiap2l2	27	0.000587	0.023
Lipo1	266	0.000589	0.023
2410012M07Rik	194	0.0006	0.0234
Tll1	226	0.000605	0.0235
Tll1	83	0.000608	0.0236
Adam12	95	0.000611	0.0236
Camk4	11	0.000614	0.0236
Lmnb1	21	0.000614	0.0236
Pttg1ip	29	0.000619	0.0236
Elavl1	47	0.00062	0.0236
Lmnb1	26	0.000622	0.0236
Macrod2	159	0.000622	0.0236
Nrgn	145	0.000622	0.0236
Col6a3	216	0.000625	0.0237
Fth1*	126	0.000627	0.0237
Efemp1	62	0.00063	0.0237
Rragb	272	0.000633	0.0238
Lmnb1	4	0.000635	0.0238
Rarres1	87	0.000636	0.0238
Slc14a1	81	0.00064	0.0239
Osbpl6	75	0.000646	0.024
Dkk2	447	0.000649	0.024
Akap1	53	0.000651	0.024
Lipo1	295	0.000651	0.024
2410012M07Rik	155	0.000656	0.0241
Capn2	42	0.000658	0.0241
Dse	277	0.000659	0.0241

Rragb	147	0.000659	0.0241
Pdgfrb	164	0.000665	0.0242
Gpc6	101	0.000666	0.0242
Camk4	230	0.00067	0.0242
Fth1*	118	0.00067	0.0242
Armc5	700	0.000671	0.0242
Pdgfrb	200	0.000675	0.0243
Clk3	319	0.000677	0.0243
Zdhhc15	46	0.000687	0.0244
S1pr3	424	0.00069	0.0244
Camk4	315	0.000692	0.0244
Slit2	319	0.000694	0.0244
Dse	204	0.000695	0.0244
Elavl1	195	0.000695	0.0244
Slc38a4	53	0.000697	0.0244
Hbegf	2	0.000699	0.0244
Lmnb1	115	0.000701	0.0244
Psma5	315	0.000701	0.0244
Slit2	1713	0.000701	0.0244
Laptm4b	11	0.000704	0.0244
Osbpl6	19	0.000704	0.0244
Rarres1	77	0.00071	0.0246
Hmcn1	43	0.000719	0.0247
Fbn1	272	0.000721	0.0247
Tll1	396	0.000725	0.0247
Macrod2	61	0.000726	0.0247
Klc1	142	0.000728	0.0247
Tll1	380	0.000728	0.0247
Lmnb1	102	0.00073	0.0247
Dse	209	0.000732	0.0247
Gjb2	215	0.000734	0.0247
Dkk2	676	0.000736	0.0247
Prss35	62	0.000738	0.0247
Hbegf	47	0.00074	0.0247
Pdgfrb	191	0.00074	0.0247
2410012M07Rik	166	0.000742	0.0247
Dse	250	0.000742	0.0247
Rc3h1	134	0.000742	0.0247
Scd2	359	0.000742	0.0247
Ptpn23	75	0.000746	0.0248
Arfgap2	150	0.000747	0.0248
Fbn2	106	0.000753	0.0248
Rragb	432	0.000753	0.0248
Cyp1b1	66	0.000757	0.0248
Laptm4b	88	0.000757	0.0248

Lipo1	205	0.000757	0.0248
Fth1*	121	0.000759	0.0249
Fbln5	289	0.000765	0.0249
Lclat1	175	0.000765	0.0249
St8sia4	8	0.000765	0.0249
Edn1	403	0.000767	0.0249
Lmnb1	86	0.000775	0.0251
Cpt2	102	0.000777	0.0251
2410012M07Rik	189	0.000781	0.0251
Scd2	487	0.000781	0.0251
Capn2	71	0.000789	0.0253
Capn2	81	0.000789	0.0253
Lclat1	136	0.000791	0.0253
Camk4	296	0.000793	0.0253
Lrrc17	84	0.000795	0.0253
Klc1	134	0.000797	0.0253
Zdhhc15	49	0.000806	0.0255
Itga11	46	0.00081	0.0256
Macrod2	48	0.000818	0.0258
S1pr3	98	0.000822	0.0259
6720456H20Rik	90	0.000827	0.0259
Rc3h1	212	0.000827	0.0259
Tll1	551	0.000827	0.0259
Efemp1	65	0.000829	0.0259
Gjb2	141	0.000829	0.0259
Gpank1	280	0.000831	0.0259
S1pr3	41	0.000836	0.0259
Fbln5	155	0.00084	0.026
Gpc6	471	0.000842	0.026
Lipo1	258	0.000844	0.0261
Dcaf7	163	0.000853	0.0262
Hmcn1	153	0.000853	0.0262
Lmnb1	9	0.000858	0.0262
Slit2	1720	0.000858	0.0262
Akap1	94	0.00086	0.0262
Wdhd1	70	0.000862	0.0262
Camk4	8	0.000869	0.0264
Mapk1ip1l	53	0.000871	0.0264
Armc5	550	0.000873	0.0264
Sh3pxd2b	53	0.000883	0.0267
Slc39a14	118	0.000887	0.0267
Tll1	162	0.000887	0.0267
Fbln5	180	0.000896	0.0267
Rc3h1	213	0.000896	0.0267
Col1a2	60	0.000899	0.0267

Tll1	360	0.000899	0.0267
Dse	206	0.000901	0.0267
Klc1	25	0.000901	0.0267
Psma5	230	0.000901	0.0267
Fth1*	135	0.000908	0.0268
Capn2	57	0.00091	0.0268
Dse	229	0.00091	0.0268
Gjb2	8	0.00091	0.0268
Osbpl6	72	0.000913	0.0268
Dse	203	0.000915	0.0268
Cd151	29	0.000917	0.0268
Nrgn	154	0.000927	0.027
Dse	282	0.00093	0.027
Slit2	273	0.00093	0.027
Scd2	602	0.000932	0.027
Fbn1	83	0.000935	0.027
Slc38a4	50	0.000937	0.027
Slit2	1312	0.000937	0.027
Fth1*	72	0.000939	0.027
Hbegf	198	0.000939	0.027
Osbpl6	61	0.000939	0.027
Gjb2	46	0.000942	0.027
Scd2	75	0.000944	0.027
Fth1*	127	0.000947	0.027
Baiap2l2	31	0.000952	0.0271
Fbln5	275	0.000962	0.0274
Hbegf	255	0.000965	0.0274
Dkk2	671	0.000967	0.0274
Clk3	305	0.000977	0.0276
Gpkow	17	0.000979	0.0276
Capn2	36	0.000985	0.0277
Slit2	405	0.000988	0.0277
Wdhd1	81	0.000988	0.0277
Gclc	107	0.000993	0.0278
Baiap2l2	68	0.000995	0.0278
Osbpl6	3	0.000995	0.0278

Publishing Agreement

It is the policy of the University to encourage the distribution of all theses, dissertations, and manuscripts. Copies of all UCSF theses, dissertations, and manuscripts will be routed to the library via the Graduate Division. The library will make all theses, dissertations, and manuscripts accessible to the public and will preserve these to the best of their abilities, in perpetuity.

I hereby grant permission to the Graduate Division of the University of California, San Francisco to release copies of my thesis, dissertation, or manuscript to the Campus Library to provide access and preservation, in whole or in part, in perpetuity.

Author Signature  Date 1-9-15